Renormalized Statistical Cumulants in Stochastic Surface Growth and Fluid Turbulence

A thesis submitted in
partial fulfillment of the requirements
for the degree of

DOCTOR OF PHILOSOPHY

in Physics

by

Tapas Singha

Department of Physics
Indian Institute of Technology Guwahati
Guwahati 781039 India

September 2016

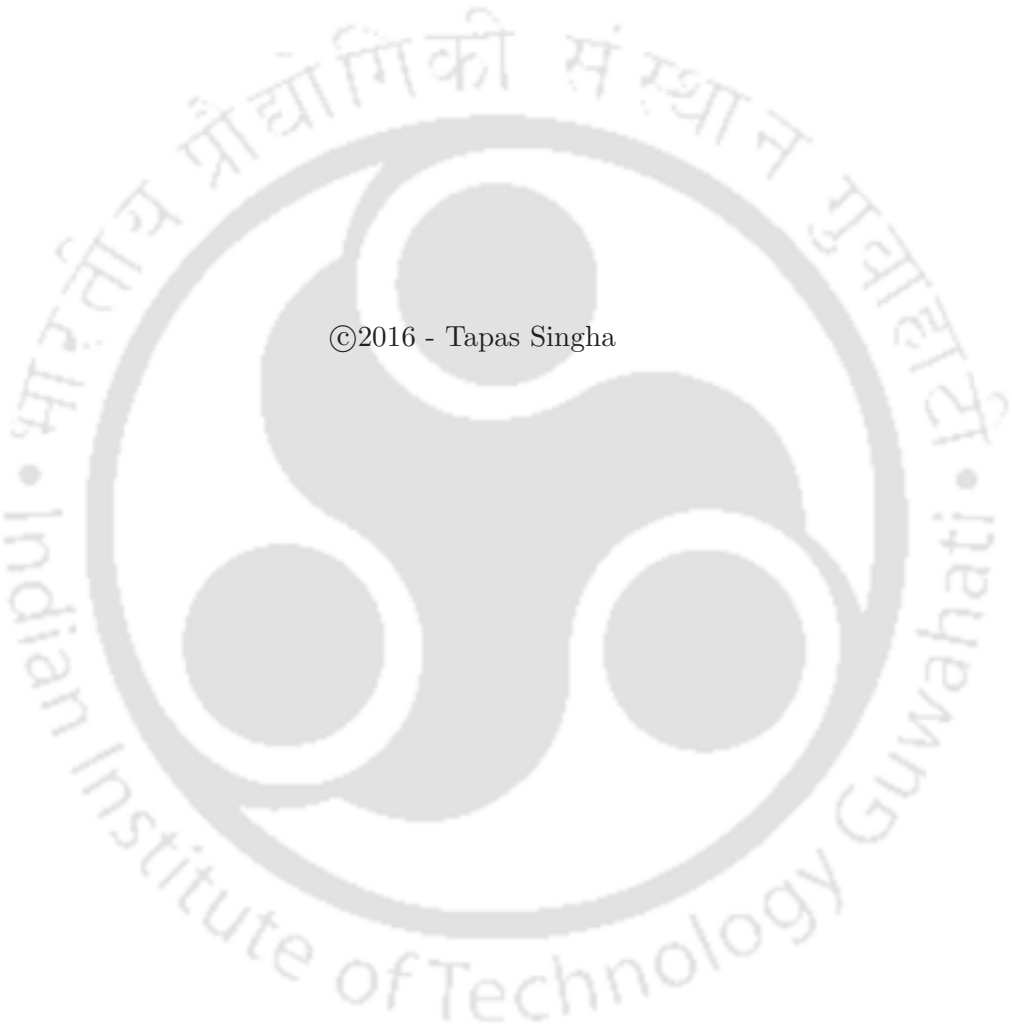

Declaration

I declare that the work contained in this thesis entitled "*Renormalized Statistical Cumulants in Stochastic Surface Growth and Fluid Turbulence*" has been carried out by me with the supervision of Dr. Malay K. Nandy at the Department of Physics, Indian Institute of Technology Guwahati, India. I further declare that no part of this thesis work has been submitted elsewhere for a degree.

(Tapas Singha)

September 9, 2016

Disclaimer

The bibliography included in this thesis is by no means complete but contains the ones which have been read fully or partially by me. I apologize for inadvertently missing out any research articles or scientific documents that may have relevance to this thesis work.

Indian Institute of Technology Guwahati
Department of Physics, Guwahati 781039, India

Dr. Malay K. Nandy
Associate Professor
Phone: +91-(361)-258-2706/ . . . 4706
Cell: +91-94010-86706
Email: mknandy@iitg.ernet.in

Certificate

This is to certify that the research work contained in this thesis, entitled "*Renormalized Statistical Cumulants in Stochastic Surface Growth and Fluid Turbulence*" has been carried out by Mr. Tapas Singha with my supervision, and that this work has not been submitted elsewhere for a degree.

(Dr. Malay K. Nandy)

September 9, 2016

To my parents...

Acknowledgements

Throughout the journey of this thesis work many ups and downs came for uplifting me and making me sorrow, respectively. Nevertheless, at the same time, I experienced supports, motivations, and love from several people during this period. It gives me immense pleasure for getting such place where I could express my gratitude to a number of people who sincerely appreciated, motivated me to smoothen this journey in various ways.

At this moment of accomplishment, first and foremost, I would like to express my sincere thank and profound gratitude to my thesis supervisor Prof. Malay Kumar Nandy for his constant supports, valuable suggestions, and encouragements. I am indebted to him for taking me as a Ph.D. student and guiding a nervous, worried student like me. He has been a constant source of academic and moral support over more than five years through the rough road to finish this thesis. Apart from the research, I enjoyed his teaching while he had taught the Statistical field theory and Quantum field theory to M.Sc. and B.Tech. students. Sometimes, when I look back, I really enjoy by remembering the long discussions, conversations, appreciations as well as disagreements. Most of the time, it enriched me which I would not forget. I would also like to thank his sister, Ms. Dipti Nandy, for her affection and support.

I am very much thankful to Prof. Amarendra Kumar Sarma for his immense supports, motivations and valuable suggestions on my thesis work and other administrative work. I am also very much thankful to Prof. Padma Kumar Padmanabhan for his constant supports, suggestions and motivations. I wish to thank Prof. Sukanta Pati and Prof. Tarak Nath Dey for their valuable suggestions on my thesis works. Once again, I would like to thank each member of my Doctoral committee for being such kind persons and for their exceptional behavior with me whenever I met them.

The last chapter of my thesis has been completed in collaboration with Dr. Kishore

Dutta. Its my pleasure to work with him who have been so much energetic, enthusiastic, and supportive. I am very much thankful to him for his supports and motivations. I would like to thank my senior Rohit for his supports and encouragements. I wish to thank Arun-da for his constant support, motivations and encouragements. I would like to thank Prof. Ravishankar and Prof. Senthilkumaran for their hospitality and for extending various facilities at IIT Delhi during my visit. I wish to thank Prof. Debaprasad Maity of for his support, motivations and friendly behavior.

I feel lucky to have friend like Sandeep, with whom I shared my academic and personal problems, who supported and helped me in various ways. He also sincerely believed and encouraged me when I feel myself down. In addition to him, there are seniors, juniors, and friends. Although the names can not be finished by listing, a few of them are indispensable to be mentioned. The names are following, namely, Biswajit-da, Himangshu-da, Ramesh-da, Bappaditya-da, Biplob, Kartik, Debashish, Ashis, Sourav, Ramiz, Kollol, Abhijit, Noor, Koushik and Sudin. I enjoyed a lot with them in various ways, such as academic and non-academic discussions, debates etc., at the tea sessions. I really enjoyed their good sense of humor, words of cheer and friendships. Besides them, I would also like to thank other research scholars at IIT Guwahati with whom I often interact.

I am grateful to Indian Institute of Technology, Guwahati for the financial support. I wish to thank Department of Physics, IITG for providing me the necessary facilities. I thank all the technical assistants of the department, specially Mr. Basab Bijoy Purkayastha for his assistance in various ways during my research period.

It should not be taken for granted that the amazing beauties of nature in and around IIT Guwahati campus make me feel good and quiet. Most often, I, either physically or mentally, go to the bank of the Brahmaputra river, situated at only four minutes walking distance away from my room. Through the window of my room, I could watch the greenish Kamakhya hill playing hide and seek with dense cloud during rainy seasons. It has been a long time, more than seven years (including my M.Sc.), I have been staying in this campus. I am very privileged to thank the river Brahmaputra and all the hills here which give me pleasure and mental peace.

Finally, I convey my gratitude and thanks to my parents and my two elder sisters for their unconditional love, constant support and inspiration during my entire career. I would like to thank my two brothers-in-law, neighbours, for their constant

support and help to my family whenever they needed it in my absence during this long period of journey.

Synopsis

Geometries associated with a variety of macroscopic non-equilibrium phenomena starting from trajectories of Brownian particles, hydrodynamic flow lines, structure of sea shores and land- scapes and also mountains, islands, rivers, glaciers, sediments, the geometrical structure of thin film's surfaces etc., are interesting topics in modern trends of research in basic sciences as well as in engineering. Most often, the dynamics of these non-equilibrium phenomena are stochastic in nature. In this thesis we shall concentrate mainly on surface growth dynamics and fluid turbulence which have been of great importance and challenging topics in modern research.

Due to stochastic behavior governed by nonlinear dynamical equations, the above phenomena can only be studied statistically via scaling analysis and probability distribution functions so that they can be classified in terms of universality classes. The studies of scaling analysis via scaling exponents are long been a important and usual procedure to characterize the system. Besides the critical exponents, the probability distribution function is an important feature to classify the universality of these processes. In experiments, measurements of normalized moments is expected to be more accurate than the measurement of scaling exponents. Thus higher-order moments can infer about the universality class in a better way than the critical exponents. Consequently, higher-order moments are very important in the study of surface morphology and the universality class can be better realized through the values of higher-order cumulants such as skewness, kurtosis and hypersewness.

It is observed that in all these problems the probability distribution functions deviate from the Gaussian distribution. A mathematically ideal situation would be to calculate the full probability distribution function. It may be noted that it is next to impossible to obtain a closed-form analytical expression for the full probability distribution starting with the nonlinear equations, namely, Kardar-Parisi-Zhang (KPZ), Villain-Lai-Das Sarma (VLDS), and Navier-Stokes equations driven by stochastic noise. Consequently, in an analytical approach, one usually evaluates a few lower and higher order moments (such as skewness, kurtosis and hyperskewness) from the

governing dynamics.

The KPZ Equation. The most generic non-linear continuum model of surface growth is the KPZ equation, which can be expressed as $\frac{\partial h(\mathbf{x},t)}{\partial t} = \nu_0 \nabla^2 h + \frac{\lambda_0}{2}(\nabla h)^2 + \eta(\mathbf{x},t)$, that is endowed with interesting properties of statistical scale invariance. The height field $h(\mathbf{x},t)$ is the height of the surface at position $\mathbf{x}$ and time t on a d dimensional substrate, ν_0 is the surface tension that has a tendency to make the surface smooth, and the coupling constant λ_0 measures the strength of the nonlinear interaction term. The nonlinear term induces local growth along the normal to the surface and gives rise to lateral correlations. On the other hand, the linear term (containing ν_0) is responsible for diffusion of particles to the local minima[111]. The driving term $\eta(\mathbf{x},t)$, describing the random deposition of particles, is assumed to obey a Gaussian distribution with covariance $\langle \eta(\mathbf{x},t)\eta(\mathbf{x}',t')\rangle = 2D_0\delta^d(\mathbf{x}-\mathbf{x}')\delta(t-t')$ where D_0 is a constant.

Various analytical approaches have been employed to study the universality class of the KPZ equation on the basis of scaling exponents in different dimensions. The dynamic renormalization-group by Kardar, Parisi, and Zhang[86] leads to the values of roughness exponent $\chi = \frac{1}{2}$ and dynamic exponent $z = \frac{3}{2}$ at one-loop order for the $(1+1)$ dimensional KPZ equation. Motivations in the theoretical study of the KPZ equation in higher dimensions have led to formulations of different analytical techniques. Examples of such theoretical studies are mode coupling scheme[28,76,189], the operator product expansion[113], the self-consistent expansion[163] and a nonperturbative renormalization group for the calculation of scaling exponents in the strong coupling regime. These exponents have also been computed numerically considering different growth rules. Apart from the numerical studies, many experiments have been carried out to find these exponents. Various experimental[71,72,179] studies have indicated that the roughness exponent is about 0.50 and the growth exponent 0.33, which have been identified with the universality class of the $(1 + 1)$-dimensional KPZ-type surface growth.

Skewness in 1D KPZ. Apart from the scaling exponents, skewness and kurtosis have been computed numerically employing a variety of deposition algorithms. Prähofer and Spohn took the polynuclear growth model (PNG) and obtained $S = 0.35941$ for the stationary self-similar case. Krug *et al.*[108] investigated the stationary state skewness for the SSM model with random uncorrelated spins ($\sigma_i = \pm 1$) and obtained $|S| \approx 0.33$. Maunuksela *et al.*[124] identified that the universality class of slow combustion fronts of a paper sheet belongs to the KPZ universality class on the basis of scaling exponents. With the same experimental conditions, Miet-

tinena *et al.*[129] performed an experiment on paper burning to find the skewness from the probability distribution function. They studied the height distribution of combustion fronts for flat initial conditions in the saturation regime and obtained the skewness value $S = 0.32$.

In Chapter-2 of the thesis, we use the (1+1)-dimensional KPZ equation driven by a Gaussian white noise by employing a perturbative renormalization scheme. Hence, we calculate the second- and third-order cumulants of height distribution using the diagrammatic method in the large-scale and long-time limits. The cumulants so calculated lead to the value $S = 0.3237$ for skewness which is independent of model parameters D_0, ν_0, λ_0, and system size L due to their exact cancellations. This value is comparable with numerical and experimental estimates.

Kurtosis in 1D KPZ. Studies of growth of an interface via simulation of the single step model with flat initial condition have been carried out by Krug[108] which yield the second and fourth cumulant $c_2 = 0.404 \pm 0.013$ and $c_4 = 0.020 \pm 0.002$, respectively suggesting a kurtosis value $Q = c_4/c_2^{3/2} = 0.123 \pm 0.020$. The PNG model of Prähofer and Spohn yields $Q = 0.289$ for stationary state. On the other hand, Halpin-Healy and Lin[61], studied the distributions of deposition models (BD, SSM, and RSOS) that strongly agree with DPRM/SHE results and they turn out to be the Baik-Rains distribution. These investigations establish that the kurtosis value in the stationary state must be the same as the universal kurtosis of the Baik-Rains distribution (for example, $Q = 0.289$ or 0.278). There are a few studies where the full Baik-Rains distribution is obtained in the context of KPZ stationary state.

In Chapter-3 of the thesis, we study the fourth order normalized cumulant of height fluctuations governed by $(1 + 1)$ dimensional KPZ equation for a growing surface. Following a diagrammatic renormalization scheme, we evaluate the kurtosis Q from the connected diagrams leading to the value $Q = 0.1523$ in the large-scale long-time limit which is free from the system size L and model parameters D_0, ν_0, and λ_0, due to their exact cancellations.

Hyperskewness in 1D KPZ. For statistical characterization to a greater degree, the normalized fifth cumulant, namely, the knowledge of hyperskewness, becomes important. The Baik-Rains value for hyperskewness is 0.3092 which may be obtained from Fredholm determinant representation as well as from the numerical data via the solution of the Painlevé-II. In Chapter-4 of the thesis, we evaluate hyperskewness of height fluctuations dictated by the $(1+1)$-dimensional KPZ equation for the stochastic growth of a surface on a flat geometry in the stationary state by following a diagrammatic approach and invoking a renormalization scheme. We

calculate the fifth cumulant given by a connected loop diagram. This, together with the result for the second cumulant, leads to the hyperskewness value $\tilde{S} = 0.0835$. The Baik-Rains value is distinctly higher than our calculated value. This underestimation is due to the fact that the method is based on a perturbative approach where the calculation is carried out only at one-loop order. Since the dynamics is governed by a white noise following a Gaussian distribution, the lowest order approximation appears to be influenced rather strongly by the Gaussian noise. A similar trend was observed in the one-loop perturbative calculation for kurtosis in the previous Chapter.

Skewness and Kurtosis in 2D KPZ. Two dimensional surface is a subject of great significance in non-equilibrium statistical mechanics due to its wide range of applicability in addition to its theoretical complexity. There exists no exact solution for the (2+1)-dimensional KPZ equation. Recently, the (2+1)-dimensional KPZ has been realized as an important problem where the higher dimensional analogs of TW GOE, TW GUE and Baik-Rains distribution have been investigated. Kim *et al.*[94] studied the minimum energy distribution of directed polymer in random potential with Gaussian distribution up to $(3+1)$ dimensions and obtained non-Gaussian distribution in those dimensions. Halpin-Healy and Takeuchi[56], throughly explored the statistics of the higher dimensional DPRM that yield non-zero skewness and kurtosis values. Alves *et al.*[5] studied the higher dimensional KPZ height distributions via the RSOS model for flat initial condition and found the distributions to be non-Gaussian.

There have been a large number of numerical works on the $(2+1)$-dimensional KPZ type growth. Quite a few growth models having a great deal of diversity, all of which belonging to the $(2+1)$-dimensional KPZ universality class, have been studied[?] for the morphology and statistics in the transient regime. The studied RSOS model, Euler integration of the KPZ equation and the mapping of the KPZ equation to a driven dimer model lead to roughness exponent $\chi = 0.383$, 0.388 and 0.375, respectively. Kelling and Odor[89] performed a simulation considering a huge size up to $2^{17} \times 2^{17}$ and estimated the scaling exponents $\chi = 0.393 \pm 0.004$. A numerically discretized RSOS model, studied by Marinari *et al.* [121] by means of multi-surface coding, yields $\chi = 0.393 \pm 0.003$. Odor *et al.*[140] found $\chi = 0.395 \pm 0.005$ by mapping the driven lattice gases of d-dimers model onto the KPZ problem.

Theoretical calculation of χ in two and higher dimensions has been a challenging work. Analytical approaches such as the perturbative RG and nonperturbative approaches, such as mode coupling and self-consistent expansion are incapable of

giving any conclusive scaling exponents as well as universality in $d = 2$ dimension. Lassig[113] employed an operator product expansion and obtained $\chi = 2/5$ and $z = 8/5$. A mode coupling calculation of Colaiori and Moore suggested the dynamic exponent $z = 1.62$ and roughness exponent $\chi = 0.38$. A nonperturbative field theoretic RG has been employed by Kloss in the stationary state and obtained roughness exponent $\chi = 0.373$ via amplitude ratio of temporal and spatial correlation.

Recently, Pagnani and Parisi[143] studied $(2+1)$-dimensional KPZ-type growth in the steady state and estimated two sets of best-fit results, namely, FIT-I and FIT-II for roughness exponent, skewness and kurtosis values. They found roughness exponent $\chi = 0.3893 \pm 0.0006$ (FIT-I), $\chi = 0.3869 \pm 0.0004$ (FIT-II), skewness $|S| = 0.2669 \pm 0.0004$ (FIT-I), $|S| = 0.2657 \pm 0.0004$ (FIT-II) and kurtosis $Q = 0.146 \pm 0.002$(FIT-I), $Q = 0.145 \pm 0.001$ (FIT-II). Halpin-Healy[60] has reported the value of average skewness ($S = 0.244$) and kurtosis ($Q = 0.177$) for three models namely, RSOS, $g5_1$ DPRM and KPZ Euler. In the literature, the roughness and dynamic exponents ($\chi \approx 0.39$, $z \approx 1.61$).

In Chapter-5 of the thesis, we consider the statistical cumulants of height fluctuations governed by the $(2+1)$-dimensional KPZ equation for flat geometry. We follow a diagrammatic scheme to derive the expressions for renormalized cumulants up to fourth order in the stationary state. Assuming a value for the roughness exponent from reliable numerical predictions, we calculate the second, third and fourth cumulants, yielding skewness $S = 0.2879$ and kurtosis $Q = 0.1995$. These values agree well with the available numerical estimations.

Skewness in 1D VLDS. The growth of a thin film using the molecular beam epitaxy (MBE) is dominated by surface diffusion at high temperatures, where atomic evaporation, desorption, bulk defects , hangs and overhangs are negligibly small. In MBE, atoms are deposited one-by-one for the preparation of high quality thin films. Considering a geometrical interpretation, Villain, Lai and Das Sarma (VLDS) proposed a nonlinear equation with non-conserved noise for the MBE processes. This dynamical equation is known as the VLDS equation, written as $\frac{\partial h(\mathbf{x},t)}{\partial t} = -\nu_0 \nabla^4 h + \frac{\lambda_0}{2}\nabla^2(\nabla h)^2 + \eta(\mathbf{x},t)$, where $h(\mathbf{x},t)$ is the height of the fluctuating surface at position x and time t, ν_0 is the diffusion constant and η is a Gaussian white noise with zero mean and covariance $\langle \eta(\mathbf{x},t)\eta(\mathbf{x}',t')\rangle = 2D_0\delta^d(\mathbf{x}-\mathbf{x}')\delta(t-t')$, where D_0 is a constant. Through one-loop dynamic RG calculations, Lai and Das Sarma as well as Tang and Nattermann independently obtained the roughness and dynamic exponent $\chi = (4-d)/3$ and $z = (8+d)/3$.

Wilby *et al.*[197] studied the SOS model by using Monte-Carlo-Simulation and

estimated the growth exponents $\beta = 0.333 \pm 0.010$ in $d = 1$ dimension which agrees with the dynamic RG result. A conserved growth model with RSOS condition, in $(1 + 1)$ dimensions, has been studied by Kim and Kim[93] and their estimated exponents (roughness and growth exponents $\chi = 0.95 \pm 0.04$ and $\beta = 0.32 \pm 0.01$ respectively) agree with the calculated exponents from dynamic RG.

In Chapter 6 of the thesis, we study the $(1 + 1)$-dimensional Villain, Lai, and Das Sarma (VLDS) equation driven by a Gaussian white noise and implement a renormalization scheme without rescaling at one-loop order. Using a diagrammatic method, we calculate the renormalized second and third moments in the large-scale and long-time limits. The ensuing skewness value is $S = -0.0441$. This (negative) value is consistent with the numerical prediction of Das Sarma *et al.*[32]. Our approach carries out the calculations of W_2 and W_3 in the large scale limit $k \to 0$ and consequently expects the statistical properties of the growth process at large scales.

It is interesting to note that we obtained the skewness value which is a negative number. This is consistent with the numerical prediction of Das Sarma *et al.*[32] who obtained $S = -0.1 \pm 0.15$ in the steady state and suggested that the skewness value is likely to be negative, although they did not exclude a zero or slightly positive value. The large error bar that they obtained is probably due to a dominant role of fluctuations in their numerical model. We observe that our value of $S = -0.0441$ is consistent with their prediction. Moreover, our calculated value asserts that the probability distribution function is negatively skewed.

Skewness in 3D Turbulence. The turbulent flow of an incompressible fluid governed by the Navier-Stokes equation has long been considered as a challenging problem due to its inherent non-linearity and complexity. Various important advances have been made over the last decades in understanding the statistical properties of turbulence following from the governing dynamical equation. The Navier-Stokes equation for an incompressible turbulent fluid is expressed as $\frac{\partial v_i}{\partial t} + v_j \frac{\partial v_i}{\partial x_j} = -\frac{1}{\rho}\frac{\partial p}{\partial x_i} + \nu_0 \frac{\partial^2 v_i}{\partial x_j \partial x_j}$, with the incompressibility condition $\frac{\partial v_i}{\partial x_i} = 0$, coming from the equation of continuity. Here $v_i(\mathbf{x}, t)$ is the velocity field, $p(\mathbf{x}, t)$ the pressure field, ρ the density, and ν_0 is the kinematic viscosity of the fluid. In three-dimensions, the turbulent energy density obeys the Kolmogorov universal scaling (neglecting intermittency correction) $E(k) = C\ \varepsilon^{2/3}\ k^{-5/3}$ in the inertial range $L^{-1} \ll k \ll \eta^{-1}$ where the turbulent energy cascades from the largest to the smallest scales of motion. In the above expression C is the universal Kolmogorov constant, ε the energy transfer rate (per unit mass) which is also the mean dissipation rate, and k is the

wavenumber. The Kolmogorov microscale η, defined as $\eta = (\nu^3/\varepsilon)^{1/4}$, signifies the scale where dissipation becomes important. Within the Kolmogorov phenomenology, the eddy-viscosity follows the universal scaling $\nu(k) = \alpha\ \varepsilon^{1/3}\ k^{-4/3}$, where α is another universal constant.

In Chapter 7 of the thesis, we apply a renormalized perturbative scheme on the Navier-Stokes equation for an incompressible isotropic turbulent velocity field. This allows us to obtain the renormalized expressions for second- and third-order cumulants of the velocity derivative directly from the corresponding Feynman diagrams. The resulting expressions are integrated numerically by excluding and including the dissipation range assuming Kolmogorov and Pao's phenomenalogical expressions for the energy spectrum. The ensuing values for skewness are found to be $S = -0.647$ (when the dissipation range is excluded) and $\mathcal{S} = -0.682$ (when the dissipation is included). These estimaed values are compared with various experimental, numerical and theoretical results.

Contents

List of Figures

List of Tables

List of Publications

Publications :

1. *Skewness in* $(1+1)$*-dimensional Kardar-Parisi-Zhang-type growth*
   Tapas Singha and Malay K. Nandy, Phys. Rev. E **90** 062402 (2014).

2. *Kurtosis of height fluctuations in* $(1+1)$ *dimensional KPZ dynamics*
   Tapas Singha and Malay K. Nandy, J. Stat. Mech. **P05020** (2015).

3. *Hyperskewness of* $(1+1)$*-dimensional KPZ height fluctuations*
   Tapas Singha and Malay K. Nandy, J. Stat. Mech. **013203** (2016).

4. *A renormalization scheme and skewness of height fluctuations in* $(1+1)$*-dimensional VLDS dynamics*
   Tapas Singha and Malay K. Nandy, J. Stat. Mech. **023205** (2016).

5. *Steady-state skewness and kurtosis from renormalized cumulants in* $(2+1)$*-dimensional stochastic surface growth*
   Tapas Singha and Malay K. Nandy, J. Stat. Mech. Sep. 2016 *(*accepted for publication) in

6. *Renormalized cumulants and velocity derivative skewness in Kolmogorov turbulence*
   Tapas Singha, Kishore Dutta and Malay K. Nandy, *(manuscript ready for submission)*

Chapter 1

Introduction

The geometry associated with a variety of macroscopic physical phenomena starting from trajectories of Brownian particles, hydrodynamic flow lines, structure of sea shores and landscape[29,68,172], and also mountains, islands, rivers, glaciers, sediments, the geometrical structure of crystals, etc., are interesting topics in research. These phenomena are most often non-equilibrium in nature due to interaction with environments. Although over the last five-six decades these systems have already been studied via different statistical approaches, they deserve much attention to fully understand the ever increasing complexities of the problems.

One of the highly interesting and technologically demanding topics among such non-equilibrium phenomena is surface and interface growth. The macroscopic fluctuations of an interface or a surface during their growth and the corresponding changes of their morphologies with time have long been a topic of increasing interest among researchers. The dynamics of growing surfaces involve many fundamental processes such as deposition, solidification, crystallization, sedimentation, inhibition, coating, sputtering, dissolution, corrosion, erosion, combustion, flame front propagation, and biological growths[119]. During growth, surface or interface advances through fluctuations which may have thermal, kinetic, chaotic origin or due to the disordered nature of the medium. Most often, the dynamics of growing surface is stochastic in nature due to the inherent randomness (spatial and temporal) of the incoming flux. A similar process takes place for the case of magnetic flux lines in superconductor being fluctuated by the pinning forces of the quenched disorder and thermal noises. Since the externally imposed random noise and the inhomogeneity of the medium enhances the complexity of such a dynamical system, these problems become analytically intractable.

1.1 Statistical characteristics of growing surfaces and interfaces

The statistical characterization of growing surfaces and interfaces are based on the most important observed property, namely, scale invariance. Due to this inherent property, the surface and interface growth problems can be described via a powerful scaling concept which enables one to connect the apparently different systems via scaling exponents. This leads to the classification in terms of *universality class*. In various physical systems with a well-defined scaling property, the scaling exponents are often found to be invariant with respect to small changes in the actual interactions or model parameters of the system. Different systems which apparently have no connection between them, are said to be in the same universality class if they possesses the same value for the scaling exponents. This is due to the fact that the scaling exponent values are independent of many details of the system, for instance, these values for an interface of a paper wetting experiment do not depend on whether the paper is immersed in ink or coffee, or whether the experiment is done with a paper or a towel.

The problem of surface growth, also known as kinetic roughening, appear in many physical processes such as material fracture[120], corrosion[67,141], electrochemical deposition[12], the propagation of flame fronts, the growth of bacteria cell colonies. Growing surfaces mainly remain scale invariant under anisotropic scale transformation. This may be understood by a single-valued function for surface height $h(x)$ at a point x satisfying $h(bx) \sim b^{\chi} h(x)$. In this case, $h(x)$ is called a self-affine function and, as such, the surface or the interface is known as self-affine fractal.

Although the roughening of surfaces or interfaces can occur under both equilibrium and non-equilibrium conditions, most often they occur under non-equilibrium conditions. The roughness of growing surface or interface determines many important physical and chemical properties of films. For instance, the electrical conductivity of a metal thin film and the hysteresis of magnetic films depend on the roughness of the surface or interface[139,159]. It controls the optical losses in optical waveguides[158] and is responsible for increase in the effective area of charge storage devices[23]. The properties of a rough surface is statistically characterized by scaling expoents.

A. Scaling exponents

The growing surfaces and interfaces are characterized by interface width. The interface width initially (in transient regime) increases with time and in the stationary state it is no longer a function of time rather it depends on the system size as

$$w(L,t) \sim t^{\beta} \quad g\left(\frac{t}{L^z}\right) \tag{1.1}$$

when $t \ll t_c$ and

$$w_{sat}(L) \sim L^{\chi}, \tag{1.2}$$

where $t \gg L^z$ and t_c is the crossover time. The exponent χ is known as the roughness exponent that characterizes the roughness of the saturated surface. The exponent β, called the growth exponent, characterizes the time-dependency of the roughening process. The dynamic exponent is defined as $z = \frac{\chi}{\beta}$ and is related to the crossover time t_c as $t_c \sim L^z$. On the other hand, the correlation length $\xi(t)$ gradually increases with time as $\sim t^{1/z}$ and becomes the order of the system size L when the system gets saturated. Thus, the dynamic exponent z indicates how fast the correlation length grows in the system. These scaling exponents characterize the dynamics of surface growth and, as such, they determine the universality class of those growth processes.

B. Representative models

A number of discrete models have been proposed to elucidate the physical properties of stochastically growing surfaces and interfaces. The simulations of these growth models played an important role in developing a better understanding of growing surfaces under non-equilibrium conditions. In what follows, we shall describe briefly some of the models that provide a basic statistical understanding about the underlying physics.

The simplest numerical model of surface growth was first proposed by Murray Eden[39,84] in one dimension to describe the shape of a cell colony being formed by random sticking of particles on the perimeters of the cluster. The fluctuation of the shape of the resulting cluster depends on the imposed microscopic growth rules.

In ballistic deposition (BD) model[194,195], particles are deposited at random sites on a substrate. As soon as the particles are deposited, they stick and settle down at nearest neighboring sites. After a long time, the bulk of the system of the structure becomes porous but non-fractal.

In restricted solid-on-solid (RSOS) model[97], the particles are also deposited at random sites $h_i \to h_i+1$. In other words, the deposition process does not violate the condition $|\Delta h| \leqslant 1$ making the bulk compact with negligibly small hangs, overhangs and vacancies.

Following these discrete models, continuous models have been constructed to describe stochastic surface growth. Edwards and Wilkinson[199], for the first time offered a differential equation which incorporates the diffusion of particles during the deposition.

C. Edwards-Wilkinson equation

To understand the sedimentation process of particles in the presence of gravitational relaxation and stochastic noise, Edwards and Wilkinson (EW) offered a partial differential equation for the interface dynamics as

$$\frac{\partial H(\mathbf{x},t)}{\partial t} = F + \nu_0 \nabla^2 H(\mathbf{x},t) + \eta(\mathbf{x},t), \tag{1.3}$$

where $H(\mathbf{x},t)$ represents the interface height, ν_0 the surface tension, F the velocity of the interface, and η is a spatially and temporally uncorrelated stochastic Gaussian noise with $\langle \eta(\mathbf{x},t) \rangle = 0$, and variance, $\langle \eta(\mathbf{x},t)\eta(\mathbf{x}',t') \rangle = 2D_0\delta^d(\mathbf{x}-\mathbf{x}')\delta(t-t')$. Here, the surface tension tries to smoothen the surface by minimizing the surface area. The term F can be excluded by viewing the growth process with such a coordinate system which is moving with velocity F, i.e., a transformation $H \to h + F\ t$ can be introduced where h is the fluctuating height field and t is time.

The values of scaling exponents χ and z can be obtained for the EW equation by exploiting the scaling concept, i.e., the growth equation would be invariant to the transformation $\mathbf{x} \to b\mathbf{x}$, $t \to b^z t$ and $h \to b^\chi h$. Under these scale transformations, the EW equation becomes

$$\frac{\partial h(\mathbf{x},t)}{\partial t} = \nu_0 b^{(z-2)} \nabla^2 h(\mathbf{x},t) + b^{(z-d-2\chi)/2} \eta(\mathbf{x},t). \tag{1.4}$$

Since the equation is scale (b) invariant, the roughness and dynamic exponents are $\chi = (2-d)/2$ and $z = 2$, respectively. The scaling exponents from EW model do not match with that of discrete models such as Eden, BD, and RSOS models indicating that these discrete models and the EW model belong to the different universality classes.

D. Kardar-Parisi-Zhang (KPZ) equation

Experiments on growing interface and surface[57] suggest that the growth propagates along the direction of the local normal to the surface or interface. One such example is the propagation of fire-front where the propagation of the front can take place along the lateral direction. The growth along the normal to the local surface is mathematically represented by $\sqrt{1+(\nabla h)^2}$. For a small spatial variation of height, a suitable term, $(\nabla h)^2$, has been incorporated into the EW equation by Kardar, Parisi, and Zhang in their seminal paper[86]. Their equation for fluctuating hight field $h(\mathbf{x},t)$, commonly known as KPZ equation, can be expressed as

$$\frac{\partial h(\mathbf{x},t)}{\partial t} = \nu_0 \nabla^2 h(\mathbf{x},t) + \frac{\lambda_0}{2}(\nabla h)^2 + \eta(\mathbf{x},t), \tag{1.5}$$

where the symbols ν_0 and $\eta(\mathbf{x},t)$ carry the same meaning as in EW equation [Eq. (1.3)]. The equation is invariant under the transformation $h \to (h+c)$. The infinitesimal change of the coordinate introduces a slight angle ϵ along the growth direction. The transformations are considered as $\mathbf{x} \to \mathbf{x}+\lambda_0\epsilon t$ and $h \to h+\epsilon\cdot\mathbf{x}$. Thus the KPZ equation remains invariant under the Galilean transformations. However, it breaks the up-down symmetry ($h \to -h$) of the growth process due to the presence of the non-linear term, which determines the direction of the growth.

The transformation of scales, namely, $x \to bx$, $t \to b^z t$ and $h \to b^\chi h$ yields

$$\frac{\partial h}{\partial t} = \nu_0 b^{z-2}\nabla^2 h + b^{(z+\chi-2)}\frac{\lambda_0}{2}(\nabla h)^2 + b^{(z-d-2\chi)/2}\eta. \tag{1.6}$$

It is the presence of the non-linear term $\lambda_0(\nabla h)^2$ in the above equation for which the scaling exponents cannot be obtained directly from the scale invariance concept.

There is a variety of systems, which are different from growing surface, behave in a similar way and have been studied using the same theoretical framework as growing surface. There are some important examples, such as the dynamics of magnetic flux lines in type-II superconductors near the pining or depinning threshold[41], the dynamics of charge-density waves driven through impure materials with the existing electric field[135], the dynamics of dislocations and polymers[40] etc. The KPZ equation in $(3+1)$ dimensions with non-Gaussian spatially and temporally correlated noise does even describe the gravitational potential in cosmology. The velocity field in Burgers equation may represent, in some stages of the standard, inflationary, big bang model for cosmology, the fluctuating velocity (on smooth background) of the overall expansion of the universe[16].

Experiments for KPZ type growth

Besides numerical simulations of growth models as discussed earlier, a number of experimental studies have been devoted to test various proposed theoretical ideas via experiments which have been motivated by the KPZ equation consisting of a nonlinear term and notably, most of the experiments have failed to provide the exponents as those of KPZ universality in $(1+1)$ dimensions. A few of them are fluid-flow in a porous medium, paper wetting, slow combustion of paper, growth of bacteria colonies, paper tearing etc., which roughly follow the $(1+1)$-dimensional KPZ growth dynamics. It is very important to mention that one-dimensional KPZ exponents are estimated in a slow combustion fronts of a paper sheet experiment [124]. Furthermore, with the same experimental conditions, an another experiment [129] on paper burning has been carried out to estimate the normalized third cumulant of the probability distribution of height fluctuations and yields comparable estimations with other numerical results. Recently, an experiment has been carried out in $(1+1)$ dimensions on growing interface in liquid crystal turbulence (TLC). The estimated scaling exponents from the experiment are the same as those of one-dimensional KPZ equation [178]. In addition to that, the probability distributions of height fluctuations have been investigated on the basis of initial conditions of the growth which are very important to determine the sub-universality class of a system under the same universality class [179].

On the other hand, there have been very few experiments which follow two-dimensional KPZ universality class. For instance, vapor deposited oligomer thin film growth [62] yields a comparable exponents values, as those of $(2+1)$-dimensional KPZ universality class, in the transient regime .

E. Mathematical methods

An explicit dynamic renormalization group (RG) analysis has been carried out by Kardar, Parisi, and Zhang in their seminal paper [86] based on the KPZ equation. Fourier transformation of the KPZ equation is obtained to implement RG on KPZ equation which is considered as the key equation of perturbative RG. Fourier transformation of the equation reads as

$$h(\mathbf{k},\omega) = G_0(\mathbf{k},\omega)\eta(\mathbf{k},\omega) - \lambda_0\, G_0(\mathbf{k},\omega)\,\mathcal{NI}[h(\mathbf{p},\Omega)h(\mathbf{k}-\mathbf{p},\omega-\Omega)] \qquad (1.7)$$

where $G_0^{-1}(\mathbf{k},\omega) = [-i\omega_k + \nu_0 k^2]$ is the bare propagator and $\mathcal{NI}[h(\mathbf{p},\Omega)h(\mathbf{k}-\mathbf{p},\omega-\Omega)]$ is the non-linear integral ($\mathcal{NI}$) of the above key equation.

There have been two basic steps in the conventional RG theory. One of them is scale-elimination and other is rescaling the parameters. In the scale-elimination process the fields of higher modes ($k \in [\Lambda_0/b, \Lambda_0]$, and $b = e^r > 1$) are eliminated out which means the elimination of microscopic degree of freedom from the system.

Once elimination process is carried out, the system has a new cut-off Λ_0/b, i.e., the upper cutoff is reduced by a factor b with $b > 1$. Since the idea is to get back the original system, the momentum, frequency, model parameters and fields are rescaled, and subsequently, these processes modify the parameters and yield the flow equations describing the change in the parameters under the RG transformation. In this context, the variation of parameters under rescaling are of interest than the perturbative solution of growth equation. The above two processes are repeatedly performed so that the parameters of the growth equation do not vary with respect to the scale parameter, signifying the system reaches a fixed point. At that point, the variations of model and coupling parameters are zero ($\frac{dg}{dr} = \frac{d\nu}{dr} = \frac{dD}{dr} = \frac{d\lambda}{dr} = 0$) and coupled equations are solved to obtain the scaling exponents of the system.

There is another approach to obtain the scaling exponents via the RG without rescaling. In this process same sort of scale elimination as before is performed and corrections to the model parameters are obtained. Here, instead of rescaling the parameter of the KPZ growth, flow is directly calculated with respect to scale elimination. The resulting recursive relations are solved for coupling and model parameters and to obtain their scale dependent expressions. To obtain a fixed point value after many recursive steps, the limit for the scale parameter $r \to \infty$ is considered. This consideration yields a scale independent value of coupling constant and scale dependent expressions of parameters. Hence, one could obtain the exponent from the scaling relations e.g., $\nu(k)k^2 = k^z$. The scale dependency in the expressions for $\nu(r)$ and $D(r)$ are same and ratio of those expressions are scale independent indicating the fluctuation-dissipation theorem in one dimensional KPZ.

F. Theoretical predictions

The exponents values in $(1+1)$-dimensional KPZ equation are exactly obtained via the RG approaches at one-loop order[86,128]. Those exponent values are $\chi = 1/2$ (roughness exponent) and $z = 3/2$ (dynamic exponent).

Various analytical approaches have been employed to study the universality class of the KPZ equation on the basis of scaling exponents in different dimensions. Motivations in the theoretical study of the KPZ equation in higher dimensions have

led to formulations of different analytical techniques. Examples of such theoretical studies are the mode coupling scheme[28,76,189], the operator product expansion[113], the self-consistent expansion[163] and a nonperturbative RG[22,100] for the calculation of scaling exponents in the strong coupling regime.

There are a few theoretical attempts to obtain the roughness exponents in two dimensions. One of them is mode-coupling approximation of Colaire and Moore[28] leading to obtain the roughness exponents $\chi = 0.38$ and other is operator product expansion of Lässig that yields $\chi = 2/5$ in $d = 2$ dimensions[113]. In a non-perturbative calculation, Kloss[100] obtain roughness exponents $\chi = 0.330(8)$ and $\chi = 0.373(1)$ in the leading and next to leading order approximations, respectively.

G. Other estimations

The exponents have also been computed numerically considering different growth rules. Apart from the numerical studies, many experiments have been carried out to find these exponents. Various experimental studies[71,72,179] have indicated that the roughness exponent is about 0.50 and the growth exponent 0.33 which have been identified with the universality class of the $(1 + 1)$ dimensional KPZ type surface growth.

Various numerical simulations have been devoted in order to obtain the scaling exponents. There have been two conjectures regarding the dimension dependent exponents. Wolf and Kertesz[203] studying the Eden model conjectured the exponents value would be $\chi = 1/(d+1)$ in d dimension. Kim and Kosterlitz[97] studied RSOS model and conjectured $\chi = 2/(d+3)$. It is important to note that both conjectures yield the exact exponents value in $d = 1$ dimensions. Quite a few growth models having a great deal of diversity, all of which belonging to the (2+1)-dimensional KPZ universality class, have been studied[59] for the morphology and the statistics in the transient regime. The studies of growth models, such as RSOS and driven dimer, and numerical (Euler) integration of the KPZ equation yield roughness exponent $\chi = 0.383$, 0.375, and 0.388, respectively in $(2 + 1)$ dimensions. On the other hand, for the stationary state, the roughness exponent is obtained as $\chi = 0.387$–0.390[60]. Meanwhile, a numerical simulation[89] has been carried out considering a huge size up to $2^{17} \times 2^{17}$ to estimate the scaling exponents $\chi = 0.393 \pm 0.004$. Considering a potts-spin representation via a multisite-coding with 11520^2 sites, Forrest and Tang[46] estimated $\chi = 0.385 \pm 0.005$. A numerically discretized RSOS model, studied by Marinari *et al.*[121] by means of multi-surface coding, yields $\chi = 0.393 \pm 0.003$

and $\beta = 0.244 \pm 0.003$. Odor *et al.*[140] found $\chi = 0.395 \pm 0.005$ by mapping the driven lattice gases of d-dimers model onto the KPZ problem. Thus, the most of the numerical work suggest that the roughness exponent to $\chi \approx 0.39$.

H. Sub-universality classes of 1D KPZ-type growth

In early days, the main focus of the numerical simulations were to estimate the scaling exponents and thereby determining the universality classes of the models where Galilean invariance guaranteed that $\chi + z = 2$ in any dimensions. Finding the scaling exponents from a theoretical model, numerical analysis and experiments have long been a usual way to conclude the universality class of the studied system. Nevertheless, there have been a few works[58,94] where probability distribution of height fluctuations or free energy fluctuations for the directed polymer in random media have been investigated. The numerical simulation of height fluctuations of ballistic deposition growth model in $(1 + 1)$ dimensions by Havlin *et al.*[64] yielded Gaussian distribution in the steady state ($t \gg L^z$) and in the transient regime ($t \ll L^z$). Later on, a lot of numerical simulations on growth models and directed polymer in random media have been performed to estimate the cumulants of probability distributions of height fluctuations in the transient regime as well as in the steady state, and most of the works estimated the non-zero skewness values in the transient regime[136].

Thereafter, Krug *et al.*[108] attempted to carry out the numerical simulations for a wide range of growth models and directed polymer in random media in one dimension to obtain the universal quantities, such as a ratio of cumulants of height distribution of surface growth phenomena and free energy fluctuations of DPRM, along with the scaling exponents from a numerical simulation. In the steady-state, they found skewness $S \approx 0.33$ from single step model (SSM) whereas in the transient regime the simulation of single step model for flat initial condition yields $S = 0.28 \pm 0.04$. After a long time, in 2000, Johansson in ref.[83] via single step model, Prähofer and Spohn in ref.[153] via the polynuclear growth have found a connection to Tracy-Widom (TW) distributions of random matrix theory[185] via polynuclear growth. Subsequently, an exact solution of the $(1 + 1)$-dimensional KPZ equation, with the full-time evolution of the probability distribution function, which is universal in the asymptotic limit, has been obtained[20,104,162]. Since then there are various work which show that although scaling exponents are same for KPZ-type growth models, the probability distributions could be different depending on the initial conditions.

For flat (curved) initial conditions, the height-distribution follows TW-GOE[21,38] (TW-GUE) distributions. At the same time, Takeuchi and Sano[178] have performed experiments on turbulent liquid crystals and found TW GOE (for flat) and TW GUE (for curved) statistics with one dimensional KPZ scaling exponents. Furthermore, they confirmed that the distribution function and two-point correlation of height fluctuations are universal. In the stationary state $(1 + 1)$-dimensional KPZ height distribution has been illustrated by Imamura and Sasamoto[78] which is found to be Baik-Rains, F_0, distribution[9]. Thus, sub-universality classes exist under the same universality class based on the initial conditions of the interface growth.

Till to date, there is no exact solution for $(2 + 1)$-dimensional KPZ equation. In 2012, Halpin-Healy, considered various models, such as different kind of DPRM models, restricted solid-on-solid (RSOS) model, a direct Euler integrations, and two dimensional driven dimmers belong to the $(2 + 1)$-dimensional KPZ universality class[59]. A higher dimensional analogs of $(1 + 1)$-dimensional KPZ height fluctuations, such as TW GOE, TW GUE, and Baik-Rains distributions have been investigated[59,60]. There have also been a variety of numerical works[5,56,94] in order to obtain the scaling exponents and distribution functions in higher dimensions. To understand these sub-universality classes the probability distribution function along with the scaling exponents are indispensable. This is understood from the extensive numerical, experimental studies of initial conditions dependent height distributions of KPZ equation in $(1 + 1)$-dimensions. The analytical study of the probability distribution function (PDF) or associated few higher order moments are scarce.

As stated earlier, the universality class of a stochastic dynamical system has many important statistical properties. In the earlier studies on surface growth, the universality classes are determined via the scaling exponents of the corresponding systems. In the last two decades, it has been realized that despite the same scaling exponents, the distribution functions can be entirely different due to different initial conditions indicating different sub-universality classes. Thus, full information about the pdf is needed to classify many similar problems into varying universality classes. Hence, it may be interesting to note that the distribution function of a stochastic system contains more statistical information than the scaling exponents. However, an analytical calculation of the full pdf is an very difficult task, whereas the calculation of higher-order moments, such as the skewness, kurtosis and hyper-skewness is a more viable approach to economize on the amount of calculations of these values which can also be used as identifiers of the universality classes.

I. Conserved growth models

Epitaxial growths are subjects of great interest from the perspective of applications to thin films where the growth processes are very sophisticated due to layer by layer deposition or even down to atom by atom deposition in a very controlled pressure, temperature and incoming flux, known as Molecular beam epitaxy (MBE) type of growth process. By applying the technique, a very high quality materials are prepared, such as various types of semiconductors, magnetic materials, sometimes structure can be prepared so precise that can be used to make quantum wells, wires and dots which are very useful in electronics and opto-electronics devices. One of the reasons behind the extremely smooth surface is the high mobility of adatoms at the growth front which enables the incoming atoms very fast to incorporate at epitaxial growth. The temperature of epitaxial growth is controlled in such a way that the temperature is high enough for fast adatom diffusion to form a multilayer growth and of course low enough to cause negligible desorption.

Theoretically, it is very interesting as well as challenging because of the scale invariance properties, self-affinity, and mainly the processes are far from equilibrium. The determination of universality class of a non-equilibrium process is an integrable part of studies describing the large-scale and long-time properties of surface growth, are usually determined by a set of exponents (χ, β and z) of that particular growth process. It has also been realized on the basis of theoretical, simulation and experimental works that the coarse-grained roughened surface of epitaxial growth follow the same type of dynamical scaling as given by Eqs. 1.1 and 1.2. However, it is very important to know the fundamental reasons that make the difference and lead to acquiring different set of exponents and thereby universality classes. For short time, the lateral correlation length $\xi(t) \sim t^{1/z}$, where z characterizes the time dependent behavior of correlation length, i.e., how fast the correlation can grow. When the system size is finite, at long times ($t \gg L^z$), the correlation (lateral) length, $\xi(t)$, would be of the order of system size is usually known as in the steady state.

However, as discussed earlier, for growth processes of KPZ universality class, the desorption or surface overhang and bulk vacancies are not negligible even at long wavelength behavior indicating the nonconserved growth process. In fact, in a real growth problem, the process of desorption, overhang, and vacancies formation are inevitable. Hence, in principle, the all epitaxial processes are non-conserved at large-scale and long-time limit [30]. Because of its simple nonlinearity and non-conserved properties, theoretically, the KPZ universality class is considered as a generic growth universality class. On the other hand, it is the matter of fact that the KPZ expo-

nents have hardly observed in any real epitaxial surface growth experiments. There have been few reasons behind this. The formation of desorption, overhangs and vacancies become dynamically insignificant with respect to the experimental time and substrate size. In addition to that epitaxial growth, especially MBE growth processes are performed with a great care and in a very controlled manner to avoid the evaporation, vacancies etc. Mullins and Herring (MH)[133] first proposed a linear conserved equation for surface growth which reads

$$\frac{\partial h(\mathbf{x},t)}{\partial t} = -\nabla \cdot \mathbf{j} + \eta(\mathbf{x},t) \tag{1.8}$$

seeming like equation of continuity where $\mathbf{j} = \nabla\mu(\mathbf{x},t)$ with the chemical potential $\mu(\mathbf{x},t) = \kappa\nabla^2 h(\mathbf{x},t)$. In the above equation, term $\mathbf{j}$ is the deposited mass current which is conserved. In the context of conservation, the KPZ nonlinearity is ruled out.

From this linear equation the exponents values are $\chi = (4-d)/2$ (roughness), $z = 4$ (dynamic) and $\beta = (4-d)/8$ (growth exponent) where d is the substrate dimension. Although in the literature, various experimental measurements have been reported having approximately same exponents values ($\beta \approx 0.25$ and $\chi \approx 0.9-1$ in (2+1) dimensions), subsequently, it has been realized that MH universality class is a crossover instead of asymptotic universality class[30].

Wolf and Villain[202] studied a surface growth model which has the close exponents ($\chi = 1.4 \pm 0.1$ and $z = 3.8 \pm 0.5$) as those of Mullins and Herring equation in $(1+1)$ dimensions. At the same time a random deposition (RD) model is proposed by Das Sarma and Tamborenea[33] to describe the $(1+1)$-dimensional MBE process which is considered as an intermidiate between two extreames RD model with and without relaxation. The estimated exponents in $(1+1)$ dimensions are following $\beta \approx 0.375 \pm 0.005$ and $\chi \approx 1.5$.

Sun, Guo and Grant (SGG)[175] proposed a nonlinear equation for surface growth where the total volume under the interface is conserved including the deposition noise. The equation reads

$$\frac{\partial h(\mathbf{x},t)}{\partial t} = -\nabla^2[\nu_0\nabla^2 h(\mathbf{x},t) + \frac{\lambda_0}{2}(\nabla h)^2] + \zeta(\mathbf{x},t) \tag{1.9}$$

where the noise is conserved and follows $\langle\eta(\mathbf{x},t)\rangle = 0$ and

$$\langle\zeta(\mathbf{x},t)\zeta(\mathbf{x}',t')\rangle = -2D_0\nabla^2\delta^d(\mathbf{x}-\mathbf{x}')\delta(t-t').$$

They obtained a distinct set of exponents given by $\chi = (2-d)/3$ and $z = (10+d)/3$ by applying one-loop dynamic RG. Furthermore, they have carried out an extensive numerical simulation (CRSOS) in one substrate dimension yielding $\chi = 0.35 \pm 0.03$ and $\beta = 0.091 \pm 0.002$ which agree with the one-loop RG results ($\chi = 1/3$ and $\beta = 1/11$) indicating the different universality class from KPZ and EW universality classes.

Subsequently, Villain, Lai and Das Sarma proposed a growth equation to mimic the actual molecular beam epitaxy growth process. The noise due to incoming particle flux is considered to be nonconserved which is the basic difference from the SGG equation. The continuum, conserved, non-linear growth equation for MBE-type growth, is known as conserved KPZ or Villain-Lai-Das Sarma (VLDS) equation which is expressed as

$$\frac{\partial h(\mathbf{x},t)}{\partial t} = -\nu_0 \nabla^4 h(\mathbf{x},t) + \frac{\lambda_0}{2}\nabla^2(\nabla h)^2 + \eta(\mathbf{x},t) \tag{1.10}$$

where h is fluctuating height field, ν_0 is the diffusivity, η is Gaussian white noise, $\langle \eta(\mathbf{x},t)\rangle = 0$ and noise correlation $\langle \eta(\mathbf{x},t)\eta(\mathbf{x}',t')\rangle = 2D_0\delta^d(\mathbf{x}-\mathbf{x}')\delta(t-t')$. Equation (1.10) is translational and rotational invariant whereas it breaks the up-down symmetry ($h \to -h$) due to its nonlinear term. Though one could easily obtain the expression for exponents from the Fourier transformation and rescaling of a linear equation, however, a nonlinear equation deserves different treatment. In a few works[31,111,183], the analytical expressions for exponents ($\chi = (4-d)/3$ and $z = (8+d)/3$) are obtained via one loop RG. Subsequently, same exponents values have been estimated via direct numerical integration[31,95,96,188] of Eq. (1.10) within the numerical accuracy (1-2%) in $(1+1)$ and $(2+1)$ dimensions. The two-loop dynamic RG calculations are carried out by Janseen which leads to very small corrections (less than 1%) to the exponents values each of the dimensions ($(1+1)$ and $(2+1)$)[82]. The VLDS equation has been investigated by Katzav[88] in a different technique closed to mode coupling approach that yields the same exponent values (as one-loop dynamic RG provides).

In real MBE growth, the deposited particles are allowed to diffuse immediately where the process of diffusion and associated processes of equilibrium depend on several factors, such as substrate temperature, the rate of incident flux, the mobility of the deposited atoms. Due to these reasons, it is obvious that the growth process will be far from equilibrium when the incident flux is high enough with respect to the atomic diffusion. In addition to the basic microscopic processes, namely, deposition, desorption, and surface diffusion, there are other effects such as shadowing which

may play an important role in shaping the interface morphology. These type of experiments usually have a lot of parameters under which thin films are grown. There have been two experimental methodology, such as diffraction methods and direct imaging methods to measure the roughness of a thin film. Since our studies are limited only at one spatial dimension, further discussion regarding these experiments are not carried out.

Along with the experiments, variuos numerical models have been introduced to study the nonequilibrium MBE growth process[111,202] It has been customary to determine the universality class of growth model, equations, and experiments via the estimated or calculated values of scaling exponents. There has been other way to characterize the surface morphology along with the scaling exponents. The estimation of moments or cumulants of probability distribution function (PDF) of height fluctuations. The lowest order moment, skewness carries the important information (up-down asymmetry of the surface morphology) of PDF. A vanishing value of skewness indicates symmetric (usually Gaussian) distribution whereas a non-zero value of skewness quantitatively measures the departure of the distribution from the Gaussian distribution. In this context, it should be noted that the height fluctuations described by linear growth dynamics following a Gaussian noise yield Gaussian height distribution function whereas the PDF becomes non-Gaussian associated with the nonlinear growth dynamics because the nonlinear term basically introduce the up-down asymmetry in the dynamics. In the asymptotic limit of the growth process (in the steady state), the non-linear term dominates over the linear term. Sometimes, in experiments and in numerical simulations, it is observed that the measured or estimated exponents are different than that of the VLDS universality class which may indicate a crossover from MH to VLDS universality class. This crossover can be better understood by the study of skewness of the PDF of height fluctuations rather than that of scaling exponents.

There have been few numerical works for (1+1)-dimensional MBE type of growth, devoted to obtain the scaling exponents as well as skewness. Das Sarma *et al.* in ref.[32] considered a minimal kinetic Monte Carlo MBE method where surface overhangs, bulk vacancies, desorption, and overhangs are negligibly small. The diffusion barrier, known as Ehrilich-Schwoebel barrier, near step edge are also neglected in the considered model to understand the dynamics of the growth in a very simple way. In their work, various growth models have been considered, such as Das Sarma and Tambornea (DT), MBE, Lai-Das Sarma (LDS), and among them LDS model yields exponents values ($\chi = 1.03$ and $z = 3.04$) which are close to the exponents values

of one dimensional VLDS equation and consequently indicating VLDS universality class. In addition, they have also studied the skewness of height fluctuations and obtained skewness value $S = -0.1 \pm 0.15$ in $(1 + 1)$ dimensions from the model.

In this thesis, we would, only, focus on the $(1 + 1)$-dimensional VLDS equation and subsequently, the skewness calculation of the probability distribution of height fluctuations. We obtain scaling exponents by implementing a renormalization scheme which agrees with the one-loop RG results of Lai-Das Sarma (LDS) and the estimations of LDS model. In the literature, as far as we know, there have been no other analytical attempts to calculate the skewness of the height fluctuations of PDF which motivated us to obtain the values in this approach. Since the skewness is an important property of a probability distribution function, it is indispensable to calculate its value for the height fluctuations governed by the VLDS dynamics, so that this fluctuations can be distinguished from those governed by other dynamical processes. Besides the scaling exponent, we study the normalized third order cumulant implementing a renormalization scheme at one-loop order by using a diagrammatic method in the large-scale and long-time limits and obtained skewness value is $S = -0.0441$. The obtained value is consistent with the numerical prediction of Das Sarma *et al.* ($S = -0.1 \pm 0.15$) within the numerical accuracy.

1.2 Homogeneous Isotropic Turbulence

In our daily life, we experience the effect of turbulence of fluids in various forms. It is very indispensable to understand the behavior of turbulent fluid due to its omnipresence nature on almost all macroscopic scales starting from the interior of biological cells, to numerous technological devices (in aeronautics, hydraulics, nuclear, mechanical, chemical engineering), to geophysical and astrophysical phenomena (including oceanography, meteorology), and to inter-galactic scales. Nevertheless, the occurrence of turbulent flow is widespread and the full understanding of turbulent flow is still a challenging problem in classical physics. Different engineering studies have been devoted to reduce the difficulties by managing the effect of turbulence. The complexity of the turbulent flow arises due to the mixing of the various spatial degree of freedom of different length scales and time scales. Scientists, engineers get motivated due to its inherent complexity and widespread practical applications.

In real life fluid turbulence, there is a production range at low wave numbers where the turbulent energy is generated. Following the production range, there occurs the innertial range where the turbulent energy cascades from low to high wave

numbers without any viscous dissipation. At high wavenumbers, viscous dissipation becomes important and there exists a dissipation range up to infinitely large wavenumbers. Dissipation of turbulent energy mainly occurred due to the kinematic viscosity of the turbulence in the length scale smaller than the Kolmogorov dissipation scales η, where the viscosity term plays an important role.

Most of the turbulence researchers believed that Navier-Stokes equation embodies the physics of all fluid flows (including the turbulent flows). In fully developed turbulence, the fluctuating field is statistically invariant under translations and rotations leading to be homogeneous and isotropy. These assumptions simplify the mathematical nature of the problem.

There have been various ways to study the Navier-Stokes equations. One of the most tried methods is direct numerical simulation of the Navier-Stokes equation which would be fine only when the considered mesh size is small enough to probe beyond the Kolmogorov length scales. Due to the limitation of computational cost, this approach is usually performed at moderate Reynolds number (R). In turbulent fluid flow, a large number of degree of freedom get excited and increases with Reynolds number $R^{9/4}$ [112]. It can roughly be estimated that to simulate an atmospheric flow covering all length scales (from the forcing length scale which is of the order of thousands of miles and dissipation range which is of the order of millimeters) of turbulence the required number of grid points would be of order 10^{25} which challenges the capabilities of present computers [201].

As the real problem have been to handle a large number of interacting degree of freedom to understand the system. So idea was to reduce the degree of freedom keeping physical properties qualitatively same. There have been a powerful theory of viewing systems at different length scales known as renormalization group. Since we are interested in long wave-length phenomena, fluctuations are integrated out in sequence starting from the smallest scale. Consequently, this approach obtains a coarse grained system as a result of elimination of microscopic fluctuations. Since physics is expected to be scale invariant, renormalization group is a tool to understand the physics of the system with the change of scale. There have been many frameworks, to implement an RG, among them momentum space perturbative formalism are widely used in which diagrammatic approach is followed to get loop diagrams. Effect of averaging out of the high momentum affect the low momentum parameters. The elimination of the short wavelength fluctuations results in an evolving differential equation with respect to the scale and the underlying physics become self-similar with respect to the change of scale. This is how bare parame-

ters of a system get modified to scale dependent parameters where the associated measurable properties can be verified through experiment to validate the theory.

A non-equilibrium physical phenomenon is immensely interesting to understand the process and at the same time extremely difficult to deal with any rigorous manner. In this thesis, relatively simpler studies (moments of a probability distribution of fluctuations at a macroscopic scale) have been investigated by proposing a renormalized perturbation scheme and comparing with existing other theoretical, numerical and experimental work to validate the proposed theory. The concerned phenomena (wherein we are interested) are surface growth fluctuations, and fluid flow turbulence which have been described by nonlinear field equations with a driving noise. These benchmark non-linear equations corresponding to the surface growth phenomena are Kardar-Parisi-Zhang (KPZ), Villian-Lai-Das Sarma (VLDS) and Navier-Stokes equation for turbulent [50,131].

1.3 Methodology

A momentum space RG of continuous decimation has first been introduced by Wilson for equilibrium critical phenomena in classical statistical mechanics [200] Eventually, many researchers successfully applied Wilson's RG approach to a large number of interacting systems and gradually becomes one of the standard tools of the statistical mechanics and condensed matter physics because of the surprisingly good results and agreement with the experiments. One of the areas of its application is stochastic differential equations for surface growth dynamics and turbulent.

Forster, Nelson, and Stephen (FNS), in 1977, applied the dynamic RG, to Navier-Stokes equation coupled with the passive scalar subjected to random driving forces in the paper [47] which is basically adapted procedure of Ma and Mazenko who used the RG to the stochastic dynamical equation of local spin density [118]. After that, implementing the dynamic RG procedure, for randomly stirred model, Kolmogorov scaling has been realized by DeDominicis and Martin [34]. Subsequently, Yakhot and Orszag developed an RG approach without rescaling to obtain several universal numbers and energy scaling considering the DeDominicis and Martin's randomly stirred turbulent model. At the same time, a nonlinear local surface growth equation has been proposed by Kardar, Parisi and Zhang (KPZ) and applied the dynamic RG approach to obtain the scaling exponents of the growth equation.

There have been two steps of the dynamic RG approach of FNS, Ma and Mazenko, and Kardar-Parisi and Zhang. The First step is the elimination of higher modes

from the evolution equation of motion (KPZ, VLDS, Navier-Stokes) which is indeed a coarse-graining process. The process effectively lowers the magnitude of the wave-vector and restricts it to go beyond some spatial scale by downgrading its spatial resolution.

Subsequently, rescaling have been carried out to get back the new equation of motion in the old form with modified system parameters. The application of this process yields differential equation of the parameter with respect to scale. At the fixed point the parameters are invariant under further transformations and the values of critical exponents are obtained. In Chapter-2 of this thesis, we carry out the renormalization group treatment without rescaling for the KPZ equation and obtain its fixed point in $(1+1)$ dimensions.

In 1961, Wyld[205] proposed a systematic perturbation theory for the problem of turbulence in an organized way depicting the mathematical terms by diagrams, analogous to the Feynman diagram of quantum field theory. The diagrams are generated by following a simple set of rules so that the perturbation series can be depicted easily. Wyld's technique has been extended to describe the Hamiltonian nonlinear fields including hydrodynamic turbulence in the Clebsch variables[206]. Moreover, Martin, Siggia, and Rose[123] proposed a different formalism to investigate the classical stochastic differential equations in statistical and condensed matter physics.

Perturbative expansion by diagrammatic approach is a useful and much simpler way than directly dealing with the long complicated mathematical expressions. In this approach, one can systematically generate the corresponding diagram of a perturbative series without missing any term due to the one to one correspondence of the mathematical term and part of a diagram. Hence, diagrams can easily be obtained from the corresponding mathematical expressions, and vice versa.

In this thesis work, we have developed a renormalization scheme by following diagrammatic method for KPZ, VLDS and Navier-Stokes equations to calculate the higher order cumulants of the corresponding distribution functions.

Statistical moments and cumulants

In the past, the surface growth analysis had mostly been based on the estimating the scaling exponents and determining the universality class from those exponents by studying only the second moment of the height fluctuations which is inherently insufficient to determine the universality class of a system.

The study of higher moments is very much interesting as it provides the more

detailed information of the PDF which helps to distinguish the PDF from the Gaussian distribution by quantifying the values of the moments which are also proved as universal quantities in stationary state. The definition of the higher moments or cumulants and the relations between them are presented below.

The generating function for the nth order moment of a random variable h can be defined as

$$Z(\beta) \equiv \langle e^{\beta h} \rangle = \sum_{n=0}^{\infty} \frac{\langle h^n \rangle}{n!} \beta^n \tag{1.11}$$

where

$$\langle h^n \rangle = \int_{-\infty}^{\infty} dh \; h^n P(h) \tag{1.12}$$

is the nth moment for a given normalised probability distribution function $P(h)$ and $n = 0, 1, 2, 3...$

Probability distribution function can also be described by the cumulants, which is alternative to the moments, and the relation between cumulant and moment is well established. In this thesis, we are interested in calculating the higher order cumulants via the diagrammatic (perturbatively) renormalization scheme and in this regard, the calculations of cumulants instead of moments are much simpler because the cumulant terms only provides connected diagramms (without disjoint pieces) instead of many connected as well as disconnected diagramms.

The cumulant generating function $F(\beta)$ is defined as

$$F(\beta) = \ln Z(\beta) = \sum_{n=1}^{\infty} \frac{\langle h^n \rangle_c}{n!} \beta^n. \tag{1.13}$$

where $\langle h^n \rangle_c$ is the nth cumulant. The moments are related to the cumulants as

$$\begin{aligned}
\langle h \rangle &= \langle h \rangle_c \\
\langle h^2 \rangle &= \langle h^2 \rangle_c + \langle h \rangle_c^2 \\
\langle h^3 \rangle &= \langle h^3 \rangle_c + 3\langle h \rangle_c \langle h^2 \rangle_c + \langle h \rangle_c^3 \\
\langle h^4 \rangle &= \langle h^4 \rangle_c + 4\langle h \rangle_c \langle h^3 \rangle_c + 3\langle h^2 \rangle_c^2 + 6\langle h \rangle_c^2 \langle h^2 \rangle_c + \langle h \rangle_c^4 \\
\langle h^5 \rangle &= \langle h^5 \rangle_c + 5\langle h \rangle_c \langle h^4 \rangle_c + 10\langle h^2 \rangle_c \langle h^3 \rangle_c + 10\langle h \rangle_c^2 \langle h^3 \rangle_c \\
&\quad + 15\langle h \rangle_c \langle h^2 \rangle_c^2 + 10\langle h \rangle_c^3 \langle h^2 \rangle_c + \langle h \rangle_c^5.
\end{aligned} \tag{1.14}$$

The fluctuating interface field $h(\mathbf{x}, t)$ has a zero mean. Thus $\langle h(\mathbf{x}, t) \rangle = \langle h(\mathbf{x}, t) \rangle_c =$

0 and hence, the above relations reduces to[108,165]

$$\langle h^2\rangle_c = \langle h^2\rangle, \tag{1.15}$$

$$\langle h^3\rangle_c = \langle h^3\rangle, \tag{1.16}$$

$$\langle h^4\rangle_c = \langle h^4\rangle - 3\langle h^2\rangle^2, \tag{1.17}$$

and

$$\langle h^5\rangle_c = \langle h^5\rangle - 10\langle h^2\rangle\langle h^3\rangle. \tag{1.18}$$

Skewness, S, kurtosis Q and hyperskewness $\widetilde{S}$ are defined as

$$S = \frac{\langle h^3\rangle_c}{\langle h^2\rangle_c^{3/2}} = \frac{\langle h^3\rangle}{\langle h^2\rangle^{3/2}} \tag{1.19}$$

$$Q = \frac{\langle h^4\rangle_c}{\langle h^2\rangle_c^{2}} = \frac{\langle h^4\rangle}{\langle h^2\rangle^{2}} - 3 \tag{1.20}$$

and

$$\widetilde{S} = \frac{\langle h^5\rangle_c}{\langle h^2\rangle_c^{5/2}} = \frac{\langle h^5\rangle}{\langle h^2\rangle^{5/2}} - 10\frac{\langle h^3\rangle}{\langle h^2\rangle^{3/2}}. \tag{1.21}$$

Another definition of nth moment of height distribution (HD) is

$$W_n = \langle [h(\mathbf{x},t) - \bar{h}(t)]^n\rangle \tag{1.22}$$

Since the fluctuating height field has a zero average $\bar{h}(t) = 0$, the definition of moments simplifies to

$$W_n = \langle h^n(\mathbf{x},t)\rangle, \tag{1.23}$$

so that skewness and extra kurtosis is defined as

$$S = \frac{W_3}{W_2^{3/2}},$$

$$Q = \frac{W_4}{W_2^{2}} - 3,$$

and

$$\tilde{S} = \frac{W_5}{W_2^{5/2}} - 10\frac{W_3}{W_2^{3/2}},$$

which are universal[3,165].

The normalised third-cumulant, skewness, measures the asymmetry of the tail from the Gaussian distribution (non-Gaussian), becomes nonzero due to the broken up-down symmetry (as in KPZ equation $h \to -h$) and vanishes where the symmetry is maintained, i.e., the valley bottoms and hill tops are equivalent for a Gaussian surface. The fourth moment kurtosis or flatness, Q, measures the sharpness or peakedness of the distribution function from the Gaussian. The value of the kurtosis $Q = 3$ for Gaussian distribution and higher (lower) value of Q describes sharper (flatter) distribution than the Gaussian.

A. Layout of the Thesis

The thesis is organized as follows.
In **Chapter 2** of the thesis, we use the $(1+1)$-dimensional KPZ equation driven by a Gaussian white noise by employing a perturbative renormalization scheme. Hence, we calculate the second- and third-order cumulants of height distribution using the diagrammatic method in the large-scale and long-time limits. The cumulants so calculated lead to the value $S = 0.3237$ for skewness which is independent of model parameters D_0, ν_0, λ_0, and system size L due to their exact cancellations. This value is comparable with numerical and experimental estimates.

In **Chapter 3** of the thesis, we study the fourth order normalized cumulant of height fluctuations governed by $(1+1)$ dimensional KPZ equation for a growing surface. Following a diagrammatic renormalization scheme, we evaluate the kurtosis Q from the connected diagrams leading to the value $Q = 0.1523$ in the large-scale long-time limit which is free from the system size L and model parameters D_0, ν_0, and λ_0, due to their exact cancellations.

In **Chapter 4** of the thesis, we evaluate hyperskewness of height fluctuations dictated by the $(1+1)$-dimensional KPZ equation for the stochastic growth of a surface on a flat geometry in the stationary state by following a diagrammatic approach and invoking a renormalization scheme. We calculate the fifth cumulant given by a connected loop diagram. This, together with the result for the second cumulant, leads to the hyperskewness value $\tilde{S} = 0.0835$.

In **Chapter 5** of the thesis, we consider the statistical cumulants of height fluctuations governed by the $(2+1)$-dimensional KPZ equation for flat geometry. We follow a diagrammatic scheme to derive the expressions for renormalized cumulants up to fourth order in the stationary state. Assuming a value for the roughness

exponent from reliable numerical predictions, we calculate the second, third and fourth cumulants, yielding skewness $S = 0.2879$ and kurtosis $Q = 0.1995$. These values agree well with the available numerical estimations.

In **Chapter 6** of the thesis, we study the $(1 + 1)$-dimensional Villain, Lai, and Das Sarma (VLDS) equation driven by a Gaussian white noise and implement a renormalization scheme without rescaling at one-loop order. Using a diagrammatic method, we calculate the renormalized second and third moments in the large-scale and long-time limits. The ensuing skewness value is $S = -0.0441$. This (negative) value is consistent with the numerical prediction of Das Sarma *et al.*[32].

In **Chapter 7** of the thesis, we apply a renormalized perturbative scheme on the Navier-Stokes equation for an incompressible isotropic turbulent velocity field. This allows us to obtain the renormalized expressions for second- and third-order cumulants of the velocity derivative directly from the corresponding Feynman diagrams. The resulting expressions are integrated numerically by excluding and including the dissipation range assuming Kolmogorov and Pao's phenomenological expressions for the energy spectrum. The ensuing values for skewness are found to be $S = -0.647$ (when the dissipation range is excluded) and $\mathcal{S} = -0.682$ (when the dissipation is included). These estimated values are compared with various experimental, numerical and theoretical results.

Chapter 2

Skewness of KPZ-type height fluctuation in $(1+1)$ dimensions

2.1 Introduction

The study of surface growth has been one of the most important problems in non-equilibrium statistical physics over the past few decades[11,43,63,105,126]. The most generic continuum model of surface growth is the Kardar-Parisi-Zhang (KPZ) equation that is endowed with interesting properties of statistical scale invariance. Kardar, Parisi and Zhang[86] suggested a nonlinear differential equation for local surface growth in the form

$$\frac{\partial h(\mathbf{x},t)}{\partial t} = \nu_0 \nabla^2 h + \frac{\lambda_0}{2}(\nabla h)^2 + \eta(\mathbf{x},t), \tag{2.1}$$

where $h(\mathbf{x},t)$ is the height of the surface at position $\mathbf{x}$ and time t on a d dimensional substrate, ν_0 is the surface tension that has a tendency to make the surface smooth, and the coupling constant λ_0 measures the strength of the nonlinear interaction term. The nonlinear term induces local growth along the normal to the surface and gives rise to lateral correlations. On the other hand, the linear term (containing ν_0) is responsible for diffusion of particles to the local minima[111]. The driving term $\eta(\mathbf{x},t)$, describing the random deposition of particles, is assumed to obey a Gaussian distribution to account for the stochastic nature of the flux of particles. It is taken to be a Gaussian white noise with zero mean, $\langle \eta(\mathbf{x},t) \rangle = 0$, and with correlation

$$\langle \eta(\mathbf{x},t)\, \eta(\mathbf{x}',t') \rangle = 2D_0\, \delta^d(\mathbf{x}-\mathbf{x}')\, \delta(t-t'), \tag{2.2}$$

where D_0 is a constant and the angular brackets denote ensemble averages.

There are many deposition models that have been identified with the KPZ universality class. A few examples are the ballistic deposition[43,127], the Eden model[84,151,152], the restricted solid-on-solid (RSOS) model[126], and the single step model (SSM)[127,150]. A large number of growth experiments show scaling exponents close to those of the KPZ growth problem. A few important phenomena are thin film growth[11], bacterial colony growth[84,191], growth of fractals[42], turbulent liquid crystal (TLC) growth[178,179], and one dimensional polynuclear growth (PNG)[54,106,153,190], etc. Apart from such growth models, the KPZ problem is related to various other processes such as the noisy Burgers equation[47], flame front propagation[110,167], directed polymer in random media[45,63,86,87,94], interface roughening due to impurities[73,74], and growing interfaces in randomly stirred fluids[91]. A great amount of work has been carried out, mostly via numerical and experimental studies, in various KPZ type surface growth problems. The interplay of non-linearity, surface tension, and uncorrelated noise in such problems establish a universality class distinct from that of the Edward-Wilkinson type growth in the large-scale long-time limit. The mean-square of the height fluctuations is related to the critical exponents[128] as

$$\langle [h(\mathbf{x},t) - h(\mathbf{x}',t')]^2 \rangle \sim |\mathbf{x}-\mathbf{x}'|^{2\chi}\ \psi\left(\frac{|t-t'|}{|\mathbf{x}-\mathbf{x}'|^z}\right), \tag{2.3}$$

where χ is the roughness exponent describing the self-affine geometry of the surface, z is the dynamic exponent (the ratio $\frac{\chi}{z} = \beta$ is the growth exponent), and $\psi(\cdot)$ is a scaling function. The roughness exponent χ is an important parameter[10] in the studies of adsorption, catalysis[148], and optical properties[132] of a thin film. The properties of a rough surface are determined by the distribution of height fluctuations and it deserves attention both in theoretical and experimental studies of growing interfaces[126].

Various analytical approaches have been employed to study the universality class of the KPZ equation on the basis of scaling exponents in different dimensions. The dynamic renormalization-group by Kardar, Parisi, and Zhang[86] leads to the values of roughness exponent $\chi = \frac{1}{2}$ and dynamic exponent $z = \frac{3}{2}$ at one-loop order for the $(1+1)$ dimensional KPZ equation. Motivations in the theoretical study of the KPZ equation in higher dimensions have led to formulations of different analytical techniques. Examples of such theoretical studies are the mode coupling scheme[28,76,189], the operator product expansion[113], the self-consistent expansion[163] and a nonper-

turbative renormalization group[22,100] for the calculation of scaling exponents in the strong coupling regime.

These exponents have also been computed numerically considering different growth rules. Apart from the numerical studies, many experiments have been carried out to find these exponents. Various experimental studies[71,72,179] have indicated that the roughness exponent is about 0.50 and the growth exponent 0.33 which have been identified with the universality class of the $(1+1)$ dimensional KPZ type surface growth.

Besides the critical exponents, the probability distribution function is an important feature to classify the universality of a physical process[94]. In experiments, measurements of normalized moments is expected to be more accurate than the measurement of scaling exponents[126]. Thus higher order moments can infer about the universality class in a better way than the critical exponents[2]. Consequently, higher order moments are very important in the study of surface morphology and the universality class can be better realized through the values of higher order moments and a parameter such as skewness.

The skewness has been computed numerically employing a variety of deposition algorithms. Krug *et al.* [108], using the simulation in a single step model for flat initial condition, obtained $|S| = 0.28 \pm 0.04$ in the transient regime. Following the same model, they prepared stationary interfaces by taking uncorrelated spins ($\sigma_i = \pm 1$) and obtained $|S| \approx 0.33$. Prähofer and Spohn[153] took the polynuclear growth model and mapped it into a random permutation through the droplet geometry thereby onto Gaussian random matrices to understand the dependence of the initial conditions on height fluctuations. They inferred that the droplet and flat substrates have the same scaling form but distinct universal distributions. They estimated the skewness for three different shapes, namely, curved, flat, and stationary self-similar in $(1+1)$ dimensions. For the flat shape, they obtained $S = 0.2935$, for the curved shape, $S = 0.2241$, and for the stationary self-similar case, $S = 0.35941$. They proposed an expression for the height distribution, namely $h(\mathbf{x},t) \simeq v_\infty t + (\Gamma t)^{1/3}\zeta$ with ζ a random variable, where $\Gamma = \frac{D_0^2\lambda_0}{8\nu_0^2}$ is a model parameter and v_∞ is the growth rate in the asymptotic limit[178]. It was found that ζ obeys the Tracy-Widom (TW) distribution corresponding to the largest eigenvalues of random matrices[179]. For curved interfaces the random matrices form a Gaussian unitary ensemble (GUE)[162] whereas for flat interfaces they form a Gaussian orthogonal ensemble (GOE).

In an experiment on growing interfaces in liquid crystal turbulence, Takeuchi *et al.*[178,179] found that the growth and roughness exponents are the same as those of

the KPZ type growth in one dimension in the asymptotic limit. Their experimental data indicated the value for skewness $S \simeq 0.29$ for a flat interface, whereas for a curved interface their experimental data converged to $S = 0.2241$. They concluded that the probability distribution function (pdf) of interface fluctuations precisely agrees with the GOE of TW distribution for the flat interface, whereas the curved interface fluctuations agree with the GUE of TW distribution, up to fourth order cumulants. Sasamoto and Spohn[161,162] solved the $(1+1)$ dimensional KPZ problem with an initial condition of curved-height profile and showed that the pdf follows the GUE of TW distribution of random matrices.

It may be noted that there have been very few analytical evaluations of the skewness and higher order moments for the KPZ type growth problem. The one known to the authors is a mean field calculation yielding $S = \pm 0.46$ in $(1+1)$ dimensions[53] with the flat initial condition $h(x,0) = 0$ for the transient regime.

In this work, we are interested in the KPZ growth problem for a flat interface and seek to calculate the skewness of height fluctuations in the stationary state. Consequently, we apply the dynamic renormalization group scheme without rescaling to the KPZ equation. This scheme was previously employed by Yakhot and Orszag[208] to calculate various universal numbers in the case of hydrodynamic turbulence. This scheme enables us to obtain the expressions for $\nu(r)$ and $D(r)$ and thereby we calculate the second and third order moments of height fluctuations in a straightforward manner. The ensuing result for skewness is compared with the findings of various numerical, experimental, and theoretical studies in Table 2.1 of the present Chapter.

This Chapter is organized as follows. In Section 2, the renormalizaiton-group scheme without rescaling is applied to the KPZ problem. Section 3 outlines the definition of statistical moments of height fluctuations and presents calculations of the second and third order statistical moments. Finally, Section 4 presents a discussion and conclusion and a comparison with other findings.

2.2 Renormalization Scheme without Rescaling

The nonlinear dynamics described by the KPZ equation (5.1) incorporates interaction among many degrees of freedom[128]. The complexity of such interactions among the collective set of height fluctuations is most easily seen when we Fourier transform the height fluctuations $h(\mathbf{x},t)$ and the driving field $\eta(\mathbf{x},t)$. The Fourier space is also suitable for employing the dynamic renormalization-group techniques[66]. The

Fourier transform of the height fluctuations $h(\mathbf{x},t)$ is expressed as

$$h(\mathbf{x},t) = \int \frac{d^d k\, d\omega}{(2\pi)^{d+1}}\, h(\mathbf{k},\omega)\, e^{i(\mathbf{k}\cdot\mathbf{x}-\omega t)}, \tag{2.4}$$

where d is the substrate dimension. The stochastic noise $\eta(\mathbf{x},t)$ is also Fourier transformed in a similar manner. The Fourier amplitude of the noise fluctuations has a zero mean, $\langle\eta(\mathbf{k},\omega)\rangle = 0$, and the noise-correlation can be expressed as

$$\langle\eta(\mathbf{k},\omega)\,\eta(\mathbf{k}',\omega')\rangle = 2D_0\,(2\pi)^d\delta^d(\mathbf{k}+\mathbf{k}')\,2\pi\delta(\omega+\omega'), \tag{2.5}$$

in the Fourier space, as a consequence of Eq. 2.2. Using Eq. (2.4), the Fourier transform of the KPZ equation [Eq. (5.1)] is obtained as

$$(-i\omega+\nu_0 k^2)\,h(\mathbf{k},\omega) = \eta(\mathbf{k},\omega) - \frac{\lambda_0}{2}\iint \frac{d^d q\, d\Omega}{(2\pi)^{d+1}}\,[\mathbf{q}\cdot(\mathbf{k}-\mathbf{q})]\,h(\mathbf{q},\Omega)\,h(\mathbf{k}-\mathbf{q},\omega-\Omega). \tag{2.6}$$

which is in a form particularly useful for implementing the renormalization-group scheme.

A. Scale Elimination

To implement the renormalization-group scheme, we eliminate height fluctuations $h^>(\mathbf{q},\Omega)$ belonging to the shell $\Lambda_0 e^{-r} \le q \le \Lambda_0$ in the wavevector space by substituting for $h^>(\mathbf{q},\Omega)$ in the equation for $h^<(\mathbf{k},\omega)$ following from Eq. (5.6). This process generates a perturbation series in powers of the coupling constant λ_0. Considering terms up to second order in λ_0 yields the equation

$$\begin{aligned}[-i\omega+\nu_0 k^2+\Sigma(\mathbf{k},\omega)]\,h^<(\mathbf{k},\omega) &= \eta^<(\mathbf{k},\omega)\\ -\frac{\lambda_0}{2}\iint \frac{d^d q\, d\Omega}{(2\pi)^{d+1}}\,&[\mathbf{q}\cdot(\mathbf{k}-\mathbf{q})]\,h^<(\mathbf{q},\Omega)\,h^<(\mathbf{k}-\mathbf{q},\omega-\Omega).\end{aligned} \tag{2.7}$$

in the range $0 \le k \le \Lambda_0 e^{-r}$ in the wavevector space, where $\Sigma(\mathbf{k},\omega)$ is the self energy correction represented by the amputated part of the Feynman diagram shown in Fig. 2.1.

Figure 2.1: Self-energy correction. The self-energy $\Sigma(\mathbf{k},\omega)$ corresponds to the loop. Propagators are indicated by arrowed lines and correlation by a wiggly line.

The corresponding loop integral is given by

$$\Sigma(\mathbf{k},\omega) = 4\left(-\frac{\lambda_0}{2}\right)^2 \int \frac{d^dq}{(2\pi)^d}\,(\mathbf{k}\cdot\mathbf{q})\,[\mathbf{q}\cdot(\mathbf{k}-\mathbf{q})] \int_{-\infty}^{\infty}\frac{d\Omega}{2\pi}\,|G_0^>(\hat{q})|^2\,(2D_0)\,G_0^>(\hat{k}-\hat{q}), \tag{2.8}$$

where $G_0(\hat{k}) \equiv G_0(\mathbf{k},\omega) = [-i\omega+\nu_0 k^2]^{-1}$ is the bare propagator and the prefactor 4 is a combinatorial factor. Following Refs.[128,208], we symmetrize the internal momenta by taking the transformation $\mathbf{q} \to (\mathbf{q}+\mathbf{k}/2)$. Performing the frequency convolution and evaluating the integral over the internal momenta in the shell $\Lambda_0 e^{-r} \le q \le \Lambda_0$ yields the self energy

$$\Sigma(k,0) = \frac{\lambda_0^2 D_0}{2\nu_0^2\Lambda_0^{2-d}}\frac{S_d}{(2\pi)^d}\left(\frac{2-d}{2d}\right)\frac{e^{(2-d)r}-1}{2-d}\,k^2 \tag{2.9}$$

in the large scale ($k \to 0$) and long time ($\omega \to 0$) limits, where $S_d = \frac{2\pi^{d/2}}{\Gamma(d/2)}$ is the surface area of a sphere of unit radius embedded in a d dimensional space. As a result of the above elimination, the effective surface tension is obtained as

$$\nu^<(r) = \nu_0\left[1+\frac{1}{4}K_d\frac{\lambda_0^2 D_0}{\nu_0^3\Lambda_0^{2-d}}\frac{e^{(2-d)r}-1}{d}\right], \tag{2.10}$$

where $K_d = \frac{S_d}{(2\pi)^d}$ and the second term in the parentheses comes from the self energy correction.

The height-height correlation is also expanded in a perturbative series in a similar manner. This gives rise to a correction to the noise amplitude, given by

$$2D^<(r) = 2D_0 + 2\left(\frac{-\lambda_0}{2}\right)^2 \int \frac{d^dq}{(2\pi)^d}\,[\mathbf{q}\cdot(\mathbf{k}-\mathbf{q})]^2 \int_{-\infty}^{\infty}\frac{d\Omega}{2\pi}\,|G_0^>(\hat{q})|^2\,(2D_0)^2\,|G_0^>(\hat{k}-\hat{q})|^2, \tag{2.11}$$

where $D^<(r)$ is the effective amplitude of noise correlation, whereas D_0 is the bare parameter appearing in the noise correlation in Eq. (2.5). The corresponding equation is shown diagrammatically in Fig. 2.2.

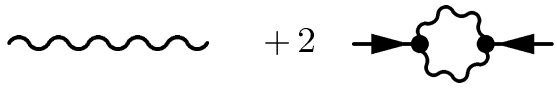

Figure 2.2: Perturbation expansion of the correlation $Q(\mathbf{k},\omega)$ at one-loop order.

Calculating the loop integral in the large scale and long time limits, $k \to 0$ and $\omega \to 0$, the correction to the noise amplitude is obtained as

$$\Delta D = D_0 \frac{\lambda_0^2 D_0^2}{4\nu_0^3 \Lambda_0^{2-d}} \frac{S_d}{(2\pi)^d} \frac{e^{(2-d)r} - 1}{2-d}. \tag{2.12}$$

Thus the effective amplitude of the noise correlation is given by

$$D^<(r) = D_0 \left[1 + \frac{1}{4} K_d \frac{\lambda_0^2 D_0}{\nu_0^3 \Lambda_0^{2-d}} \frac{e^{(2-d)r} - 1}{2-d} \right]. \tag{2.13}$$

We observe that the surface tension ν_0 and noise amplitude D_0 acquire corrections due to the elimination of small scales belonging to the high-momentum shell $\Lambda_0 e^{-r} \leq k \leq \Lambda_0$.

B. Flow Equations and Fixed Point

To implement the renormalization scheme, we shall follow a procedure suggested by Yakhot and Orszag[207,208] where the renormalized parameters are not rescaled after the above scale elimination operation. A particular advantage with this scheme is that the flow equations for the renormalized parameters are obtained directly with respect to the elimination parameter r. Implementing this scheme, we obtain, from Eqs. 2.10 and 2.13, the flow equations for the renormalized surface tension $\nu(r)$ and renormalized noise amplitude $D(r)$ as the differential equations

$$\frac{d\nu}{dr} = \frac{1}{4} K_d \left(\frac{2-d}{d} \right) \frac{\lambda_0^2 D(r)}{\nu^2(r) \Lambda^{2-d}(r)} \tag{2.14}$$

and

$$\frac{dD}{dr} = \frac{1}{4} K_d \frac{\lambda_0^2 D^2(r)}{\nu^3(r) \Lambda^{2-d}(r)}, \tag{2.15}$$

where $\Lambda(r) = \Lambda_0 e^{-r}$. In this scheme, there is no flow equation for the coupling constant λ_0 as it does not acquire any correction due to Galilean invariance. In

order to find the fixed point, we define an effective coupling, $g(r)$, as

$$g(r) = K_d \frac{\lambda_0^2 D(r)}{\nu^3(r)\Lambda^{2-d}(r)}. \tag{2.16}$$

Using Eqs. 6.22 and 2.15, the flow equation for this effective coupling is obtained as

$$\frac{dg}{dr} = a\, g(r) - b\, g^2(r), \tag{2.17}$$

where $a = 2-d$, and $b = \frac{3-2d}{2d}$. Integrating this equation, we obtain an r-dependent expression for the effective coupling, given by

$$g(r) = \frac{g_0 e^{ar}}{1 + \frac{b}{a} g_0 (e^{ar} - 1)}, \tag{2.18}$$

where $g_0 = g(0) = K_d \frac{\lambda_0^2 D_0}{\nu_0^3 \Lambda_0^{2-d}}$. The fixed point value g^* is obtained in the limit $r \to \infty$. For $d \leq 2$, we get

$$g^* = \frac{a}{b} = \frac{2d(2-d)}{(3-2d)}. \tag{2.19}$$

We see that the fixed point value g^* diverges for the substrate dimension $d = 1.5$ and it is finite and positive in the range $0 \leq d < 1.5$. However, in the range $1.5 < d < 2$, the coupling constant is finite but negative, and it vanishes at $d = 2$. These fixed point values are consistent with Frey and Täuber's one-loop calculation[48] (Cf. Eq. (3.18)). In this paper, we are interested in the substrate dimension $d = 1$; thus the effective coupling constant approaches the fixed point value $g^* = 2$.

Using Eqs. (2.16) and (2.18), the differential equations (6.22) and (2.15) yield the exact solutions

$$\nu(r) = \nu_0 \left[1 + \frac{b g_0}{a}(e^{ar} - 1)\right]^{a/4bd} \tag{2.20}$$

and

$$D(r) = D_0 \left[1 + \frac{b g_0}{a}(e^{ar} - 1)\right]^{1/4b}. \tag{2.21}$$

For very large r, the above solutions lead to the asymptotic expressions

$$\nu(r) \simeq \nu_0 \left(\frac{b g_0}{a} e^{ar}\right)^{a/4bd} \tag{2.22}$$

and

$$D(r) \simeq D_0 \left(\frac{b g_0}{a} e^{ar}\right)^{1/4b}. \tag{2.23}$$

in the large scale limit. Noting that $a = 1$ and $b = \frac{1}{2}$ for our case $d = 1$, these expressions for surface tension and noise amplitude reduce to

$$\nu(r) \simeq \nu_0 \sqrt{\frac{g_0}{2}} e^{r/2} \tag{2.24}$$

and

$$D(r) \simeq D_0 \sqrt{\frac{g_0}{2}} e^{r/2}. \tag{2.25}$$

These asymptotic expressions, for very large r, correspond to the renormalized surface tension

$$\nu(k) \simeq \nu_0 \sqrt{\frac{\lambda_0^2 D_0}{2\pi\nu_0^3}}\, k^{-1/2} \tag{2.26}$$

and renormalized noise amplitude

$$D(k) \simeq D_0 \sqrt{\frac{\lambda_0^2 D_0}{2\pi\nu_0^3}}\, k^{-1/2} \tag{2.27}$$

in the large scale long time limit.

The dynamic exponent z can be defined via the renormalized response function as

$$G^{-1}(\mathbf{k}, \omega) = \left[-i\omega + \nu(k)k^2\right]^{-1} \propto k^z\, \phi\left(\frac{\omega}{k^z}\right), \tag{2.28}$$

suggesting the scaling $\nu(k)k^2 \sim k^z$. This leads to the dynamic exponent $z = \frac{3}{2}$ and roughness exponent $\chi = \frac{1}{2}$, the latter being a consequence of the scaling relation $\chi + z = 2$.

2.3 Statistical Moments and Skewness

The nth moment of the height fluctuations is defined as

$$W_n = \langle [h(\mathbf{x}, t) - \bar{h}(t)]^n \rangle. \tag{2.29}$$

These moments obey power laws in the stationary state and they scale as $W_n \sim L^{n\chi}$, where L is the size of the substrate.

The statistical measure corresponding to the (square of) interface width (or standard deviation) is given by the second moment

$$W_2 = \langle h^2(\mathbf{x}, t) \rangle - \langle h(\mathbf{x}, t) \rangle^2. \tag{2.30}$$

The skewness is related to the third moment

$$W_3 = \langle h^3(\mathbf{x},t)\rangle - 3\langle h^2(\mathbf{x},t)\rangle\langle h(\mathbf{x},t)\rangle + 2\langle h(\mathbf{x},t)\rangle^3. \tag{2.31}$$

In this paper, we calculate the skewness S of surface height fluctuations in the KPZ surface growth model. It is defined as

$$S = \frac{W_3}{(W_2)^{3/2}}. \tag{2.32}$$

We present the calculations of the moments W_2 and W_3 in the following subsections.

A. The Second Moment

The second moment is expressed in the Fourier space as

$$\langle h^2(\mathbf{x},t)\rangle = \int \frac{d^dk\,d\omega}{(2\pi)^{d+1}} \int \frac{d^dk'\,d\omega'}{(2\pi)^{d+1}} \langle h(\mathbf{k},\omega)\,h(\mathbf{k}',\omega')\rangle\; e^{i(\mathbf{k}+\mathbf{k}')\cdot\mathbf{x}}\; e^{-i(\omega+\omega')t}. \tag{2.33}$$

We shall assume the growth process to be statistically homogeneous in space and stationary in time. This assumption yields the form

$$\langle h(\mathbf{k},\omega)\,h(\mathbf{k}',\omega')\rangle = Q(\mathbf{k},\omega)\,(2\pi)^d\,\delta^d(\mathbf{k}+\mathbf{k}')\,2\pi\,\delta(\omega+\omega') \tag{2.34}$$

From Eq. (5.6), we see that $\langle h(\mathbf{k},\omega)\rangle = 0$ for any $\mathbf{k} \neq 0$, implying $\langle h(\mathbf{x},t)\rangle = 0$ for all practical purposes. Thus from Eqs. 6.27, 6.35, and 2.34, we obtain

$$W_2 = \langle h^2(\mathbf{x},t)\rangle = \int \frac{d^dk\,d\omega}{(2\pi)^{d+1}}\; Q(\mathbf{k},\omega) \tag{2.35}$$

We write the integrand in terms of renormalized quantities as

$$W_2 = \int \frac{d^dk\,d\omega}{(2\pi)^{d+1}}\; G(\mathbf{k},\omega)\,L_2(\mathbf{k},\omega)\,G(-\mathbf{k},-\omega) \tag{2.36}$$

We first consider the bare value

$$L_2^{(0)}(\mathbf{k},\omega) = 2D_0 + 2\left(\frac{-\lambda_0}{2}\right)^2 \int \frac{d^dq\,d\Omega}{(2\pi)^{d+1}}\; [\mathbf{q}\cdot(\mathbf{k}-\mathbf{q})]^2 |G_0(\mathbf{q},\Omega)|^2\; |G_0(\mathbf{k}-\mathbf{q},\omega-\Omega)|^2\,(2D_0)^2 \tag{2.37}$$

where the propagators are unrenormalized.

We evaluate the second term in Eq. 2.37 which corresponds to the amputated

part of the loop diagram in Fig. 2.2. Performing the integrations over the internal frequency and internal momentum in the shell $\Lambda_0 e^{-r} \leq q \leq \Lambda_0$, we obtain

$$L_2^{<}(r) = 2D_0 + K_d \frac{\lambda_0^2 D_0^2}{2\nu_0^3 \Lambda_0^{2-d}} \frac{e^{(2-d)r} - 1}{2-d}, \tag{2.38}$$

Following Yakhot and Orszag's procedure of renormalization, we make the assumption that thin shells in momentum space are eliminated recursively in iterative steps. This leads to a differential equation for $L_2(r)$,

$$\frac{dL_2}{dr} = \frac{1}{2\pi} \frac{\lambda_0^2 D^2(r)}{\nu^3(r)\,\Lambda(r)}, \tag{2.39}$$

representing the evolution of $L_2(r)$ with respect to the recursive steps of the shell elimination scheme. Using Eqs. 2.24 and 2.25, and integrating over r, Eq. 2.39 yields

$$L_2(r) = D_0 \sqrt{\frac{2\lambda_0^2 D_0}{\pi \nu_0^3 \Lambda_0}}\, e^{r/2} \tag{2.40}$$

for $d = 1$, in the asymptotic limit of large r. We transform this expression into a wavenumber and frequency dependent expression identifying $\Lambda_0 e^{-r}$ as $k f(\frac{\omega}{k^z})$ where z is the dynamic exponent and $f(\cdot)$ is a dimensionless scaling function. Thus, we obtain the renormalized function corresponding to Eq. 6.39 as

$$L_2(\mathbf{k}, \omega) = D_0 \sqrt{\frac{2\lambda_0^2 D_0}{\pi \nu_0^3}}\; k^{-1/2} f^{-1/2} \left(\frac{\omega}{k^z}\right). \tag{2.41}$$

We identify the scaling function by considering consistency in the $\omega \to 0$ limit, so that

$$k\, f\left(\frac{\omega}{k^z}\right) = \frac{1}{k^3\, \nu^2(k)\, |G(\mathbf{k}, \omega)|^2} \tag{2.42}$$

where the modulus of the response function $G(\mathbf{k}, \omega)$ signifies further consistency with the fact that $\Lambda_0 e^{-r}$ is a real quantity. Thus the renormalized quantity $L_2(\mathbf{k}, \omega)$ is expressed as

$$L_2(\mathbf{k}, \omega) = \frac{\lambda_0^2 D_0^2}{\pi \nu_0^2}\, k\, |G(\mathbf{k}, \omega)|. \tag{2.43}$$

We notice that the first diagram in Fig. 2.2 does not contribute to L_2 and the contribution comes solely from the loop diagram.

Substituting the expression 3.40 in Eq. 2.36 and treating the propagators as renormalized given by Eq. 2.28, with the renormalized surface tension $\nu(k)$ coming

from Eq. 2.26, we obtain the contribution to the second moment as

$$W_2 = \frac{\lambda_0^2 D_0^2}{\pi \nu_0^2} \int \frac{d^d k}{(2\pi)^d}\; k \int_{-\infty}^{+\infty} \frac{d\omega}{2\pi} \left[\frac{1}{\omega^2 + \nu^2(k)\, k^4}\right]^{3/2} \tag{2.44}$$

Performing the frequency integration using

$$\int_{-\infty}^{+\infty} \frac{d\omega}{(\omega^2 + m^2)^\alpha} = \frac{\sqrt{\pi}}{(m^2)^{\alpha - 1/2}} \frac{\Gamma(\alpha - \frac{1}{2})}{\Gamma(\alpha)} \tag{2.45}$$

and carrying out the momentum integration in Eq. 2.44, we obtain

$$W_2 = \frac{4}{\pi} \left(\frac{D_0}{2\pi\nu_0}\right) \frac{1}{\mu} \tag{2.46}$$

where μ is an infrared cutoff in the momentum integration.

B. The Third Moment and Skewness

The third moment $\langle h^3(\mathbf{x}, t)\rangle$ can be expressed in the Fourier space as

$$W_3 = \langle h^3(\mathbf{x}, t)\rangle = \int \frac{d^d k\, d\omega}{(2\pi)^{d+1}} \int \frac{d^d k'\, d\omega'}{(2\pi)^{d+1}} \int \frac{d^d k''\, d\omega''}{(2\pi)^{d+1}}$$
$$\langle h(\mathbf{k}, \omega)\, h(\mathbf{k}', \omega')\, h(\mathbf{k}'', \omega'')\rangle\; e^{i(\mathbf{k}+\mathbf{k}'+\mathbf{k}'')\cdot\mathbf{x}}\, e^{-i(\omega+\omega'+\omega'')t} \tag{2.47}$$

Contribution to W_3 comes from the one-loop diagram shown in Fig. 2.3. Thus W_3 can be written in terms of the one-loop contribution $L_3(\hat{k}, \hat{k}')$ as

$$W_3 = \int \frac{d^{d+1}\hat{k}}{(2\pi)^{d+1}} \int \frac{d^{d+1}\hat{k}'}{(2\pi)^{d+1}}\, G(\hat{k})\, G(\hat{k}')\, L_3(\hat{k}; \hat{k}')\, G(-\hat{k} - \hat{k}') \tag{2.48}$$

where $\hat{k}$ stands for $(\mathbf{k}, \omega)$ and $\hat{k}'$ for $(\mathbf{k}', \omega')$.

We first consider the bare value of the loop integral. Integrating over ω'', the bare loop integral can be written as

$$L_3^{(0)}(\mathbf{k}, \omega; \mathbf{k}', \omega') = 8 \left(\frac{-\lambda_0}{2}\right)^3 \int \frac{d^d q\, d\Omega}{(2\pi)^{d+1}}\; [(\mathbf{q} - \mathbf{k}) \cdot (\mathbf{k}' + \mathbf{k} - \mathbf{q})]\, [\mathbf{q} \cdot (\mathbf{k} - \mathbf{q})]$$
$$[-\mathbf{q} \cdot (\mathbf{q} - \mathbf{k}' - \mathbf{k})]\, Q_0(\mathbf{q}, \Omega)\, Q_0(\mathbf{k} - \mathbf{q}, \omega - \Omega)\, Q_0(\mathbf{k} + \mathbf{k}' - \mathbf{q}, \omega + \omega' - \Omega) \tag{2.49}$$

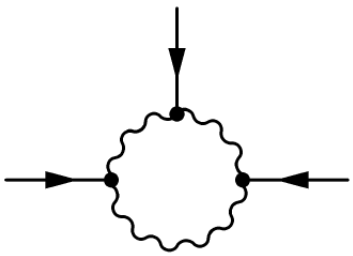

Figure 2.3: The third-order moment.

Carrying out the frequency convolution in Eq. 5.9, we extract the leading order contribution from this integral in the large scale and long time limits, namely the limits $k \to 0$, $k' \to 0$, $\omega \to 0$, $\omega' \to 0$ for the external momenta and frequencies. Working out the momentum integration in the high-momentum shell $\Lambda_0 e^{-r} \leq q \leq \Lambda_0$, we obtain

$$L_3^<(r) = \frac{3}{2} K_d \frac{\lambda_0^3 D_0^3}{\nu_0^5 \Lambda_0^{4-d}} \frac{e^{(4-d)r} - 1}{4-d}. \tag{2.50}$$

As before, we consider the iterative nature of the shell elimination scheme in thin shells in the momentum space, and obtain the flow of $L_3(r)$ in the form of a differential equation

$$\frac{dL_3}{dr} = \frac{3}{2\pi} \frac{\lambda_0^3 D^3(r)}{\nu^5(r)} \frac{1}{\Lambda^3(r)} \tag{2.51}$$

for $d = 1$. The functions $\nu(r)$ and $D(r)$ being known from Eqs. 2.24 and 2.25, the differential equation is solved to obtain

$$L_3(r) = \frac{3}{2} \frac{\lambda_0 D_0^2}{\nu_0^2 \Lambda_0^2} e^{2r} \tag{2.52}$$

in the asymptotic limit of large r.

The corresponding renormalized function $L_3(\hat{k}; \hat{k}')$, being symmetric with respect to interchange of $\hat{k}$ and $\hat{k}'$, its frequency dependent expression can be obtained by replacing $(\Lambda_0 e^{-r})^{-2}$ with the expression

$$k^{-1} k'^{-1} f^{-1}\left(\frac{\omega}{k^z}\right) f^{-1}\left(\frac{\omega'}{k'^z}\right). \tag{2.53}$$

Employing Eq. 2.42 in 2.52, we thus obtain

$$L_3(\mathbf{k},\omega;\mathbf{k}',\omega') = \frac{3}{8\pi^2}\frac{\lambda_0^5 D_0^4}{\nu_0^4}\; k^2\, k'^2\, |G(\mathbf{k},\omega)|^2\; |G(\mathbf{k}',\omega')|^2. \tag{2.54}$$

Using this expression in Eq. 5.8, the third moment is obtained as

$$W_3 = \frac{3}{8\pi^2}\frac{\lambda_0^5 D_0^4}{\nu_0^4}\int \frac{d^{d+1}\hat{k}}{(2\pi)^{d+1}}\int \frac{d^{d+1}\hat{k}'}{(2\pi)^{d+1}}\, k^2 k'^2\, G(\hat{k})\, |G(\hat{k})|^2\, G(\hat{k}')\, |G(\hat{k}')|^2\, G(-\hat{k}-\hat{k}') \tag{2.55}$$

where the propagators are treated as renormalized as expressed in Eq. 2.28 with the renormalized surface tension $\nu(k)$ given by Eq. 2.26. Performing the frequency integrations over ω and ω' yields

$$W_3 = \frac{3}{2}\left(\frac{D_0}{2\pi\nu_0}\right)^{3/2}\int_{-\infty}^{+\infty} dk_x \int_{-\infty}^{+\infty} dk'_x\; F(k_x,k'_x), \tag{2.56}$$

in one dimension, where

$$F(k_x,k'_x) = \frac{U(k_x,k'_x)}{V(k_x,k'_x)} \tag{2.57}$$

with

$$U(k_x,k'_x) = 3\left(|k_x|^3+|k'_x|^3\right)+4|k_x+k'_x|^{3/2}\left(|k_x|^{3/2}+|k'_x|^{3/2}\right)+14|k_x|^{3/2}|k'_x|^{3/2}+|k_x+k'_x|^3 \tag{2.58}$$

and

$$V(k_x,k'_x) = 16\,|k_x|\,|k'_x|\,\left(|k_x|^{3/2}+|k'_x|^{3/2}+|k_x+k'_x|^{3/2}\right)^3. \tag{2.59}$$

The integrations in Eq. 2.56 can be decomposed to obtain

$$W_3 = \frac{3}{2}\left(\frac{D_0}{2\pi\nu_0}\right)^{3/2}\left[2\int_\mu^\infty dk_x\int_\mu^\infty dk'_x\, F(k_x,k'_x)+2\int_\mu^\infty dk_x\int_\mu^\infty dk'_x\, F(-k_x,k'_x)\right]. \tag{2.60}$$

where we have set infrared cut offs at μ as these integrals have infrared divergences. Thus we write

$$W_3 = \frac{3}{2}\left(\frac{D_0}{2\pi\nu_0}\right)^{3/2}\left[2I(\mu)+2J(\mu)\right] \tag{2.61}$$

where

$$I(\mu) = \int_\mu^\infty dk_x\int_\mu^\infty dk'_x\, F(k_x,k'_x) \tag{2.62}$$

and

$$J(\mu) = \int_{\mu}^{\infty} dk_x \int_{\mu}^{\infty} dk'_x \, F(-k_x, k'_x). \tag{2.63}$$

The infrared divergences in these integrals suggest the following forms

$$I(\mu) = I_0 \, \mu^{-3/2} \tag{2.64}$$

$$J(\mu) = J_0 \, \mu^{-3/2} \tag{2.65}$$

where I_0 and J_0 are dimensionless constants.

Substituting from Eqs. (2.64) and (2.65) in Eq. (2.61), we obtain the third moment as

$$W_3 = 3 \left(\frac{D_0}{2\pi\nu_0} \right)^{3/2} (I_0 + J_0) \, \frac{1}{\mu^{3/2}} \tag{2.66}$$

According to the definition of skewness, we thus obtain from Eqs. 4.34 and 2.66

$$S = \frac{W_3}{W_2^{3/2}} = \frac{3}{8} \, (I_0 + J_0) \, \pi^{3/2}. \tag{2.67}$$

We calculate the constants I_0 and J_0 from Eqs. 2.62 and 2.63, using the expressions given by Eqs. 2.57, 2.58 and 2.59, and obtain

$$I_0 = \lim_{\mu \to 0^+} [\mu^{3/2} I(\mu)] = 0.034946 \tag{2.68}$$

$$J_0 = \lim_{\mu \to 0^+} [\mu^{3/2} J(\mu)] = 0.120089 \tag{2.69}$$

by means of numerical integrations. The computation shows convergence to the above numerical values as the parameter μ is chosen to approach values close to zero.

From Eq. 2.67, the value of skewness is thus found to be

$$S = \frac{3}{8} \, (0.155035) \, \pi^{3/2} = 0.323732. \tag{2.70}$$

2.4 Discussion and Conclusion

We employed Yakhot and Orszag's scheme of renormalization without rescaling and obtained the renormalized surface tension and the strength of the noise correlation for the surface growth problem governed by the KPZ dynamics on a flat substrate. This scheme of renormalization is slightly different from the usual perturbative renormalization group analysis with rescaling that has been employed for dynamical prob-

lems by Ma and Mazenko[118], Forster *et al.*[47], and Medina *et al.*[128]. This method allowed us the advantage of obtaining the flow equations directly without rescaling by considering the iterative nature of the scale elimination procedure. This yielded the fixed point from the r-dependent expression of effective coupling constant $g(r)$ in the limit $r \to \infty$. Similar to the other calculations, the renormalized surface tension and the strength of the noise correlation are found to be renormalized in the same way so that $D(r)/\nu(r)$ is r-independent, a consequence of fluctuation dissipation theorem for the case of $(1+1)$ dimensional KPZ equation[35,47].

To obtain a numerical value for the skewness, we employed the diagrammatic approach for the second and third order moments W_2 and W_3. The Fourier integrals of these moments involve the loop integrals L_2 and L_3. The simplicity of Yakhot and Orszag's renormalization scheme allowed us to find renormalized expressions for these loop integrals in a straightforward manner. Although the renormalized diagrams are infrared divergent, the calculated value of skewness turns out to be finite due to cancellation of the infrared cutoff parameter μ. We obtained a value of skewness $S = 0.323732$ for the flat geometry in the stationary state which is compared with the results of numerical simulations for various growth models and those of experiments in Table 2.1. We present a discussion with regard to these results in the following paragraphs.

It has been shown by numerical simulations for polynuclear growth (PNG) that the roughness and growth exponents are in good agreement with the one dimensional KPZ exponents[54,190]. Further numerical work by Krug *et al.*[108] and Bartelt and Evance[13] have ensured that the PNG model belongs to the universality class of the KPZ growth model[126]. Prähofer and Spohn[153] have shown that the PNG model follows the TW distribution with different initial conditions. They estimated the skewness for three different shapes, namely, $S = 0.2241$ for the curved shape (GUE TW), $S = 0.2935$ for the flat shape (GOE TW), and $S = 0.35941$ for the stationary self-similar case[153]. On the other hand, the distribution of height fluctuations for the KPZ growth model with sharp wedge initial condition was shown to be the same as that of the GUE TW distribution, as established by Sasamoto and Spohn[161,162]. Calabrese and Doussal[21] obtained the GOE TW distribution by mapping the one dimensional KPZ problem with flat initial condition to a one end free directed polymer, referred to as a point-to-line configuration. The curved initial condition, on the other hand, maps on to a point-to-point configuration of the directed polymer.

For the case of directed polymers at zero temperature in a random potential (DPRP), Kim *et al.*[94] introduced two types of random site potentials $\mu(\mathbf{x}, t)$,

namely, uniform and Gaussian distributions for $\mu(\mathbf{x}, t)$, with the bending energy (γ) of the polymer as the only tunable parameter. They obtained skewness $S = -0.29 \pm 0.02$ of the minimum energy distribution in $1+1$ dimensions for uniform distribution of $\mu(\mathbf{x}, t)$ for a point-to-line configuration via simulations for $\gamma > 1$. The same value of skewness was obtained for Gaussian distribution of $\mu(\mathbf{x}, t)$, which is independent of γ. Kim and others[94,97] studied height fluctuations of surface growth using the RSOS model with a flat initial condition where the scaling form of the height distribution matches with the energy distribution of the DPRP within numerical accuracy. The skewness in the same model turned out to be $S \approx -0.29$, suggesting universality of the probability distribution function.

Using a mean field theory in terms of densities at different heights applied to the KPZ equation in $(1+1)$ dimensions, Ginelli and Hinrichsen[53] started with the flat initial condition $h(x, 0) = 0$ and obtained the skewness $S = \pm 0.46$ for the transient regime. Takeuchi *et al.*[179] carried out an experiment on a growing interface in liquid crystal turbulence and established that it is in the KPZ universality class. For flat initial conditions, their experimental asymptotic value for skewness was close to $\simeq 0.29$ as suggested by their experimental plots. These values are displayed in Table 2.1 for comparison with our result.

Table 2.1: Values of Skewness in one dimension

System of Study	*Reference*	*Methodology*	*Skewness*
SSM (flat)	[108]	Numerical	0.28 ± 0.04
SSM (stationary)	[108]	Numerical	≈ 0.33
DPRM (point-to-line)	[108]	Numerical	-0.296 ± 0.028
DPRP (point-to-line)	[94]	Numerical	-0.29 ± 0.02
RSOS (flat)	[94,97]	Numerical	≈ -0.29
TLC (flat)	[179]	Experimental	0.29
PNG (curved)	[153]	Numerical	0.2241
PNG (flat)	[153]	Numerical	0.2935
PNG (stationary)	[153]	Numerical	0.35941
KPZ (mean field, flat)	[53]	Analytical	± 0.46
Combustion front (flat)	[129]	Experimental	0.33
Combustion front (stationary)	[129]	Experimental	0.32
KPZ (present calculation)	Eq. (2.70)	Analytical	0.3237

We observe that our calculated result for the skewness is comparable with some of the experimental values and numerical simulations. It deviates from the non-

stationary results and the deviation is more pronounced from the result for curved interfaces. This is expected as our calculations are applicable for a flat geometry in the stationary state. We also observe that the result of the mean field calculation deviates somewhat strongly from all other results. Since skewness is determined by the underlying probability distribution, its calculation following from the governing dynamics is of importance in inferring the universality class. Moreover, the existing studies indicate that the pdf is determined by not only the governing dynamics but also by the boundary conditions. Thus it may be said that there are different subclasses belonging to the same universality class. Different numerical values of skewness may thus be said to correspond to different universality subclasses although they may have the same scaling exponents for the correlation and response functions.

Since the renormalization scheme involves calculations of the statistical moments in the large scale limit $k \to 0$, such calculations are expected to lead to the statistical properties of the growth process at large scales. The fact that W_2 and W_3 turn out to be infrared divergent implies a dominant role of the large scale fluctuations in determining these statistical moments. Moreover since the renormalization scheme involves calculations in the long time limit $\omega \to 0$, such calculations are expected to capture the statistical properties of the growth process in the stationary state.

However, for a large system, achieving a stationary state is difficult [78], especially in experiments and numerical simulations, unless a stationary state is taken as an initial condition [177]. To achieve a stationary pdf for the flat one dimensional KPZ problem, Imamura and Sasamoto took both sided Brownian motion as an initial condition [78,79] and obtained the generating function for the replica partition function as a Fredholm determinant. This allowed for the calculation of the pdf which was found to approach the Baik-Rains F_0 distribution in the long time limit. Krug *et al.* [108] investigated the stationary state skewness for the SSM model with random uncorrelated spins ($\sigma_i = \pm 1$). They obtained $|S| \approx 0.33$ which agrees well with our calculated value. Maunuksela *et al.* [124] identified that the universality class of slow combustion fronts of a paper sheet belongs to the KPZ universality class on the basis of scaling exponents. With the same experimental conditions, Miettinena *et al.* [129] performed an experiment on paper burning to find the skewness from the pdf. They studied the height distribution of combustion fronts for flat initial conditions in the saturation regime and obtained the value $S = 0.32$ which agrees well with our calculated value. It may however be noted that Takeuchi [176] has suggested that their analysis of the pdf may need modifications.

Although our calculated value for the skewness (0.3237) compares excellently

well (within 1–2%) with the above mentioned stationary values (0.33 and 0.32), we observe that there is a slight departure (of about 10%) from the value $S = 0.3594$ coming from the PNG model[153]. This departure may be due to the dominating role of large scale fluctuations in determining the moments W_2 and W_3. The infrared cutoff μ may be interpreted as the inverse of the size L of the substrate and thus the calculations appear to be influenced by finite size effects. In spite of this slight departure, together with the agreements with the experimental results, our calculation for the skewness seems to identify the relevant universality subclass of the KPZ equation.

Ideally speaking, full information about the pdf enables one to classify many seemingly similar problems into varying universality classes. However, an analytical calculation of the full pdf is an extremely difficult task, whereas the calculation of higher order moments such as the skewness is a more viable approach. Thus a classification scheme for universality beyond the scaling exponents can be formulated via the values of skewness for various processes. Takeuchi and Sano[178] have proved through the TLC experiment that the KPZ class has geometry dependent subclasses in spite of having the same scaling exponents. Thus, to characterize the subclasses, knowledge of skewness and higher order moments is very much essential. The calculation of skewness, directly from the KPZ dynamics, is therefore an important step in identifying a universality subclass of the KPZ equation.

Chapter 3

Kurtosis of height fluctuations in $(1+1)$ dimensional KPZ Dynamics

3.1 Introduction

Growth of a surface or interface has been one of the most important and well-studied fields in nonequilibrium statistical physics since a long time[11,43,63,105,126]. Kardar, Parisi and Zhang[86] first proposed a paradigmatic nonlinear equation for local surface growth capable of describing many growth phenomena. The equation, called the KPZ equation, is expressed as

$$\frac{\partial h}{\partial t} = \nu_0 \nabla^2 h + \frac{\lambda_0}{2}(\nabla h)^2 + \eta, \tag{3.1}$$

where $h(\mathbf{x}, t)$ is the field of height fluctuations, ν_0 is the surface tension that relaxes particles from local maxima to local minima, and λ_0 is the strength of local interaction. Here $\eta(\mathbf{x}, t)$ is the deposition noise with zero average, $\langle \eta(\mathbf{x}, t) \rangle = 0$, and its covariance is modeled as a short range correlation

$$\langle \eta(\mathbf{x}, t)\, \eta(\mathbf{x}', t') \rangle = 2D_0\, \delta^d(\mathbf{x} - \mathbf{x}')\, \delta(t - t'), \tag{3.2}$$

with d the substrate dimension.

The roughness of a self-affine surface is characterized by the width w of the interface (or standard deviation w of the height fluctuations), given by the dynamic scaling relation

$$w(L, t) \sim L^{\chi} f\left(\frac{t}{L^z}\right), \tag{3.3}$$

as suggested by Family and Vicsek[43], where L is the size of the interface and $f(\cdot)$

is a universal function having asymptotics such that $w(L,t) \sim t^{\beta}$ when $t \ll L^z$ and $w(L,t) \sim L^{\chi}$ for $t \gg L^z$. Here the exponent χ characterizes the roughness of the surface, z is the dynamic exponent, and the ratio $\beta = \frac{\chi}{z}$ is known as the growth exponent. The roughness exponent χ is an important parameter in experiments; adsorption, catalysis[148] and optical properties[132] of a thin film are affected by the roughness of the surface. The exponents are related via the scaling relation $\chi + z = 2$[107,127,128], which is independent of the substrate dimension.

There are various growth phenomena that are believed to be in the KPZ universality class on the basis of the numerical values of the scaling exponents[11]. A few of them are thin film deposition[144], bacteria colony growth[71,191], fluid flow in porous media[160], turbulent liquid crystal[178,179], one dimensional polynuclear growth (PNG)[54,106,153,190], slow combustion of a sheet of paper[129,134]. In addition, many problems are equivalent to the KPZ equation, e.g., Burgers equation[47] describes the vorticity free velocity, directed polymer in random media[45,87] and in random potentials (DPRP)[108], sequence alignment of gene or protein[75,77], heat equation of multiplicative noise obtained via the Cole-Hopf transformation of the KPZ equation.

A renormalization group (RG) analysis[86] of the $1+1$ dimensional KPZ equation yielded roughness exponent $\chi = \frac{1}{2}$ and dynamic exponent $z = \frac{3}{2}$ which are consistent with various numerical models, e.g., ballistic deposition[43,127], Eden model[39,84,151,152], restricted solid on solid model (RSOS)[126], single step model (SSM)[127,150]. RG calculation in $2+1$ dimensions is unable to yield the exponents of KPZ equation. A number of analytical techniques have been employed to study the higher dimensional scaling exponents of KPZ equation, e.g., the mode coupling[28,189], the operator product expansion[113], the self-consistent expansion[163] and the non-perturbative RG[22,100].

Although many physical problems are described by the $1+1$ dimensional KPZ equation, enough attention has not been payed to understand the statistical probability distribution of the height fluctuations as it is a challenging task to obtain it directly from the KPZ equation. Nevertheless, it is a highly desirable objective and it demands extensive theoretical and experimental studies[126]. Prähofer and Spohn[153] studied the PNG model for three different initial conditions namely flat, droplet and stationary self similar which are in the KPZ universality class on the basis of scaling exponents. For the droplet initial condition the distribution was found to be the Gaussian unitary ensemble (GUE) Tracy-Widom (TW) whereas for the flat initial condition it is the Gaussian orthogonal ensemble (GOE) Tracy-

Widom (TW) distribution. The height distribution was modeled through the relation $h(x,t) \sim v_\infty t + (\Gamma t)^{1/3}\phi$ (with the parameter $\Gamma = \frac{D_0^2\lambda_0}{8\nu_0^2}$) where ϕ is a random variable determined by appropriate random matrices and v_∞ is the rate of growth at long times[178].

Imamura and Sasamoto[78] considered a Brownian motion as an initial condition from both sides of the substrate and used the Bethe ansatz and a replica trick to find the height distribution in terms of a Fredholm determinant. Takeuchi[177] obtained scaling functions smoothly connecting the crossover between the GOE-TW and Baik-Rains F_0 distributions. He observed that the moments pass through minimum values, known as the Takeuchi minima. Such behavior was also noticed via TLC experimental studies apart from the numerical study of the PNG model.

In spite of the same scaling exponents, the statistical behavior of stochastic processes may be different due to difference in the underlying probability distribution functions (pdf) that incorporate the basic features of a dynamical process[165]. In principle, the pdf can be calculated analytically by solving the Fokker-Planck equation[74,147] corresponding to the KPZ equation. However, this is practically infeasible due to the nonlinear term. As an alternative, a few higher order moments can be calculated to understand the statistical behavior of the interface and the corresponding universality class. It may be noted that the measurement accuracy of higher order moments is greater than that of the scaling exponents[2] in experiments.

In this Chapter, we consider the $1+1$ dimensional KPZ equation with a flat substrate and focus on the evaluation of the fourth order cumulant relevant to the kurtosis in stationary state. We apply a diagrammatic approach to find a renormalized expression for the loop integral corresponding to the fourth order cumulant in the large scale long time limit.

The present Chapter is organized as follows. Section 2 defines the moments and cumulants and states the relations between them. Section 3 is devoted to the calculation of fourth order cumulant. In Section 4, the calculation of excess kurtosis is presented. Section 5 presents a discussion and conclusion and a comparison the kurtosis value with other numerical and experimental findings.

3.2 Moments and Cumulants

Higher order moments and cumulants are usually defined in terms of a generating function. The moment generating function $Z(\beta)$ is defined as

$$Z(\beta) \equiv \langle e^{\beta h} \rangle = \sum_{n=0}^{\infty} \frac{\beta^n}{n!} \langle h^n \rangle, \tag{3.4}$$

where $\langle h^n \rangle$ is the nth order moment of a random variable h, given by

$$\langle h^n \rangle = \int_{-\infty}^{+\infty} h^n P(h)\, dh, \tag{3.5}$$

for a given normalized probability distribution function $P(h)$. The cumulant generating function $F(\beta)$ is defined as

$$F(\beta) = \ln Z(\beta) = \sum_{n=1}^{\infty} \frac{\beta^n}{n!} \langle h^n \rangle_c, \tag{3.6}$$

where $\langle h^n \rangle_c$ is the nth order cumulant. The moments are related to the cumulants as

$$\begin{aligned}
\langle h \rangle &= \langle h \rangle_c \\
\langle h^2 \rangle &= \langle h^2 \rangle_c + \langle h \rangle_c^2 \\
\langle h^3 \rangle &= \langle h^3 \rangle_c + 3\langle h \rangle_c \langle h^2 \rangle_c + \langle h \rangle_c^3 \\
\langle h^4 \rangle &= \langle h^4 \rangle_c + 4\langle h \rangle_c \langle h^3 \rangle_c + 3\langle h^2 \rangle_c^2 + 6\langle h \rangle_c^2 \langle h^2 \rangle_c + \langle h \rangle_c^4.
\end{aligned} \tag{3.7}$$

The fluctuating interface field $h(\mathbf{x}, t)$ has a zero mean; $\langle h(\mathbf{x}, t) \rangle = \langle h(\mathbf{x}, t) \rangle_c = 0$. Hence the second and fourth order cumulants[108,165] are related to the moments as

$$\langle h^2 \rangle_c = \langle h^2 \rangle, \tag{3.8}$$

and

$$\langle h^4 \rangle_c = \langle h^4 \rangle - 3\langle h^2 \rangle^2. \tag{3.9}$$

Kurtosis Q is defined by the "normalized" fourth order cumulant as

$$Q = \frac{\langle h^4 \rangle_c}{\langle h^2 \rangle_c^2} = \frac{\langle h^4 \rangle}{\langle h^2 \rangle^2} - 3. \tag{3.10}$$

In the diagrammatic approach, a connected diagram with n external legs corresponds to the nth order cumulant. Henceforth, we focus on the fourth cumulant instead of the moment and therefore we evaluate the connected loop diagram to obtain the cumulant in order to evaluate the kurtosis.

3.3 The Fourth-order Cumulant

The fourth order cumulant $\langle h^4(\mathbf{x},t)\rangle_c$ of the height fluctuations measures the degree of flatness of the probability distribution. Using the Fourier transform

$$h(\mathbf{x},t) = \int \frac{d^d k\, d\omega}{(2\pi)^{d+1}}\, h(\mathbf{k},\omega)\, e^{i(\mathbf{k}\cdot\mathbf{x}-\omega t)}, \tag{3.11}$$

the KPZ equation (5.1) is written in momentum and frequency space as

$$(-i\omega+\nu_0 k^2)\, h(\mathbf{k},\omega) = \eta(\mathbf{k},\omega) - \frac{\lambda_0}{2}\int \frac{d^d q\, d\Omega}{(2\pi)^{d+1}}\, [\mathbf{q}\cdot(\mathbf{k}-\mathbf{q})]\, h(\mathbf{q},\Omega)\, h(\mathbf{k}-\mathbf{q},\omega-\Omega). \tag{3.12}$$

This equation forms the basis of developing a perturbation theory.

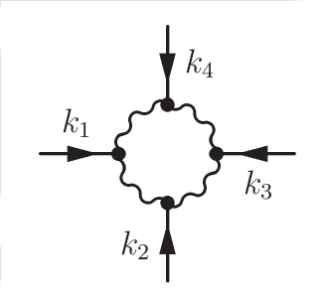

Figure 3.1: Feynman Diagram corresponding to the fourth cumulant

The expression for the fourth cumulant is given by the connected fourth order correlation in momentum and frequency space as

$$\begin{aligned}\langle h^4(\mathbf{x},t)\rangle_c \;=\; & \int \frac{d^{d+1}\hat{k}_1}{(2\pi)^{d+1}} \int \frac{d^{d+1}\hat{k}_2}{(2\pi)^{d+1}} \int \frac{d^{d+1}\hat{k}_3}{(2\pi)^{d+1}} \int \frac{d^{d+1}\hat{k}_4}{(2\pi)^{d+1}} \\ & \langle h(\hat{k}_1)h(\hat{k}_2)h(\hat{k}_3)h(\hat{k}_4)\rangle_c\, e^{i(\hat{k}_1+\hat{k}_2+\hat{k}_3+\hat{k}_4)\cdot\hat{x}},\end{aligned} \tag{3.13}$$

where $\hat{x} \equiv (\mathbf{x},t)$ and $\hat{k}_i \equiv (\mathbf{k}_i,\omega_i)$ are vectors in $(d+1)$-vector notation. We use the diagrammatic approach and obtain a connected loop diagram for the fourth cumulant as shown in Fig. 3.1, where a wiggly line represents the correlation and a

solid line the response function. We express the correlation in accordance with the connected loop diagram in Fig. 3.1, so that

$$\begin{aligned}\langle h^4(\mathbf{x},t)\rangle_c &= \int \frac{d^{d+1}\hat{k}_1}{(2\pi)^{d+1}} \int \frac{d^{d+1}\hat{k}_2}{(2\pi)^{d+1}} \int \frac{d^{d+1}\hat{k}_3}{(2\pi)^{d+1}}\, G(\hat{k}_1)\, G(\hat{k}_2)\, G(\hat{k}_3) \\ &\quad L_4(\hat{k}_1,\hat{k}_2,\hat{k}_3)\, G(-\hat{k}_1-\hat{k}_2-\hat{k}_3), \end{aligned} \tag{3.14}$$

where L_4 represents the renormalized loop corresponding to the amputated part of the diagram (excluding the external legs). Its bare value is written as

$$\begin{aligned}L_4^{(0)}(\hat{k}_1,\hat{k}_2,\hat{k}_3) &= 16\left(-\frac{\lambda_0}{2}\right)^4 (2D_0)^4 \int \frac{d^{d+1}\hat{q}}{(2\pi)^{d+1}} [\mathbf{q}\cdot(\mathbf{q}-\mathbf{k}_1)][\mathbf{q}\cdot(\mathbf{k}_2+\mathbf{q})] \\ &\quad [(\mathbf{q}+\mathbf{k}_2)\cdot(\mathbf{k}_3+\mathbf{k}_2+\mathbf{q})][(\mathbf{k}_4+\mathbf{k}_3+\mathbf{k}_2+\mathbf{q})\cdot(\mathbf{q}+\mathbf{k}_2+\mathbf{k}_3)] \\ &\quad G_0(\hat{q})G_0(-\hat{q}+\hat{k}_1)G_0(-\hat{q})G_0(\hat{q}+\hat{k}_2)G_0(-\hat{q}-\hat{k}_2)G_0(\hat{q}+\hat{k}_3+\hat{k}_2) \\ &\quad G_0(\hat{q}+\hat{k}_2+\hat{k}_3+\hat{k}_4)G_0(-\hat{q}-\hat{k}_2-\hat{k}_3), \end{aligned} \tag{3.15}$$

where the prefactor 16 is a combinatorial factor.

Now we evaluate Eq. 5.27 by performing frequency and momentum integrations where the momentum is restricted to the shell $\Lambda_0 e^{-r} \le q \le \Lambda_0$. This leads to

$$L_4^{<}(r) = \frac{5}{2} K_d \frac{\lambda_0^4 D_0^4}{\nu_0^7 \Lambda_0^5} \left(\frac{e^{5r}-1}{5}\right), \tag{3.16}$$

where $K_d = \frac{S_d}{(2\pi)^d}$, with S_d the surface area of a unit sphere in d dimensional space.

We follow Yakhot and Orszag's[207,208] scheme of renormalization without rescaling and obtain from Eq. 3.16 the differential equation

$$\frac{dL_4}{dr} = \frac{5}{2\pi} \frac{\lambda_0^4 D^4(r)}{\nu^7(r)\Lambda^5(r)}, \tag{3.17}$$

in one dimension.

Noting that $\Lambda(r) = \Lambda_0 e^{-r}$ and using the asymptotic expressions

$$\nu(r) = \lambda_0 \sqrt{\frac{D_0}{2\pi\nu_0\Lambda_0}}\, e^{r/2} \tag{3.18}$$

and

$$D(r) = \frac{\lambda_0 D_0}{\nu_0} \sqrt{\frac{D_0}{2\pi\nu_0\Lambda_0}}\, e^{r/2} \tag{3.19}$$

obtained from renormalization-group calculations[169], we obtain the solution to the

differential equation (3.17) as

$$L_4(r) = \frac{10\pi}{7}\lambda_0 \left(\frac{2D_0^5}{\pi\nu_0^5\Lambda_0^7}\right)^{1/2} e^{7r/2}. \tag{3.20}$$

The factor $\Lambda_0 e^{-r}$ is interpreted as a momentum k_i in the large scale limit. Since the loop integral must be symmetric with respect to interchange of the external momenta k_1, k_2 and k_3, we replace $\Lambda_0 e^{-r}$ by the fully symmetric form $k_1^{1/3}k_2^{1/3}k_3^{1/3}$. Thus we have

$$L_4(\mathbf{k}_1, 0; \mathbf{k}_2, 0; \mathbf{k}_3, 0) = \frac{10\pi}{7}\lambda_0 \left(\frac{2D_0^5}{\pi\nu_0^5}\right)^{1/2} k_1^{-7/6}k_2^{-7/6}k_3^{-7/6}, \tag{3.21}$$

when the external frequencies are zero. To obtain the frequency dependency, we take the scaling function as

$$k_i^{7/6} f_4\left(\frac{\omega_i}{k_i^z}\right) = \frac{1}{k_i^{17/6}\nu^2(k_i)|G(\mathbf{k}_i, \omega_i)|^2}, \tag{3.22}$$

where the renormalized response function is given by $G(\mathbf{k}_i, \omega_i) = [-i\omega_i + \nu(k_i)\mathbf{k}_i^2]^{-1}$ with the renormalized surface tension

$$\nu(k_i) = \lambda_0\sqrt{\frac{D_0}{2\pi\nu_0}}\, k_i^{-1/2}. \tag{3.23}$$

The above scaling relation (3.22) obeys consistency with the zero frequency limit and with the real valuedness of $\Lambda_0 e^{-r}$, in addition to being of the correct dimension. Now with the aid of Eq. (3.22), Eq. (3.21) is modified to the frequency dependent form

$$\begin{aligned} L_4(\hat{k}_1, \hat{k}_2, \hat{k}_3) \;=\; & \frac{10\pi}{7}\lambda_0 \left(\frac{2D_0^5}{\pi\nu_0^5}\right)^{1/2} k_1^{17/6}k_2^{17/6}k_3^{17/6}\, \nu^2(k_1)|G(k_1, \omega_1)|^2 \\ & \nu^2(k_2)|G(k_2, \omega_2)|^2\, \nu^2(k_3)|G(k_3, \omega_3)|^2, \end{aligned} \tag{3.24}$$

representing the renormalized loop diagram in Fig. 3.1. We substitute the renormalized expression for the loop diagram from Eq. 3.24 in Eq. 5.26 and treat the external legs representing the response functions as renormalized. Carring out the frequency integration, we obtain

$$\langle h^4(\mathbf{x}, t)\rangle_c = \frac{10}{7}\left(\frac{D_0}{2\pi\nu_0}\right)^2 \int_{-\infty}^{\infty} dk_1 \int_{-\infty}^{\infty} dk_2 \int_{-\infty}^{\infty} dk_3\, \Phi(k_1, k_2, k_3) \tag{3.25}$$

where

$$\Phi(k_1,k_2,k_3)=\frac{u(k_1,k_2,k_3)}{v(k_1,k_2,k_3)} \tag{3.26}$$

with

$$\begin{aligned} u(k_1,k_2,k_3) &= (3(|\mathbf{k}_1|^{9/2}+|\mathbf{k}_2|^{9/2}+|\mathbf{k}_3|^{9/2})+5(|\mathbf{k}_1|^{3/2}+|\mathbf{k}_2|^{3/2}+|\mathbf{k}_3|^{3/2})|\mathbf{k}_1+\mathbf{k}_2+\mathbf{k}_3|^3 \\ &+7(|\mathbf{k}_1|^3+|\mathbf{k}_2|^3+|\mathbf{k}_3|^3)|\mathbf{k}_1+\mathbf{k}_2+\mathbf{k}_3|^{3/2}+17(|\mathbf{k}_1|^3|\mathbf{k}_2|^{3/2}+|\mathbf{k}_1|^{3/2}|\mathbf{k}_2|^3 \\ &+|\mathbf{k}_1|^3|\mathbf{k}_3|^{3/2}+|\mathbf{k}_1|^{3/2}|\mathbf{k}_3|^3+|\mathbf{k}_2|^3|\mathbf{k}_3|^{3/2}+|\mathbf{k}_2|^{3/2}|\mathbf{k}_3|^3) \\ &+22(|\mathbf{k}_1|^{3/2}|\mathbf{k}_2|^{3/2}+|\mathbf{k}_1|^{3/2}|\mathbf{k}_3|^{3/2}+|\mathbf{k}_2|^{3/2}|\mathbf{k}_3|^{3/2})|\mathbf{k}_1+\mathbf{k}_2+\mathbf{k}_3|^{3/2} \\ &+90|\mathbf{k}_1|^{3/2}|\mathbf{k}_2|^{3/2}|\mathbf{k}_3|^{3/2}+|\mathbf{k}_1+\mathbf{k}_2+\mathbf{k}_3|^{9/2}) \end{aligned} \tag{3.27}$$

and

$$v(k_1,k_2,k_3)=64|\mathbf{k}_1|^{7/6}|\mathbf{k}_2|^{7/6}|\mathbf{k}_3|^{7/6}(|\mathbf{k}_1|^{3/2}+|\mathbf{k}_2|^{3/2}+|\mathbf{k}_3|^{3/2}+|\mathbf{k}_1+\mathbf{k}_2+\mathbf{k}_3|^{3/2})^4. \tag{3.28}$$

The symmetry of the function $\Phi(k_1,k_2,k_3)$ allows us to write Eq. 3.25 as

$$\langle h^4(\mathbf{x},t)\rangle_c=\frac{10}{7}\left(\frac{D_0}{2\pi\nu_0}\right)^2\int_\mu^\infty dk_1\int_\mu^\infty dk_2\int_\mu^\infty dk_3\,[2\Phi(k_1,k_2,k_3)+6\Phi(-k_1,k_2,k_3)] \tag{3.29}$$

where μ is an infrared cut off. Now we write the integrations separately as

$$I_1(\mu)=\int_\mu^\infty dk_1\int_\mu^\infty dk_2\int_\mu^\infty dk_3\,\Phi(k_1,k_2,k_3) \tag{3.30}$$

and

$$I_2(\mu)=\int_\mu^\infty dk_1\int_\mu^\infty dk_2\int_\mu^\infty dk_3\,\Phi(-k_1,k_2,k_3). \tag{3.31}$$

These integrals are expected to be of the forms

$$I_1(\mu)=a_1\mu^{-2} \tag{3.32}$$

$$I_2(\mu)=a_2\mu^{-2}. \tag{3.33}$$

where a_1 and a_2 are dimensionless constants. Substituting Eqs. 3.32 and 3.33 in Eq. 3.29 yields

$$\langle h^4(\mathbf{x},t)\rangle_c=\frac{10}{7}[2a_1+6a_2]\left(\frac{D_0}{2\pi\nu_0}\right)^2\frac{1}{\mu^2} \tag{3.34}$$

We evaluate the integrals in Eqs. 3.30 and 3.31 by integrating over k_1, k_2 and k_3

numerically and obtain the dimensionless constants as

$$a_1 = \lim_{\mu \to 0^+} [\mu^2 I_1(\mu)] = 0.007505 \tag{3.35}$$

and

$$a_2 = \lim_{\mu \to 0^+} [\mu^2 I_2(\mu)] = 0.026297, \tag{3.36}$$

the numerical values having converged to the above values for decreasing values of the parameter μ very close to zero.

3.4 The Kurtosis

Having calculated the fourth-order cumulant given by Eq. (3.34), we now need the value of the second-order cumulant to determine the value of kurtosis given by Eq. (5.65). The second moment is written as

$$\langle h^2(\mathbf{x},t)\rangle = \int \frac{d^d k_1\, d\omega_1}{(2\pi)^{d+1}} \int \frac{d^d k_2\, d\omega_2}{(2\pi)^{d+1}} \langle h(\mathbf{k}_1,\omega_1) h(\mathbf{k}_2,\omega_2)\rangle\, e^{i(\mathbf{k}_1+\mathbf{k}_2)\cdot\mathbf{x}}\, e^{-i(\omega_1+\omega_2)t}. \tag{3.37}$$

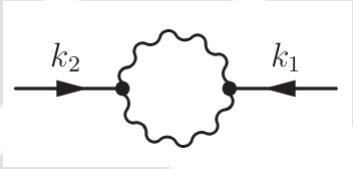

Figure 3.2: Feynman diagram corresponding to the second cumulant

Homogeneity in space and time implies that the correlation takes the form

$$\langle h(\mathbf{k}_1,\omega_1)\, h(\mathbf{k}_2,\omega_2)\rangle = Q(\mathbf{k}_1,\omega_1)\,(2\pi)^d \delta^d(\mathbf{k}_1+\mathbf{k}_2)\,(2\pi)\delta(\omega_1+\omega_2). \tag{3.38}$$

The correlation function $Q(\mathbf{k},\omega)$ can be written in accordance with the one-loop diagram in Fig. 3.2, so that

$$\langle h^2(\mathbf{x},t)\rangle_c = \langle h^2(\mathbf{x},t)\rangle = \int \frac{d^d k\, d\omega}{(2\pi)^{d+1}}\, G(\mathbf{k},\omega)\, L_2(\mathbf{k},\omega)\, G(-\mathbf{k},-\omega) \tag{3.39}$$

The renormalized value of L_2, given by the loop integral coming from the amputated

part of Fig. 3.2, can be obtained as

$$L_2(\mathbf{k},\omega) = \frac{\lambda_0^2 D_0^2}{\pi \nu_0^2}\, k\, |G(\mathbf{k},\omega)|, \tag{3.40}$$

by means of a renormalization scheme as shown in Ref.[169]. This yields the second cumulant as

$$\langle h^2(\mathbf{x},t)\rangle_c = \frac{4}{\pi}\left(\frac{D_0}{2\pi\nu_0}\right)\frac{1}{\mu}. \tag{3.41}$$

Employing Eqs. (3.25) and (4.34) in the definition of kurtosis leads to

$$Q = \frac{\langle h^4(\mathbf{x},t)\rangle_c}{\langle h^2(\mathbf{x},t)\rangle_c^2} = \frac{5\pi^2}{28}(a_1 + 3a_2), \tag{3.42}$$

free from the infra-red cutoff μ and the model parameters ν_0, D_0, and λ_0. Employing the numerical values of a_1 and a_2 from Eqs. 3.35 and 3.36 yields the kurtosis as

$$Q = 0.152267. \tag{3.43}$$

We compare this value with other stationary values of kurtosis in Table 3.1.

Table 3.1: Values of Kurtosis in $(1+1)$ dimensions.

System of study	*Method*	*Kurtosis*	*Reference*
PNG (stationary)	Numerical	0.289	[153]
g1 DPRM (stationary)	Numerical	0.278	[61]
KPZ (present calculation)	Analytical	0.1523	Eq. (3.43)

3.5 Discussion and Conclusion

In this work, we followed a perturbative renormalization approach to evaluate the Feynman diagram in Fig. 3.1 that represents the fourth cumulant, noting that contribution to cumulants are given by the connected loop diagrams. To calculate the connected diagram, we first renormalized its amputated part in the limit of internal momenta and frequencies much greater than the external ones and followed Yakhot and Orszag's iterative renormalization scheme without rescaling[208]. This results in a scale dependent function for the amputated part of the loop diagram at zero frequency. Introducing a frequency dependent scaling function that smoothly joins

with the obtained scaling behavior and that preserves the property of real valuedness, we evaluated the resulting frequency and momentum integrations to obtain an expression for the fourth order cumulant depending on the infrared cutoff in the momentum integration. The evaluation of the second cumulant is simpler which also depends on the the infrared cutoff as shown in Ref.[169]. The behaviors of both the fourth and second order cumulants are seen to be exactly in accordance with the well-known behavior of the nth moment, namely $W_n \sim L^{n\chi}$, where L is the substrate size (so that $\mu \sim L^{-1}$) and χ is the roughness exponent. These cumulants yield the value of kurtosis $Q = 0.1523$ which is free from the infrared cutoff μ and model dependent parameters D_0 , ν_0, and λ_0, due to their exact cancellations.

Incidentally, it may be worth mentioning that the calculation of cumulant amplitudes have been regarded as an important objective by some researchers. For example, Krug et al.[108] studied the growth of an interface via simulation of the single step model with flat initial condition and obtained the estimates for the cumulant amplitudes as $c_2 = 0.404 \pm 0.013$ and $c_4 = 0.020 \pm 0.002$, suggesting a kurtosis value $Q = \frac{c_4}{c_2^2} = 0.123 \pm 0.020$. Furthermore, they showed that c_2 is higher for the steady state case, namely, $c_2 = 0.712 \pm 0.003$, due to the additional role of fluctuations in the initial conditions besides those operating during the growth. Earlier, Hwa and Frey[76] had obtained $c_2 = 0.69$ via mode-coupling calculations. Tang[181] estimated $c_2 = 0.725 \pm 0.005$ using a Monte-Carlo simulation with the single-step model, giving an excellent estimate for the Baik-Rains constant[60,153]. A slightly different result, $c_2 = 0.71$, was obtained through mode-coupling calculation by Amar and Family[7].

In Table 3.1, our calculated kurtosis value is compared with other stationary values. Prähofer and Spohn[153] studied the PNG model belonging to the $1 + 1$ dimensional KPZ universality class to find the effect of initial conditions on the statistical behavior of growing interfaces. They obtained different kurtosis values for different initial conditions, namely, $Q = 0.0934$ for curved, $Q = 0.1652$ for flat, and $Q = 0.289$ for stationary initial conditions. Halpin-Healy and Lin[61] studied the DPRM with different configurations such as point-to-point, point-to-line, and stationary cases, leading to GUE-TW, GOE-TW and Baik-Rains F_0 distributions, respectively. Through g_1 DPRM, they estimated the stationary kurtosis value to be $Q = 0.278$.

Apart from the values shown in Table 3.1, there are a few studies where the full Baik-Rains distribution is obtained in the context of KPZ stationary state. Takeuchi[177] obtained, via a numerical simulation of the PNG model and an experiment on the TLC, a universal function that undergoes a crossover from a transient

state to the stationary regime. Miettinen *et al.*[129] carried out an experimental study of the slow propagation of the combustion front on a sheet of paper to investigate upon the front fluctuation distribution. Their experimental data for the transient and stationary states were found to fit well with the GOE-TW and F_0 distributions, respectively. On the other hand, Halpin-Healy and Lin[61], studied the distributions of deposition models (BD, SSM, and RSOS) that strongly agree with DPRM/SHE results and they turn out to be the Baik-Rains distribution. These investigations establish that the kurtosis value in the stationary state must be the same as the universal kurtosis of the Baik-Rains distribution (for example, $Q = 0.289$[153] or 0.278[61]).

In our calculation based on the RG scale elimination scheme, we obtained the renormalized quantities in the large-scale and long-time limits. Thus our methodology inexorably selects the stationary regime. However, the resulting kurtosis value does not agree well with the stationary kurtosis value and it is distinctly lower than the Baik-Rains value, $Q = 0.28916$. In our simplified scheme of calculation, we obtained the fourth cumulant at one-loop order. While a one-loop scheme for the third cumulant was nearly successful in estimating the stationary skewness value[169], a higher order calculation would appear to be more appropriate for the fourth cumulant. Noting that the perturbation expansion is about a Gaussian state, the Gaussian behavior seems to play some role with the increase in order of the cumulant, lowering the estimated value. This opens the door for further investigations into the rather unexplored stationary KPZ problem that is expected to illuminate upon its semantic relation with Baik-Rains distribution.

We conclude by recalling that there are many growth processes governed by nonequilibrium dynamics that are believed to be in the KPZ universality class on the basis of scaling exponents. However, as shown by the PNG and TLC studies, the statistical behavior, that is the probability distribution, depends on the initial conditions. The full probability distribution function of the KPZ height fluctuations has never been studied analytically due to the inherent difficulty in the problem. However, relevant information about the probability distribution can be obtained through the study a few higher order moments and cumulants. Thus the present theoretical study may be viewed as an initial attempt at the quantification of higher order statistical property of the $1+1$ dimensional KPZ dynamics. We hope that such analytical scheme would be useful for the study of statistical behavior of other important stochastic processes as well.

Chapter 4

Hyperskewness of $(1+1)$-dimensional KPZ Height Fluctuations

4.1 Introduction

The dynamics of surface growth has extensively been studied in nonequilibrium statistical physics in the last few decades[11,43,63,105]. To describe a local surface growth, Kardar, Parisi and Zhang[86] (KPZ) first proposed a prototypical nonlinear equation for the fluctuating height field $h(\mathbf{x},t)$, expressed as

$$\frac{\partial}{\partial t}h(\mathbf{x},t) = \nu_0\nabla^2 h + \frac{\lambda_0}{2}(\nabla h)^2 + \eta(\mathbf{x},t), \tag{4.1}$$

where ν_0 is the surface tension that smoothens the surface curvature and minimizes the surface area and λ_0 is a coupling constant representing the strength of the nonlinear term. The stochastic term $\eta(\mathbf{x},t)$ is modeled as a Gaussian white noise of zero average, $\langle\eta(\mathbf{x},t)\rangle = 0$, and its covariance

$$\langle\eta(\mathbf{x},t)\eta(\mathbf{x}',t')\rangle = 2D_0\delta^d(\mathbf{x}-\mathbf{x}')\delta(t-t') \tag{4.2}$$

where d is the substrate dimension. We shall consider the stationary state for the growth of a surface on a flat substrate of dimension $d = 1$.

There are various systems that are mathematically equivalent to the KPZ dynamics. A few examples are: vorticity free noisy Burgers equation[47], stochastic heat equation, diffusion equation governed by random source and sink, directed polymer in random potentials[108], in random media[45,87], the sequence alignment of gene or protein[75,77] etc. Various growth phenomena belong to the $(1+1)$-dimensional

KPZ universality class (on the basis of scaling exponents[11]). For example, growth of a bacteria colony[71,191], fluid flow in a porous media[160], turbulent liquid crystal[178,179], slow combustion of a sheet of paper[129,134] etc.

The $1+1$-dimensional KPZ equation satisfies the fluctuation dissipation theorem. The standard RG treatment of the $1+1$-dimensional KPZ equation leads to the same scaling exponents for the renormalised noise amplitude $D(k)$ and the renormalised surface tension $\nu(k)$. The resulting roughness and dynamic exponents are $\chi = \frac{1}{2}$ and $z = \frac{3}{2}$ respectively[86,87] that satisfies the scaling relation $\chi + z = 2$. There have been various numerical models, namely, ballistic deposition[43,127], Eden model[39,84,151,152], restricted solid on solid model[126], single step model[127,150], polynuclear growth[54,106,153,190] which have the same scaling exponents, and consequently, belong to the universality class of the $(1+1)$-dimensional KPZ equation.

The identification of the universality class of experimental processes and numerical models have long been based on the numerical values of the scaling exponents. New insights have been gained by Prähofer and Spohn[153] via the study of PNG model by mapping the problem to the longest permutation of random Gaussian matrices. Thus they[153] arrived at different probability distributions such as Gaussian unitary ensemble (GUE) Tracy-Widom (TW), Gaussian orthogonal ensemble (GOE) TW, and stationary self-similar for the curved, flat and random initial conditions, respectively. The effects of these initial conditions on the growth have further been studied in various works. GUE TW distribution has been observed for sharp-wedge initial condition[161,162]. Calabrese and Doussal[21] mapped the one end free directed polymer to the flat initial condition KPZ equation and obtained GOE TW distribution. A universal crossover function from GOE TW to Baik-Rains (F_0) distribution has been studied in the experiment of turbulent liquid crystal (TLC) and numerical simulation of the PNG model by Takeuchi[177]. Imamura and Sasamoto[78] considered a two-sided Brownian motion as an initial condition and obtained an exact solution of the $(1+1)$-dimensional KPZ equation as a function of time t which goes to the Baik-Rains distribution asymptotically. Thus the probability distributions of the $(1+1)$-dimensional KPZ height fluctuations is governed by the nature of the initial conditions despite having the same scaling exponents[165]. In principle the probability distribution function can be obtained from the solution of the Fokker-Planck version[74,147] of the KPZ equation which is next to impossible due to the nonlinear term. A more viable way to obtain a partial information of the PDF is to calculate the higher order cumulants such as third, fourth and fifth cu-

mulants. These cumulants, when normalized with respect to the second cumulant, yield skewness, kurtosis and hyperskewness, respectively.

In this Chapter, we employ a diagrammatic approach and an RG scheme to calculate the fifth cumulant. We follow an RG approach without rescaling that was found to be successful for calculating the skewness[?] and kurtosis[170]. We evaluate the loop diagram for the fifth cumulant in the large scale and long time limits that yields $\tilde{S} = 0.0835$.

The rest of the Chapter is organized as follows. In Section II, the definition of hyperskewness in terms of moments and cumulants are presented. In Section III the calculations of fifth cumulant and the resulting hyperskewness is presented. Finally, a Discussion and Conclusion appear in in Section-IV.

4.2 Moments and Cumulants

Relations between moments and cumulants can be obtained by means of generating functions. The moment generating function $Z(\beta)$ and cumulant generating function $F(\beta)$ are defined as

$$Z(\beta) \equiv \langle e^{\beta h} \rangle = \sum_{n=0}^{\infty} \frac{\langle h^n \rangle}{n!} \beta^n \tag{4.3}$$

$$F(\beta) = \ln Z(\beta) = \sum_{n=1}^{\infty} \frac{\langle h^n \rangle_c}{n!} \beta^n, \tag{4.4}$$

respectibely where $\langle h^n \rangle$ is the nth moment and $\langle h^n \rangle_c$ is the nth cumulant, the angular bracket denotes an average with respect to the probability distribution. The relations among the first few moments and cumulants are expressed as

$$\begin{aligned}
\langle h \rangle &= \langle h \rangle_c \\
\langle h^2 \rangle &= \langle h^2 \rangle_c + \langle h \rangle_c^2 \\
\langle h^3 \rangle &= \langle h^3 \rangle_c + 3\langle h \rangle_c \langle h^2 \rangle_c + \langle h \rangle_c^3 \\
\langle h^4 \rangle &= \langle h^4 \rangle_c + 4\langle h \rangle_c \langle h^3 \rangle_c + 3\langle h^2 \rangle_c^2 + 6\langle h \rangle_c^2 \langle h^2 \rangle_c + \langle h \rangle_c^4 \\
\langle h^5 \rangle &= \langle h^5 \rangle_c + 5\langle h \rangle_c \langle h^4 \rangle_c + 10\langle h^2 \rangle_c \langle h^3 \rangle_c + 10\langle h \rangle_c^2 \langle h^3 \rangle_c \\
&\quad + 15\langle h \rangle_c \langle h^2 \rangle_c^2 + 10\langle h \rangle_c^3 \langle h^2 \rangle_c + \langle h \rangle_c^5 .
\end{aligned} \tag{4.5}$$

Since h represents height fluctuations with respect to the mean height, $\langle h(\mathbf{x},t)\rangle = 0$ in the stationary state. Consequently, the relevant quantities for hyperskewness are

$$\langle h^2\rangle_c = \langle h^2\rangle \tag{4.6}$$

and

$$\langle h^5\rangle_c = \langle h^5\rangle - 10\langle h^2\rangle\langle h^3\rangle. \tag{4.7}$$

Hyperskewness $\widetilde{S}$ is defined as

$$\widetilde{S} = \frac{\langle h^5\rangle_c}{\langle h^2\rangle_c^{5/2}} = \frac{\langle h^5\rangle}{\langle h^2\rangle^{5/2}} - 10\frac{\langle h^3\rangle}{\langle h^2\rangle^{3/2}}. \tag{4.8}$$

Contribution to nth cumulant $\langle h^n(\mathbf{x},t)\rangle_c$ comes from connected loop diagrams with n external legs.

4.3 The Fifth Cumulant

In this section, we calculate the fifth order cumulant via a renormalization scheme at one loop order. The Fourier transformation of $h(\mathbf{x},t)$ is expressed as

$$h(\mathbf{x},t) = \int \frac{d^dk\ d\omega}{(2\pi)^{d+1}} h(\mathbf{k},\omega)e^{i(\mathbf{k}\cdot\mathbf{x}-\omega t)} \tag{4.9}$$

The Fourier transformation of Eq. 5.1 leads to obtain the following form as

$$(-i\omega+\nu_0k^2)h(\mathbf{k},\omega) = \eta(\mathbf{k},\omega) - \frac{\lambda_0}{2}\int \frac{d^d\mathbf{q}d\Omega}{(2\pi)^{d+1}}[\mathbf{q}\cdot(\mathbf{k}-\mathbf{q})]h(\mathbf{q},\Omega)h(\mathbf{k}-\mathbf{q},\omega-\Omega) \tag{4.10}$$

We shall treat $[-i\omega+\nu_0k^2]^{-1} = G_0(k,\omega)$ as the bare propagator. The Fourier transformation of fifth cumulant is expressed as

$$\langle h^5(\mathbf{x},t)\rangle_c = \int \frac{d^{d+1}\hat{k}_1}{(2\pi)^{d+1}}\int \frac{d^{d+1}\hat{k}_2}{(2\pi)^{d+1}}\int \frac{d^{d+1}\hat{k}_3}{(2\pi)^{d+1}}\int \frac{d^{d+1}\hat{k}_4}{(2\pi)^{d+1}}\int \frac{d^{d+1}\hat{k}_5}{(2\pi)^{d+1}} e^{i(\hat{k}_1+\hat{k}_2+\hat{k}_3+\hat{k}_4+\hat{k}_5)\cdot\hat{x}}\ \langle h(\hat{k}_1)h(\hat{k}_2)h(\hat{k}_3)h(\hat{k}_4)h(\hat{k}_5)\rangle_c \tag{4.11}$$

where $\hat{x}\equiv(\mathbf{x},t)$ and $\hat{k}_i\equiv(\mathbf{k}_i,\omega_i)$. The connected loop diagram corresponding to the fifth order cumulant is shown in Fig. .

We write Eq. 4.11 in more compact form where the amputated part of the loop

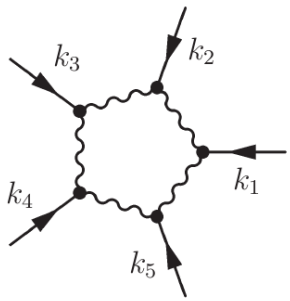

Figure 4.1: Feynman diagram corresponding to the fifth cumulant where the solid and wiggly lines represent the response and correlation functions, respectively

and the external legs are presented distinctly as

$$\langle h^5(\mathbf{x},t)\rangle_c = \int \frac{d^{d+1}\hat{k}_1}{(2\pi)^{d+1}} \int \frac{d^{d+1}\hat{k}_2}{(2\pi)^{d+1}} \int \frac{d^{d+1}\hat{k}_3}{(2\pi)^{d+1}} \int \frac{d^{d+1}\hat{k}_4}{(2\pi)^{d+1}} G(\hat{k}_1)G(\hat{k}_2)G(\hat{k}_3) G(\hat{k}_4)G(-\hat{k}_1-\hat{k}_2-\hat{k}_3-\hat{k}_4)L(\hat{k}_1,\hat{k}_2,\hat{k}_3,\hat{k}_4). \tag{4.12}$$

where L is the amputated part of the loop diagram (excluding the external legs). The unrenormalised (bare) form of the loop is written as

$$\begin{aligned} L^{(0)}(\hat{k}_1,\hat{k}_2,\hat{k}_3,\hat{k}_4) = \quad & 32\left(\frac{-\lambda_0}{2}\right)^5 (2D_0)^5 \int \frac{d^{d+1}\hat{q}_1}{(2\pi)^{d+1}} [\mathbf{q}_1\cdot(\mathbf{q}_1-\mathbf{k}_1)][\mathbf{q}_1\cdot(\mathbf{q}_1+\mathbf{k}_2)] \\ & \times[(\mathbf{q}_1+\mathbf{k}_2)\cdot(\mathbf{q}_1+\mathbf{k}_2+\mathbf{k}_3)][(\mathbf{q}_1+\mathbf{k}_2+\mathbf{k}_3)\cdot(\mathbf{q}_1+\mathbf{k}_2+\mathbf{k}_3+\mathbf{k}_4)] \\ & [(\mathbf{q}_4-\mathbf{k}_4)\cdot(\mathbf{k}_1+\mathbf{k}_2+\mathbf{k}_3+\mathbf{k}_4+\mathbf{k}_5)]G_0(\hat{q}_1)G_0(\hat{k_1}-\hat{q}_1) \\ & \times G_0(-\hat{q}_1)G_0(\hat{k}_2+\hat{q}_1)G_0(-\hat{q}_1-\hat{k}_2)G_0(\hat{k}_3+\hat{q}_1+\hat{k}_2)G_0(-\hat{q}_1-\hat{k}_2-\hat{k}_3) \\ & G_0(\hat{k}_4+\hat{q}_1+\hat{k}_2+\hat{k}_3)G_0(-\hat{q}_1-\hat{k}_2-\hat{k}_3-\hat{k}_4)G_0(\hat{q}_1+\hat{k}_5+\hat{k}_2+\hat{k}_3+\hat{k}_4) \end{aligned} \tag{4.13}$$

We shall find a renormalized equivalent of this bare quantity by means of a renormalization scheme employed earlier for the calculation of skewness and kurtosis[170?]. We perform the internal frequency integration in Eq. 4.13 and carry out the integration over the internal momentum restricted in the shell $\Lambda_0 e^{-r} \leq q \leq \Lambda_0$, leading to

$$L^{<}(r) = \frac{35}{8}\frac{\lambda_0^5 D_0^5}{\pi\nu_0^9\Lambda_0^7}\left[\frac{e^{7r}-1}{7}\right]. \tag{4.14}$$

Considering the iterative nature of the momentum shell elimination in the RG

scheme, we obtain the differential equation

$$\frac{dL}{dr} = \frac{35}{8}\frac{\lambda_0^5 D^5(r)}{\pi\nu^9(r)\Lambda^7(r)}. \tag{4.15}$$

For large r, $\Lambda(r) = \Lambda_0 e^{-r}$ is identified as the momentum k. Substituting the following functional forms

$$\nu(k) = \lambda_0\sqrt{\frac{D_0}{2\pi\nu_0}}k^{-1/2}, \tag{4.16}$$

and

$$D(k) = \lambda_0\sqrt{\frac{D_0}{2\pi\nu_0}}k^{-1/2}, \tag{4.17}$$

we integrate the differential equation Eq. 4.15 and obtain

$$L(r) = \frac{7\pi}{2}\lambda_0\frac{D_0^3}{\nu_0^3\Lambda_0^5}e^{5r}. \tag{4.18}$$

This expression for the renormalized loop needs to be expressed as a symmetric combination of the external momentum $\hat{k}_i$. Consequently $\Lambda_0 e^{-r}$ is expressed as the fully symmetric combination

$$L(\mathbf{k}_1,0;\mathbf{k}_2,0;\mathbf{k}_3,0;\mathbf{k}_4,0) = \frac{7\pi}{2}\lambda_0\left(\frac{D_0}{\nu_0}\right)^3 k_1^{-5/4}k_2^{-5/4}k_3^{-5/4}k_4^{-5/4} \tag{4.19}$$

for vanishing external frequencies. The frequency dependence is constructed by considering a scaling fuction of the form

$$k_i^{5/4} f_5\left(\frac{\omega_i}{k_i^z}\right) = \frac{1}{k_i^{11/4}\nu^2(k_i)|G(k_i,\omega_i)|^2}. \tag{4.20}$$

This form satisfies the property of real valuedness and it has the desired zero frequency (long time) limit. Consequently, the renormalized loop in Fig. is written as

$$\begin{aligned} L(\mathbf{k}_1,\omega_1;\mathbf{k}_2,\omega_2;\mathbf{k}_3,\omega_3;\mathbf{k}_4,\omega_4) = \quad & \frac{7\pi}{2}\lambda_0\left(\frac{D_0}{\nu_0}\right)^3 k_1^{11/4}k_2^{11/4}k_3^{11/4}k_4^{11/4}\nu^2(k_1)\nu^2(k_2)\nu^2(k_3)\nu^2(k_4) \\ & |G(k_1,\omega_1)|^2|G(k_2,\omega_2)|^2|G(k_3,\omega_3)|^2|G(k_4,\omega_4)|^2. \end{aligned} \tag{4.21}$$

Substituting from Eq. 4.21 in Eq. 4.12, and carrying out the frequency integrations

over ω_1, ω_2, ω_3 and ω_4, the fifth cumulant is obtained as

$$\langle h^5(\mathbf{x},t)\rangle_c = \frac{7}{4}\left(\frac{D_0}{2\pi\nu_0}\right)^{5/2}\int_{-\infty}^{\infty}dk_1\int_{-\infty}^{\infty}dk_2\int_{-\infty}^{\infty}dk_3\int_{-\infty}^{\infty}dk_4 \; J(k_1,k_2,k_3,k_4) \tag{4.22}$$

where

$$J(k_1,k_2,k_3,k_4) = \frac{X(k_1,k_2,k_3,k_4)}{Y(k_1,k_2,k_3,k_4)} \tag{4.23}$$

with

$$\begin{aligned} X(k_1,k_2,k_3,k_4) = \; & (-3|k_1|^6 - 3|k_2|^6 - 10|k_2|^{9/2}(2|k_3|^{3/2} + 2|k_4|^{3/2} + |k_1+k_2+k_3+k_4|^{3/2}) \\ & -10|k_1|^{9/2}(2|k_2|^{3/2} + 2|k_3|^{3/2} + 2|k_4|^{3/2} + |k_1+k_2+k_3+k_4|^{3/2}) \\ & -(|k_3|^{3/2} + |k_4|^{3/2} + |k_1+k_2+k_3+k_4|^{3/2})^2(3|k_3|^3 + 3|k_4|^3 + \\ & 4|k_4|^{3/2}|k_1+k_2+k_3+k_4|^{3/2} + |k_1+k_2+k_3+k_4|^3 \\ & +2|k_3|^{3/2}(7|k_4|^{3/2} + 2|k_1+k_2+k_3+k_4|^{3/2})) \\ & -2|k_2|^3(17|k_3|^3 + 17|k_4|^3 + 23|k_4|^{3/2}|k_1+k_2+k_3+k_4|^{3/2} \\ & +6|k_1+k_2+k_3+k_4|^3 + |k_3|^{3/2}(62|k_4|^{3/2} + 23|k_1+k_2+k_3+k_4|^{3/2})) \\ & -2|k_1|^3(17|k_2|^3 + 17|k_3|^3 + 17|k_4|^3 + 23|k_4|^{3/2}|k_1+k_2+k_3+k_4|^{3/2} \\ & +6|k_1+k_2+k_3+k_4|^3 + |k_3|^{3/2}(62|k_4|^{3/2} + 23|k_1+k_2+k_3+k_4|^{3/2}) \\ & +|k_2|^{3/2}(62|k_3|^{3/2} + 62|k_4|^{3/2} + 23|k_1+k_2+k_3+k_4|^{3/2}))) \end{aligned} \tag{4.24}$$

and

$$\begin{aligned} Y(k_1,k_2,k_3,k_4) \; & = 256|k_1|^{5/4}|k_2|^{5/4}|k_3|^{5/4}|k_4|^{5/4}(|k_1|^{3/2} + |k-2|^{3/2} + |k_3|^{3/2} \\ & +|k_4|^{3/2} + |k_1+k_2+k_3+k_4|^{3/2})^5 \end{aligned}$$

Considering the symmetry of the function $J(k_1,k_2,k_3,k_4)$, the integrations in Eq. 4.22 can be written as

$$\begin{aligned} \langle h^5(\mathbf{x},t)\rangle_c = \; & \frac{7}{4}\left(\frac{D_0}{2\pi\nu_0}\right)^{5/2}\int_{\mu}^{\infty}dk_1\int_{\mu}^{\infty}dk_2\int_{\mu}^{\infty}dk_3\int_{\mu}^{\infty}dk_4 \\ & [2J(k_1,k_2,k_3,k_4) + 8J(-k_1,k_2,k_3,k_4) \\ & +6J(-k_1,-k_2,k_3,k_4)]. \end{aligned} \tag{4.25}$$

where an infrared cut off μ has been set due to the infrared divergences in the

integrations. We write the integrations as

$$J_1(\mu) = \int_\mu^\infty dk_1 \int_\mu^\infty dk_2 \int_\mu^\infty dk_3 \int_\mu^\infty dk_4 J(k_1, k_2, k_3, k_4), \tag{4.26}$$

$$J_2(\mu) = \int_\mu^\infty dk_1 \int_\mu^\infty dk_2 \int_\mu^\infty dk_3 \int_\mu^\infty dk_4 J(-k_1, k_2, k_3, k_4) \tag{4.27}$$

and

$$J_3(\mu) = \int_\mu^\infty dk_1 \int_\mu^\infty dk_2 \int_\mu^\infty dk_3 \int_\mu^\infty dk_4 J(-k_1, -k_2, k_3, k_4) \tag{4.28}$$

So that Eq. 4.25 becomes

$$\langle h^5(\mathbf{x}, t)\rangle_c = \frac{7}{4}\left(\frac{D_0}{2\pi\nu_0}\right)^{5/2} [2J_1(\mu) + 8J_2(\mu) + 6J_3(\mu)] \tag{4.29}$$

The IR cut off dependent integrals are of the form

$$\begin{aligned} J_1(\mu) &= a_1 \mu^{-5/2} \\ J_2(\mu) &= a_2 \mu^{-5/2} \\ J_3(\mu) &= a_3 \mu^{-5/2} \end{aligned} \tag{4.30}$$

where a_1, a_2 and a_3 are dimensionless constants. Numerical integrations yield the dimensionless constants as

$$\begin{aligned} a_1 &= \lim_{\mu\to 0^+} [\mu^{5/2} J_1(\mu)] = 0.00197 \\ a_2 &= \lim_{\mu\to 0^+} [\mu^{5/2} J_2(\mu)] = 0.00607 \\ a_3 &= \lim_{\mu\to 0^+} [\mu^{5/2} J_3(\mu)] = 0.00583 \end{aligned} \tag{4.31}$$

via numerical convergences. Substituting Eqs. 4.31, 4.26, 4.27, 4.28, 4.30 in Eq. 4.29, we finally obtain the expression for fifth cumulant as

$$\langle h^5(\mathbf{x}, t)\rangle_c = \frac{7}{4}[2a_1 + 8a_2 + 6a_3]\left(\frac{D_0}{2\pi\nu_0}\right)^{5/2} \frac{1}{\mu^{5/2}} \tag{4.32}$$

4.4 Hyperskewness

To calculate the hyperskewness, the expression for the second cumulant is needed. The second cumulant in the frequency and momentum space is expressed as

$$\langle h^2(\mathbf{x},t)\rangle_c = \langle h^2(\mathbf{x},t)\rangle \quad = \int \frac{d^dk}{[2\pi]^d} \int \frac{d\omega}{[2\pi]} \int \frac{d^dk'}{(2\pi)^d} \int \frac{d\omega'}{2\pi} \langle h(\mathbf{k},\omega)h(\mathbf{k}',\omega')\rangle_c \; e^{i[(\mathbf{k}+\mathbf{k}')\cdot\mathbf{x}-(\omega+\omega')t]} \tag{4.33}$$

The Feynman loop corresponding to the correlation function is shown in Fig. **??**.

Figure 4.2: Feynman diagram corresponding to the second cumulant.

The frequency and momentum integrations in Eq. 6.35 can be evaluated [170?] and it can be obtained as

$$\langle h^2(\mathbf{x},t)\rangle_c = \frac{4}{\pi}\left(\frac{D_0}{2\pi\nu_0}\right)\frac{1}{\mu} \tag{4.34}$$

Using Eq. 4.32 and 4.34 in 4.8, we obtain

$$\widetilde{S} = \frac{\langle h^5(\mathbf{x},t)\rangle_c}{\langle h^2(\mathbf{x},t)\rangle_c^{5/2}} = \frac{7}{2}\left(\frac{\pi}{4}\right)^{5/2}(a_1+4a_2+3a_3) \tag{4.35}$$

Substituting the values of a_1, a_2 and a_3 in Eq. 4.35 we obtain

$$\widetilde{S} = 0.0835. \tag{4.36}$$

4.5 Discussion and Conclusion

In this Chapter, we considered the stochastic growth of a surface on a flat geometry (in the stationary state) governed by the $(1+1)$-dimensional KPZ equation. We followed a diagrammatic RG scheme to evaluate the Feynman diagram [Fig.] for the fifth cumulant at one loop order corresponding to the $(1+1)$-dimensional KPZ dynamics. We started with the unrenormalized loop with bare parameters (ν_0, λ_0 and D_0) and invoked a shell elimination scheme (belonging to the shell $\Lambda_0 e^{-r} \leq q \leq$

Λ_0) to obtain a differential equation (Eq. 4.15) representing the recursion relation for successive elimination of momenta in thin shells. The solution of the differential equation yielded the renormalized expression (Eq. 4.18) for the loop diagram. This facilitated the evaluation of the cumulant $\langle h^5(\mathbf{x},t)\rangle_c$ given by Eq. 4.12 involving renormalized quantities. The resulting integrals are found to be infrared divergent and hence $\langle h^5(\mathbf{x},t)\rangle_c$ depends on the infrared cutoff μ. The momentum integrals are evaluated numerically to obtain $\langle h^5(\mathbf{x},t)\rangle_c$ as given by Eq. 4.32. Normalizing this value with respect to the $\langle h^2(\mathbf{x},t)\rangle_c^{5/2}$ resulted in the hyperskewness value as $\widetilde{S} = 0.0835$. It is interesting to note that all parameters of the KPZ dynamics (ν_0, λ_0, D_0) and the momentum cutoffs (Λ_0 and μ) finally cancel out to yield this value, suggesting its universality.

Although there have been many studies on the lower order normalized moments such as skewness and kurtosis, the study of hyperskewness remains a rarity. However, there have been studies based on numerical models that focus on the probability distribution function belonging to the KPZ universality class[61,153,177]. In the steady state, this distribution is believed to be identical with the Baik-Rains distribution[61,177]. with zero mean[9,153].

The universal Baik-Rains F_0 distribution is a function of the solutions of the Painlevé-II equation, namely, $u''(x) = 2u^3(x) + xu(x)$. Hastings and McLeod[65] obtained a unique solution with the asymptotic boundary conditions $u(x) \sim -Ai(x)$ as $x \to \infty$ and $u(x) \sim \sqrt{x/2}$ as $x \to -\infty$ where $Ai(x)$ is the Airy function. To solve the Painlevé-II equation, Tracy and Widom performed a numerical integration[185]. Subsequently, Prähofer and Spohn[154] obtained an arbitrary high precision solution by performing Taylor expansions. The Baik-Rains distribution is obtained from these solutions via known mathematical relations. On the other hand, the Fredholm determinant representation of the random matrix theory has been observed to be conceptually simpler and more numerically efficient than Painlevé-II to obtain the probability distributions [47] (F_2, F_1, F_0, etc).

It may, however, be noted that the Baik-Rains value for hyperskewness is 0.3092, which may be obtained from Fredholm determinant representation[17] as well as from the numerical data via the solution of the Painlevé-II. This Baik-Rains value is distinctly higher than our calculated value $S = 0.0835$. This underestimation via the RG calculation is due to the fact that the method is based on a perturbative approach where the calculation is carried out only at one-loop order. Since the dynamics is governed by a white noise following a Gaussian distribution, the lowest order approximation appears to be influenced rather strongly by the Gaussian noise.

A similar trend was observed in the one-loop perturbative calculation for kurtosis, namely, $Q = 0.1523$ [170], which is lower than the Baik-Rains value 0.2892. However, the value for skewness via the perturbative scheme, namely, $S = 0.3237$ [169] is slightly lower than the Baik-Rains value 0.3594. Thus, it appears that the Gaussian white noise plays a more dominant role in the perturbative calculations for the higher order moments, namely, kurtosis and hyperskewness. More involved calculations with the incorporation of higher order contributions in the perturbative expansion are expected to yield better estimates for these higher order moments.

We note that it is next to impossible to obtain a closed-form analytical expression for the full probability distribution starting with the KPZ equation driven by the stochastic noise. Consequently, in an analytical approach, it is sufficient to evaluate a few lower and higher order moments (such as skewness, kurtosis and hyperskewness) from the governing dynamics. This outlook has motivated us to evaluate these numbers and we have seen that the analytical values for skewness, kurtosis and hyperskewness turn out to be $S = 0.3237$ [169], $Q = 0.1523$ [170] and $\widetilde{S} = 0.0835$ [Eq. 4.36], respectively. Thus, it is seen that the normalized cumulants decrease in magnitude with respect to the order of the cumulant. We thus expect that the value of the normalized sixth order cumulant would be a number smaller than $\widetilde{S}$. Consequently, this suggests that the values of S, Q and $\widetilde{S}$ capture most of the information contained in the full probability distribution.

Chapter 5

Steady-state skewness and kurtosis from renormalized cumulants in $(2+1)$-dimensional stochastic surface growth

5.1 Introduction

The scale invariant growth of a two dimensional surface is a subject of great significance in nonequilibrium statistical mechanics. This is due to its wide range of applicability in addition to its theoretical complexity[11,43,63,105,126]. It has almost been three decades that Kardar, Parisi, and Zhang[86] proposed a generic equation for surface growth, namely,

$$\frac{\partial h}{\partial t} = \nu_0 \nabla^2 h + \frac{\lambda_0}{2}(\nabla h)^2 + \eta, \tag{5.1}$$

known as the KPZ equation, where $h(\mathbf{x}, t)$ is the fluctuating height field and ν_0 is the surface tension. The surface grows due to aggregation of particles, modeled by the stochastic noise term $\eta(\mathbf{x}, t)$, which is considered to be Gaussian of zero average with the correlation

$$\langle \eta(\mathbf{x}, t)\eta(\mathbf{x}', t')\rangle = 2D_0\delta^d(\mathbf{x} - \mathbf{x}')\delta(t - t'), \tag{5.2}$$

where D_0 is referred to as the deposition noise strength and d is the dimension of the substrate.

The KPZ equation in one dimension plays an important role in the application domain. The $(1+1)$-dimensional KPZ equation has a semantic relation to a variety of systems. For example, directed polymers in random media (DPRM)[45,87], vorticity free fluid velocity described by the Burgers equation[47], the stochastic heat equation (SHE)[60], and even sequence alignments in proteins and genes[75,77], growth phenomena in bacteria colonies[71,191], turbulent liquid crystals (TLC)[178,179], slow combustion of a sheet of paper[124,129,134], etc., exhibit the same scaling exponents as the $(1+1)$-dimensional KPZ equation.

The KPZ equation has been analyzed through renormalization group[48,128], mode coupling calculation[49,73,189], and numerical simulations[6,46,97]. Moreover, the scaling functions[76], as well as scaling exponents and the probability distribution function have been studied through finite temperature DPRM in $(1+1)$ dimensions[58] and zero temperature DPRM in $(1+1)$ and $(2+1)$ dimensions[94].

A considerable amount of understanding of the probability distribution function and its dependence on the initial conditions (namely flat, curved, and stationary) has been achieved through the study of various analytical[21,78], numerical[153] and experimental[178–180] methods for different systems that are governed by the $(1+1)$-dimensional KPZ type dynamics. The evolution of a growing surface from a flat initial condition to the stationary state has been studied[177] both numerically (PNG) and experimentally (TLC). The corresponding crossover function is established as universal[61] by considering DPRM, stochastic heat equation (SHE) and growth models which share the universality class of the $(1+1)$-dimensional KPZ dynamics.

There exists no exact solution for the $(2+1)$-dimensional KPZ equation, which represents a wide variety of surface growth phenomena in real life. Recently the $(2+1)$-dimensional KPZ has been realized as an important problem where the higher dimensional analogs of TW GOE, TW GUE and Baik-Rains distribution have been investigated[59,60]. Kim *et al.*[94] studied the minimum energy distribution of directed polymer in random potential with Gaussian distribution up to $(3+1)$ dimensions and obtained non-Gaussian distribution in those dimensions. Halpin-Healy and Takeuchi[56], throughly explored the statistics of the higher dimensional DPRM that yield non-zero skewness and kurtosis values. Alves *et al.*[5] studied the higher dimensional KPZ height distributions via the RSOS model for flat initial condition and found the distributions to be non-Gaussian.

There have been a large number of numerical works on the $(2+1)$-dimensional KPZ type growth. For instance, the study of the RSOS model by Kim and Koster-

litz[97] leads to estimation of the scaling exponents that agree with their proposed relations $z = 2(d+2)/(d+3)$ and $\beta = 1/(d+2)$ for spatial dimensions $d \leq 4$. Kondev *et al.*[102] developed an approach wherein properties of scaling of loops of constant height are analyzed to conclude upon geometrical and roughness exponents. They obtained the roughness exponent $\chi = 0.38 \pm 0.08$ via nonlinear estimation. Quite a few growth models having a great deal of diversity, all of which belonging to the $(2+1)$-dimensional KPZ universality class, have been studied[59] for the morphology and statistics in the transient regime. The studied RSOS model, Euler integration of the KPZ equation and the mapping of the KPZ equation to a driven dimer model lead to roughness exponent $\chi = 0.383$, 0.388 and 0.375, respectively. On the other hand, for the stationary state, $\beta = 0.241 \pm 0.001$[60] and thereby via the well known KPZ scaling relation $\chi(1 + 1/\beta) = 2$ the roughness exponent is obtained as $\chi = 0.387$–0.390. Kelling and Odor[89] performed a simulation considering a huge size up to $2^{17} \times 2^{17}$ and estimated the scaling exponents $\chi = 0.393 \pm 0.004$ and $\beta = 0.2415$ where the growth exponent of the simulation is higher than $\beta = 0.221$[51] and $\beta = 0.229$[3]. Considering a potts-Spin representation via a multisite-coding with 11520^2 sites, Forrest and Tang[46] estimated $\chi = 0.385 \pm 0.005$. An effort via a Monte-Carlo simulation of the hypercube-stacking model of Tang *et al.* [182] yields the growth exponent $\beta = 0.240 \pm 0.001$. A numerically discretized RSOS model, studied by Marinari *et al.*[121] by means of multisurface coding, yields $\chi = 0.393 \pm 0.003$ and $\beta = 0.244 \pm 0.003$. Odor *et al.*[140] found $\chi = 0.395 \pm 0.005$ by mapping the driven lattice gases of d-dimers model onto the KPZ problem.

Theoretical calculation of χ in two and higher dimensions has been a challenging work. Analytical approaches such as the perturbative RG[48,86,128,137] and nonperturbative approaches, such as mode coupling[18,49,187,189] and self-consistent expansion[163] are incapable of giving any conclusive scaling exponents as well as universality in $d = 2$ dimension. Lässig[113] employed an operator product expansion and obtained $\chi = 2/5$ and $z = 8/5$. A mode coupling calculation of Colaiori and Moore[28] suggested the dynamic exponent $z = 1.62$ and roughness exponent $\chi = 0.38$. A nonperturbative field theoretic RG has been employed by Kloss[100] in the stationary state and obtained roughness exponent $\chi \simeq 0.373$ via amplitude ratio of temporal and spatial correlation[99].

There have been experiments that mimic the $(2+1)$-dimensional KPZ scaling and the distribution of height fluctuations. Growth of oligmer thin film due to vapor deposition on a silicon substrate[145] yields the roughness and growth exponents as

$\chi = 0.45 \pm 0.04$ and $\beta = 0.28 \pm 0.05$. For the same system, the measured value of skewness $S = 0.23$[186] in the transient regime indicates that the growth is in the $(2+1)$-dimensional KPZ universality class. It is interesting to note that Almeida *et al.* [4] studied the height fluctuations on a polycrystalline CdTe/Si(100) sample and measured $\beta = 0.27 \pm 0.04$.

From the knowledge of geometry dependent subclasses in $(1+1)$ dimensions, it is well known that the scaling exponents are not sufficient to understand the KPZ universality class. For the identification of the universality class, information about the whole distribution function is essential. Moreover, it has been suggested that the measurements of moments are more stable and accurate[126] than the scaling exponents.

Marinari *et al.*[121] estimated higher order moments through multi-surface coding in different dimensions. From their reported moments in 2D, the skewness and kurtosis can be calculated as $|S| \sim 0.266$ and $Q \sim 0.121$, respectively. Recently, two authors of the same group, Pagnani and Parisi[143] refined the study of $(2+1)$-dimensional KPZ-type growth in the steady state and estimated two sets of best-fit results, namely, FIT-I and FIT-II for roughness exponent, skewness and kurtosis values. They found roughness exponent $\chi = 0.3893 \pm 0.0006$ (FIT-I), $\chi = 0.3869 \pm 0.0004$ (FIT-II), skewness $|S| = 0.2669 \pm 0.0004$ (FIT-I), $|S| = 0.2657 \pm 0.0004$ (FIT-II) and kurtosis $Q = 0.146 \pm 0.002$(FIT-I), $Q = 0.145 \pm 0.001$ (FIT-II). Chin and den Nijs[26] have performed a numerical study of the $(2+1)$-dimensional KPZ equation in the stationary state and obtained the roughness exponent $\chi \approx 0.38$ considering finite size scaling. They concluded that the third moment is more stable and more sensitive (than the roughness exponent) so that it is more suitable to determine and verify the universality class. They found skewness $|S| = 0.27$ and excess kurtosis $Q = 0.15$ which are the same as those in Kim-Kosterlitz (KK) and BCSOS models, thus identifying them to belong to the universality class of the $(2+1)$-dimensional KPZ dynamics.

Halpin-Healy[60] has reported the value of average skewness ($S = 0.244$) and kurtosis ($Q = 0.177$) for three models namely, RSOS, $g5_1$ DPRM and KPZ Euler. In the literature, the roughness and dynamic exponents ($\chi \approx 0.39$, $z \approx 1.61$) have been estimated from a considerable amount of numerical effort. For the purpose of calculating the skewness and kurtosis in $(2+1)$ dimensions, we take $\chi = 9/23$ (and $z = 37/23$, satisfying $\chi + z = 2$) as the sole input. The advantage of taking χ as a rational number is to avoid uncontrollable truncation errors in the subsequent exponents occuring in the calculations. We thus write the renormalized surface

tension and noise amplitude as

$$\nu(k) = A\ k^{-9/23} \tag{5.3}$$

and

$$D(k) = B\ k^{-27/23} \tag{5.4}$$

where A and B are scale independent constants. The noise correlation in the Fourier space is written as

$$\langle \eta(\mathbf{k},\omega)\eta(\mathbf{k}',\omega')\rangle = 2D_0(2\pi)^d\delta^d(\mathbf{k}+\mathbf{k}')(2\pi)\delta(\omega+\omega'). \tag{5.5}$$

Although the scaling exponents and universality class of (1+1)-dimensional KPZ have been studied extensively, there are few numerical estimations of moments in the $(2+1)$-dimensional case, whereas analytical treatments are extremely rare. In this Chapter, we calculate the higher order statistical moments of height fluctuation of the (2+1)-dimensional flat KPZ equation in the stationary state. This is achieved by calculating the cumulants up to the fourth order by employing a perturbation scheme to obtain the connected loop diagrams.

This Chapter is organized in the following way. Section II and Section III present the calculations of the third and fourth cumulants, respectively. In Section IV, we calculate the second cumulant. Skewness and kurtosis values are obtained from the calculated cumulants in Section V. Finally discussions and conclusions are given in Section VI.

5.2 The Third Cumulant

Fourier transform of the KPZ equation (Eq. 5.1) is written as

$$(-i\omega+\nu_0k^2)h(\mathbf{k},\omega) = \eta(\mathbf{k},\omega) - \frac{\lambda_0}{2}\iint \frac{d^d\mathbf{q}d\Omega}{(2\pi)^{d+1}}[\mathbf{q}\cdot(\mathbf{k}-\mathbf{q})]h(\mathbf{q},\Omega)h(\mathbf{k}-\mathbf{q},\omega-\Omega), \tag{5.6}$$

which will be used for perturbation calculations of cumulants.

The third cumuant $\langle h^3(\mathbf{x},t)\rangle_c$ can be expressed in the Fourier space as

$$W_3 = \langle h^3(\mathbf{x},t)\rangle_c = \int \frac{d^dk_1\,d\omega_1}{(2\pi)^{d+1}}\int \frac{d^dk_2\,d\omega_2}{(2\pi)^{d+1}}\int \frac{d^dk_3\ d\omega_3}{(2\pi)^{d+1}}$$
$$\langle h(\mathbf{k}_1,\omega_1)\,h(\mathbf{k}_2,\omega_2)\,h(\mathbf{k}_3,\omega_3)\rangle_c\ e^{i(\mathbf{k}_1+\mathbf{k}_2+\mathbf{k}_3)\cdot\mathbf{x}}\,e^{-i(\omega_1+\omega_2+\omega_3)t} \tag{5.7}$$

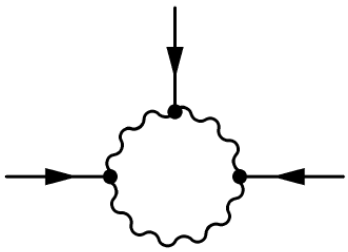

Figure 5.1: Feynman diagram corresponding to the third cumulant where a wiggly line represents correlation and solid line represents response.

The third cumulant in Eq. 5.7 is constructed by using Eq. 5.6 in a perturbative frame-work. We follow the diagrammatic approach and obtain a one-loop diagram which contributes to $\langle h^3(\mathbf{x},t)\rangle_c$ as shown in Fig. 5.1. Consequently, $\langle h^3(\mathbf{x},t)\rangle_c$ is written as

$$\langle h^3(\mathbf{x},t)\rangle_c = \int \frac{d^{d+1}\hat{k}_1}{(2\pi)^{d+1}} \int \frac{d^{d+1}\hat{k}_2}{(2\pi)^{d+1}}\, G(\hat{k}_1)\, G(\hat{k}_2)\, L_3(\hat{k}_1;\hat{k}_2)\, G(-\hat{k}_1-\hat{k}_2) \tag{5.8}$$

where $L_3(\hat{k}_1;\hat{k}_2)$ indicates the amputated loop (excluding the external legs) and $\hat{k}_1$ stands for $(\mathbf{k}_1,\omega_1)$. We first consider bare value of the loop integral[?] which is expressed as

$$L_3^{(0)}(\mathbf{k}_1,\omega_1;\mathbf{k}_2,\omega_2) = 8\left(\frac{-\lambda_0}{2}\right)^3 \int \frac{d^dq\, d\Omega}{(2\pi)^{d+1}}\, [(\mathbf{q}-\mathbf{k}_1)\cdot(\mathbf{k}_2+\mathbf{k}_1-\mathbf{q})]\,[\mathbf{q}\cdot(\mathbf{k}_1-\mathbf{q})]$$
$$[-\mathbf{q}\cdot(\mathbf{q}-\mathbf{k}_2-\mathbf{k}_1)]\, Q_0(\mathbf{q},\Omega)\, Q_0(\mathbf{k}_1-\mathbf{q},\omega_1-\Omega)\, Q_0(\mathbf{k}_1+\mathbf{k}_2-\mathbf{q},\omega_1+\omega_2-\Omega) \tag{5.9}$$

Frequency and momentum integrations are performed in Eq. 5.9 in the limit of zero external momenta and frequencies. This gives the leading order contribution in an expansion when the external momenta and frequencies are small with respect to internal ones in the loop integral. The momentum is integrated in the thin shell $\Lambda_0 e^{-r} \le q \le \Lambda_0$, yielding

$$L_3^{<}(r) = \frac{3}{2} K_d \frac{\lambda_0^3 D_0^3}{\nu_0^5 \Lambda_0^{4-d}} \frac{e^{(4-d)r}-1}{4-d}. \tag{5.10}$$

where $K_d = S_d/(2\pi)^d$ with S_d the surface area of unit sphere embedded in a d-dimensional space. Assuming that shell elimination is performed in recursive

steps[208], we obtain a differential equation for the scale dependent loop as

$$\frac{dL_3}{dr} = \frac{3}{2}K_d \frac{\lambda_0^3 D^3(r)}{\nu^5(r)\Lambda^{4-d}(r)} \tag{5.11}$$

where $\Lambda(r) = \Lambda_0 e^{-r}$. Using the scaling relations Eq. 5.3 and 5.4, and identifying k as $\Lambda_0 e^{-r}$, we integrate Eq. 5.11 over r, and obtain

$$L_3(r) = \lambda_0^3 \frac{69}{328\pi}\left(\frac{B^3}{A^5}\right)\Lambda_0^{-82/23} e^{82r/23} \tag{5.12}$$

for $d = 2$. Since $L_3(\hat{k}_1;\hat{k}_2)$ appearing in Eq. 5.8 represents the (renormalized) loop diagram, its value is determined by the independent momenta $\hat{k}_1$ and $\hat{k}_2$ that flow along two internal lines belonging to the loop. Moreover, $L_3(\hat{k}_1;\hat{k}_2)$ should be symmetric with respect to interchange of momenta $\hat{k}_1$ and $\hat{k}_2$ because the right hand expression in Eq. (5.8) is expected to be symmetric with respect to the same momentum exchange. Consequently, we construct the momentum dependence in $L_3(\hat{k}_1;\hat{k}_2)$ by considering $\Lambda_0 e^{-r}$ in Eq. (5.8) as $k_1^{1/2}k_2^{1/2}$. To obtain the dependence on the corresponding external frequencies ω_1 and ω_2, we identify $(\Lambda_0 e^{-r})^{-41/23}$ as $k_i^{-41/23} f_1\left(\frac{\omega_i}{k_i^z}\right)$ where $f_1(.)$ is a dimensionless scaling function given by

$$k_i^{-41/23} f_1\left(\frac{\omega_i}{k_i^z}\right) = k_i^{143/23}\nu^4(k_1)|G(k_i,\omega_i)|^4 \tag{5.13}$$

with $i = 1, 2$. We thus write

$$L_3(\hat{k}_1;\hat{k}_2) = \lambda_0^3 \frac{69}{328\pi}\left(\frac{B^3}{A^5}\right) k_1^{143/23}k_2^{143/23}\nu^4(k_1)\nu^4(k_2)|G(\mathbf{k}_1,\omega_1)|^4|G(\mathbf{k}_2,\omega_2)|^4. \tag{5.14}$$

Using the expression from Eq. 5.14 in Eq. 5.8, we obtain

$$\langle h^3(\mathbf{x},t)\rangle_c = \frac{69}{328\pi}(\lambda_0 AB)^3 \int \frac{d^{d+1}\hat{k}_1}{(2\pi)^{d+1}} \int \frac{d^{d+1}\hat{k}_2}{(2\pi)^{d+1}} k_1^{107/23}k_2^{107/23}|G(\hat{k}_1)|^4|G(\hat{k}_2)|^4 G(\hat{k}_1)G(\hat{k}_2)$$

$$G(-\hat{k}_1 - \hat{k}_2) \tag{5.15}$$

We perform the frequency integrations over ω and ω', leading to

$$\langle h^3(\mathbf{x},t)\rangle_c = \lambda_0^3\left(\frac{B}{A^2}\right)^3 \frac{69}{328\pi}\int \frac{d^2k_1}{(2\pi)^2}\int \frac{d^2k_2}{(2\pi)^2}F(\mathbf{k}_1,\mathbf{k}_2) \tag{5.16}$$

The algebric form of the function $F(\mathbf{k}_1,\mathbf{k}_2)$ is given in Appendix. We perform

the integrations in Eq. 5.16 in cartesian coordinates. The function $F(\mathbf{k}_1, \mathbf{k}_2)$ is symmetric with respect to interchange of $\mathbf{k}_1$ and $\mathbf{k}_2$. Consequently, we can write

$$I = \int d^2k_1 \int d^2k_2 F(\mathbf{k}_1, \mathbf{k}_2) = 4[I_1(\mu) + 2I_2(\mu) + I_3(\mu)] \tag{5.17}$$

where

$$I_1(\mu) = \int_0^\infty dk_{1x} \int_0^\infty dk_{2x} \int_\mu^\infty dk_{1y} \int_\mu^\infty dk_{2y} F(k_{1x}, k_{1y}, k_{2x}, k_{2y}), \tag{5.18}$$

$$I_2(\mu) = \int_0^\infty dk_{1x} \int_0^\infty dk_{2x} \int_\mu^\infty dk_{1y} \int_\mu^\infty dk_{2y} F(k_{1x}, -k_{1y}, k_{2x}, k_{2y}), \tag{5.19}$$

and

$$I_3(\mu) = \int_0^\infty dk_{1x} \int_0^\infty dk_{2y} \int_\mu^\infty dk_{2x} \int_\mu^\infty dk_{1y} F(-k_{1x}, -k_{1y}, k_{2x}, k_{2y}) \tag{5.20}$$

where we have introduced an infrared cutoff μ because these integrals diverges at the lower limit. We perform numerical integrations of these functions over k_{1x}, k_{1y}, k_{2x} and k_{2y}, leading to the values

$$I_1(\mu) = 0.032196\ \mu^{-27/23}, \tag{5.21}$$

$$I_2(\mu) = 0.062963\ \mu^{-27/23}, \tag{5.22}$$

$$I_3(\mu) = 0.0043277\ \mu^{-27/23}, \tag{5.23}$$

for very small values of μ close to zero. The value of the third cumulant coming from Eq. 5.16, in terms of these integration values, is given by

$$\langle h^3(\mathbf{x}, t)\rangle_c = \left(\frac{\lambda_0 B}{A^2}\right)^3 \frac{69}{328\pi} \frac{1}{4\pi^4} \left[I_1(\mu) + 2I_2(\mu) + I_3(\mu)\right]. \tag{5.24}$$

5.3 The Fourth Cumulant

The fourth order cumulant, written in Fourier space, assumes the form

$$\begin{aligned} \langle h^4(\mathbf{x}, t)\rangle_c \;=\; & \int \frac{d^{d+1}\hat{k}_1}{(2\pi)^{d+1}} \int \frac{d^{d+1}\hat{k}_2}{(2\pi)^{d+1}} \int \frac{d^{d+1}\hat{k}_3}{(2\pi)^{d+1}} \int \frac{d^{d+1}\hat{k}_4}{(2\pi)^{d+1}} \\ & \langle h(\hat{k}_1) h(\hat{k}_2) h(\hat{k}_3) h(\hat{k}_4)\rangle_c\, e^{i(\hat{k}_1+\hat{k}_2+\hat{k}_3+\hat{k}_4)\cdot\hat{x}}. \end{aligned} \tag{5.25}$$

Following the diagrammatic approach, we obtain a connected loop diagram for the fourth order cumulant in Fourier space occurring in the integrand. The corresponding loop diagram is shown in Fig. 5.2, which suggests the expression

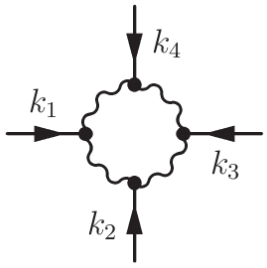

Figure 5.2: Feynman diagram corresponding to the fourth cumulant where a wiggly line represents correlation and solid line response.

$$\begin{aligned}\langle h^4(\mathbf{x},t)\rangle_c &= \int \frac{d^{d+1}\hat{k}_1}{(2\pi)^{d+1}} \int \frac{d^{d+1}\hat{k}_2}{(2\pi)^{d+1}} \int \frac{d^{d+1}\hat{k}_3}{(2\pi)^{d+1}} G(\hat{k}_1)\, G(\hat{k}_2)\, G(\hat{k}_3) \\ &\quad L_4(\hat{k}_1;\hat{k}_2;\hat{k}_3)\, G(-\hat{k}_1-\hat{k}_2-\hat{k}_3), \end{aligned} \tag{5.26}$$

where $L_4(\hat{k}_1;\hat{k}_2;\hat{k}_3)$ is the contribution coming from the renormalized amputated loop (without the external legs) and $G(\hat{k}_i)$ are the renormalized propagators.

The unrenormalized expression for the amputated loop, in $(d+1)$ dimensions, corresponding to the fourth order cumulant is expressed as[170]

$$\begin{aligned} L_4^{(0)}(\hat{k}_1;\hat{k}_2;\hat{k}_3) &= 16\left(-\frac{\lambda_0}{2}\right)^4 (2D_0)^4 \int \frac{d^{d+1}\hat{q}}{(2\pi)^{d+1}} [\mathbf{q}\cdot(\mathbf{q}-\mathbf{k}_1)][\mathbf{q}\cdot(\mathbf{k}_2+\mathbf{q})] \\ &\quad [(\mathbf{q}+\mathbf{k}_2)\cdot(\mathbf{k}_3+\mathbf{k}_2+\mathbf{q})][(\mathbf{q}-\mathbf{k}_1)\cdot(\mathbf{q}+\mathbf{k}_2+\mathbf{k}_3)] G_0(\hat{q}) \\ &\quad G_0(-\hat{q}+\hat{k}_1) G_0(-\hat{q}) G_0(\hat{q}+\hat{k}_2) G_0(-\hat{q}-\hat{k}_2) G_0(\hat{q}+\hat{k}_3+\hat{k}_2) \\ &\quad G_0(\hat{q}-\hat{k}_1) G_0(-\hat{q}-\hat{k}_2-\hat{k}_3), \end{aligned} \tag{5.27}$$

where the suffix 0 signifies unrenormalized quantities. Carrying out the frequency and momentum integration in Eq. 5.27, we obtain the following expression on elimination of modes from the shell $\Lambda(r) \le q \le \Lambda_0$.

$$L_4^<(r) = \frac{5}{2} K_d \frac{\lambda_0^4 D_0^4}{\nu_0^7 \Lambda_0^{6-d}} \frac{e^{(6-d)r}-1}{d-6} \tag{5.28}$$

Assuming that shell elimination is performed in recursive steps, we obtain

$$\frac{dL_4}{dr} = \frac{5}{2} K_d \frac{\lambda_0^4 D^4(r)}{\nu^7(r)\Lambda^{6-d}(r)} \tag{5.29}$$

Employing Eq. 5.3 and 5.4 with k identified as $\Lambda_0 e^{-r}$ and integrating Eq. 5.29 over r for $d = 2$ substrate dimensions, we obtain

$$L_4(r) = \frac{115}{548\pi} \left[\frac{\lambda_0^4 D^4(r)}{\nu^7(r)\Lambda^4(r)} \right]. \tag{5.30}$$

Since the loop $L_4(\hat{k}_1; \hat{k}_2; \hat{k}_3)$ depends on the three external momenta k_1, k_2 and k_3, the expression for $L_4(\hat{k}_1; \hat{k}_2; \hat{k}_3)$ appearing in Eq. 5.26 is expected to be symmetric with respect to interchange of $\hat{k}_1$, $\hat{k}_2$ and $\hat{k}_3$. Thus the momentum dependence is constructed by considering $\Lambda_0 e^{-r}$ in Eq. 5.30 as $k_1^{1/3} k_2^{1/3} k_3^{1/3}$. To obtain the dependence on external frequencies ω_1, ω_2 and ω_3, we identify $(\Lambda_0 e^{-r})^{-137/69}$ as $k_j^{-137/69} f_2\left(\frac{\omega_j}{k_j^z}\right)$ where $f_2(.)$ is a dimensionless scaling function. The form of the scaling function is introduced as

$$k_j^{-137/69} f_2\left(\frac{\omega_j}{k_j^z}\right) = k_j^{415/69} \nu^4(k_j) |G(k_j, \omega_j)|^4 \tag{5.31}$$

where $\hat{k}_j$ represents $\hat{k}_1$ or $\hat{k}_2$ or $\hat{k}_3$. Employing this scaling relation, the renormalized loop in Fig. 5.3 assumes the form

$$L_4(\hat{k}_1; \hat{k}_2; \hat{k}_3) = \lambda_0^4 \left(\frac{B^4}{A^7}\right) \frac{115}{548\pi} \prod_{j=1}^{3} k_j^{415/69} \nu^4(k_j) |G(\hat{k}_j)|^4 \tag{5.32}$$

Using the expression from Eq. 5.32 in Eq. 5.26, we obtain

$$\begin{aligned} \langle h^4(\mathbf{x}, t) \rangle_c \;=\; & \lambda_0^4 A^5 B^4 \frac{115}{548\pi} \int \frac{d^{d+1}\hat{k}_1}{(2\pi)^{d+1}} \int \frac{d^{d+1}\hat{k}_2}{(2\pi)^{d+1}} \int \frac{d^{d+1}\hat{k}_3}{(2\pi)^{d+1}} G(-\hat{k}_1 - \hat{k}_2 - \hat{k}_3) \\ & \prod_{j=1}^{3} k_j^{307/69} |G(\hat{k}_j)|^4 G(\hat{k}_j) \end{aligned} \tag{5.33}$$

where the response function involves the renormalized surface tension $\nu(\mathbf{k})$. Carrying out the frequency integrations yields

$$\langle h^4(\mathbf{x}, t) \rangle_c = \left(\frac{\lambda_0 B}{A^2}\right)^4 \frac{115}{548\pi} \int \frac{d^2 k_1}{(2\pi)^2} \int \frac{d^2 k_2}{(2\pi)^2} \int \frac{d^2 k_3}{(2\pi)^2} T(\mathbf{k}_1, \mathbf{k}_2, \mathbf{k}_3) \tag{5.34}$$

where the form of $T(\mathbf{k}_1, \mathbf{k}_2, \mathbf{k}_3)$ is given in Appendix. For brevity in notations, henceforth we rename the momenta $\mathbf{k}_1$, $\mathbf{k}_2$ and $\mathbf{k}_3$ as $\mathbf{k}$, $\mathbf{p}$ and $\mathbf{q}$. Subsequently, we express the integrations in cartesian coordinates, so that

$$\langle h^4(\mathbf{x},t)\rangle_c = \frac{\lambda_0^4}{(2\pi)^6}\frac{B^4}{A^8}\frac{115}{548\pi}[\int_{-\infty}^{\infty}dk_x\int_{-\infty}^{\infty}dk_y\int_{-\infty}^{\infty}dp_x\int_{-\infty}^{\infty}dp_y \int_{-\infty}^{\infty}dq_x\int_{-\infty}^{\infty}dq_y T(k_x,k_y;p_x,p_y;q_x,q_y)] \tag{5.35}$$

Due to the symmetry of the integrand in momentum variables, we can break the function as

$$\langle h^4(\mathbf{x},t)\rangle_c = \frac{4}{(2\pi)^6}\left(\frac{\lambda_0 B}{A^2}\right)^4\frac{115}{548\pi}\int_0^{\infty}dk_x\int_0^{\infty}dk_y\int_0^{\infty}dp_x\int_0^{\infty}dp_y\int_0^{\infty}dq_x\int_0^{\infty}dq_y \{T(k_x,k_y;p_x,p_y;q_x,q_y)+6T(k_x,-k_y;p_x,p_y;q_x,q_y)+9T(-k_x,-k_y;p_x,p_y;q_x,q_y)\} \tag{5.36}$$

The momentum dependence causes the integrations to diverge in the infrared limit. Therefore, we set μ as the lower cutoff of the integrations and express the integration in terms of

$$J_1(\mu) = \int_0^{\infty}dk_x\int_0^{\infty}dk_y\int_0^{\infty}dp_x\int_{\mu}^{\infty}dp_y\int_{\mu}^{\infty}dq_x\int_{\mu}^{\infty}dq_y T(k_x,k_y;p_x,p_y;q_x,q_y), \tag{5.37}$$

$$J_2(\mu) = \int_0^{\infty}dk_x\int_0^{\infty}dk_y\int_0^{\infty}dp_x\int_{\mu}^{\infty}dp_y\int_{\mu}^{\infty}dq_x\int_{\mu}^{\infty}dq_y T(k_x,-k_y;p_x,p_y;q_x,q_y) \tag{5.38}$$

and

$$J_3(\mu) = \int_0^{\infty}dk_x\int_0^{\infty}dk_y\int_0^{\infty}dp_x\int_{\mu}^{\infty}dp_y\int_{\mu}^{\infty}dq_x\int_{\mu}^{\infty}dq_y T(-k_x,-k_y;p_x,p_y;q_x,q_y) \tag{5.39}$$

so that

$$\langle h^4(\mathbf{x},t)\rangle_c = \frac{4}{(2\pi)^6}\left(\frac{\lambda_0 B}{A^2}\right)^4\frac{115}{548\pi}\left[J_1(\mu)+6J_2(\mu)+9J_3(\mu)\right]. \tag{5.40}$$

Performing the integrations numerically, we obtain

$$J_1(\mu) = 0.0069369\mu^{-36/23}, \tag{5.41}$$

$$J_2(\mu) = 0.0000151\mu^{-36/23}, \tag{5.42}$$

and

$$J_3(\mu) = 0.0219628\mu^{-36/23}. \tag{5.43}$$

We shall employ these numerical values in the next Section while calculating the value of kurtosis.

5.4 The Second Cumulant

In order to calculate the skewness and kurtosis, we need in addition to the third and fourth, the second cumulant. The first moment, $\langle h(\mathbf{x},t)\rangle$, is zero in the steady state, where the angular brackets denote as ensemble average. The second cumulant is expressed in the Fourier space as

$$W_2 = \langle h^2(\mathbf{x},t)\rangle_c = \int \frac{d^d k d\omega}{(2\pi)^{d+1}} \int \frac{d^d k' d\omega'}{(2\pi)^{d+1}} \langle h(\mathbf{k},\omega) h(\mathbf{k}',\omega')\rangle_c e^{i(\mathbf{k}+\mathbf{k}')\cdot\mathbf{x}} e^{-i(\omega+\omega')t}. \tag{5.44}$$

where the height-height correlation is given by

$$\langle h(\mathbf{k},\omega) h(\mathbf{k}',\omega')\rangle = Q(\mathbf{k},\omega)(2\pi)^d \delta^d(\mathbf{k}+\mathbf{k}')(2\pi)\delta(\omega+\omega') \tag{5.45}$$

with $Q(\mathbf{k},\omega)$ the renormalized correlation. Using Eq. (5.45) in Eq. (5.44) leads to

$$\langle h^2(\mathbf{x},t)\rangle_c = \int \frac{d^d k\ d\omega}{(2\pi)^{d+1}} Q(\mathbf{k},\omega). \tag{5.46}$$

The correlation, $Q(\mathbf{k},\omega)$, can be obtained perturbatively using Eqs. (5.6) and (5.45). To obtain the leading order contribution to the second cumulant, we consider the one loop diagram shown in Fig. 5.3, that satisfies the expression

$$Q(\mathbf{k},\omega) = G(\mathbf{k},\omega) L_2(\mathbf{k},\omega) G(-\mathbf{k},-\omega) \tag{5.47}$$

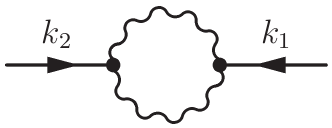

Figure 5.3: Feynman diagram corresponding to the second cumulant where a wiggly line represents correlation and solid line response.

Equation 5.47 corresponds to the loop diagram in Fig. 5.3. The unrenormalized

amputated loop (excluding the external legs) is expressed as

$$L_2^{(0)}(\mathbf{k},\omega) = 2\left(\frac{-\lambda_0}{2}\right)^2 \int_{\Lambda(r)}^{\Lambda_0} \frac{d^dq}{(2\pi)^d} \int_{-\infty}^{\infty} \frac{d\omega}{(2\pi)} [\mathbf{q}\cdot(\mathbf{k}-\mathbf{q})]^2 |G_0(\hat{\mathbf{q}})|^2 |G_0(\hat{\mathbf{k}}-\hat{\mathbf{q}})|^2 |(2D_0)^2 \tag{5.48}$$

that contains unrenormalized noise amplitude D_0 and unrenormalized response function $G_0(\mathbf{k},\omega) = [-i\omega + \nu_0 k^2]^{-1}$. Carrying out the frequency integration in the whole range and the momentum integration in the shell $\Lambda_0 e^{-r} \leq q \leq \Lambda_0$, we obtain

$$L_2^{<}(r) = \frac{\lambda_0^2 D_0^2 K_d}{2\nu_0^3} \left[\frac{\Lambda_0^{d-2} - \Lambda^{d-2}(r)}{(d-2)}\right]. \tag{5.49}$$

We construct a differential equation for L_2 with respect to the scale parameter r,

$$\frac{dL_2}{dr} = K_d \frac{\lambda_0^2 D^2(r)}{2\nu^3(r)\Lambda^{2-d}(r)} \tag{5.50}$$

where $\Lambda(r) = \Lambda_0 e^{-r}$. Using the scale dependence from Eqs. 5.3 and 5.4, and integrating over r leads to

$$L_2(r) = \frac{23}{108\pi}\left(\frac{\lambda_0^2 B^2}{A^3}\right)(\Lambda_0 e^{-r})^{-27/23} \tag{5.51}$$

for $d = 2$. We consider the scale dependent parameter $(\Lambda_0 e^{-r})^{-27/23}$ as $k^{-27/23}\, f\left(\frac{\omega}{k^z}\right)$, where $f(.)$ dimensionless scaling function and z is the dynamic exponent. Thus $L_2(\mathbf{k};\omega)$ is expressed as

$$L_2(\mathbf{k};\omega) = \frac{23}{108\pi}\left(\frac{\lambda_0^2\ B^2}{A^3}\right) k^{-27/23}\ f\left(\frac{\omega}{k^z}\right). \tag{5.52}$$

As before, we write

$$k^{-27/23} f\left(\frac{\omega}{k^z}\right) = k^{3861/943} \nu^{108/41}(k) |G(\mathbf{k},\omega)|^{108/41} \tag{5.53}$$

so that $L_2(\mathbf{k};\omega)$ becomes

$$L_2(\mathbf{k};\omega) = \frac{23}{108\pi}\left(\frac{\lambda_0^2\ B^2}{A^3}\right) k^{3861/943} \nu^{108/41}(k)\ |G(\mathbf{k},\omega)|^{108/41} \tag{5.54}$$

From Eqs. 5.46 and 5.47, we have

$$\langle h^2(\mathbf{x},t)\rangle_c = \int \frac{d^dk}{(2\pi)^d} \int \frac{d\omega}{(2\pi)} |G(\mathbf{k},\omega)|^2 L_2(\mathbf{k};\omega) \tag{5.55}$$

where we substitute the expression for L_2 given by Eq. 5.54, so that

$$\langle h^2(\mathbf{x},t)\rangle_c = \frac{23}{108\pi}\left(\frac{\lambda_0^2 B^2}{A^3}\right) A^{108/41} \int \frac{d^2k}{(2\pi)^2} k^{2889/943} \int \frac{d\omega}{(2\pi)} \frac{1}{[\omega^2+\nu^2(k)k^4]^{95/41}}, \tag{5.56}$$

where the surface tension $\nu(k)$ in the denominator is renormalized. Performing the frequency integration and expressing the momentum integration in cartesian coordinates, we obtain

$$\langle h^2(\mathbf{x},t)\rangle_c = \frac{23}{108\pi}\left(\frac{\lambda_0 B}{A^2}\right)^2 \left(\frac{\Gamma\left(\frac{149}{82}\right)}{2\sqrt{\pi}\,\Gamma\left(\frac{95}{41}\right)}\right) \left[\frac{4}{4\pi^2}\int_0^\infty dk_x \int_0^\infty dk_y \frac{1}{[k_x^2+k_y^2]^{32/23}}\right]. \tag{5.57}$$

The factor of 4 appears because the integrand is an even function of k_x and k_y. Moreover, the integration in the Eq. 5.57 is symmetric with respect to interchange of k_x and k_y. We first do the momentum integration over k_x with limits, $0 \le k_x \le \infty$ yielding

$$\langle h^2(\mathbf{x},t)\rangle_c = \frac{23}{108\pi^3}\left(\frac{\lambda_0 B}{A^2}\right)^2 \left(\frac{\Gamma\left(\frac{149}{82}\right)}{2\sqrt{\pi}\,\Gamma\left(\frac{95}{41}\right)}\right) \left(\frac{\sqrt{\pi}}{2}\frac{\Gamma\left(\frac{41}{46}\right)}{\Gamma\left(\frac{32}{23}\right)}\right) \left[\int_\mu^\infty dk_y k_y^{-41/23}\right] \tag{5.58}$$

We have introduced an infrared cutoff μ as the integral on k_y diverges at the lower limit. We thus obtain by integration

$$\langle h^2(\mathbf{x},t)\rangle_c = [0.211105\times 10^{-2}] \left(\frac{\lambda_0 B}{A^2}\right)^2 \frac{1}{\mu^{18/23}} \tag{5.59}$$

where we have used $\Gamma\left(\frac{149}{82}\right) = 0.936026$, $\Gamma\left(\frac{95}{41}\right) = 1.178818$, $\Gamma\left(\frac{41}{46}\right) = 1.075746$ and $\Gamma\left(\frac{32}{23}\right) = 0.887772$. This is the second cumulant of the height fluctuations in the stationary state of the $2+1$ KPZ equation.

5.5 Skewness and Kurtosis

In this section, we calculate the skewness and kurtosis of the height fluctuations obeying the $(2+1)$-dimensional KPZ equation in the stationary state. For this purpose, we use the values of the second, third and fourth order moments evaluated above. The n th moments is expressed as

$$W_n = \langle [h(\mathbf{x},t) - \langle h\rangle]^n\rangle \tag{5.60}$$

which is related to the system size as $W_n \sim L^{n\chi}$, where L is the size of the system. Substituting $n = 3$ and 4 in Eq. 5.60, we obtain the expressions

$$W_2 = \langle h^2 \rangle - \langle h \rangle^2, \tag{5.61}$$

$$W_3 = \langle h^3 \rangle - 3\langle h \rangle \langle h^2 \rangle + 2\langle h \rangle^3$$

$$W_4 = \langle h^4 \rangle - 4\langle h \rangle \langle h^3 \rangle + 6\langle h^2 \rangle \langle h \rangle^2 - 3\langle h^2 \rangle^2. \tag{5.62}$$

The moments and cumulants are related as

$$\begin{aligned} \langle h \rangle &= \langle h \rangle_c \\ \langle h^2 \rangle &= \langle h^2 \rangle_c + \langle h \rangle_c^2 \\ \langle h^3 \rangle &= \langle h^3 \rangle_c + 3\langle h \rangle_c \langle h^2 \rangle_c + \langle h \rangle_c^3 \\ \langle h^4 \rangle &= \langle h^4 \rangle_c + 4\langle h \rangle_c \langle h^3 \rangle_c + 3\langle h^2 \rangle_c^2 + 6\langle h \rangle_c^2 \langle h^2 \rangle_c + \langle h \rangle_c^4 \end{aligned} \tag{5.63}$$

These higher order moments determine the values of skewness and kurtosis. Taking ensemble average on both sides of Eq. (6), we find that both terms on the right hand side vanish because the noise is Gaussian and the second term yields a Dirac delta function $\delta^d(\mathbf{k})$ upon using Eq. (45). Finiteness of the substrate (although it is assumed to be large) implies that $\langle h \rangle = 0$. Thus, skewness and kurtosis may be expressed as

$$S = \frac{\langle h^3 \rangle}{\langle h^2 \rangle^{3/2}} = \frac{\langle h^3 \rangle_c}{\langle h^2 \rangle_c^{3/2}} \tag{5.64}$$

and

$$Q = \frac{\langle h^4 \rangle}{\langle h^2 \rangle^2} - 3 = \frac{\langle h^4 \rangle_c}{\langle h^2 \rangle_c^2} \tag{5.65}$$

where the suffix c indicates the cumulants that correspond to connected diagramms in the perturbative expansion. Skewness S measures the asymmetry of the distribution function with respect to the Gaussian. A positive (negative) value of skewness is obtained when the distribution has a longer tail on the right (left) side. The Q value indicates sharpness with respect to the Gaussian distribution. A positive (negative) value of Q signifies a sharper (flatter) distribution than the Gaussian.

We obtain the skewness and kurtosis employing the above definitions. Using the

numerically evaluated integrations of $I_1(\mu)$, $I_2(\mu)$ and $I_3(\mu)$ in Eq. 5.24, we obtain

$$\langle h^3(\mathbf{x},t)\rangle_c = [0.027922 \times 10^{-3}] \left(\frac{\lambda_0 B}{A^2}\right)^3 \mu^{-27/23}. \tag{5.66}$$

Substituting from equations 6.45 and 5.66 in Eq. 5.64, we calculate the skewness of the $(2+1)$-dimensional KPZ height distribution as

$$S = \frac{\langle h^3(\mathbf{x},t)\rangle_c}{\langle h^2(\mathbf{x},t)\rangle_c^{3/2}} = \frac{0.027922}{(0.211105)^{3/2}} = 0.2879. \tag{5.67}$$

Similarly, we substitute the results of the evaluated numerical integrations $J_1(\mu)$, $J_2(\mu)$ and $J_3(\mu)$ in Eq. 5.40, obtaining

$$\langle h^4(\mathbf{x},t)\rangle_c = [0.008889 \times 10^{-4}] \left(\frac{\lambda_0 B}{A^2}\right)^4 \mu^{-36/23}. \tag{5.68}$$

Using Eq. 5.68 and Eq. 6.45 in Eq. 5.65 leads to the kurtosis value as

$$Q = \frac{\langle h^4(\mathbf{x},t)\rangle_c}{\langle h^2(\mathbf{x},t)\rangle_c^2} = \frac{0.008889}{(0.211105)^2} = 0.1995 \tag{5.69}$$

We note that these values for skewness and kurtosis are obtained for the $(2+1)$-dimensional KPZ dynamics corresponding to the stationary state.

5.6 Discussion and Conclusion

Our main motivation in this work comes from two facts. First, the growth of a surface on a 2D substrate is a commonly occurring phenomenon in Nature. Second, analytical methodologies to obtain the skewness and kurtosis values directly from the dynamical equation are unavailable in the existing literature. The obtained skewness $S = 0.2879$ and kurtosis $Q = 0.1995$ values are independent of model parameters (ν_0, D_0, and λ_0), scaling coefficients (A and B) and the momentum cutoffs (Λ_0 and μ) in the calculations. The sole input to our calculations is the roughness exponent $\chi = 9/23 = 0.391304$ which is a good approximation to high resolution numerical results.

In this context it may be noted that most analytical approaches have been unsuccessful to obtain the scaling exponents in $(2+1)$ dimensions, apart from the works of Lässig[113], Tu[187] Colaiori and Moore[28] and Kloss *et al.*[99], as mentioned earlier. At the same time, a huge amount of numerical approaches suggest the roughness

and dynamic exponents to be $\chi \approx 0.39$ and $z \approx 1.61$, respectively.

We employed perturbation theory directly on the KPZ equation to obtain expressions for $L_3^<(r)$, $L_4^<(r)$ and $L_2^<(r)$ that contain the bare parameters ν_0 and D_0. Obtaining these expressions solely depend on the use of perturbation theory and they do not incorporate the renormalization group in the conventional sense. We use these expressions for $L_3^<(r)$, $L_4^<(r)$, and $L_2^<(r)$ to obtain the flow equations for the renormalized quantities $L_3(r)$, $L_4(r)$, and $L_2(r)$ that involve the renormalized quantities $\nu(r)$ and $D(r)$. In this process, we are able to find explicit mathematical relations including the prefactors once the scaling laws for the effective surface tension $\nu(k)$ and the noise amplitude $D(k)$ are assumed (Eqs. (3) and (4)) in consistency with the scaling relation $\chi + z = 2$. We incorporate frequency dependence of these loops by scaling functions that preserve their real valuedness and their correct zero frequency limits. This allows for the calculation of the corresponding cumulants that are found to depend on the infrared cutoff μ as $W_n \sim \mu^{-n\chi}$. This is expected because the cumulants have the semi-extensive property $W_n \sim L^{n\chi}$ in the stationary state where L is the substrate size. Thus the infrared cutoff can be identified as $\mu \sim L^{-1}$. We finally obtain the skewness value $S = 0.2879$ and the kurtosis value $Q = 0.1995$, relevant to the case of $(2+1)$-dimensional KPZ growth in the stationary state.

It may be noted that it is not possible to incorporate the results of the standard renormalization group analyses that do not yield a strong coupling fixed point and thereby providing no prediction for the value of χ in two dimensions. On the other hand, mode-coupling theories suggest that the upper critical dimension is 3.6, 4 or ∞[28,37,187]. Interestingly, a non-perturbative renormalization group analysis[100] indicated the existence of a stable strong coupling fixed point for $d \leq 2$, whereas for $d > 2$, there exist two basins of attraction containing a Gaussian fixed point and a strong coupling fixed point. The resulting roughness exponent was found to be $\chi = 0.330(8)$ and $\chi = 0.373(1)$ (in two dimensions) in the leading and next to leading order approximations, respectively. The latter result agrees very well with the numerical estimation $\chi \approx 0.39$ that we have used in our calculations. We further note that the values for the amplitudes A and B (that determine the fixed point value $g^* \sim \lambda_0^2 B/A^3$) are not required in our calculations because they cancel out in the ratios determining S and Q.

It can be seen that the scalings of the renormalized quantities are $\nu(k) \sim k^{-\chi}$ and $D(k) \sim k^{-3\chi+2-d}$ in d dimensions. Consequently, the scalings for the loop functions turn out to be $L_3(k) = C_3\, k^{-4\chi-2d+2}$, $L_4(k) = C_4\, k^{-5\chi-3d+2}$ and

$L_2(k) = C_2\, k^{-3\chi-d+2}$. We expect these scaling relations to be correct for any (non-zero) value of χ because they have been obtained on the basis of counting momentum dimensions. These relations suggest that $dL_3/dr = (4\chi + 2d - 2)\, C_3\, \Lambda_0^{-4\chi-2d+2}\, e^{(4\chi+2d-2)r}$, $dL_4/dr = (5\chi + 3d - 2)\, C_4\, \Lambda_0^{-5\chi-3d+2}\, e^{(5\chi+3d-2)r}$ and $dL_2/dr = (3\chi + d - 2)\, C_2\, \Lambda_0^{-3\chi-d+2}\, e^{(3\chi+d-2)r}$. These flow equations for $L_3(r)$, $L_4(r)$ and $L_2(r)$ contain unknown constants C_3, C_4 and C_2 respectively. The use of perturbation theory in our calculations serves to find these flow equations, along with the unknown constants, directly from the KPZ equation. In addition, we see that a good numerical input for χ results in good estimates for skewness and kurtosis values.

All recent numerical simulations in $(2+1)$ dimensions suggest that the roughness exponent χ is very close to 0.39 which is close to 9/23 (0.391304). We therefore slightly vary the value of the roughness exponent to $\chi = 19/50$ $(= 0.38)$ and $\chi = 2/5$ $(= 0.40)$ and recalculate the integrals. We find that skewness and kurtosis values undergo shifts by less than 5% from the calculated values given in Eqs. (67) and (69).

The estimated skewness and kurtosis values of Chin and den Nijs[26] via the Kim-Kosterlitz (KK) and BCSOS models are given in Table 5.1 of this Chapter. Although their roughness exponents differed in the two models (KK: $\chi = 2/5$ and BCSOS: $\chi \sim 0.38$), their skewness value ($|S| = 0.27 \pm 0.01$) was the same for both models. Consequently, they concluded that the third moment is more reliable than the roughness exponent for a better identification of the universality class. Their kurtosis value was $Q = 0.15 \pm 0.02$ for both models.

Reis[3] considered the stationary states for etching, ballistic deposition, and body-centered restricted solid-on-solid (BCRSOS) models that suggested the universality of the absolute values of skewness and kurtosis. The best estimates come from etching model which yielded $|S| = 0.26 \pm 0.01$ and $Q = 0.134 \pm 0.015$.

Miranda and Reis[130] used Euler discretization method for numerical integration of the KPZ equation and obtained roughness exponent $0.37 \leq \chi \leq 0.40$. In addition, they estimated skewness $S = 0.25 \pm 0.01$ and kurtosis $Q = 0.15 \pm 0.1$ by extrapolating data in the limit of large substrate size L. Marinari *et al.* [121] obtained skewness $S \sim 0.266$ and kurtosis $Q \sim 0.121$ through a numerical RSOS model.

Halpin-Healy[60] considered the $(2+1)$-dimensional numerical models such as $g5_1$ DPRM, RSOS and KPZ Euler in the asymptotic limit of time ($t >> L^z$) and obtained a $(2+1)$-dimensional analog of $(1+1)$-dimensional Baik-Rains distribution from these numerical models. In addition, they calculated the Baik-Rains constant

from those numerical models. On the other hand, instead of full probability distribution function only the skewness and kurtosis values have been estimated via the Kim-Kosterlitz (KK), BCSOS models[26], etching model[3], and KPZ Euler discretization approach[130], as displayed in Table-5.1 of present Chapter.

Experiments on vapor deposited oligmer thin film growth[145,186] yield the roughness and growth exponents $\chi = 0.45 \pm 0.04$ and $\beta = 0.28 \pm 0.05$, and the measured value of skewness $S = 0.23$, suggesting that this growth is in the KPZ universality class. Halpin-Healy and Palasantzas[62] examined two point statistics, in particular, spatial covariance by using the experimental results[145]. In addition, they studied the local squared roughness distribution and extremal height distribution via Euler integration of $(2+1)$ KPZ and compared with the experimental results.

Derrida and Appert[36] (DA) defined a ratio $R_{DA} = S^2/Q$ in $1+1$ dimensions, called the Derrida-Appert ratio[56], and estimated the ratio as $R_{DA} = 0.41517$, which is very close to the estimations from asymmetric simple exclusion principle (ASEP), BD and Brick models in asymptotic time limit, suggesting that R_{DA} is universal for the KPZ dynamics. In these dimensions, R_{DA} is conjectured to be universal via the Derrida-Lebowitz universal scaling function (DLSF) which is independent of any model parameters[25]. Subsequently, Prähofer and Spohn[153] estimated skewness $S = 0.35941$ and kurtosis $Q = 0.28916$ for $(1+1)$-dimensional KPZ height fluctuations in the stationary state and thereby, DA ratio is calculated as $R_{DA} = 0.44673$. Halpin-Healy and Takeuchi[56] studied the higher dimensional numerical models of KPZ class and different geometrical sub-classes namely point-point, point-line and point-plane in the transient regime and found a approximate constant value of R_{DA}. Alves *et al.*[5] studied the transient state RSOS model starting from the flat initial condition in higher dimensions $d = 3, 4, 5, 6$ and found $S \sim d^{0.46}$ and $Q \sim d^{0.92}$. This appears to suggest that S^2/Q is independent of d, supporting the greater universality of Derrida-Appert ratio proposed in[56], via their extensive examination of KPZ systems in the transient regime, across dimensions, as well as geometry. Our calculated skewness and kurtosis values yield $R_{DA} = 0.41547$, the normalized values of which is compared with the other stationary values in Table 5.1 of this Chapter.

The universality class of a dynamical system is an important statistical property. In the earlier studies on surface growth, the universality class used to be obtained from only the scaling exponents. In the last two decades, it has been realized that despite the same scaling exponents, the distribution functions can be entirely different due to different initial conditions corresponding to different sub-universality classes. Thus the distribution function contains more statistical information about

Table 5.1: Stationary state values of Skewness and Kurtosis in $(2+1)$ dimensions.

System of study	*Method*	$\lvert S\rvert$	Q	R_{DA}	*Reference*
$g5_1$ DPRM	Numerical	0.240	0.18	0.32	[60]
$2+1$ RSOS	Numerical	0.256	0.18	0.364	[60]
KPZ Euler	Numerical	0.236	0.17	0.328	[60]
KPZ Equation	Numerical	0.25 ± 0.01	0.15 ± 0.1	0.42 ± 0.31	[130]
Etching model	Numerical	0.26 ± 0.01	0.134 ± 0.015	0.50 ± 0.09	[3]
KK and BCSOS	Numerical	0.27 ± 0.01	0.15 ± 0.02	0.49 ± 0.08	[26]
(2+1) RSOS (FIT-I)	Numerical	0.2669 ± 0.0004	0.146 ± 0.002	0.488 ± 0.008	[143]
(2+1) RSOS (FIT-II)	Numerical	0.2657 ± 0.0004	0.145 ± 0.001	0.487 ± 0.005	[143]
Present work	Analytical	0.2879	0.1995	0.4155	Eqs. 5.67, 5.69

the system than the scaling exponents. The analytical calculation of the distribution function is hardly possible. To economize on the amount of calculations, one can calculate a few higher order cumulants of the distribution function, the normalized values of which can be used as identifiers of the universality classes.

Appendix

The term $F(\mathbf{k}, \mathbf{p})$ appearing in Eq. 5.16 is defined as

$$F = (F_1 + F_2 + F_3 + F_4)/R$$

We define $a = 37/23$, $b = 41/23$, and $P = |\mathbf{k}_1 + \mathbf{k}_2|$, so that

$$\begin{aligned}
F_1(\mathbf{k}_1, \mathbf{k}_2) &= 33\ k_1^{4a} + 4\ k_1^{3a}(47\ k_2^a + 24\ P^a) \\
F_2(\mathbf{k}_1, \mathbf{k}_2) &= 3(k_2^a + P^a)^2(11k_2^{2a} + 10k_2^a P^a + 3P^{2a}) \\
F_3(\mathbf{k}_1, \mathbf{k}_2) &= 2k_1^{2a}(203k_2^{2a} + 176k_2^a P^a + 51P^{2a}) \\
F_4(\mathbf{k}_1, \mathbf{k}_2) &= 4k_1^a(47k_2^{3a} + 88k_2^{2a} P^a + 53k_2^a P^{2a} + 12P^{3a})
\end{aligned}$$

$$R(\mathbf{k}_1, \mathbf{k}_2) = 256 k_1^b k_2^b (k_1^a + k_2^a + P^a)^5$$

The function $T(\mathbf{k},\mathbf{p},\mathbf{q})$ appearing in Eq. 5.34 is expressed as

$$T = (T_1 + T_2 + T_3 + T_4 + T_5 + T_6)/S$$

where

$$T_1(\mathbf{k},\mathbf{p},\mathbf{q}) = 3\{33k^{6a} + 2k^{5a}(127p^a + 127q^a + 81Q^a)\}$$

$$T_2(\mathbf{k},\mathbf{p},\mathbf{q}) = 3[k^{4a}\{815p^{2a} + 815q^{2a} + 986q^aQ^a + 327Q^{2a} + 34p^a(51q^a + 29Q^a)\}]$$

$$\begin{aligned}T_3(\mathbf{k},\mathbf{p},\mathbf{q}) = 3[4k^{3a}\{&297p^{3a} + 297q^{3a} + 585q^{2a}Q^a + 375q^aQ^{2a} + 87Q^{3a}\\ &+3p^{2a}(397q^a + 195Q^a) + p^a(1191q^{2a} + 1234q^aQ^a + 375Q^{2a})\}]\end{aligned}$$

$$\begin{aligned}T_4(\mathbf{k},\mathbf{p},\mathbf{q}) = 3[(p^a + q^a + Q^a)^2\{&(33p^{4a} + 4p^{3a}(47q^a + 24Q^a)\\ &+3(q^a + Q^a)^2(11q^{2a} + 10q^aQ^a + 3Q^{2a}) + 2p^{2a}(203q^{2a} + 176q^aQ^a + 51Q^{2a})\\ &+4p^a(47q^{3a} + 88q^{2a}Q^a + 53q^aQ^{2a} + 12Q^{3a})\}]\end{aligned}$$

$$\begin{aligned}T_5(\mathbf{k},\mathbf{p},\mathbf{q}) = 3[k^{2a}\{&815p^{4a} + 12p^{3a}(397q^a + 195Q^a) + (q^a + Q^a)^2\\ &(815q^{2a} + 710q^aQ^a + 207Q^{2a}) + 2p^{2a}(5277q^{2a} + 4366q^aQ^a + 1221Q^{2a})\\ &+4p^a(1191q^{3a} + 2183q^{2a}Q^a + 1273q^aQ^{2a} + 281Q^{3a})\}]\end{aligned}$$

$$\begin{aligned}T_6(\mathbf{k},\mathbf{p},\mathbf{q}) = 3[2k^a\{&127p^{5a} + 17p^{4a}(51q^a + 29Q^a) + (q^a + Q^a)^3(127q^{2a} + 112q^aQ^a + 33Q^{2a})\\ &+p^a(q^a + Q^a)^2(867q^{2a} + 734q^aQ^a + 211Q^{2a}) + p^{3a}(2382q^{2a} + 2468q^aQ^a + 750Q^{2a})\\ &+p^{2a}(2382q^{3a} + 4366q^{2a}Q^a + 2546q^aQ^{2a} + 562Q^{3a})\}]\end{aligned}$$

and

$$S(\mathbf{k},\mathbf{p},\mathbf{q}) = 4096k^{4a}p^{4a}q^{4a}(k^a+p^a+q^a+Q^a)^7$$

where $Q = |\mathbf{k}+\mathbf{p}+\mathbf{q}|$

Chapter 6

A renormalization scheme and skewness of height fluctuations in $(1+1)$-dimensional VLDS dynamics

6.1 Introduction

In the last few decades, one of the most widespread, useful and fascinating topics of research in nonequilibrium statistical physics is kinetic interface roughening[11,44,63,105,126]. A great deal of experiments and numerical simulations have been carried out in this field and a few analytical methods have been employed including the renormalization group (RG) to understand the scaling behavior, exponents and thereby universality of a growing surface. A linear continuum dynamics of surface growth is described by the Edwards-Wilkinson[199] (EW) equation where the surface profile evolves due to random deposition and surface tension.

A nonlinear paradigmatic equation for surface growth, as proposed by Kardar, Parisi and Zhang (KPZ)[86,128], describes a wide range of surface growth phenomena such as the eden model[152], ballistic deposition[127], restricted solid-on-solid model (RSOS), all belonging to a common universality class as they exhibit the same scaling exponents.

The growth of a thin film using the molecular beam epitaxy (MBE) is dominated by surface diffusion[166] at high temperatures, where atomic evaporation[150], desorption, bulk defects[209], hangs and overhangs are negligibly small. In MBE, atoms are deposited one-by-one for the preparation of high quality thin films[2]. On the other hand, at low temperatures, a growing surface would be amorphous instead of crystalline[192] because deposited particles would not have much energy

to overcome the height barriers so that they can settle down at the lowest energy positions. According to Mullins's theory [133] such surface growth obeys the equation of continuity

$$\frac{\partial h}{\partial t} = -\nabla \cdot \mathbf{j} \tag{6.1}$$

where the particle current is $\mathbf{j} = \nabla\mu(\mathbf{x},t)$ and local chemical potential $\mu(\mathbf{x},t)$ is related to the surface curvature as $\mu(\mathbf{x},t) = \kappa\nabla^2 h(\mathbf{x},t)$. Fourier transforming and rescaling of equation 6.1 yield roughness, dynamic and growth exponents as $\chi = (4-d)/2$, $z = 4$ and $\beta = (4-d)/8$ respectively, d being the substrate dimension. Wolf and Villain [204] (WV) studied a model with random deposition and surface diffusion in one dimension, where the particles are relaxed to the minimum energy positions yielding roughness and dynamic exponents, $\chi = 1.4 \pm 0.1$ and $z = 3.8 \pm 0.5$, that indicates a different universality class from those of EW and KPZ. These exponents are close to those obtained from equation 6.1. Das Sarma and Tamborenea (DT) [33] investigated a deposition model with surface relaxation and estimated roughness and growth exponents as $\chi \approx 1.5$ and $\beta = 0.375 \pm 0.005$ in one spatial dimension. Krug [?] studied the height-height correlation function and structure factor in one dimension by taking the solid-on-solid (SOS) model with DT [33] relaxation rule where overhangs are not present. His obtained growth exponent is $\beta = 0.37 \pm 0.01$, satisfying the scaling relation of equation 6.1. The step size distribution of his study yields a non zero skewness in one substrate dimension. This implies that the distribution of height fluctuations is not Gaussian unlike that of equation 6.1 and consequently suggesting that the continuum model for the MBE growth process must be a nonlinear dynamical equation.

Sun, Guo and Grant (SGG) [175] proposed a nonlinear equation for surface growth where total volume under the interface is conserved, including noise conservation. They obtained a distinct set of exponents given by $\chi = \frac{2-d}{3}$ and $z = \frac{10+d}{3}$ that agree with the conserved restricted solid on solid (CRSOS) model for $d = 1$.

Considering a geometrical interpretation, Villain, Lai and Das Sarma (VLDS) [111,192] proposed a nonlinear equation with non-conserved noise for the MBE process. This dynamical equation is known as the VLDS equation, written as

$$\frac{\partial h}{\partial t} = -\nu_0\nabla^4 h + \frac{\lambda_0}{2}\nabla^2(\nabla h)^2 + \eta, \tag{6.2}$$

where $h(\mathbf{x},t)$ is the height of the fluctuating surface at position $\mathbf{x}$ and time t, ν_0 is the diffusion constant and $\eta(\mathbf{x},t)$ is a Gaussian white noise with zero mean and

covariance

$$\langle \eta(\mathbf{x},t)\eta(\mathbf{x}',t')\rangle = 2D_0\delta^d(\mathbf{x}-\mathbf{x}')\delta(t-t'). \tag{6.3}$$

where D_0 is a constant.

Family and Vicsek[43] proposed the dynamic scaling for the surface width (standard deviation) as

$$w(L,t) \sim L^{\chi} F\left(\frac{t}{L^z}\right). \tag{6.4}$$

For large τ, $F(\tau) = Const.$ and for small τ, $F(\tau) \sim \tau^{\beta}$. The ratio $\beta = \frac{\chi}{z}$ is called the growth exponent.

Through one-loop dynamic RG calculations[111], Lai and Das Sarma as well as Tang and Nattermann[183] independently obtained the roughness, dynamic and growth exponents as $\chi = \frac{4-d}{3}$, $z = \frac{8+d}{3}$ and $\beta = \frac{4-d}{8+d}$. Janssen argued in the ref.[82] that KPZ like Galilean transformation in SGG and VLDS equations are mathematically ill defined and thereby the exponents following from an RG calculations are to be corrected. Accounting for two-loop corrections in an RG calculation, he obtained small corrections to the exponents in each dimensions. Subsequently, numerical works[210,211] were devoted to capture corrections to the exponents. These numerical corrections turned out to be larger than Janssen's corrections. However, no conclusions could be reached regarding the role of vertex corrections in their numerical simulations. Katzav[88] investigated equation 6.2 via a self-consistent-expansion method which has close relation to mode-coupling approach and obtained the same set of exponents as the one-loop dynamic RG results. It may however be noted that Katzav's self-consistent integral equations were equivalent to a renormalized perturbation theory at one-loop order without vertex renormalization.

There exist two types of investigations in the literature. One of them is finding the scaling exponents through different growth models and comparing them with the calculated exponents corresponding to the continuum equations. The other type of work is the derivation of a continuum equation from the discrete model using the principle of symmetry or re-parametrization of invariance[122] (alternatively using the master equation[69,70,149,196]). Wilby *et al.*[197] studied the SOS model by using Monte-Carlo-Simulation and estimated the growth exponents $\beta = 0.333 \pm 0.010$ in $d = 1$ dimension which agrees with the dynamic RG result. A conserved growth model with RSOS condition, in $1+1$ dimensions, has been studied by Kim and Kim in the refs.[93,98] and their estimated exponents (roughness and growth exponents $\chi = 0.95 \pm 0.04$ and $\beta = 0.32 \pm 0.01$ respectively) agree with the calculated exponents from dynamic RG.

There exist many numerical studies to obtain the scaling exponents which in turn determine the universality classes. A detailed study of the height fluctuations involves the determination of its probability distribution function that determines the universality class of the growth process. However, obtaining the full probability distribution function is an analytically impossible task and alternatively a few lower order moments yielding the skewness and kurtosis could be studied. The nth moment of the height fluctuations is defined as

$$W_n = \langle [h(\mathbf{x},t) - \bar{h}(t)]^n \rangle, \tag{6.5}$$

and the moments follow the power laws at stationary state as, $W_n \sim L^{n\chi}$, where L is the substrate size. Skewness is defined as

$$S = \frac{W_3}{(W_2)^{3/2}}. \tag{6.6}$$

It may be noted that numerical attempts to obtain the skewness for the VLDS type growth is rather rare. For example, Das Sarma *et al.*[32] considered a discrete LDS model and obtained $S = -0.1 \pm 0.15$ in the steady state.

However, there appears to be no attempts to obtain the value of skewness via analytical means directly from the VLDS equation. Since skewness is an important property of the probability distribution function, it is indispensable to calculate its value for the height fluctuations governed by the VLDS dynamics so that this fluctuations can be distinguished from those governed by other dynamical processes.

In this Chapter we calculate the second and third moments of the height fluctuations in the stationary state directly from the VLDS equation starting from flat initial condition employing a diagrammatic methods and a renormalization scheme without rescaling. This allows for the calculation of the skewness given by equation 6.6.

This Chapter is organized in the following way. Section II presents a renormalization group scheme without rescaling. Section III presents the calculation of the second moment W_2. In Section-IV, we calculate the third moment W_3 and thereby the value of skewness is obtained. Section-V calculates the skewness and Section-VI gives a Discussion and Conclusion.

6.2 Renormalization Scheme Without Rescaling

In this section, we employ an RG scheme without rescaling that was previously used by Yakhot and Orszag[207,208] in the case of fluid turbulence and, later, it was applied to the stochastic KPZ dynamics[169,170] We begin with the Fourier transformation of the VLDS equation (equation 6.2), namely,

$$(-i\omega+\nu_0 k^4)h(\mathbf{k},\omega)=\eta(\mathbf{k},\omega)-\frac{\lambda_0}{2}k^2\int\!\!\int\frac{d^dqd\Omega}{[2\pi]^{d+1}}[\mathbf{q}\cdot(\mathbf{k}-\mathbf{q})]h(\mathbf{q},\Omega)h(\mathbf{k}-\mathbf{q},\omega-\Omega). \tag{6.7}$$

We shall use equation 6.7 to obtain the renormalized surface diffusivity as well as the skewness of the height fluctuations in $(1+1)$-dimensions.

A. Scale Elimination

In the Fourier space, we split the height and noise fields into slow and fast modes, namely, $h^<(\mathbf{k},\omega)$ and $h^>(\mathbf{k},\omega)$, and $\eta^<(\mathbf{k},\omega)$ and $\eta^>(\mathbf{k},\omega)$, where $h^>(\mathbf{k},\omega)$ and $\eta^>(\mathbf{k},\omega)$ belong to the shell $\Lambda_0 e^{-r}\leq k\leq\Lambda_0$. The fluctuating modes $h^>(\mathbf{k},\omega)$ are eliminated by means of integration and its effect is accounted for as corrections to the model parameters (ν_0, D_0 and λ_0). As a consequence, we obtain an equation for the slow modes $h^<(\mathbf{k},\omega)$

$$\begin{aligned}&[-i\omega+\nu_0k^4+\Sigma(\mathbf{k},\omega)]h^<(\mathbf{k},\omega)=\eta^<(\mathbf{k},\omega)\\&-\left(\frac{\lambda_0}{2}\right)k^2\int\!\!\int\frac{d^dq\;d\Omega}{[2\pi]^{d+1}}[\mathbf{q}\cdot(\mathbf{k}-\mathbf{q})]h^<(\mathbf{q},\Omega)h^<(\mathbf{k}-\mathbf{q},\omega-\Omega),\end{aligned} \tag{6.8}$$

in the momentum space $0\leq(k,p,q)\leq\Lambda_0e^{-r}$. Here, the self energy correction is given by

$$\begin{aligned}\Sigma(k,\omega)&=4\left(\frac{-\lambda_0}{2}\right)^2(2D_0)k^2\int^>\frac{d^dq}{[2\pi]^d}[\mathbf{q}\cdot(\mathbf{k}-\mathbf{q})]\;[\mathbf{k}\cdot(\mathbf{q}-\mathbf{k})]\;q^2\\&\times\int_{-\infty}^{\infty}\frac{d\Omega}{[2\pi]}\,G_0^>(\hat{q})\,|G_0^>(\hat{k}-\hat{q})|^2\end{aligned} \tag{6.9}$$

with $G_0(\hat{k})\equiv G_0(\mathbf{k},\omega)=[-i\omega+\nu_0k^4]^{-1}$ is a bare propagator. Following Ref.[47,207,208], we integrate over the internal frequency Ω and invoke the transformation $\mathbf{q}\to(\mathbf{q}+\mathbf{k}/2)$. Performing the internal momentum integration in the shell $\Lambda_0e^{-r}\leq q\leq\Lambda_0$,

a correction to the surface diffusivity is obtained as

$$\Delta\nu = \frac{\lambda_0^2 D_0}{\nu_0^2}\frac{S_d}{[2\pi]^d}\left(\frac{6-d}{4d}\right)\left[\frac{e^{(4-d)r}-1}{(4-d)\Lambda_0^{4-d}}\right] \tag{6.10}$$

in the large-scale ($q >> k$) long-time limits ($\omega \to 0$). Here $S_d = \frac{2\pi^{d/2}}{\Gamma(d/2)}$ is the area of a sphere of unit radius embedded in a d-dimensional space and $\Sigma(\mathbf{k},0) = k^4\Delta\nu$. Consequently, we obtain an effective diffusivity as

$$\nu^<(r) = \nu_0\left[1 + \frac{\lambda_0^2 D_0}{\nu_0^2}\frac{S_d}{[2\pi]^d}\left(\frac{6-d}{4d}\right)\left(\frac{e^{(4-d)r}-1}{(4-d)\Lambda_0^{4-d}}\right)\right]. \tag{6.11}$$

The two point height-height correlation function corresponding to one-loop perturbative expansion can be written as

$$\langle h^<(\mathbf{k},\omega)h^<(\mathbf{k}',\omega')\rangle = 2[D_0+\Delta D]|G(\mathbf{k},\omega)|^2[2\pi]^{d+1}\delta^d(\mathbf{k}+\mathbf{k}')\delta(\omega+\omega') \tag{6.12}$$

where

$$\Delta D = \left(\frac{-\lambda_0}{2}\right)^2(2D_0)^2k^4\int^> \frac{d^dq}{[2\pi]^d}\left[\mathbf{q}\cdot(\mathbf{k}-\mathbf{q})\right]^2\int_{-\infty}^{\infty}\frac{d\Omega}{[2\pi]}\left|G_0^>(\hat{q})\right|^2\left|G_0^>(\hat{k}-\hat{q})\right|^2 \tag{6.13}$$

which comes from the amputated part of the loop diagram shown in figure 6.1(b). The frequency and momentum integrations in equation 6.13 are carried out yielding

$$\Delta D = k^4\left(\frac{K_d\lambda_0^2D_0^2}{4\nu_0^3}\right)\left[\frac{\Lambda_0^{d-8}-\Lambda^{d-8}(r)}{d-8}\right] \tag{6.14}$$

Since ΔD goes like k^4, this correction to D_0 is irrelevant in the large-scale and long-time limits. Hence

$$D^<(r) = D_0. \tag{6.15}$$

According to Lai and Das Sarma[111], the vertex (λ_0) does not get any corrections from the RG transformation at one-loop order, consequently

$$\lambda^<(r) = \lambda_0. \tag{6.16}$$

B. Flow equations and Fixed point

We obtained the flow equations as differential equations with respect to variation of the parameter r from equations 6.11, 6.15 and 6.16 giving

$$\begin{aligned} \frac{d\nu}{dr} &= K_d \frac{\lambda_0^2 D_0 \Lambda^{d-4}(r)}{\nu^2(r)} \left(\frac{6-d}{4d}\right) \\ \frac{dD}{dr} &= 0 \\ \frac{d\lambda}{dr} &= 0 \end{aligned} \tag{6.17}$$

where $\Lambda(r) = \Lambda_0 e^{-r}$. We define an effective coupling parameter

$$g(r) = K_d \frac{\lambda_0^2 D(r)}{\nu^3(r)\Lambda^{4-d}(r)}. \tag{6.18}$$

Using equations 6.17 and 6.18, we obtain the flow equation for the coupling constant

$$\frac{dg(r)}{dr} = a\ g(r) - b\ g^2(r) \tag{6.19}$$

where $a = (4-d)$ and $b = \frac{3(6-d)}{4d}$. Integrating equation 6.19 over r, yields

$$g(r) = \frac{g_0 e^{ar}}{1 + \frac{b}{a} g_0\ (e^{ar} - 1)}, \tag{6.20}$$

where $g(0) = g_0 = \frac{K_d \lambda_0^2 D_0}{\nu_0^3 \Lambda_0^{4-d}}$. In the asymptotic limit of r ($r \to \infty$), equation 6.20 approaches to r independent quantity

$$g* = \frac{4d(4-d)}{3(6-d)}. \tag{6.21}$$

The fixed point, expressed by equation 6.21, is stable for $d < 4$, thereby the upper critical dimension of the VLDS equation is $d_c = 4$ which agrees with refs.[111,183].

C. Renormalized Surface Diffusivity

Integrating the first flow equation in equation 6.17 using equation 6.19, we obtain

$$\nu(r) = \nu_0 \left[1 + \frac{b}{a} g_0\ (e^{ar} - 1)\right]^{1/3}. \tag{6.22}$$

In the asymptotic limit of large r, equation 6.22 takes the form

$$\nu(r) = \nu_0 \left(\frac{b\ g_0}{a} e^{ar} \right)^{1/3}, \tag{6.23}$$

and, in $(1+1)$ dimensions, the above equation becomes

$$\nu(r) = \nu_0 \left(\frac{5\ g_0}{4} \right)^{1/3} e^r. \tag{6.24}$$

Thus the corresponding renormalized surface diffusivity reads

$$\nu(k) = \quad \nu_0 \left(\frac{5\lambda_0^2 D_0}{4\pi\nu_0^3} \right)^{1/3} k^{-1}, \tag{6.25}$$

in the large-scale long-time limits. The renormalized response function $G(\mathbf{k},\omega)$ and the dynamic exponent z is related through the expression

$$G^{-1}(\mathbf{k},\omega) = [-i\omega + \nu(k)k^4] \ \propto \ k^z\, \xi\left(\frac{\omega}{k^z}\right). \tag{6.26}$$

The above equation indicates that $\nu(k)k^4 \sim k^z$ implying dynamic exponent $z = 3$ in $d = 1$ dimension. The roughness exponent, $\chi = 1$, can be obtained from the scaling relation $\chi + z = 4$.

6.3 The Second Moment

Using the definition of nth moment of the height fluctuations expressed in equation 6.5, the second and third moments are obtained as

$$W_2 = \langle h^2(\mathbf{x},t)\rangle - \langle h(\mathbf{x},t)\rangle^2. \tag{6.27}$$

and

$$W_3 = \langle h^3(\mathbf{x},t)\rangle - 3\langle h^2(\mathbf{x},t)\rangle\langle h(\mathbf{x},t)\rangle + 2\langle h(\mathbf{x},t)\rangle^3, \tag{6.28}$$

respectively. Here $h(\mathbf{x},t)$ is the height fluctuations satisfying $\langle h(\mathbf{x},t)\rangle = 0$, and consequently equation 6.27 and equation 6.28 become

$$W_2 = \langle h^2(\mathbf{x},t)\rangle \tag{6.29}$$

and

$$W_3 = \langle h^3(\mathbf{x}, t)\rangle, \tag{6.30}$$

A. Calculation of $W_2^{(1)}$

The perturbative expansion at one-loop order of the second moment yields

$$W_2 = \langle [h(\mathbf{x}, t)]^2\rangle = W_2^{(1)} + W_2^{(2)} + W_2^{(3)}, \tag{6.31}$$

where $W_2^{(1)}$ and $W_2^{(2)}$ are non-zero contributions corresponding to $O[\lambda_0^0]$ and $O[\lambda_0^2]$ of the perturbation series. In Fourier space, the expression for $W_2^{(1)}$ is written as

$$W_2^{(1)} = \int \frac{d^d k d\omega}{[2\pi]^{d+1}} \int \frac{d^d k' d\omega'}{[2\pi]^{d+1}} Q^{(0)}(\mathbf{k}, \omega; \mathbf{k}', \omega') e^{i(\mathbf{k}+\mathbf{k}')\cdot\mathbf{x}} e^{-i(\omega+\omega')t}. \tag{6.32}$$

The diagrammatic representation of $W_2^{(1)}$ is shown in figure 6.1(a). We incorporate two point correlation (zeroth order), namely, $Q^{(0)}(\mathbf{k}, \omega; \mathbf{k}', \omega') \equiv \langle h(\mathbf{k}, \omega) h(\mathbf{k}', \omega')\rangle = 2D_0[2\pi]^{d+1}|G(\mathbf{k}, \omega)|^2 \delta^d(\mathbf{k} + \mathbf{k}')\delta(\omega + \omega')$ and carry out integration over k' yielding

$$W_2^{(1)} = 2D_0 \int \frac{d^d k}{[2\pi]^d} \int \frac{d\omega}{[2\pi]} |G(\mathbf{k}, \omega)|^2. \tag{6.33}$$

We use the functional form of $\nu(k)$ from equation 6.25. Consequently performing the frequency integration and carrying out the momentum integration in $(1 + 1)$ dimensions in equation 6.33, we obtain

$$W_2^{(1)} = \frac{1}{2\pi^{2/3}} \left(\frac{4D_0^2}{5\lambda_0^2}\right)^{1/3} \frac{1}{\mu^2} \tag{6.34}$$

where μ is the lower limit of the momentum integration.

B. Calculation of $W_2^{(2)}$

The expression for $W_2^{(2)}$ is expressed in momentum and frequency spaces as

$$W_2^{(2)} = \int \frac{d^d k d\omega}{[2\pi]^{d+1}} \int \frac{d^d k' d\omega'}{[2\pi]^{d+1}} Q^{(2)}(\mathbf{k}, \omega; \mathbf{k}', \omega')\, e^{i(\mathbf{k}+\mathbf{k}')\cdot\mathbf{x}} e^{-i(\omega+\omega')t}. \tag{6.35}$$

where $Q^{(2)}(\mathbf{k}, \omega; \mathbf{k}', \omega') = [2\pi]^{d+1} L_2(\mathbf{k}, \omega)|G(\mathbf{k}, \omega)|^2 \delta^d(\mathbf{k} + \mathbf{k}')\delta(\omega + \omega')$. Feynman diagram for $W_2^{(2)}$ is given in figure 6.1 (b). One-loop contribution to the second

moment is given by

$$W_2^{(2)} = \int \frac{d^d k d\omega}{[2\pi]^{d+1}} G(\mathbf{k},\omega) L_2(\mathbf{k},\omega) G(-\mathbf{k},-\omega) \tag{6.36}$$

where L_2 [$L_2 = k^4 l_2(\hat{k})$] corresponds to the amputated loop of figure 6.1 (b) expressed in equation 6.13. We carry out the integrations over the internal frequencies and internal momenta in the shell $\Lambda_0 e^{-r} \leq k \leq \Lambda_0$ and obtain

$$l_2^{<}(r) = \left(\frac{\lambda_0^2 D_0^2}{2\pi\nu_0^3}\right)\left[\frac{\Lambda_0^{-7} - \Lambda^{-7}(r)}{-7}\right] \tag{6.37}$$

leading to the differential equation

$$\frac{dl_2}{dr} = \frac{\lambda_0^2 D_0^2}{2\pi\nu^3(r)\Lambda^7(r)}. \tag{6.38}$$

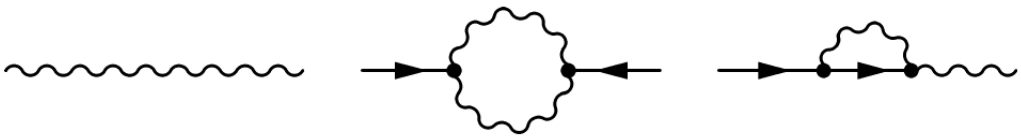

(a) (b) (c)

Figure 6.1: Feynman diagrams : (a) $W_2^{(1)}$, (b) $W_2^{(2)}$ and (c) $W_2^{(3)}$. Responses are indicated by solid lines with arrow and correlations are indicated by wiggly lines.

The function $\nu(r)$ being known from equation 6.24, the above differential equation is solved to obtain

$$l_2(r) = \left(\frac{D_0}{10\Lambda_0^4}\right) e^{4r} \tag{6.39}$$

in the asymptotic limit of large r. Identifying $\Lambda_0 e^{-r} = k$, we get

$$l_2(k,0) = \frac{1}{10} D_0\ k^{-4}. \tag{6.40}$$

The vertex of figure 6.1(b) contains k^4 and consequently the loop contribution (without the external legs) becomes we define $L_2(k,0) = k^4 l_2(k,0)$

$$L_2 = \frac{1}{10} D_0. \tag{6.41}$$

which is scale independent. Now substituting equation 6.41 in equation 6.36, we get

$$W_2^{(2)} = \int \frac{d^d k}{(2\pi)^d} \int \frac{d\,\omega}{[2\pi]} |G(\mathbf{k},\omega)|^2 L_2 \tag{6.42}$$

Performing the frequency integration in equation 6.42, we obtain

$$W_2^{(2)} = \frac{1}{20\pi^{2/3}} \left(\frac{4D_0^2}{5\lambda_0^2}\right)^{1/3} \int_\mu^\infty dk k^{-3}. \tag{6.43}$$

We carry out the momentum integration in the above equation leading to

$$W_2^{(2)} = \frac{1}{40\pi^{2/3}} \left(\frac{4D_0^2}{5\lambda_0^2}\right)^{1/3} \frac{1}{\mu^2}. \tag{6.44}$$

Feynman diagram corresponding to $W_2^{(3)}$ is shown in figure 6.1(c). The contribution to $W_2^{(3)}$ vanishes in the large-scale limit. Adding the contributions $W_2^{(1)}$ and $W_2^{(2)}$ from equations 6.34 and 6.44, we obtain W_2 as

$$W_2 = W_2^{(1)} + W_2^{(2)} = \frac{21}{40\pi^{2/3}} \left(\frac{4D_0^2}{5\lambda_0^2}\right)^{1/3} \frac{1}{\mu^2} \tag{6.45}$$

6.4 The Third Moment and Skewness

The third moment of height fluctuations is expressed as

$$W_3 = \sum_{i=1}^{8} W_3^{(i)} \tag{6.46}$$

where $W_3^{(1)}$ and $W_3^{(2)}$, corresponding to Feynman diagrams Figs. 6.2 (a) and 6.2(b) respectively, give non-zero contributions. The terms $W_3^{(3)}$ and $W_3^{(4)}$, corresponding to figures 6.3(a) and 6.3(b), respectively, give equal magnitudes of logarithmic corrections with opposite signs and thus they cancel each other. The rest of the terms in equation 6.46, namely, $W_3^{(5)}$, $W_3^{(6)}$, $W_3^{(7)}$ and $W_3^{(8)}$, are depicted in Figs. 4(a), 4(b), 4(c) and 4(d), respectively, which give zero contributions individually in the large-scale long-time limits.

A. Calculation of $W_3^{(1)}$

In this subsection, we calculate Feynman diagram given in figure 6.2(a). The integral expression for $W_3^{(1)}$ in the Fourier space is given by

$$W_3^{(1)} = \int \frac{d^d k_1\, d\omega_1}{[2\pi]^{d+1}} \int \frac{d^d k_2\, d\omega_2}{[2\pi]^{d+1}} \int \frac{d^d k_3\, d\omega_3}{[2\pi]^{d+1}} \langle h(\mathbf{k}_1,\omega_1)\, h(\mathbf{k}_2,\omega_2)\, h(\mathbf{k}_3,\omega_3)\rangle\; e^{i(\mathbf{k}_1+\mathbf{k}_2+\mathbf{k}_3)\cdot\mathbf{x}}\, e^{-i(\omega_1+\omega_2+\omega_3)t}, \tag{6.47}$$

The third order height correlation appearing in equation 6.47 is expressed as

$$\langle h(\mathbf{k}_1,\omega_1)\, h(\mathbf{k}_2,\omega_2)\, h(\mathbf{k}_3,\omega_3)\rangle = G(\hat{k}_1)\, G(\hat{k}_2)\, G(\hat{k}_3)\, L_3^{(1)}(\hat{k}_1;\hat{k}_2;\hat{k}_3) \times[(2\pi)^{d+1}\, \delta^{d+1}(\hat{k}_1+\hat{k}_2+\hat{k}_3)] \tag{6.48}$$

where $L_3^{(1)}(\hat{k}_1;\hat{k}_2;\hat{k}_3) = \mathbf{k}_1^2\,\mathbf{k}_2^2\,\mathbf{k}_3^2\, l_3(\hat{k}_1;\hat{k}_2;\hat{k}_3)$ represents the renormalized amputated part of the loop diagram [figure 6.2 (a)]. Substituting equation 6.48, in equation 6.47, we obtain

$$W_3^{(1)} = \int \frac{d^{d+1}\hat{k}_1}{[2\pi]^{d+1}} \int \frac{d^{d+1}\hat{k}_2}{[2\pi]^{d+1}}\, G(\hat{k}_1)\, G(\hat{k}_2)\, L_3^{(1)}(\hat{k}_1;\hat{k}_2)\, G(-\hat{k}_1-\hat{k}_2) \tag{6.49}$$

The bare value of $l_3^{(1,0)}(\hat{k}_1;\hat{k}_2)$ is given by

$$l_3^{(1,0)}(k_1,\omega_1;k_2,\omega_2) = 8 \left(\frac{-\lambda_0}{2}\right)^3 \int \frac{d^d q\; d\omega}{[2\pi]^{d+1}} [(\mathbf{q}-\mathbf{k}_1)\cdot(\mathbf{k}_2+\mathbf{k}_1-\mathbf{q})][\mathbf{q}\cdot(\mathbf{k}_1-\mathbf{q})] \times[-\mathbf{q}\cdot(\mathbf{q}-\mathbf{k}_2-\mathbf{k}_1)] Q_0(\hat{\mathbf{q}}) Q_0(\hat{\mathbf{k}}_1-\hat{\mathbf{q}}) Q_0(\hat{\mathbf{k}}_1+\hat{\mathbf{k}}_2-\hat{\mathbf{q}})]. \tag{6.50}$$

where $Q_0(\mathbf{q}) = 2D_0\,[2\pi]^{d+1}\, G_0(\hat{q})\, G_0(\hat{q}')\, \delta^{d+1}(\hat{q}+\hat{q}')$ are the correlations. Considering the external momenta and frequencies to be much smaller in magnitude than internal momenta and frequencies, we carry out frequency convolution and momentum integrations yielding

$$l_3^{(1)<}(r) = \frac{3}{2}\left[\frac{\lambda_0^3 D_0^3 K_d}{\nu_0^5 \Lambda_0^{14-d}}\right]\left[\frac{e^{(14-d)r}-1}{(14-d)}\right]. \tag{6.51}$$

The iterative nature of the shell elimination scheme yields

$$\frac{dl_3^{(1)}}{dr} = \frac{3}{2}\left[\frac{\lambda_0^3 D_0^3 K_d}{\nu^5(r)\Lambda^{14-d}(r)}\right] \tag{6.52}$$

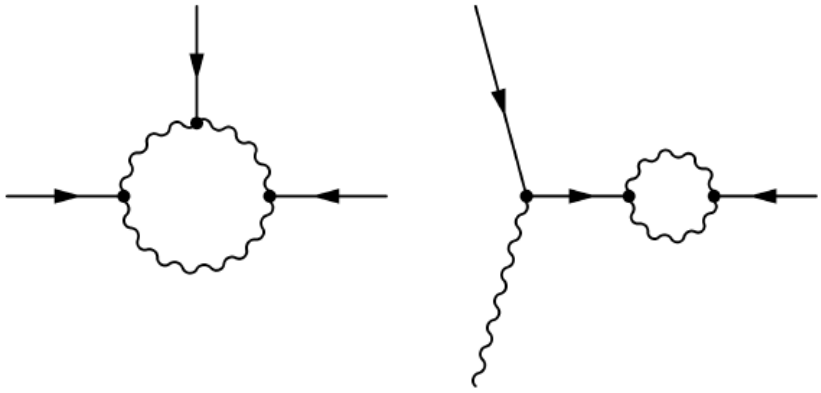

Figure 6.2: Feynman diagrams: (a) $W_3^{(1)}$ and (b) $W_3^{(2)}$. These diagrams contribute to W_3.

Solving this equation in the asymptotic limit of large r in $d = 1$ dimension, we obtain

$$l_3^{(1)}(r) = \frac{3}{20}\lambda_0 D_0^2 \left(\frac{4\pi}{5\lambda_0^2 D_0}\right)^{2/3} \frac{1}{\Lambda^8(r)}. \tag{6.53}$$

$\Lambda_0 e^{-r}$ is identified as the external momenta, yielding

$$l_3^{(1)}(k_1, 0; k_2, 0) = \frac{3}{20}\lambda_0 D_0^2 \left(\frac{4\pi}{5\lambda_0^2 D_0}\right)^{2/3} k_1^{-4} k_2^{-4}. \tag{6.54}$$

So, $L_3^{(1)}$ becomes

$$L_3^{(1)}(\mathbf{k}_1, \mathbf{k}_2) = \mathbf{k}_1^2 \mathbf{k}_2^2 \mathbf{k}_3^2 \, l_3^{(1)} \tag{6.55}$$

Now to find the wave vector and frequency dependence in equation 6.54 a form of scaling function is introduced by replacing k_i^{-2} by

$$k_i^{-2} f_d\left(\frac{\omega_i}{k_i^z}\right) = k_i^6 \nu^2(k_i) |G(\mathbf{k}_i, \omega_i)|^2 \tag{6.56}$$

where $i = 1, 2$ and $f(0) = 1$. This expression is the same as k_i^{-2} for $\omega_i = 0$. Incorporating equation 6.56 in equation 6.54, we obtain

$$L_3^{(1)}(\hat{k}_1, \hat{k}_2) = \frac{3}{20} A \; k_1^4 k_2^4 |\mathbf{k}_1 + \mathbf{k}_2|^2 |G(\hat{k}_1)|^2 |G(\hat{k}_2)|^2 \tag{6.57}$$

with $A = \lambda_0 D_0^2 \left(\frac{5\lambda_0^2 D_0}{4\pi}\right)^{2/3}$. We substitute equation 6.57 in equation 6.49 yielding

$$W_3^{(1)} = \frac{3}{20} A \int \frac{d^2\hat{k}_1}{[2\pi]^2} \int \frac{d^2\hat{k}_2}{[2\pi]^2} \quad k_1^4 \, k_2^4 \, |\mathbf{k}_1 + \mathbf{k}_2|^2 \, |G(\hat{k}_1)|^2 \, |G(\hat{k}_2)|^2 \times [G(\hat{k}_1) G(\hat{k}_2) \; G(-\hat{k}_1 - \hat{k}_2)] \tag{6.58}$$

Carrying out the frequency integrations over ω_1 and ω_2, we obtain

$$W_3^{(1)} = \left(\frac{3}{20}\right) \frac{A_1}{[2\pi]^2} \int_{-\infty}^{\infty} dk_1 \int_{-\infty}^{\infty} dk_2 \; F_1(k_1, k_2). \tag{6.59}$$

where

$$F_1(k_1, k_2) = \frac{3\sigma^2(k_1) + (\sigma(k_2) + \sigma(|k_1 + k_2|)(3\sigma(k_2) + \sigma(|k_1 + k_2|)) + 2\sigma(k_1)(7\sigma(k_2) + 2\sigma(|k_1 + k_2|))}{16\sigma^2(k_1)\sigma^2(k_2)(\sigma(k_1) + \sigma(k_2) + \sigma(|k_1 + k_2|))^3}$$

with $\sigma(k_i) = k_i^3$ and $A_1 = \frac{A \; (4\pi)^{5/3}}{\left(5\lambda_0^2 D_0\right)^{5/3}} = \left(\frac{4\pi D_0}{5\lambda_0}\right)$. Now the integrations become

$$I_1(\mu) = \int_{\mu}^{\infty} dk_1 \int_{\mu}^{\infty} dk_2 F_1(k_1, k_2)$$

and

$$J_1(\mu) = \int_{\mu}^{\infty} dk_1 \int_{\mu}^{\infty} dk_1 F_1(-k_1, k_2).$$

Since these integrals are infrared divergent, we write them as

$$\begin{aligned} I_1(\mu) &= I_1^{(0)} \mu^{-3} \\ J_1(\mu) &= J_1^{(0)} \mu^{-3}. \end{aligned} \tag{6.60}$$

where $I_1^{(0)}$ and $J_1^{(0)}$ are dimensionless numerical constants. Carrying out numerical integrations, we obtain the values for the constants as

$$\begin{aligned} I_1^{(0)} &= \lim_{\mu \to 0^+} [\mu^3 I_1(\mu)] = 0.0148673 \\ J_1^{(0)} &= \lim_{\mu \to 0^+} [\mu^3 J_1(\mu)] = 0.0039435, \end{aligned} \tag{6.61}$$

Substituting equations 6.60 and 6.61 in equation 6.59, we obtain

$$W_3^{(1)} = \frac{3}{100\pi}\left(\frac{D}{\lambda_0}\right)(2I_1^{(0)} + 2J_1^{(0)})\frac{1}{\mu^3}$$
$$= \frac{3}{50\pi}\left(\frac{D}{\lambda_0}\right)(0.018811)\frac{1}{\mu^3}. \quad (6.62)$$

B. Calculation of $W_3^{(2)}$

Feynman diagram for $W_3^{(2)}$ is shown in figure 6.2(b). The integral expression for $W_3^{(2)}$ is written as

$$W_3^{(2)} = \int \frac{d^{d+1}\hat{k}}{[2\pi]^{d+1}} \int \frac{d^{d+1}\hat{k}'}{[2\pi]^{d+1}} \int \frac{d^{d+1}\hat{k}''}{[2\pi]^{d+1}} \int \frac{d^{d+1}\hat{q}}{[2\pi]^{d+1}} \int \frac{d^{d+1}\hat{p}}{[2\pi]^{d+1}} \int \frac{d^{d+1}\hat{Q}}{[2\pi]^{d+1}}$$
$$[k'^2 G(\hat{k}') k''^2 G(\hat{k}'') Q^2 G(\hat{Q})][\mathbf{q}\cdot(\mathbf{k}'-\mathbf{q})][\mathbf{Q}\cdot(\mathbf{k}''-\mathbf{Q})][\mathbf{p}\cdot(\mathbf{Q}-\mathbf{p})]$$
$$\times[\langle h(\hat{k})h(\hat{q})h(\hat{k}'-\hat{q})h(\hat{k}''-\hat{q})h(\hat{p})h(\hat{Q}-\hat{p})\rangle] \quad (6.63)$$

The height correlation appearing in equation 6.63 is expressed as

$$\langle h(\hat{k})h(\hat{q})h(\hat{k}'-\hat{q})h(\hat{k}''-\hat{Q})h(\hat{p})h(\hat{Q}-\hat{p})\rangle = 24(2D_0)^3[2\pi]^{3(d+1)}[|G_0(\hat{q})|^2]|G_0(\hat{k}'-\hat{q})|^2$$
$$\times|G(\hat{k})|^2[G(\hat{k}')k'^2][G(-\hat{k}-\hat{k}')|\mathbf{k}+\mathbf{k}'|^2][\mathbf{k}'^2 G(-\hat{k}')]\delta^{d+1}(\hat{k}+\hat{k}'+\hat{k}'')[\delta^{d+1}(\hat{p}+\hat{q})]$$
$$\times[\delta^{d+1}(\hat{Q}+\hat{k}')] \quad (6.64)$$

Substituting the above form in equation 6.63, we obtain

$$W_3^{(2)} = 12(\lambda_0 D_0)\int \frac{d^{d+1}\hat{k}}{[2\pi]^{d+1}} \int \frac{d^{d+1}\hat{k}'}{[2\pi]^{d+1}} |\mathbf{k}+\mathbf{k}'|^2[\mathbf{k}'\cdot(-\mathbf{k})]|G(\hat{k}')|^2|G(\hat{k})|^2 G(\hat{k}-\hat{k}')$$
$$L_3^{(2)}(\hat{k}') \quad (6.65)$$

where $L_3^{(2)}(\hat{k}') = k'^4 l_3^{(2)}(\hat{k}')$ and

$$l_3^{(2)}(\hat{k}') = 2(\lambda_0 D_0)^2 \int \frac{d^{d+1}q}{[2\pi]^{d+1}}[\mathbf{q}\cdot(\mathbf{q}-\mathbf{k}')]^2[\mathbf{q}\cdot(\mathbf{k}'-\mathbf{q})]|G_0(\hat{k}'-\hat{q})|^2|G_0(\hat{q})|^2 \quad (6.66)$$

We consider the external momenta and frequencies are much smaller in magnitude than internal momenta and frequencies and perform the frequency integration and

momentum integration in the range $\Lambda_0 e^{-r} \leq q \leq \Lambda_0$ leading

$$l_3^{(2)<}(r) = \frac{(\lambda_0 D_0)^2 K_d}{2\nu_0^3}\left[\frac{\Lambda_0^{d-8} - \Lambda^{d-8}(r)}{(d-8)}\right]. \tag{6.67}$$

We construct a differential equation for $l_3^{(2)}(r)$ by considering the iterative nature of the procedure

$$\frac{dl_3^{(2)}}{dr} = \frac{\lambda_0^2 D_0^2 K_d}{2\nu^3(r)}\Lambda^{d-8}(r) \tag{6.68}$$

Integrating over r, we obtain

$$l_3^{(2)}(r) = \frac{D_0}{10}\Lambda^{-4}(r) \tag{6.69}$$

in $d = 1$ dimension. We identify $\Lambda(r)$ as an external momentum and obtain

$$L_3^{(2)} = k'^4 l_3^{(2)}(k', 0) = D_0/10 \tag{6.70}$$

which is an scale independent quantity. We substitute equation 6.70 in equation 6.65 leading to

$$W_3^{(2)} = \frac{6}{5}(\lambda_0 D_0^2)\int \frac{d^2\hat{k}}{[2\pi]^2}\int \frac{d^2\hat{k}'}{[2\pi]^2}[-\mathbf{k}'\cdot\mathbf{k}]|\mathbf{k}+\mathbf{k}'|^2|G(\hat{k}')|^2|G(\hat{k})|^2 G(-\hat{k}-\hat{k}') \tag{6.71}$$

Carrying out the frequency integration, we obtain

$$W_3^{(2)} = -\frac{6\pi}{25}\left(\frac{D_0}{\lambda_0}\right)\int_{-\infty}^{\infty}\frac{dk}{[2\pi]}\int_{-\infty}^{\infty}\frac{dk'}{[2\pi]}F_2(k,k') \tag{6.72}$$

where

$$F_2(k,k') = \frac{(k'k)(k+k')^2}{|k|^3|k'|^3[|k|^3+|k'|^3+|k+k'|^3]} \tag{6.73}$$

We write

$$W_3^{(2)} = -\left(\frac{3}{50\pi}\right)\left(\frac{D_0}{\lambda_0}\right)[2(I_2(\mu)+J_2(\mu))] \tag{6.74}$$

where

$$I_2(\mu) = \int_{\mu}^{\infty} dk \int_{\mu}^{\infty} dk' F_2(k,k')$$

and

$$J_2(\mu) = \int_{\mu}^{\infty} dk \int_{\mu}^{\infty} dk' F_2(-k,k').$$

As before we write the integrals as

$$I_2(\mu) = I_2^{(0)}\mu^{-3}$$
$$J_2(\mu) = J_2^{(0)}\mu^{-3}. \tag{6.75}$$

Numerical evaluations yield

$$I_2^{(0)} = \lim_{\mu\to 0^+}[\mu^3 I_2(\mu)] = 0.154439$$
$$J_2^{(0)} = \lim_{\mu\to 0^+}[\mu^3 J_2(\mu)] = -0.020075, \tag{6.76}$$

Substituting equations 6.76 and 6.75 in equation 6.74, we obtain

$$\begin{aligned} W_3^{(2)} = & \frac{3}{50\pi}(2I_2^{(0)} + 2J_2^{(0)})\left(\frac{D}{\lambda_0}\right)\frac{1}{\mu^3} \\ & = -\frac{3}{50\pi}(0.268728)\left(\frac{D}{\lambda_0}\right)\frac{1}{\mu^3}. \end{aligned} \tag{6.77}$$

C. Calculation of $W_3^{(3)}$

The integral expression for $W_3^{(3)}$ can be written as

$$\begin{aligned} W_3^{(3)} = & \left(\frac{-\lambda_0}{2}\right)^3 \int \frac{d^{d+1}\hat{k}}{(2\pi)^{d+1}} \int \frac{d^{d+1}\hat{k}'}{(2\pi)^{d+1}} \int \frac{d^{d+1}\hat{p}}{(2\pi)^{d+1}} \int \frac{d^{d+1}\hat{q}}{(2\pi)^{d+1}} \int \frac{d^{d+1}\hat{q}'}{(2\pi)^{d+1}} \int \frac{d^{d+1}\hat{Q}}{(2\pi)^{d+1}} \\ & \times[\mathbf{Q}\cdot(\mathbf{k}'-\mathbf{Q})][\mathbf{q}'\cdot(\mathbf{Q}-\mathbf{q}')]][\mathbf{q}\cdot(\mathbf{q}'-\mathbf{q})][G(\hat{k}')|k'|^2|Q^2||q'|^2 G_0(\hat{Q})G_0(\hat{q}') \\ & \times\langle h(\hat{p})h(\hat{k})h(\hat{k}'-\hat{Q})h(\hat{Q}-\hat{q}')h(\hat{q})h(\hat{q}'-\hat{q})\rangle \end{aligned} \tag{6.78}$$

which is depicted in figure 6.3(a). The height correlation appearing in equation 6.78 is expressed as

$$\begin{aligned} \langle h(\hat{p})h(\hat{k})h(\hat{k}'-\hat{Q})h(\hat{Q}-\hat{q}')h(\hat{q})h(\hat{q}'-\hat{q})\rangle = & \; 48(2D_0)^3[2\pi]^{3(d+1)}|G_0(\hat{q}'+\hat{k})|^2|G_0(\hat{p})|^2 \\ & |G_0(\hat{k})|^2\delta^{d+1}(\hat{Q}+\hat{p}-\hat{q}')\delta^{d+1}(\hat{q}'+\hat{k}-\hat{q}) \\ & \delta^{d+1}(\hat{q}'-\hat{p}-\hat{k}') \end{aligned} \tag{6.79}$$

Substituting equation 6.79 in equation 6.78, we obtain

$$W_3^{(3)} = -48(\lambda_0 D_0)^3 \int \frac{d^{d+1}\hat{k}}{(2\pi)^{d+1}} \int \frac{d^{d+1}\hat{p}}{(2\pi)^{d+1}} |\mathbf{k}+\mathbf{p}|^2|G(\hat{p})|^2|G(\hat{k})|^2]G(-\hat{k}-\hat{p})L_3(\hat{k};\hat{p}) \tag{6.80}$$

where

$$l_3^{(3)}(\hat{k};\hat{p}) = \int \frac{d^{d+1}\hat{q}'}{(2\pi)^{d+1}}|\mathbf{q}'-\mathbf{p}|^2|q'|^2[\mathbf{q}'\cdot\mathbf{p}][(\mathbf{q}'-\mathbf{p})\cdot(\mathbf{k}+\mathbf{q}')][(\mathbf{q}'+\mathbf{k})\cdot\mathbf{k}]G_0(\hat{q}') \\ G_0(\hat{q}'-\hat{p})|G_0(\hat{q}'+\hat{k})|^2 \tag{6.81}$$

Assuming the internal wave vector q' is much greater than external wave vectors p and k, we get

$$L_3^{(3)}(\mathbf{k},0;\mathbf{p},0) = -\int \frac{d^{d+1}q'}{[2\pi]^{d+1}}|q'|^6[\mathbf{q}'\cdot\mathbf{p}][\mathbf{q}'\cdot\mathbf{k}]|G_0(\hat{q}')|^2G_0^2(\hat{q}'). \tag{6.82}$$

Carrying out the frequency and momentum ($\Lambda_0 e^{-r} \leq q' \leq \Lambda_0$) integration in $d=1$ dimension, we follow the same procedure as in Sec. 4.1 and obtain

$$L_3^{(3)}(p,0;k,0) = -\frac{p\,k}{10\lambda_0^2 D_0}\ln(\Lambda_0/k). \tag{6.83}$$

We substitute equation 6.83 in equation 6.80 and obtain

$$W_3^{(3)} = \frac{24}{5}\left(\lambda_0 D_0^2\right)\ I_3 \tag{6.84}$$

where

$$I_3 = \int \frac{dk\,d\omega_1}{[2\pi]^2}\int \frac{dp\,d\omega_2}{[2\pi]^2}[k\,p]([k+p])^2|G(\hat{k})|^2|G(\hat{p})|^2G(-\hat{k}-\hat{p})\ln(\Lambda_0/k) \tag{6.85}$$

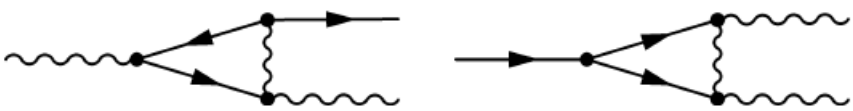

(a) (b)

Figure 6.3: Feynman diagrams: (a) $W_3^{(3)}$ and (b) $W_3^{(4)}$. These diagrams yield logarithmic corrections same in magnitude with opposite signs.

D. Calculation of $W_3^{(4)}$

We express $W_3^{(4)}$ in momentum and frequency spaces as

$$\begin{aligned} W_3^{(4)} &= \left(\frac{-\lambda_0}{2}\right)^3 \int \frac{d^{d+1}\hat{k}}{[2\pi]^{d+1}} \int \frac{d^{d+1}\hat{k}'}{[2\pi]^{d+1}} \int \frac{d^{d+1}\hat{p}}{[2\pi]^{d+1}} \int \frac{d^{d+1}\hat{q}}{[2\pi]^{d+1}} \int \frac{d^{d+1}\hat{q}'}{[2\pi]^{d+1}} \int \frac{d^{d+1}\hat{Q}}{[2\pi]^{d+1}} \\ &\times [\mathbf{q}\cdot(\mathbf{k}'-\mathbf{Q}-\mathbf{q})][\mathbf{Q}\cdot(\mathbf{k}'-\mathbf{Q})][\mathbf{q}'\cdot(\mathbf{Q}-\mathbf{q}')]|\mathbf{k}'-\mathbf{Q}|^2|Q|^2|k'|^2 G(\hat{Q})G(\hat{k}') \\ &\times G(\hat{k}'-\hat{Q})[\langle h(\hat{p})h(\hat{k})h(\hat{q})h(\hat{q}')h(\hat{k}'-\hat{Q}-\hat{q})h(\hat{Q}-\hat{q}')\rangle] \end{aligned} \tag{6.86}$$

and the corresponding Feynman diagram is depicted in figure 6.3(b). Height correlation in equation 6.86 is written as

$$\begin{aligned} \langle h(\hat{p})h(\hat{k})h(\hat{q})h(\hat{q}')h(\hat{k}'-\hat{Q}-\hat{q})h(\hat{Q}-\hat{q}')\rangle &= 24(2D_0)^3[2\pi]^{3(d+1)}|G_0(\hat{k}+\hat{Q})|^2|G_0(\hat{p})|^2 \\ &\quad |G_0(\hat{k})|^2\delta^{d+1}(\hat{q}+\hat{k}+\hat{Q})\delta^{d+1}(\hat{Q}+\hat{q}'-\hat{k}) \\ &\quad \delta^{d+1}(\hat{k}+\hat{k}'+\hat{p}). \end{aligned} \tag{6.87}$$

We substitute equation 6.87 in equation 6.86 and obtain

$$W_3^{(4)} = -24(\lambda_0 D_0)^3 \int \frac{d^{d+1}\hat{k}}{[2\pi]^{d+1}} \int \frac{d^{d+1}\hat{p}}{[2\pi]^{d+1}} |\mathbf{k}+\mathbf{p}|^2|G(\hat{p})|^2|G(\hat{k})|^2]G(\hat{k}-\hat{p})L_3^{(4)}(\hat{p};\hat{k}) \tag{6.88}$$

where

$$\begin{aligned} l_3^{(4)}(\hat{p};\hat{k}) &= \int \frac{d^{d+1}\hat{Q}}{[2\pi]^{d+1}} [\mathbf{Q}\cdot(-\mathbf{k}-\mathbf{p}-\mathbf{Q})][(-\mathbf{k}-\mathbf{Q})\cdot -\mathbf{p}][(\mathbf{k}+\mathbf{Q})\cdot -\mathbf{k}]|\mathbf{k}+\mathbf{p}+\mathbf{Q}|^2 \\ &\quad |Q|^2 G_0(\hat{Q})G(-\hat{k}-\hat{p}-\hat{Q})|G(\hat{k}+\hat{Q})|^2 \end{aligned} \tag{6.89}$$

Considering external momenta and frequencies ($\hat{p}$ and $\hat{k}$) are much smaller than the internal momenta and frequency ($\hat{Q}$), we obtain

$$l_3^{(4)}(\mathbf{p},0;\mathbf{k},0) = \int \frac{d^{d+1}\hat{Q}}{[2\pi]^{d+1}} [\mathbf{Q}\cdot\mathbf{k}]\,[\mathbf{Q}\cdot\mathbf{p}]|Q|^6\, G_0(\hat{Q})G(-\hat{k}-\hat{p}-\hat{Q})|G(\hat{Q})|^2 \tag{6.90}$$

Performing the frequency integration and working out the momentum integration in the high-momentum shell $\Lambda_0 e^{-r} \le Q \le \Lambda_0$, we follow the same procedure as in Sec. 4.1 and 4.2 and obtain

$$l_3^{(4)}(p,0;k,0) = -\frac{p\,k}{5\lambda_0^2 D_0}\ln(\Lambda_0/k) \tag{6.91}$$

in $d = 1$ dimension. We substitute equation 6.91 in equation 6.87 and get

$$W_3^{(4)} = -\frac{24}{5}\left(\lambda_0 D_0^2\right)\ I_4 \tag{6.92}$$

where

$$I_4 = \int \frac{dk\, d\omega_1}{[2\pi]^2} \int \frac{dp\, d\omega_2}{[2\pi]^2} [k\, p]([k+p])^2 |G(\hat{k})|^2 |G(\hat{p})|^2 G(-\hat{k}-\hat{p}) \ln(\Lambda_0/k). \tag{6.93}$$

It is seen that the integral form of I_3 and I_4, expressed in equations 6.85 and 6.93, respectively, are identical. Hence the logarithmic contributions $W_3^{(3)}$ and $W_3^{(4)}$, obtained in equations 6.84 and 6.92, respectively, are same in magnitude and opposite in signs. Thus, they cancel each other exactly and effectively do not contribute to W_3.

E. Calculation of $W_3^{(5)}$

The expression for $W_3^{(5)}$ in momentum and frequency space is given by

$$\begin{aligned} W_3^{(5)} \;=\; & \left(\frac{-\lambda_0}{2}\right)^3 \int \frac{d^{d+1}\hat{k}}{[2\pi]^{d+1}} \int \frac{d^{d+1}\hat{k}'}{[2\pi]^{d+1}} \int \frac{d^{d+1}\hat{p}}{[2\pi]^{d+1}} \int \frac{d^{d+1}\hat{q}}{[2\pi]^{d+1}} \int \frac{d^{d+1}\hat{q}'}{[2\pi]^{d+1}} \int \frac{d^{d+1}\hat{Q}}{[2\pi]^{d+1}} \\ & [\mathbf{Q}\cdot(\mathbf{k}'-\mathbf{Q})][\mathbf{q}\cdot(\mathbf{p}-\mathbf{q})][\mathbf{q}'\cdot(\mathbf{Q}-\mathbf{q}')]|k'|^2|p|^2|Q|^2 G(\hat{k}')G(\hat{p})G(\hat{Q}) \\ & \langle h(\hat{k}'-\hat{Q})h(\hat{q}')h(\hat{Q}-\hat{q}')h(\hat{q})h(\hat{p}-\hat{q})h(\hat{k}')\rangle \end{aligned} \tag{6.94}$$

Feynman diagram corresponding to $W_3^{(5)}$ is shown in figure 6.4(a). We express the height correlation appearing in equation 6.94 as

$$\begin{aligned} \langle h(\hat{k}'-\hat{Q})h(\hat{q}')h(\hat{Q}-\hat{q}')h(\hat{q})h(\hat{p}-\hat{q})h(\hat{k})\rangle \;=\; & 48(2D_0)^3[2\pi]^{3(d+1)} G(\hat{p}+\hat{k}')G(\hat{k})|G(\hat{k}')|^2 \\ & |G_0(\hat{k}'-\hat{Q})|^2\, \delta^{d+1}(\hat{k}'+\hat{q})\, \delta^{d+1}(\hat{k}'-\hat{q}') \\ & \delta^{d+1}(\hat{k}+\hat{p}+\hat{k}'). \end{aligned} \tag{6.95}$$

Substituting equation 6.95 in equation 6.94, we obtain

$$\begin{aligned} W_3^{(5)} \;=\; & 48(2D_0)^2 \left(\frac{-\lambda_0}{2}\right)^3 \int \frac{d^{d+1}\hat{k}}{[2\pi]^{d+1}} \int \frac{d^{d+1}\hat{p}}{[2\pi]^{d+1}} |\mathbf{k}+\mathbf{p}|^2 |p|^2 G(-\hat{k}-\hat{p})G(\hat{p})G(\hat{k}) \\ & |G(\hat{k}+\hat{p})|^2 [(\mathbf{k}+\mathbf{p})\cdot\mathbf{k}] L_3^{(5)}(\hat{k}+\hat{p}) \end{aligned} \tag{6.96}$$

where

$$L_3^{(5)}(\hat{k}+\hat{p}) = (2D_0)\int \frac{d^{d+1}\hat{Q}}{[2\pi]^{d+1}}[\mathbf{Q}\cdot(\mathbf{Q}+\mathbf{k}+\mathbf{p})][(\mathbf{Q}-\mathbf{k}-\mathbf{p})\cdot(\mathbf{k}+\mathbf{p})]|Q|^2 G_0(\hat{Q}) \\ |G_0(\hat{k}+\hat{p}+\hat{Q})|^2 \tag{6.97}$$

Considering internal momenta are much larger than the external momenta, we obtain

$$L_3^{(5)}(\hat{k}+\hat{p}) = -(2D_0)\int \frac{d^{d+1}\hat{Q}}{[2\pi]^{d+1}}|Q|^4[\mathbf{Q}\cdot(\mathbf{k}+\mathbf{p})]G_0(\hat{Q})|G_0(\hat{k}+\hat{p}+\hat{Q})|^2 \tag{6.98}$$

We perform the frequency integration and obtain

$$L_3^{(5)}(k+p) = -\frac{D_0}{4\nu_0^2}(k+p)\int_{-\infty}^{\infty}\frac{dQ}{[2\pi]}\,\frac{Q}{|Q|^4} = 0 \tag{6.99}$$

in $d=1$ dimension. Hence, $W_3^{(5)}$ yields zero contribution. Similarly other terms such as $W_3^{(6)}$, $W_3^{(7)}$ and $W_3^{(8)}$, shown in figures. 6.4(b), 6.4(c) and 6.4(d), respectively, give vanishing contributions individually.

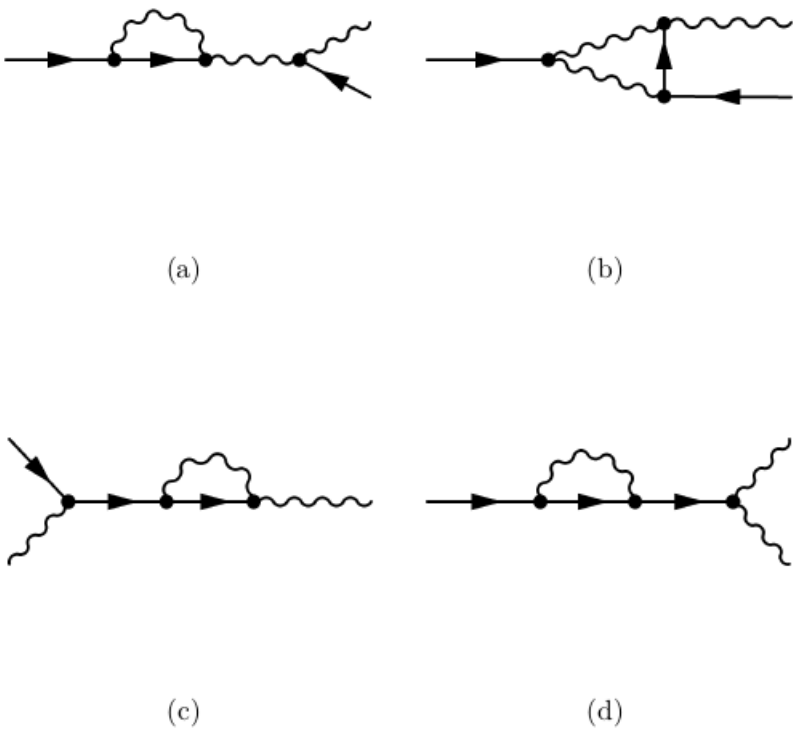

Figure 6.4: Feynman diagrams: (a) $W_3^{(5)}$, (b) $W_3^{(6)}$, (c) $W_3^{(7)}$ and (d) $W_3^{(8)}$. These diagrams yield zero contributions individually.

F. Skewness in One dimension

Adding all the terms on the right hand side of equation 6.46, we observe that the effective contribution to W_3 comes from $W_3^{(1)}$ and $W_3^{(2)}$, given in equations 6.45 and 6.100, yielding

$$W_3 = W_3^{(1)} + W_3^{(2)} = -\frac{3}{50\pi}[0.249917]\left(\frac{D_0}{\lambda_0}\right)\frac{1}{\mu^3}. \tag{6.100}$$

Hence, we calculate the skewness employing the definition given in equation 6.6 wherein we substitute the calculated values for W_2 and W_3 from equations 6.45 and 6.100 . Thus we obtain

$$S = \frac{W_3}{W_2^{3/2}} = -0.044072 \tag{6.101}$$

which is independent of the model parameters (λ_0 ν_0 D_0) and the momentum cutoffs (μ_0, Λ_0).

6.5 Discussion and Conclusion

In this Chapter, we considered the conserved stochastic growth of a surface due to particle deposition on a flat substrate and we find the statistical properties of the surface in the large-scale long-time limits. The corresponding dynamics is represented by the VLDS equation driven by a stochastic Gaussian white noise. We followed an RG scheme without rescaling akin to Yakhot and Orszag[207,208].

This RG scheme differs from the conventional dynamical RG scheme of Ma and Mazenko[118], Forster *et al.*[47], and Medina *et al.*[128] in the sense that the renormalized quantity are not rescaled and their flow equation are directly worked out. Thus, we obtained the renormalized diffusivity $\nu(r)$ at large r and the roughness exponent $\chi = 1$. This is consistent with the previous RG results obtained by Lai and Das Sarma[111].

Subsequently, we calculate the skewness of height fluctuations of the VLDS equation. A similar scheme was employed earlier for the calculation of skewness[?] and kurtosis[170] in the case of non-conserved interface growth governed by the $(1+1)$-dimensional KPZ equation. The amputated parts of the connected loop diagrams, namely, l_2, $l_3^{(1)}$, $l_3^{(2)}$, $l_3^{(3)}$, $l_3^{(4)}$ etc., for the second and third moments as shown in Figs. 1(b), 2(a), 2(b), 3(a), 3(b) etc., respectively, are renormalized by means of scale elimination and by constructing differential equations representing how these renormalized quantities flow with respect to the RG decimation scheme. The so-

lutions to the differential equations immediately yield their renormalized values. Employing this RG scheme, we directly find the renormalized expressions for these loop integrals which are indispensable for the calculation of moments. These renormalized amputated parts of the loops are used in conjunction with the external legs to numerically evaluate the integrals for the second and third moments.

Our approach consideres calculations of W_2 and W_3 in the large scale limit $k \to 0$ and consequently expects the statistical properties of the growth process at large scales. It is to be noted that these moments are independent of the upper cutoff Λ_0 and functions of lower cutoff μ which may be identified with the inverse of the substrate size L. These moments are also observed to follow the expected scaling $W_n \sim L^{n\chi}$. The value for the skewness is immediately obtained from these calculated values which is found to be independent of the model parameters (λ_0, D_0, ν_0) and the UV and IR cutoffs (Λ_0, μ), suggesting its universality.

It is interesting to note that we obtained the skewness value which is a negative number. This is consistent with the numerical prediction of Das Sarma *et al.*[32] who obtained $S = -0.1 \pm 0.15$ in the steady state and suggested that the skewness value is likely to be negative, although they did not exclude a zero or slightly positive value. The large error bar that they obtained is probably due to a dominant role of fluctuations in their numerical model. We observe that our value of $S = -0.0441$ is consistent with their prediction. Moreover our calculated value asserts that the probability distribution function is negatively skewed.

Chapter 7

Renormalized cumulants and velocity derivative skewness in Kolmogorov turbulence

7.1 Introduction

The turbulent flow of an incompressible fluid governed by the Navier-Stokes (NS) equation has long been considered as a challenging problem due to its inherent non-linearity and complexity[50,114,116,125]. Various important advances have been made over the last decades in understanding the statistical properties of turbulence following from the governing dynamical equation. The Navier-Stokes equation for an incompressible turbulent fluid is expressed as

$$\frac{\partial u_i}{\partial t} + u_j \frac{\partial u_i}{\partial x_j} = -\frac{1}{\rho}\frac{\partial p}{\partial x_i} + \nu_0 \frac{\partial^2 u_i}{\partial x_j \partial x_j}, \tag{7.1}$$

with the incompressibility condition

$$\frac{\partial u_i}{\partial x_i} = 0, \tag{7.2}$$

coming from the equation of continuity. Here $u_i(\mathbf{x}, t)$ is the velocity field, $p(\mathbf{x}, t)$ the pressure field, ρ the density, and ν_0 is the kinematic viscosity of the fluid. The pressure field can be expressed in terms of the velocity field using the incompressibility condition $\partial u_i/\partial x_i = 0$. The relative importance of the inertial convective term $u_j \partial u_i/\partial x_j$ and the viscous term $\nu_0 \partial^2 u_i/\partial x_j \partial x_j$ is determined by the Reynolds number $R = UL/\nu_0$, where L and U are the integral length and velocity scales,

respectively.

In three-dimensions, the turbulent energy density obeys the Kolmogorov universal scaling (neglecting intermittency correction)

$$E(k) = C\ \varepsilon^{2/3}\ k^{-5/3} \tag{7.3}$$

in the inertial range $L^{-1} \ll k \ll \eta^{-1}$ where the turbulent energy cascades from the largest to the smallest scales of motion[50,101,116]. In the above expression, C is the universal Kolmogorov constant, ε the energy transfer rate (per unit mass) which is also the mean dissipation rate, and k is the wavenumber. The Kolmogorov microscale η, defined as $\eta = (\nu^3/\varepsilon)^{1/4}$, signifies the scale where dissipation becomes important. Within the Kolmogorov phenomenology, the eddy-viscosity follows the universal scaling

$$\nu(k) = \alpha\ \varepsilon^{1/3}\ k^{-4/3}, \tag{7.4}$$

where α is another universal constant.

Statistical characterization of Navier-Stokes turbulence begins most often with an equal-time n-th order structure function $\Phi_n(r) = \langle|\Delta\mathbf{u}_\mathbf{r}|^n\rangle$ that represents the n-th order cumulant (with respect to the probability distribution) of the velocity difference $\Delta\mathbf{u}_r = \mathbf{u}(\mathbf{x}+\mathbf{r}) - \mathbf{u}(\mathbf{x})$ between two points separated by a displacement $\mathbf{r}$ at the same time t[52,114,117,156,157,164,173,174]. Within the Kolmogorov's phenomenological picture, the PDF in the inertial-range is universal and, as a consequence, its statistical characterization is expected to be described in terms of universal numbers[50,114,116]. It has been observed, both experimentally[14,109] and numerically[81], that the full probability distribution deviates from the normal distribution. The increasingly non-Gaussian statistics of velocity differences towards small scales has usually been attributed to the spatially intermittent character of the fine-scale structure in such flows. As the velocity-gradient field in high Reynolds number turbulent flows is increasingly dominated by the velocity fluctuations towards the smaller scales of motion, knowledge of the statistical cumulants of velocity-gradient for a turbulent flow is important to understand the fine-scale statistics of turbulence.

In the past couple of decades, extensive experimental[15,19,50], numerical[55,80,142,193,198], and theoretical[8,24,103,115,138,155,171,208] investigations on the statistical cumulants of velocity gradient for homogeneous and isotropic turbulent flows have been carried out. Experimentally, the longitudinal velocity gradient $\partial u_1/\partial x_1$ is found to be negatively skewed[15,19], yielding $S = \langle(\frac{\partial u_1}{\partial x_1})^3\rangle/\langle(\frac{\partial u_1}{\partial x_1})^2\rangle^{3/2} \approx -0.5$. This was also confirmed via a numerical simulation with the three-dimensional Navier-Stokes equation

for incompressible flow[142] that led to $S = -0.47$ at moderate Taylor-microscale Reynolds numbers ($20 \leqslant R_\lambda \leqslant 45$). Subsequently, direct numerical simulations (DNSs) for three-dimensional homogeneous isotropic turbulence[55,80,193,198] also suggested that S is independent of R_λ at moderate R_λ. At $R_\lambda \approx 150$, Vincent and Meneguzzi[193] obtained $S = -0.5$ in their DNS. Wang *et al.*[198] performed a set of DNSs on both the freely decaying and forced stationary isotropic turbulence fields for $21 < R_\lambda < 195$ and showed that the velocity derivative skewness $S \approx -0.5$ is almost independent of the flow Reynolds number. Performing a high resolution DNS, Gotoh[55] suggested that the skewness factor of the longitudinal velocity derivative is very insensitive to R_λ over a range $38 \leqslant R_\lambda \leqslant 460$, and its average value is $S = -0.53$. In another recent DNS with 4096^3 grid points, Ishihara *et al.*[80] showed that the $S \approx -0.5$ for $R_\lambda < 200$.

In theoretical investigations, namely in eddy-damped quasi-normal Markovian (EDQNM) closure[8,103,115,155], multi-fractal (MF) model[24,50,138], and dynamic RG analyses[171,208], the value of skewness turned out to be comparable to the above mentioned experimental and numerical predictions. Using EDQNM closure, André and Lesieur[8] showed that the value of S increases with R_λ and tends to the value $S = -0.495$ for large R_λ. Kraichnan[103] applied a mapping closure model on the Navier-Stokes equation and showed that skewness of turbulent velocity derivative is asymptotically independent of the Reynolds number. Using the EDQNM closuer, Lesieur and Ossia[115] investigated three-dimensional isotropic turbulence at very high Reynolds numbers and obtained $S = -0.547$, independent of Reynolds number. Qian[155], on the other hand found a constant value of skewness, namely $S = -0.515$ for very high value of Reynolds numbers. The MF model[138] suggested that the skewness increases with Reynolds number as $S \sim -R_\lambda^{0.14}$. The dynamic RG scheme of Yakhot and Orszag[?] yields $S = -0.4878$ in three dimensions. Smith and Reynolds[171] made a correction in their calculation and obtained $S = -0.59$.

While these theoretical studies provide estimates for the velocity derivative skewness comparable to the experimental estimates[15,19,50] and numerical predictions[55,193,198] mentioned above, a few recent experiments and a high-resolution DNS suggest higher magnitudes for skewness at high Reynolds numbers. Particularly, recent hot-wire anemometer measurements in active-grid wind-tunnel turbulence[1] yielded the velocity derivative skewness over a range $149 \leqslant R_\lambda \leqslant 729$. From the measured data for S, they obtained an R_λ-dependent empirical relation $S = -0.33R_\lambda^{0.09}$, indicating that the value of S slowly becomes more negative with increasing Reynolds number [the skewness value is $S = -0.597$ for $R_\lambda = 729$ (corresponding to $R \approx \frac{R_\lambda^2}{16} =$

3.3×10^4)[114]]. A similar behavior was observed in a very high resolution DNS[80] carried out up to $R_\lambda = 1130$ where the skewness data for $200 < R_\lambda \leq 680$ were found to fit well with a power law $S \sim -(0.32 \mp 0.02)\ R_\lambda^{0.11 \pm 0.01}$. They reported the skewness value $S = -0.648 \pm 0.003$ for $R_\lambda = 680$ (corresponding to $R \approx 2.9 \times 10^4$).

The dynamic RG scheme was initially used by Forster, Nelson and Stephen[47] for the case of Navier-Stokes fluid along with the coupled problem of the advection of a passive scalar subjected to a random driving force. They adopted the procedure developed earlier by Ma and Mazenko[118]. It was observed by DeDominicis and Martin[34] that for a particular case of randomly stirred model, Kolmogorov's inertial-range scaling for the energy spectrum, $E(k) \sim k^{-5/3}$, is realizable. Yakhot and Orszag[208] applied the dynamic RG scheme on the randomly stirred model of DeDominicis and Martin and calculated various universal numbers including the velocity derivative skewness associated with Kolmogorov turbulence. Using an amplitude ratio coming from the energy transport equation, they obtained $S = \langle(\frac{\partial u_1}{\partial x_1})^3\rangle / \langle(\frac{\partial u_1}{\partial x_1})^2\rangle^{3/2} = -0.4878$ which was corrected to $S = -0.59$ in Ref.[171]. Here we consider an alternative scheme that yields renormalized quantities relevant for the calculation of skewness. This scheme is different from the above RG schemes as it finds a relation between the renormalized Feynman diagrams involving the renormalized viscosity. Recently this procedure was found to be successful in determining the experimentally observed statistical characteristics in KPZ[169,170] and VLDS[168] surface growth dynamics. This scheme enables us to calculate the second- and third-order cumulants of velocity derivative and the resulting value for skewness is obtained as $S = -0.647$. This value is obtined when only the innertial range with Kolmogorov scaling is considered. It is however important to take the dissipation range into account in order to calculate the integrals for the second and third order cumulants. Consequently, we employ Pao's model that joins the innertial range smoothly with the dissipation range and evaluate the integrals for the second and third order cumulants. The resulting skewness value $\mathcal{S}$ turns out to be $\mathcal{S} = -0.682$.

This Chapter is organized as follows. In Section II we introduce the randomly stirred model and calculate an amplitude ratio needed later. Calculations of second- and third-order renormalized cumulants and skewness in the Kolmogorov range are presented in Section III. Section IV generalizes teh calculations of second and third order cumulants and skewness to include the dissipation range. Finally, a discussion and conclusion are given in Section V.

Figure 7.1: Feynman diagram giving contribution to Υ. The propagators are indicated by solid lines and correlation by a wiggly line.

7.2 Randomly stirred dynamics

In order to calculate the velocity derivative skewness, we use Fourier transformation of the velocity field

$$u_i(\mathbf{x},t) = \int \frac{d^dk}{[2\pi]^d} \int_{-\infty}^{\infty} \frac{d\omega}{[2\pi]} u_i(\mathbf{k},\omega) e^{i(\mathbf{k}\cdot\mathbf{x}-\omega t)}, \tag{7.5}$$

along with the incompressibility condition

$$k_i u_i(\mathbf{k},\omega) = 0.$$

Thus, the Fourier transformed Navier-Stokes equation becomes

$$\left(-i\omega + \nu_0 k^2\right) u_i(\mathbf{k},\omega) = f_i(\mathbf{k},\omega) - \frac{i\lambda_0}{2} P_{ijl}(\mathbf{k}) \int \frac{d^dq}{[2\pi]^d} \int_{-\infty}^{\infty} \frac{d\Omega}{[2\pi]} u_j(\mathbf{q},\Omega) u_l(\mathbf{k}-\mathbf{q},\omega-\Omega), \tag{7.6}$$

where $P_{ijl}(\mathbf{k}) = k_j P_{il}(\mathbf{k}) + k_l P_{ij}(\mathbf{k})$ with $P_{ij}(\mathbf{k}) = (\delta_{ij} - \frac{k_i k_j}{\mathbf{k}^2})$. A random force term $f_i(\mathbf{k},\omega)$ is introduced in Eq. (7.6) following the randomly stirred model of DeDominicis and Martin[34]. This forcing field maintains a statistically steady state and it is assumed to have a Gaussian white-noise statistics with the correlation

$$\langle f_i(\mathbf{k},\omega) f_j(\mathbf{k}',\omega')\rangle = F(k) P_{ij}(\mathbf{k}) [2\pi]^d \delta^d(\mathbf{k}+\mathbf{k}') [2\pi] \delta(\omega+\omega'), \tag{7.7}$$

where $F(k)$ is modeled as

$$F(k) = \frac{2D_0}{k^y}, \tag{7.8}$$

with d the space dimension, D_0 a constant and y is a parameter which is taken as $y = d$ for consistency with Kolmogorov spectrum given by Eq. 7.3. An expansion parameter $\lambda_0(=1)$ is introduced in the non-linear term of Eq. (7.6).

Since the nonlinear term poses mathematical difficulty in the problem, it is customary to treat it as a perturbation. It is in fact possible to construct renormalized

expressions for the second and third cumulants from the perturbation theory. We shall calculate the renormalized cumulants in the next two sections. We shall see that the expressions for the second and third cumulants contain the amplitude ratio α^2/C. We evaluate its value using a recursive shell elimination procedure that we shall also use latter while evaluating the second and third cumulants. The value of $\nu(k)k^2$ is determined by the renormalized loop in Fig. 7.1. The bare value of the loop is determined by the expression

$$\Upsilon = 2\lambda_0^2 D_0 P_{ijl}(\mathbf{k}) \int \frac{d^{d+1}\hat{q}}{[2\pi]^{d+1}} P_{jni}(\mathbf{k}-\mathbf{q}) P_{ln}(\mathbf{q}) |\mathbf{q}|^{-y} |G_0(\hat{q})|^2 G_0(\hat{k}-\hat{q}), \tag{7.9}$$

where we use the short-hand notation $\int d^{d+1}\hat{q} \equiv \int d^d q \int_{-\infty}^{\infty} d\Omega$ with $G_0(\hat{q}) \equiv G_0(\mathbf{q},\Omega) = [-i\Omega + \nu_0 q^2]^{-1}$ the bare propagator. We perform the integration over frequency Ω and expand the integrand in the limit $q \gg k$ because we wish to eliminate the high wavenumber band $\Lambda_0 e^{-r} \leq q \leq \Lambda_0$. Consequently, we find that Υ is proportional to k^2 in the large scale long time limit. The quantity $\nu^<(r) = \Upsilon^<(r)/k^2$, where $\Upsilon^<(r)$ is the value of Υ after the elimination of the high wavenumber band, is given by

$$\nu^<(r) = \frac{S_d}{[2\pi]^d} \left(\frac{\lambda_0^2 D_0}{\nu_0^2}\right) \left(\frac{d^2-4-y}{2d(d+2)}\right) \int_{\Lambda_0 e^{-r}}^{\Lambda_0} q^{d-y-5} dq \tag{7.10}$$

This yields

$$\nu^<(r) = \frac{S_d}{[2\pi]^d} \frac{\lambda_0^2 D_0}{2\nu_0^2 \Lambda_0^{4+y-d}} \left(\frac{\Lambda_0^{d-y-4} - (\Lambda_0 e^{-r})^{d-y-4}}{d-y-4}\right) \tag{7.11}$$

Assuming that the wave number band is eliminated in recursive steps, we find a differential equation from the above expression, yielding

$$\frac{d\nu}{dr} = \frac{S_d}{[2\pi]^d} \left(\frac{d^2-4-y}{2d(d+2)}\right) \left(\frac{\lambda_0^2 D_0}{\nu^2(r)\Lambda^{4+y-d}(r)}\right) \tag{7.12}$$

Using Eq. (4) and with the identifications $k = \Lambda_0 e^{-r} = \Lambda(r)$, $\lambda_0 = 1$, and $D_0 = 2\pi^2 \alpha C \varepsilon$ that follows from the scaling relations given by Eqs. (7.3) and (7.4), we obtain

$$\alpha^2/C = \left(\frac{d^2-4-y}{2d(d+2)}\right) \left(\frac{3}{4+3y-3d}\right). \tag{7.13}$$

We thus obtain $\alpha^2/C = 0.050$ for $y = d = 3$. This numerical value is consistent with the EDQNM prediction, namely, $\alpha = 0.28$ for $C = 1.6$ [27], as indicated in Ref. [171].

(a) (b)

Figure 7.2: Feynman diagrams for the second cumulant W_2. Fig.(a) and (b) correspond to $W_2^{(1)}$ and $W_2^{(2)}$, respectively

7.3 Evaluation of skewness in the Kolmgorov range

In this section, we shall calculate the value of velocity derivative skewness assuming the Kolmogorov scaling given by Eq. (7.3) to be valid in the innertial range. We shall neglect the small correction (to the $-5/3$ exponent) due to intermittency.

A. The Second Cumulant of Velocity Derivative

The second cumulant of the derivative of fluctuating velocity distribution is defined as

$$W_2 = \left\langle \left(\frac{\partial u_1(\mathbf{x},t)}{\partial x_1} \right)^2 \right\rangle - \left\langle \frac{\partial u_1(\mathbf{x},t)}{\partial x_1} \right\rangle^2 . \tag{7.14}$$

With the assumption of homogeneity and isotropy the ensemble average $\langle u_i(\mathbf{x},t)\rangle = 0$, so that $\langle \partial u_1(\mathbf{x},t)/\partial x_1\rangle = 0$. Thus we write Eq. (7.14) as

$$W_2 = \left\langle \left(\frac{\partial u_1(\mathbf{x},t)}{\partial x_1} \right)^2 \right\rangle = \left\langle \left(\frac{\partial u_3(\mathbf{x},t)}{\partial x_3} \right)^2 \right\rangle = W_2^{(1)} + W_2^{(2)}, \tag{7.15}$$

where the second equality follows from the assumption of homogeneity and isotropy. $W_2^{(1)}$ and $W_2^{(2)}$ are contributions coming from $O[\lambda_0^{(0)}]$ and $O[\lambda_0^{(2)}]$ terms of the perturbation series due to the elimination of velocity fluctuations belonging to the shell $\Lambda_0 e^{-r} \leqslant q \leqslant \Lambda_0$. Figs. 7.2(a) and 7.2(b) represent the contributions $W_2^{(1)}$ and $W_2^{(2)}$, respectively. The corresponding expressions are written as

$$W_2^{(1)} = -\int \frac{d^{d+1}\hat{k}}{[2\pi]^{d+1}} \int \frac{d^{d+1}\hat{k}'}{[2\pi]^{d+1}} k_3\ k_3'\ \langle u_3(\mathbf{k},\omega) u_3(\mathbf{k}',\omega')\rangle, \tag{7.16}$$

and

$$W_2^{(2)} = \left(\frac{\lambda_0}{2}\right)^2 \int \frac{d^{d+1}\hat{k}}{[2\pi]^{d+1}} \int \frac{d^{d+1}\hat{k}'}{[2\pi]^{d+1}} k_3\, k_3'\, P_{3mn}(\mathbf{k}) P_{3sl}(\mathbf{k}') G(\hat{k}) G(\hat{k}') \int \frac{d^{d+1}\hat{p}}{[2\pi]^{d+1}} \int \frac{d^{d+1}\hat{q}}{[2\pi]^{d+1}} \langle v_m(\hat{p}) v_n(\hat{k}-\hat{p}) v_s(\hat{q}) v_l(\hat{k}'-\hat{q})\rangle, \tag{7.17}$$

The ensemble average appearing in the right-hand side of Eq. (7.17) can be expressed as

$$\langle u_m(\hat{p}) u_n(\hat{k}-\hat{p}) u_s(\hat{q}) u_l(\hat{k}'-\hat{q})\rangle = \langle u_m(\hat{p}) u_n(\hat{k}-\hat{p})\rangle \langle u_s(\hat{q}) u_l(\hat{k}'-\hat{q})\rangle + 2\langle u_m(\hat{p}) u_s(\hat{q})\rangle \langle u_n(\hat{k}-\hat{p}) u_l(\hat{k}'-\hat{q})\rangle \tag{7.18}$$

from which first term does not contribute because it occurrs with the vertex factor $P_{lmn}(k)$. Assuming that the flow field is statistically homogeneous in space and stationary in time, we can express the velocity correlation in terms of the renormalized quantities as

$$\langle u_i(\mathbf{k},\omega) u_j(\mathbf{k}',\omega')\rangle = 2D_0 |\mathbf{k}|^{-y} P_{ij}(\mathbf{k}) |G(\mathbf{k},\omega)|^2 [2\pi]^{d+1} \delta^d(\mathbf{k}+\mathbf{k}') \delta(\omega+\omega') \tag{7.19}$$

Thus we obtain Eq. (7.16) as

$$W_2^{(1)} = 2D_0 \int \frac{d^{d+1}\hat{k}}{[2\pi]^{d+1}} k^{-y} P_{33}(\mathbf{k})\; k_3^2\; |G(k,\omega)|^2, \tag{7.20}$$

and Eq. (7.17) as

$$W_2^{(2)} = \int \frac{d^{d+1}\hat{k}}{[2\pi]^{d+1}} k_3^2 P_{3mn}(\mathbf{k}) P_{3sl}(\mathbf{k}) |G(k,\omega)|^2 K^{(2)}_{mnsl}(\mathbf{k},\omega). \tag{7.21}$$

The unrenormalized expression for $K^{(2)}_{mnsl}(\mathbf{k},\omega)$ is given by

$$K^{(2)}_{mnsl}(\mathbf{k},\omega) = 2\lambda_0^2 D_0^2 \int \frac{d^d p}{[2\pi]^d} \int \frac{d\Omega}{[2\pi]} |\mathbf{p}|^{-2y} P_{ms}(\mathbf{p}) P_{nl}(\mathbf{p}) |G(p,\Omega)|^4 \tag{7.22}$$

representing the loop diagram without the external legs in Fig. 7.2(b).

Now we perform the integration over frequency in Eq. (7.20) and obtain

$$W_2^{(1)} = \frac{S_{d-1}}{[2\pi]^d} (2\pi^2 \alpha C \varepsilon) \int_0^{\Lambda_0} dk \frac{k^{d-y+1}}{\zeta(k)} \int_0^{\pi} \sin^{(d-2)}\theta \cos^2\theta [1-\cos^2\theta] d\theta \tag{7.23}$$

where $\zeta(k)$ is related to the renormalized viscosity $\nu(k)$ as $\zeta(k) = k^2\nu(k)$. Carrying out the angular and wave vector integrations, we arrive at

$$W_2^{(1)} = \frac{1}{10} C\varepsilon^{2/3}\Lambda_0^{4/3} \tag{7.24}$$

in three dimensions where we have substituted $D_0 = 2\pi^2\alpha C\varepsilon$. Further, Eq. (7.22) yields

$$K_{mnsl}^{(2)<}(r) = \frac{S_d}{[2\pi]^d}\frac{(d^2-2)}{2d(d+2)}\left(\frac{\lambda_0^2 D_0^2}{\nu_0^3}\right)\left[\frac{\Lambda_0^{d-2y-6} - (\Lambda_0 e^{-r})^{d-2y-6}}{d-2y-6}\right]\delta_{ml}\delta_{ns}, \tag{7.25}$$

which leads to the differential equation

$$\frac{dK_{mnsl}^{(2)}(r)}{dr} = \frac{S_d}{[2\pi]^d}\frac{(d^2-2)\lambda_0^2 D_0^2}{2d(d+2)\nu^3(r)}(\Lambda_0 e^{-r})^{(d-2y-6)}\delta_{ml}\delta_{ns}. \tag{7.26}$$

Integrating with respect to r, we obtain

$$K_{mnsl}^{(2)}(r) = \frac{S_d}{[2\pi]^d}\frac{(d^2-2)}{2d(d+2)(2+2y-d)}\left(\frac{\lambda_0^2 D_0^2}{\nu^3(r)}\right)(\Lambda_0 e^{-r})^{(d-2y-6)}\delta_{ml}\delta_{ns}. \tag{7.27}$$

Substituting $y = d$ in three dimensions, we obtain

$$K_{mnsl}^{(2)}(r) = \frac{7\lambda_0^2 D_0^2}{300\pi^2\nu^3(r)}(\Lambda_0 e^{-r})^{-9}\delta_{ml}\ \delta_{ns}. \tag{7.28}$$

Now we construct k and ω dependences of $K_{mnsl}^{(2)}(k,\omega)$ by identifying $\Lambda_0 e^{-r}$ with k and a dimensionless scaling function is employed to obtain $(\Lambda_0 e^{-r})^{-5}$ as

$$k^{-1}\nu^2(k)|G(k,\omega)|^2 \tag{7.29}$$

which has the desired limit k^{-5} in the limit of $\omega \to 0$. Thus, Eq. (7.28) can be expressed as

$$K_{mnsl}^{(2)}(k,\omega) = \frac{7\pi^2\varepsilon C^2}{75\alpha}k^{-1}\nu^2(k)|G(k,\omega)|^2\delta_{ml}\delta_{ns}. \tag{7.30}$$

Substituting Eq. (7.30) in Eq. (7.21) and performing frequency and angular integrations, we obtain

$$W_2^{(2)} = \frac{7}{2250}\frac{C^2\varepsilon^{2/3}}{\alpha^2}\int_0^{\Lambda_0} q^{1/3}dq. \tag{7.31}$$

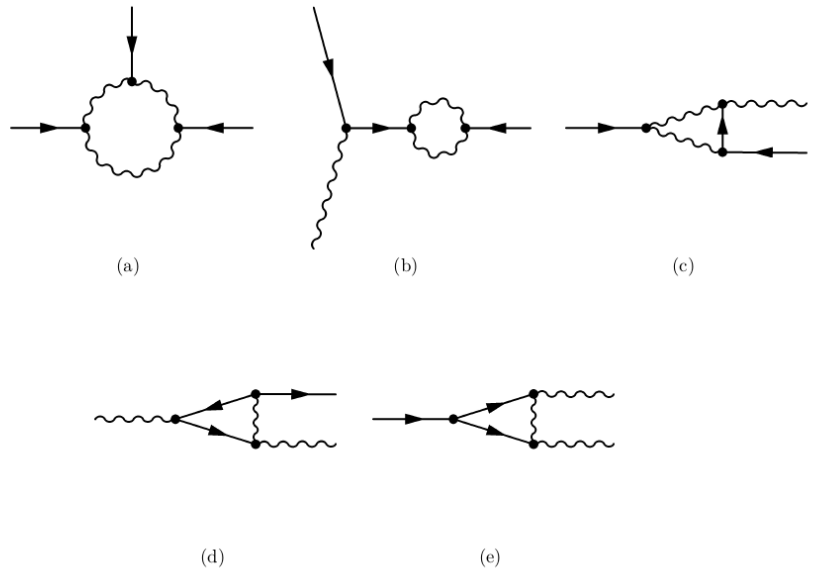

Figure 7.3: Feynman diagrams for the third cumulant W_3. Fig. (a), (b), (d), and (e) correspond to non-zero contributions, namely, $W_3^{(1)}$, $W_3^{(2)}$, $W_3^{(3)}$, and $W_3^{(4)}$, respectively. Fig. (c) gives vanishing contribution.

in three dimensions. This yields

$$W_2^{(2)} = \frac{7}{3000(\alpha^2/C)}\, C\varepsilon^{2/3}\Lambda_0^{4/3} \tag{7.32}$$

. Thus, adding the contributions $W_2^{(1)}$ and $W_2^{(2)}$ from Eqs. (7.24) and (7.32), we obtain the second cumulant of velocity derivative as

$$W_2 = \left[1 + \frac{7}{300(\alpha^2/C)}\right]\, \frac{C}{10}\varepsilon^{2/3}\Lambda_0^{4/3}. \tag{7.33}$$

B. The Third Cumulant of Velocity Derivative

The third cumulant of the velocity derivative $W_3 = \langle\left(\frac{\partial u_1}{\partial x_1}\right)^3\rangle$ can be expressed as

$$W_3 = \left\langle\left(\frac{\partial u_3}{\partial x_3}\right)^3\right\rangle = W_3^{(1)} + W_3^{(2)} + W_3^{(3)} + W_3^{(4)}, \tag{7.34}$$

where $W_3^{(1)}$, $W_3^{(2)}$, $W_3^{(3)}$, and $W_3^{(4)}$ are $[O(\lambda_0^3)]$ with non-zero contributions coming from the perturbation series. The corresponding Feynman diagrams are shown in Fig. 7.3 including the one that gives vanishing contribution to W_3. Figs.7.3 (a), 7.3(b), 7.3(d), and 7.3(e) correspond to $W_3^{(1)}$, $W_3^{(2)}$, $W_3^{(3)}$, and $W_3^{(4)}$, respectively.

The other diagram, namely, 7.3(c) gives vanishing contribution in the large scale limit. Here, we evaluate separately the contributions coming from $W_3^{(1)}$, $W_3^{(2)}$, $W_3^{(3)}$, and $W_3^{(4)}$. We shall see that Figs. 7.3(d) and 7.3(e), corresponding to $W_3^{(3)}$ and $W_3^{(4)}$, yield logarithmic contributions of opposite signs and equal magnitude and thus they cancel each other out. Consequently, the contribution to W_3 comes only from the two diagrams, namely, Figs. 7.3(a) and 7.3(b).

Calculation of $W_3^{(1)}$

The integral expression for $W_3^{(1)}$ in the Fourier space is given by

$$W_3^{(1)} = -i \int \frac{d^{d+1}\hat{k}}{[2\pi]^{d+1}} \int \frac{d^{d+1}\hat{k}'}{[2\pi]^{d+1}} \; k_3 \; k_3'(-k_3 - k_3') \; \langle u_3(\hat{k}) u_3(\hat{k}') u_3(-\hat{k} - \hat{k}') \rangle, \quad (7.35)$$

the corresponding Feynman diagram is displayed in Fig. 7.3(a). The three-point velocity correlation appearing here can be expressed in terms of the renormalized quantities as

$$\langle u_3(\hat{k}) u_3(\hat{k}') u_3(\hat{k}'') \rangle = P_{3mn}(\mathbf{k}) P_{3ij}(\mathbf{k}') P_{3sl}(-\mathbf{k} - \mathbf{k}') L^{(1)}_{ijlmns}(\hat{k}, \hat{k}')$$
$$G(\hat{k}) G(\hat{k}') G(-\hat{k} - \hat{k}') (2\pi)^{d+1} \delta^{d+1}(\hat{k} + \hat{k}' + \hat{k}''), \quad (7.36)$$

where $L^{(1)}_{ijlmns}$ represents the renormalized amputated part of the loop diagram. Substituting Eq. (7.36) in Eq. (7.35), we obtain

$$W_3^{(1)} = -i \int \frac{d^d\mathbf{k} d\omega}{[2\pi]^{d+1}} \int \frac{d^d\mathbf{k}' d\omega'}{[2\pi]^{d+1}} k_3 \; k_3'(-k_3 - k_3') P_{3mn}(\mathbf{k}) P_{3ij}(\mathbf{k}') P_{3sl}(-\mathbf{k} - \mathbf{k}')$$
$$G(\mathbf{k}, \omega) \; G(\mathbf{k}', \omega') L^{(1)}_{ijlmns}(\mathbf{k}, \omega, \mathbf{k}', \omega') \; G(-\mathbf{k} - \mathbf{k}', -\omega - \omega'). \quad (7.37)$$

The bare value of $L^{(1)}_{ijlmns}(\mathbf{k}, \omega, \mathbf{k}', \omega')$ is given by

$$L^{(1)}_{ijlmns}(\mathbf{k}, \omega, \mathbf{k}', \omega') = 8 \left(\frac{-i\lambda_0}{2} \right)^3 \int \frac{d^{d+1}\hat{q}}{[2\pi]^{d+1}} \int \frac{d^{d+1}\hat{q}'}{(2\pi)^{d+1}} \int \frac{d^{d+1}\hat{Q}}{[2\pi]^{d+1}} G_0(\hat{q}) G_0(\hat{k} - \hat{q}) G_0(\hat{q}')$$

$$G_0(\hat{k}' - \hat{q}') G_0(\hat{Q}) G_0(-\hat{k} - \hat{k}' - \hat{Q}) \langle f_m(\hat{q}) f_j(\hat{k}' - \hat{q}') \rangle \langle f_n(\hat{k} - \hat{q}) f_s(\hat{Q}) \rangle \langle f_i(\hat{q}') f_l(-\hat{k} - \hat{k}' - \hat{Q}) \rangle. \quad (7.38)$$

Using the expression for noise correlation as given by Eq. (7.7), we evaluate the above integral employing the delta functions. The internal wave vector $\mathbf{q}$ is assumed to be much greater in magnitude than external wave vectors. Consequently

we obtain

$$L^{(1)}_{ijlmns} = i\lambda_0^3(2D_0)^3 \int \frac{d^dq}{[2\pi]^d} \int \frac{d\Omega}{[2\pi]} P_{mj}(\mathbf{q})P_{ns}(\mathbf{q})P_{il}(\mathbf{q})|G_0(\mathbf{q},\Omega)|^6|\mathbf{q}|^{-3y}. \quad (7.39)$$

Performing frequency convolution, we obtain

$$L^{(1)}_{ijlmns} = \frac{3}{2}\frac{i\lambda_0^3 D_0^3}{\nu_0^5} \int \frac{d^dq}{[2\pi]^d}\ P_{mj}(\mathbf{q})P_{ns}(\mathbf{q})P_{il}(\mathbf{q})\ |\mathbf{q}|^{-3y-10}. \quad (7.40)$$

Eliminating the high wave number band $\Lambda_0 e^{-r} \leq q \leq \Lambda_0$, we obtain

$$L^{(1)<}_{ijlmns}(r) = \frac{S_d}{[2\pi]^d}\frac{3i\lambda_0^3 D_0^3}{2\nu_0^5} F_{ijlmns}(d) \int_{\Lambda_0 e^{-r}}^{\Lambda_0} q^{d-3y-11} dq, \quad (7.41)$$

where we define

$$\begin{aligned} F_{ijlmns}(d) = \quad & [f_1(d)\delta_{mj}\delta_{ns}\delta_{il} + f_2(d)(\delta_{ms}\delta_{nj}\delta_{il} + \delta_{mj}\delta_{is}\delta_{nl} + \delta_{im}\delta_{ns}\delta_{jl}) \\ & - f_3(d)(\delta_{ml}\delta_{in}\delta_{js} + \delta_{ms}\delta_{in}\delta_{jl} + \delta_{im}\delta_{nl}\delta_{js} + \delta_{ml}\delta_{is}\delta_{nj})] \end{aligned} \quad (7.42)$$

with

$$f_1(d) = 1 - \frac{3}{d} + \frac{3}{d(d+2)} - \frac{1}{d(d+2)(d+4)}, \quad f_2(d) = \frac{1}{d(d+2)} - \frac{1}{d(d+2)(d+4)},$$

$$f_3(d) = \frac{1}{d(d+2)(d+4)}. \quad (7.43)$$

We consider the iterative nature of the shell elimination scheme in thin shells in the wave vector space and obtain the flow of $L^{(1)}_{ijlmns}(r)$ in the form of a differential equation

$$\frac{dL^{(1)}_{ijlmns}}{dr} = \frac{S_d}{[2\pi]^d}\frac{3i\lambda_0^3 D_0^3}{2\nu^5(r)}\Lambda^{d-3y-10}(r)F^{(1)}_{ijlmns}(d). \quad (7.44)$$

Solving this equation in the asymptotic limit of large r, we obtain for $y = d$

$$L^{(1)}_{ijlmns}(r) = \frac{S_d}{[2\pi]^d}\frac{3i\lambda_0 D_0^2}{2(2d+10/3)}\left(\frac{\lambda_0^2 D_0}{\alpha^3\ \varepsilon}\right)\frac{\Lambda^{-2d-6}(r)}{\nu^2(r)}F^{(1)}_{ijlmns}(d). \quad (7.45)$$

To find the wave vector and frequency dependence, we identify $\Lambda_0 e^{-r}$ with k and a dimensionless scaling function is employed to obtain $(\Lambda_0 e^{-r})^{(-d-5/3)}$ as

$$k^{(7-3d)/3}\nu^2(k)|G(\hat{k})|^2, \quad (7.46)$$

yielding the renormalized amputated loop diagram in Fig. (2a) as

$$L^{(1)}_{ijlmns}(\mathbf{k},\omega,\mathbf{k}',\omega') = \frac{S_d}{[2\pi]^d}\frac{3i(2\pi^2\alpha C\varepsilon)^3}{2\alpha\ \varepsilon^{1/3}(2d+10/3)}F^{(1)}_{ijlmns}(d)k^{-(d+1/3)}k'^{-(d+1/3)}|G(\hat{k})|^2|G(\hat{k'})|^2. \tag{7.47}$$

Substituting Eq. (7.47) in Eq. (7.37) and carrying out the frequency integrations, we obtain

$$W^{(1)}_3 = -\frac{S_d}{[2\pi]^d}\frac{3(2\pi^2\alpha C\varepsilon)^3}{2\alpha\ \varepsilon^{1/3}(2d+10/3)}\int\frac{d^dk}{[2\pi]^d}\int\frac{d^dk'}{[2\pi]^d}k_3k'_3(k_3+k'_3)$$
$$[P_{3mn}(\mathbf{k})P_{3ij}(\mathbf{k}')P_{3sl}(-\mathbf{k}-\mathbf{k}')]\ k^{-(d+1/3)}\ k'^{-(d+1/3)}R(\mathbf{k},\mathbf{k}'), \tag{7.48}$$

where

$$R(\mathbf{k},\mathbf{k}') = \frac{N(\mathbf{k},\mathbf{k}')}{D(\mathbf{k},\mathbf{k}')} \tag{7.49}$$

with

$$N(\mathbf{k},\mathbf{k}') = 3[\zeta^2(k)+\zeta^2(k')]+4\zeta(|\mathbf{k}+\mathbf{k}'|)[\zeta(k)+\zeta(k')]+\zeta^2(|\mathbf{k}+\mathbf{k}'|)+14\zeta(k)\zeta(k'), \tag{7.50}$$

and

$$D(\mathbf{k},\mathbf{k}') = 16\ \zeta^2(k)\ \zeta^2(k')\left[\zeta(k)+\zeta(k')+\zeta(|\mathbf{k}+\mathbf{k}'|)\right]^3. \tag{7.51}$$

$$R'(\mathbf{k},\mathbf{k}') = (\alpha\varepsilon^{1/3})^5R(\mathbf{k},\mathbf{k}') \tag{7.52}$$

For $d=3$, tensorial contraction leads to

$$F^{(1)}_{ijlmns}(d)[P_{3mn}(\mathbf{k})P_{3ij}(\mathbf{k}')P_{3sl}(\mathbf{k}+\mathbf{k}')] = \frac{34}{105}[P_{3js}(\mathbf{k})P_{3jl}(\mathbf{k}')P_{3sl}(\mathbf{k}+\mathbf{k}')], \tag{7.53}$$

yielding

$$W^{(1)}_3 = \frac{S_d}{[2\pi]^d}\frac{17\lambda_0(2\pi^2\alpha C\varepsilon)}{35[2\pi]^{2d}(2d+10/3)}\left(\frac{\lambda_0 2\pi^2C}{\alpha^2}\right)^2 I_1(\Lambda_0), \tag{7.54}$$

with

$$I_1(\Lambda_0) = \int_0^{\Lambda_0}dk\int_0^{\Lambda_0}dk'\int_0^{\pi}\sin\theta d\theta\int_0^{\pi}\sin\theta' d\theta'\int_0^{2\pi}d\phi\int_0^{2\pi}d\phi'\ M(\mathbf{k},\mathbf{k}',\theta,\theta',\phi,\phi'), \tag{7.55}$$

where

$$M(\mathbf{k},\mathbf{k}',\theta,\theta',\phi,\phi') = -R'(\mathbf{k},\mathbf{k}')\ k^{-4/3}\ k'^{-4/3}J(\mathbf{k},\mathbf{k}',\theta,\theta',\phi,\phi'), \tag{7.56}$$

with

$$J(\mathbf{k},\mathbf{k}',\theta,\theta',\phi,\phi') = k_3 k_3'(-k_3-k_3')[P_{3js}(\mathbf{k})P_{3jl}(\mathbf{k}')P_{3sl}(-\mathbf{k}-\mathbf{k}')]. \tag{7.57}$$

The expression for $J(\mathbf{k},\mathbf{k}',\theta,\theta',\phi,\phi')$ is given in the appendix. Scaling the wave numbers with respect to Λ_0 and performing the integration numerically in Eq. (7.55) for large ultra-violet limits, we obtain

$$c_1 = \lim_{\Lambda_0\to\infty}[I_1(\Lambda_0)/\Lambda_0^2] = 0.553. \tag{7.58}$$

We thus obtain

$$W_3^{(1)} = \frac{51c_1}{15680\pi^2}\,\frac{\varepsilon\, C^{3/2}\Lambda_0^2}{(\alpha^2/C)^{3/2}}. \tag{7.59}$$

Calculation of $W_3^{(2)}$

Contribution to $W_3^{(2)}$ comes from the Feynman diagram shown in Fig. 7.3(b). The integral expression is written as

$$W_3^{(2)} = \left(\frac{\lambda_0}{2}\right)^3 \int \frac{d^{d+1}\hat{k}}{[2\pi]^{d+1}} \int \frac{d^{d+1}\hat{k}'}{[2\pi]^{d+1}} \int \frac{d^{d+1}\hat{k''}}{[2\pi]^{d+1}} k_3\ k_3'\ k_3'' G(\hat{k}')G(\hat{k''})P_{3mn}(\mathbf{k}')P_{3ij}(\mathbf{k}'')$$

$$\int \frac{d^{d+1}\hat{Q}}{[2\pi]^{d+1}} \int \frac{d^{d+1}\hat{q}}{[2\pi]^{d+1}} \int \frac{d^{d+1}\hat{q}}{[2\pi]^{d+1}} G(\hat{Q})P_{iab}(\mathbf{Q})\langle u_3(\hat{k})u_m(\hat{q})u_n(\hat{k'}-\hat{q})u_j(\hat{k''}-\hat{Q})u_a(\hat{q})u_b(\hat{Q}-\hat{q})\rangle, \tag{7.60}$$

The velocity correlation appearing in Eq. (7.60) is expressed as

$$\langle u_3(\hat{k})u_m(\hat{q})u_n(\hat{k'}-\hat{q})u_j(\hat{k''}-\hat{Q})u_a(\hat{q})u_b(\hat{Q}-\hat{q})\rangle = 24(2D_0)^3\,(2\pi)^{3(d+1)}\delta^{d+1}(\hat{k}+\hat{k}'+\hat{k}'')P_{ma}(\mathbf{q})$$

$$P_{nb}(\mathbf{k}'-\mathbf{q})P_{3j}(\mathbf{k})|G(\hat{q})|^2|G(\hat{k}'-\hat{q})|^2|G(\hat{k})|^2\ |\mathbf{q}|^{-y}|\mathbf{k}'-\mathbf{q}|^{-y}|\mathbf{k}|^{-y}, \tag{7.61}$$

giving

$$W_3^{(2)} = 24(\lambda_0 D_0)^3 \int \frac{d^{d+1}\hat{k}}{[2\pi]^{d+1}} \int \frac{d^{d+1}\hat{p}}{[2\pi]^{d+1}} k_3 p_3 (k_3+p_3)P_{3mn}(\mathbf{p})P_{3ij}(\mathbf{k}+\mathbf{p})$$

$$P_{iab}(-\mathbf{p})]P_{3j}(\mathbf{k})|\mathbf{k}|^{-y}[|G(\hat{p})|^2|G(\hat{k})|^2G(-\hat{k}-\hat{p})L^{(2)}_{mnab}(\mathbf{p},\Omega), \tag{7.62}$$

where $L^{(2)}_{mnab}(\mathbf{p},\Omega)$ comes from the amputated part of the loop diagram in Fig. 7.3(b). The bare value of $L^{(2)}_{mnab}(\mathbf{p},\Omega)$ is given by

$$L^{(2)}_{mnab}(\mathbf{p},\Omega) = \int \frac{d^dq}{[2\pi]^d} \int \frac{d\Omega}{[2\pi]} |G(q,\Omega)|^2 |G(p-q,\omega-\Omega)|^2 P_{ma}(\mathbf{q}) P_{nb}(\mathbf{p}-\mathbf{q}) |\mathbf{q}|^{-y} |\mathbf{p}-\mathbf{q}|^{-y}. \tag{7.63}$$

Performing frequency integration, we obtain

$$L^{(2)<}_{mnab}(r) = \frac{S_d}{[2\pi]^d} \frac{1}{4\nu_0^3} \; F^{(2)}_{mnab}(d) \; \left[\frac{\Lambda_0^{d-12} - (\Lambda_0 e^{-r})^{(d-12)}}{d-12} \right], \tag{7.64}$$

where

$$F^{(2)}_{mnab}(d) = \left[\delta_{ma}\delta_{nb} - \frac{2}{d}\delta_{ma}\delta_{nb} + \frac{\delta_{ma}\delta_{nb} + \delta_{mb}\delta_{na} + \delta_{mn}\delta_{ab}}{d(d+2)} \right]. \tag{7.65}$$

Using a similar procedure as in Sec. B., we obtain renormalized amputated loop as

$$L^{(2)}_{mnab}(r) = \frac{S_d}{[2\pi]^d} \frac{1}{20\alpha^3\varepsilon} F^{(2)}_{mnab}(d) \Lambda^{-5}(r). \tag{7.66}$$

For wave vector and frequency dependences, we identify $(\Lambda_0 e^{-r})^{-5}$ as

$$p^{-1}\, \nu(p)^2\, |G(p,\Omega)|^2, \tag{7.67}$$

so that we write

$$L^{(2)}_{mnab}(\mathbf{p},\Omega) = \frac{S_d}{[2\pi]^d} \frac{F^{(2)}_{mnab}(d)}{20\;\alpha\varepsilon^{1/3}}\, p^{-11/3} |G(p,\Omega)|^2. \tag{7.68}$$

Substituting this expression in Eq. (7.69), we obtain

$$W_3^{(2)} = \frac{6}{5} \frac{S_d}{[2\pi]^d} \frac{(2\pi^2\alpha C\varepsilon)^3 F^{(2)}_{mnab}(d)}{\alpha\varepsilon^{1/3}} \int \frac{d^{d+1}\hat{k}}{[2\pi]^{d+1}} \int \frac{d^{d+1}\hat{p}}{[2\pi]^{d+1}} k_3 p_3 (k_3+p_3) P_{3mn}(\mathbf{p}) P_{3ij}(\mathbf{k}+\mathbf{p})$$

$$P_{iab}(-\mathbf{p}) P_{3j}(\mathbf{k}) |k|^{-y}\; |p|^{-11/3} |G(\hat{p})|^2 |G(\hat{k})|^2 G(-\hat{k}-\hat{p}) |G(\hat{p})|^2 \tag{7.69}$$

We carry out the frequency integrations in Eq. (7.69) and obtain

$$W_3^{(2)} = \frac{56}{25}\pi^4\alpha^2 C^3 \varepsilon^{8/3} \int \frac{d^3k}{[2\pi]^3} \int \frac{d^3p}{[2\pi]^3} R_2(\mathbf{k},\mathbf{p}) |k|^{-y} |p|^{-11/3}\, T(\mathbf{k},\mathbf{p},\theta_1,\theta_2,\phi_1,\phi_2), \tag{7.70}$$

in $d = 3$ where

$$R_2(\mathbf{k},\mathbf{p}) = \frac{\zeta(k) + 2\zeta(p) + \zeta(|\mathbf{k}+\mathbf{p}|)}{8\,\zeta(k)\zeta^3(p)\{\zeta(k)+\zeta(p)+\zeta(|\mathbf{k}+\mathbf{p}|)\}^2}, \tag{7.71}$$

coming from frequency integrations and

$$T(\mathbf{k},\mathbf{p},\theta,\theta',\phi,\phi') = 2(p_3 p_i - \delta_{3i}p^2)P_{3ij}(\mathbf{k}+\mathbf{p})P_{3j}(\mathbf{k}), \tag{7.72}$$

The expression for $T(\mathbf{k},\mathbf{p},\theta,\theta',\phi,\phi')$ is given in the Appendix. Eq. (7.70) is expressed as

$$W_3^{(2)} = \frac{7}{200\pi^2}\frac{\varepsilon\, C^{3/2}}{(\alpha^2/C)^{3/2}}\, I_2(\Lambda_0) \tag{7.73}$$

where

$$I_2(\Lambda_0) = \int_0^{\Lambda_0} dk \int_0^{\Lambda_0} dp \int_0^{\pi} \sin\theta\, d\theta \int_0^{\pi} \sin\theta'\, d\theta' \int_0^{2\pi} d\phi \int_0^{2\pi} d\phi'\, R_2'(\mathbf{k},\mathbf{p})$$
$$k^{-y}p^{-11/3}\, T(\mathbf{k},\mathbf{p},\theta,\theta',\phi,\phi'). \tag{7.74}$$

with

$$R_2'(\mathbf{k},\mathbf{p}) = \alpha^5\varepsilon^{5/3}R_2(\mathbf{k},\mathbf{p}) \tag{7.75}$$

We carry out the integrations in Eq. (7.74) numerically for large ultra-violet limits and obtain

$$c_2 = \lim_{\Lambda_0\to\infty}[I_2(\Lambda_0)/\Lambda_0^2] = -0.166. \tag{7.76}$$

Thus, we obtain

$$W_3^{(2)} = \frac{7c_2}{200\pi^2}\frac{\varepsilon\, C^{3/2}}{(\alpha^2/C)^{3/2}}\,\Lambda_0^2 \tag{7.77}$$

Calculation of $W_3^{(3)}$

The contribution $W_3^{(3)}$ comes from the one-loop Feynman diagram shown in Fig. 7.3(d). The corresponding integral expression can be written as

$$W_3^{(3)} = 48\left(\frac{\lambda_0}{2}\right)^3 (2D_0)^2 \int \frac{d^{d+1}\hat{k}}{[2\pi]^{d+1}} \int \frac{d^{d+1}\hat{k}'}{[2\pi]^{d+1}} [k_3 k_3'(-k_3-k_3')]G(-\hat{k}-\hat{k}')P_{3ij}(-\mathbf{k}-\mathbf{k}')$$
$$|G(\hat{k}')|^2|G(\hat{k})|^2[P_{3b}(\mathbf{k}')P_{3n}(\mathbf{k})]|k|^{-y}|k'|^{-y}L_{ibnj}^{(3)}(\hat{k}') \tag{7.78}$$

where the amputated part $L^{(3)}_{ibnj}(\hat{k}')$ is given by

$$L^{(3)}_{ibnj}(\hat{k}') = 2D_0 \int \frac{d^{d+1}\hat{q}}{[2\pi]^{d+1}} |\mathbf{q}+\mathbf{k}|^{-y} G(\hat{q}) G(\hat{q}-\hat{k}') |G(\hat{q}+\hat{k})|^2 [P_{iab}(\mathbf{q}-\mathbf{k}') P_{amn}(\mathbf{q}) P_{mj}(\mathbf{q}+\mathbf{k})]. \tag{7.79}$$

Assuming the internal wave number q to be much greater than external wave numbers k and k', we obtain

$$L^{(3)}_{ibnj}(\mathbf{0}, 0) = 2D_0 \int \frac{d^{d+1}\hat{q}}{[2\pi]^{d+1}} [q_b q_n \delta_{ij} - \frac{q_i q_b q_n q_j}{q^2}] G^2(\hat{q}) |G(\hat{q})|^2 |q|^{-y}. \tag{7.80}$$

Carrying out the angular and frequency integrations, we have

$$L^{(3)<}_{ibnj}(r) = -\frac{S_d}{[2\pi]^d} \frac{D_0(\delta_{ib}\delta_{nj} + \delta_{in}\delta_{bj})}{4\nu_0^3 d(d+2)} \int_{\Lambda_0 e^{-r}}^{\Lambda_0} dq\, q^{-5}. \tag{7.81}$$

Now, following the same procedure as in Sec. B., we obtain

$$L^{(3)<}_{ibnj}(r) = -\frac{S_d}{[2\pi]^d} \frac{D_0(\delta_{ib}\delta_{nj} + \delta_{in}\delta_{bj})}{4\alpha^3 \varepsilon d(d+2)} r. \tag{7.82}$$

Considering $\Lambda_0 e^{-r} = k'$, that is $r = \ln(\frac{\Lambda_0}{k'})$, Eq. (7.82) yields

$$L^{(3)}_{ibnj} = -\frac{S_d}{[2\pi]^d} \frac{2\pi^2 C(\delta_{ib}\delta_{nj} + \delta_{in}\delta_{bj})}{4\alpha^2\ d(d+2)} \ln\left(\frac{\Lambda_0}{k'}\right). \tag{7.83}$$

Thus, substituting Eq. (7.83) in Eq. (7.78), we obtain

$$W_3^{(3)} = -\frac{12}{d(d+2)} \frac{S_d}{[2\pi]^d} \left(2\pi^2 C\varepsilon^{2/3}\right)^3 \int \frac{d^{d+1}\hat{k}}{[2\pi]^{d+1}} \int \frac{d^{d+1}\hat{k}'}{[2\pi]^{d+1}} [k_3 k_3'(k_3+k_3')] G(-\hat{k}-\hat{k}') P_{3ij}(\mathbf{k}+\mathbf{k}')$$
$$|G(\hat{k}')|^2 |G(\hat{k})|^2 [P_{3i}(\mathbf{k}') P_{3j}(\mathbf{k})]\, |\mathbf{k}|^{-y} |\mathbf{k}'|^{-y}\ \ln(\Lambda_0/k'). \tag{7.84}$$

Calculation of $W_3^{(4)}$

The contribution $W_3^{(4)}$ comes from the one-loop Feynman diagram shown in Fig. 7.3(e). The corresponding integral expression is written as

$$W_3^{(4)} = 24 \left(\frac{\lambda_0}{2}\right)^3 (2D_0)^2 \int \frac{d^{d+1}\hat{k}}{[2\pi]^{d+1}} \int \frac{d^{d+1}\hat{k}'}{[2\pi]^{d+1}} [k_3 k_3'(-k_3-k_3')] G(-\hat{k}-\hat{k}') P_{3ij}(-\mathbf{k}-\mathbf{k}')$$
$$|G(\hat{k}')|^2 |G(\hat{k})|^2 [P_{3b}(\mathbf{k}) P_{3n}(\mathbf{k}')] |\mathbf{k}|^{-y} |\mathbf{k}'|^{-y} L^{(4)}_{ibnj}(\hat{k}, \hat{k}') \tag{7.85}$$

where the amputated part of the loop diagram in Fig. 7.3(b) is given by

$$L^{(4)}_{ibnj}(\hat{k},\hat{k}') = 2D_0 \int \frac{d^{d+1}\hat{Q}}{[2\pi]^d} G(\hat{Q})G(-\hat{k}-\hat{k}'-\hat{Q})|G(\hat{k}+\hat{Q})|^2 P_{jmn}(-\mathbf{k}-\mathbf{k}'-\mathbf{Q})P_{iab}(\mathbf{Q})P_{ma}(\mathbf{k}+\mathbf{Q}). \tag{7.86}$$

Now we consider the external wave numbers k and k' to be much smaller compared to the internal wave number Q. This yields

$$L^{(4)}_{ibnj} = 2D_0 \int \frac{d^{d+1}\hat{Q}}{[2\pi]^d} G(\hat{Q})G(-\hat{Q})|G(\hat{Q})|^2 P_{jmn}(-\mathbf{Q})P_{iab}(\mathbf{Q})P_{ma}(\mathbf{Q}). \tag{7.87}$$

Performing the angular and frequency integrations in the above expression, we obtain

$$L^{(4)<}_{ibnj}(r) = \frac{S_d}{[2\pi]^d}\frac{D_0(\delta_{ib}\delta_{nj}+\delta_{in}\delta_{bj})}{2d(d+2)\nu_0^3}\int_{\Lambda_0 e^{-r}}^{\Lambda_0} dQ|Q|^{-5}. \tag{7.88}$$

Following the similar procedure as in Sec. B., we obtain

$$L^{(4)<}_{ibnj}(r) = \frac{S_d}{[2\pi]^d}\frac{D_0(\delta_{in}\delta_{bj})}{d(d+2)\alpha^3\,\varepsilon}r. \tag{7.89}$$

This yields

$$L^{(4)}_{ibnj} = \frac{S_d}{[2\pi]^d}\frac{2\pi^2 C}{d(d+2)\alpha^2}\ln(\Lambda_0/k')\,\delta_{in}\delta_{bj} \tag{7.90}$$

Substituting the expression for $L^{(4)}_{ibnj}(k')$ in Eq. (7.85), we obtain

$$W_3^{(4)} = \frac{12}{d(d+2)}\frac{S_d}{[2\pi]^d}\left(2\pi^2 C\varepsilon^{2/3}\right)^3\int\frac{d^{d+1}\hat{k}}{[2\pi]^{d+1}}\int\frac{d^{d+1}\hat{k}'}{[2\pi]^{d+1}}[k_3k_3'(k_3+k_3')]G(-\hat{k}-\hat{k}')P_{3ij}(\mathbf{k}+\mathbf{k}')$$
$$|G(\hat{k}')|^2|G(\hat{k})|^2[P_{3i}(\mathbf{k}')P_{3j}(\mathbf{k})]\,|\mathbf{k}|^{-y}|\mathbf{k}'|^{-y}\ln(\Lambda_0/k'). \tag{7.91}$$

which is a logarithmic contribution to the third cumulant of the velocity derivative. Thus, we see the logarithmic contributions $W_3^{(3)}$ and $W_3^{(4)}$, given by Eqs. (7.84) and (7.91), respectively cancel each other out.

C. Inertial range skewness

Adding the two contributions, namely, $W_3^{(1)}$ and $W_3^{(2)}$ from Eqs. (7.59) and (7.77), we obtain the third cumulant for the fluctuating velocity derivative as

$$W_3 = \frac{1}{40\pi^2}\left(\frac{51c_1}{392}+\frac{7c_2}{5}\right)\frac{\varepsilon\,C^{3/2}}{(\alpha^2/C)^{3/2}}\Lambda_0^2. \tag{7.92}$$

Using the obtained expressions for W_2 and W_3 from Eqs. (7.101) and (7.92), we obtain the expression for the velocity derivative skewness as

$$S = \frac{W_3}{W_2^{3/2}} = \frac{\sqrt{10}}{4\pi^2} \frac{(\frac{51c_1}{392} + \frac{7c_2}{5})}{\{1 + \frac{7}{300(\alpha^2/C)}\}^{3/2}} \frac{1}{(\alpha^2/C)^{3/2}} \tag{7.93}$$

Using $c_1 = 0.553$, $c_2 = -0.166$ and $\alpha^2/C = 0.050$ from Eqs. (7.58), (7.76), and (7.13), respectively, we obtain

$$S = -0.647. \tag{7.94}$$

Recent DNS and experimental values as displayed in Table 1 of this Chapter, where various theoretical, experimental and numerical predictions for skewness are also displayed for comparison.

Table 7.1: Various experimental, numerical, and theoretical estimates for the velocity derivative skewness in three-dimensional homogeneous isotropic turbulence. The value shown against Ref.[1] is evaluated from their predicted scaling law. The number of significant digits displayed are according to the availability from the sources.

Method	R_λ	Ref.	Skewness
Rotating disk	200 to 700	[15]	-0.5
Hot-wire	149 to 729	[1]	-0.518 to -0.597
Hot-wires	11 to 47	[19]	-0.5 ($\pm 5\%$)
Numerical	20 to 45	[142]	-0.47
Numerical	28.9 to 82.9	[90]	-0.505 ± 0.005
DNS	150	[193]	-0.5
DNS	21 to 195	[198]	-0.5
DNS	38 to 460	[55]	-0.53
DNS	680	[80]	-0.648 ± 0.003
EDQNM	asymptotic	[8]	-0.495
EDQNM	asymptotic	[115]	-0.547
RG	asymptotic	[208]	-0.4878
RG	asymptotic	[171]	-0.59
MSCE	asymptotic	[184]	-0.65
MLRA	asymptotic	[85]	-0.66
LDIA	asymptotic	[92]	-0.66
Present scheme (excluding dissipation)	asymptotic	Eq. (7.93)	-0.647
Present scheme (with dissipation)	asymptotic	Eq. (7.107)	-0.682

7.4 Evaluation of skewness including the dissipation range

It is well known that following the inertial range there occurs a dissipation range where dissipative effects due to the viscosity are dominant. It would be interesting to obtain the skewness value taking the dissipative effects into account. However, it may be noted that there exists no standard theory for the dissipation range and the renormalization schemes including the clouser approximations have not been able to address the behavior of this range. Consequently, such schemes so far have calculated only inertial range quantities where power like spectra exist. There has been a lot of studies in the structure of fine scales turbulence within the inertial range. The corresponding statistical characterization is important in the sense that Kolmogrov 1941 theory of universal range would predict a skewness independent of the Reynolds number.

Despite the above fact, we expect that a renormalized theory can be extended to include the dissipation range, an example being the EDQNM formulation. Since our formulation is based on renormalized quantities, we expect a similar kind of extension to be valid.

The energy spectrum $E(k)$ including the dissipative effects has been modeled in different ways in the literature. Here we take the model of Pao[146], namely,

$$E(k) = C\varepsilon^{2/3}k^{-5/3}e^{-\beta(k\eta)^{4/3}} \tag{7.95}$$

where $\beta = 2.400$ for $C = 1.600$ and η is the kolmogorov dissipation length scale defined as $\eta = (\nu_0^3/\varepsilon)^{1/4}$ [171].

In this section we shall denote the second and third cumulants as $\mathcal{W}_2$ and $\mathcal{W}_3$ that include the contributions due to the dissipation range.

A. Evaluation of $\mathcal{W}_2$

We generalize the expression for $W_2^{(1)}$ as

$$\mathcal{W}_2^{(1)} = \frac{S_{d-1}2\pi^2 C\varepsilon^{2/3}}{[2\pi]^d}\int_0^\infty dk\ k^{1/3}e^{-\beta(k\eta)^{4/3}}\int_0^\pi d\theta\cos^2\theta[1-\cos^2\theta]\sin\theta \tag{7.96}$$

that incorporates the dissipation range as the energy spectrum due to Pao, namely, Eq. (7.95), has been employed. The ultra-violet limit has been extended to infinity to include all dissipative effects occurring in the small scales of motions.

We make the change of variable as $\beta^{3/4}k\eta = s$ and obtain

$$\mathcal{W}_2^{(1)} = \frac{2a}{15}\frac{C\varepsilon^{2/3}}{\beta\eta^{4/3}} \tag{7.97}$$

where

$$a = \int_0^\infty ds\ s^{1/3}e^{-s^{4/3}} \tag{7.98}$$

We make a similar generalization of the expression for $W_2^{(2)}$ to incorporate Pao's model and obtain

$$\mathcal{W}_2^{(2)} = \frac{7}{2250}\frac{C^2\varepsilon^{2/3}}{\alpha^2}\int_0^\infty dk\ k^{1/3}e^{-\beta(k\eta)^{4/3}} \tag{7.99}$$

Using the same change of variables, it can be written as

$$\mathcal{W}_2^{(2)} = \frac{7\,a}{2250(\alpha^2/C)}\frac{C\varepsilon^{2/3}}{\beta\eta^{4/3}} \tag{7.100}$$

so that

$$\mathcal{W}_2 = \mathcal{W}_2^{(1)} + \mathcal{W}_2^{(2)} = \frac{2\,a}{15}\left(1 + \frac{7}{300\,(\alpha^2/C)}\right)\frac{C\varepsilon^{2/3}}{\beta\eta^{4/3}} \tag{7.101}$$

B. Evaluation of $\mathcal{W}_3$

Here we generalize the expression for $W_3^{(1)}$ to include the dissipation range so that

$$\mathcal{W}_3^{(1)} = \frac{51\ b_1}{15680\pi^2(\alpha^2/C)^{3/2}}\ \frac{\varepsilon\ C^{3/2}}{\beta^{3/2}\eta^2} \tag{7.102}$$

with

$$b_1 = \int_0^\infty ds \int_0^\infty ds' \int_0^\pi \sin\theta d\theta \int_0^\pi \sin\theta' d\theta' \int_0^{2\pi} d\phi \int_0^{2\pi} d\phi'$$
$$M(\mathbf{s},\mathbf{s}',\theta,\theta',\phi,\phi')\ e^{-3s^{4/3}/4}e^{-3s'^{4/3}/4} \tag{7.103}$$

where $s = \beta^{3/4}k\eta$ and $s' = \beta^{3/4}k'\eta$.

In a similar way as above, we generalize the expression for $W_3^{(2)}$ to include the dissipative effects as

$$\mathcal{W}_3^{(2)} = -\frac{7\ b_2}{200\pi^2}\ \frac{1}{(\alpha^2/C)^{3/2}}\frac{\varepsilon\ C^{3/2}}{\beta^{3/2}\eta^2}. \tag{7.104}$$

where

$$b_2 = \int_0^\infty ds \int_0^\infty ds' \int_0^\pi \sin\theta\, d\theta \int_0^\pi \sin\theta'\, d\theta' \int_0^{2\pi} d\phi \int_0^{2\pi} d\phi'\, R_2(\mathbf{s},\mathbf{s}')\, s^{-y}\ s'^{-11/3}$$

$$T(\mathbf{s},\mathbf{s}',\theta_1,\theta_2,\phi_1,\phi_2) e^{-(3/4)\ s^{4/3}}\ e^{-(3/4)s'^{4/3}} \tag{7.105}$$

The contributions from $\mathcal{W}_3^{(3)}$ and $\mathcal{W}_3^{(4)}$ are irrelevant because they cancel each other out in this case also.

C. Evaluation of Skewness

We obtain the total contribution to $\mathcal{W}_3$ as

$$\mathcal{W}_3 = \mathcal{W}_3^{(1)} + \mathcal{W}_3^{(2)} = \frac{1}{40\pi^2}\left(\frac{51 b_1}{392} + \frac{7 b_2}{5}\right) \frac{1}{(\alpha^2/C)^{3/2}} \frac{\varepsilon C^{3/2}}{\beta^{3/2}\eta^2}. \tag{7.106}$$

The resulting expression for skewness, from Eqs 7.101 and 7.106, turns out to be

$$\mathcal{S} = \frac{\mathcal{W}_3}{\mathcal{W}_2^{3/2}} = \frac{3\sqrt{15}}{16\sqrt{2}\, a^{3/2}\pi^2} \frac{\left(\frac{51\ b_1}{392} + \frac{7\ b_2}{5}\right)}{\{1 + \frac{7}{300(\alpha^2/C)}\}^{3/2}} \frac{1}{(\alpha^2/C)^{3/2}}. \tag{7.107}$$

We observe that the skewness value $\mathcal{S}$ depends on the parameters a, b_1, b_2 and α^2/C. Evaluating numerically the constants a, b_1 and b_2 from the integrals given by Eqs. 7.98, 7.103 and 7.105, we obtain $a = 0.750$, $b_1 = 0.928$ and $b_2 = -0.207$. Using them in the above expressions for $\mathcal{S}$ we obtain

$$\mathcal{S} = -0.682 \tag{7.108}$$

It is interesting to observe that the skewness value does not change drastically from the inertial range value when the dissipation range is included. In fact the magnitude of skewness acquires a slightly higher value than the innertial range value.

7.5 Discussion and Conclusion

In this Chapter, we obtained renormalized expressions for the second- and third-order cumulants of velocity derivative by applying a renormalized perturbative scheme on the Navier-Stokes equation for an incompressible isotropic turbulent velocity field. This scheme of calculation finds out the renormalized quantities directly from various loop diagrams for the second and third order cumulants of

velocity derivative. This type of scheme has previously been used for the calculation of statistical cumulants in Kardar-Parisi-Zhang (KPZ)[169,170] and Villain-Lai-Das Sarma[168] surface growth dynamics. Employing diagrammatic approach, we have seen that there are two contributing Feynman diagrams [Fig. 7.2] at one-loop order for the second cumulant W_2. We evaluated the amputated part of the loop-diagram appearing in Fig. 7.2(b) as given by Eq. (7.101). In total, there are five Feynman diagrams for the third cumulant W_3 as shown in Fig. 7.3. Calculating each of the diagrams, we have seen that one diagram, namely, Figs. 7.3(c), gives vanishing contribution. Further, Figs. 7.3(d) and 7.3(e), corresponding to $W_3^{(3)}$ and $W_3^{(4)}$, yield logarithmic contributions with opposite signs and they cancel each other out. The remaining two diagrams, namely, Figs. 7.3(a) and 7.3(b), finally leads to a negative value of W_3 as given by Eq. (7.92). This result, combined with the result for W_2 given by Eq. (7.101), yields the expression for velocity derivative skewness given by Eq. 7.93 when only the innertial range, namely, the energy spectrum given by Eq. (7.3) is employed and the dissipation range is neglected. We see that the resulting expression for skewness depends on three constants c_1, c_2 and α^2/C. We numerically evaluated the integral expressions determining c_1 and c_2 yielding $c_1 = 0.553$ and $c_2 = -0.166$. The value of amplitude ratio α^2/C is determined employing the same procedure to obtain the $\alpha^2/C = 0.050$.The skewness value S is calculated using these values to yield $S = -0.647$.

It is however important to take the dissipation range into account in order to calculate the integrals for the second and third cumulants, W_2 and W_3. To do so, we employed Pao's model with the energy spectrum given by Eq. 7.95 that joins the innertial range smoothly with the dissipation range. We repeated the calculations and obtained the expression for the corresponding skewness value $\mathcal{S}$ as given by Eq. 7.107. This expression for $\mathcal{S}$ depends on the constants a , b_1, b_2 and α^2/C. We evaluated the the integral expressions determining a, b_1 and b_2 yielding $a = 0.750$, $b_1 = 0.928$ and $b_2 = -0.207$. The skewness value turns out to be $\mathcal{S} = -0.682$. We observe that this value is somewhat close to the innertial range skewness value giving us the impression that inclusion or exclusion of the dissipation range does not affect the skewness value drastically.

There have been various other theoretical attempts for the calculation of velocity derivative skewness. Andre and Leisure[8] employed the EDQNM formulation of homogeneous isotropic turbulence and obtained. $S = -0.495$ at a very high Reynolds number, namely, $R = 5.24 \times 10^5$. In another work, Leisure and Ossia[115] obtained $S = -0.547$ at high Reynolds numbers from the EDQNM appro imation. Yakhot

and Orszag[208] obtained $S = -0.4878$ through a dynamic RG calculation using the randomly stirred Navier-Stokes dynamics. However, Smith and Reynolds[171] corrected this value to $S = -0.59$. Tatsumi *et al.*[184], through a MSCE scheme, showed that the magnitude of skewness increases with R_λ and saturates to $S = -0.65$ at very high Reynolds numbers. With a different choice for the initial energy spectrum, they obtain a slightly different value, namely, $S = -0.67$. Kaneda[85], employing the Markovianized Lagrangian renormalized approximation (MLRA) for freely decaying homogeneous isotropic turbulence, obtained $S = -0.66$. Kida and Goto[92] applied Lagrangian direct interaction approximation for stationary turbulence and obtained $S = -0.66$, in agreement with that of the decaying turbulence. As shown in Table 1 of this Chapter, our present theoretical skewness values are in the vicinity of the other theoretical estimates coming from MSCE[184], and the closure theories, namely, LRA[85] and LDIA[92].

In Table 7.1 of this Chapter, we have also displayed the values of the velocity derivative skewness obtained via a number of experiments and DNSs over a range of R_λ, in addition to the above theoretical estimates. Belin[15] performed hot wire measurements on the flow of low temperature helium gas between counter rotating disks. Their experimental data indicated $S \approx -0.5$ in the range $200 < R_\lambda < 700$. On the other hand, Gylfason *et al.*[1] obtained an empirical relation $S = -0.33R_\lambda^{0.09}$ in the range $149 \leqslant R_\lambda \leqslant 729$ by performing hot wire measurements on active grid wind-tunnel turbulence. For the maximum value of R_λ in their experiment, $S = -0.597$ is obtained. Burattini *et al.*[19] carried out measurements with single and crossed wire configurations on grid and box turbulence in the range $11 \leq R_\lambda \leq 47$ and found a constant value, namely, $S = -0.5$ with an uncertainty of $\pm 5\%$, that let them to support the validity of Kolmogorov 1941 theory. Orszag and Patterson[142] performed a numerical simulation of homogeneous isotropic turbulence based on the NS equation. They found that the time evolution of S was independent of the initial value of R_λ in the range $20 \leq R_\lambda \leq 45$. They reported that the small scale structure of turbulence is Reynolds number independent even at moderate values. Kerr[90] considered a DNS with 128^3 grid points up to $R_\lambda = 82.9$ for forced steady state turbulence and found $S = -0.505 \pm 0.005$ that does not increase with Reynolds number over the range $28.9 \leq R_\lambda \leq 82.9$. Vincent and Maniguzzi performed a DNS with resolution of 240^3 to obtain a homogeneous isotropic turbulence field for $R_\lambda \approx 150$. They found the probability distribution function for the velocity derivative to be close to, but not quite, exponential. Similar to Kerr's[90] result, they also found $S = -0.5$ and thus they indicated that the skewness is independent

of Reynolds number. Wang *et al.*[198] performed a DNS at a resolution of 512^3 grid points and considered cases such as freely decaying, stationary turbulence forced at large scales. Their simulation in the range $21 \leq R_\lambda \leq 195$ indicated a skewness value $S \sim -0.5$ which was almost independent of the Reynolds number in agreement with Kerr's result. Gotoh *et al.*[55] performed a DNS up to 1024^3 grid points for homogeneous steady turbulence and found the average value $S = -0.53$ in the range $38 \leq R_\lambda \leq 460$. They also reported the scaling $S \propto R_\lambda^{0.0370}$ via least square fit of the DNS data. Ishihara *et al.*[80] performed a high resolution DNS (4096^3 grid points) and obtained $S = -0.648 \pm 0.003$ for $R_\lambda = 680$. Their DNS suggested an empirical relation $S \sim -(0.32 \mp 0.02)\ R_\lambda^{0.11 \pm 0.01}$, via a least square fit of the DNS data in the range $200 < R_\lambda \leq 680$, whereas their DNS up to $R_\lambda = 1130$ was consistent with Gylfason's[1] scaling relation.

We thus see that some of the experimental and numerical studies suggest that the skewness value is a constant with respect to the Reynolds number while others support that the skewness is a mildly growing function of Reynolds number following a scaling relation over a range of Reynolds numbers. We would like to note that we have calculated the second and third order velocity derivatives, and hence the skewness, assuming the Kolmogorov phenomenology and Pao's modification for inclusion of the dissipation range to be valid. These phenomenological considerations are in fact valid for infinitely large Reynolds numbers leading us to state that our calculations for skewness correspond to infinite Reynolds number.

Since our theoretical estimates are in the limit of infinite Reynolds number, it is difficult to compare them with the experimental and numerical results that are usually obtained for finite (although high) Reynolds numbers. As discussed above, experimental and numerical estimates for skewness have been expressed in the form $S = -\sigma R_\lambda^\delta$ (with σ and δ positive). This empirical relation is usually valid for a (finite) range of high R_λ values beyond which its validity is unknown. However, this scaling law, if assume to be extended to Reynolds numbers higher than those considered in the experiments and numerical simulations, the skewness would grow indefinitely (although slowly) with increasing Reynolds numbers. This situation appears to be quite unlikely as the skewness can not be infinitely large[114]. Our theoretical estimates, on the other hand, indicate that the skewness is a finite quantity in the limit of infinite Reynolds number. In fact, Tatsumi *et al.*[184] showed through the MSCE method that the skewness value saturates to a constant value as the Reynolds number increases boundlessly. Our calculated skewness values $S = -0.647$ and $\mathcal{S} = -0.682$ compares well with Tatsumi's asymptotic value -0.65 for

infinitely large Reynolds number. It can be guessed that beyond the scaling regime ($S \sim R_\lambda^\delta$) observed in experiments and numerical simulations, the skewness ought to saturate to a constant value.

Appendix

A. Expression for $J(k_1, k_2, \theta_1, \theta_2, \phi_1, \phi_2)$

The expression given by Eq. (7.57) can be simplified by using the spherical polar coordinate where $k_{13} = k_1\, x = k_1 \cos\theta_1$, $k_{23} = k_2\, y = k_2 \cos\theta_2$ and $\mathbf{k}_1 \cdot \mathbf{k}_2 = k_1\, k_2\, z = k_1\, k_2\, [\sin\theta_1 \sin\theta_2 \cos(\phi_1 - \phi_2) + \cos\theta_1 \cos\theta_2]$. Thus, we obtain

$$\begin{aligned} J(k_1, k_2, \theta_1, \theta_2, \phi_1, \phi_2) = 2|k_1|^3|k_2|^3 \left[\rho_1(x,y,z) + \rho_2(x,y,z)\frac{(k_1x + k_2y)^2}{k_1^2 + k_2^2 + 2k_1k_2z}\right] \\ +2|k_1|^2|k_2|^4 \left[\sigma_1(x,y,z) + \sigma_2(x,y,z)\frac{(k_1x + k_2y)^2}{k_1^2 + k_2^2 + 2k_1k_2z}\right] \\ +2|k_1|^4|k_2|^2 \left[\tau_1(x,y,z) + \tau_2(x,y,z)\frac{(k_1x + k_2y)^2}{k_1^2 + k_2^2 + 2k_1k_2z}\right], \end{aligned} \tag{7.109}$$

where

$$\rho_1(x,y,z) = x(y^3 - y^5 - y^3z^2) + 2x^2(y^2z - y^4z) + x^3(4y^3z^2 + y - yz^2) - 2x^4y^2z - x^5y,$$

$$\rho_2(x,y,z) = xy\left[x^2(1+4z^2) + y^2(1+4z^2) - z^2 - 1 - 4xyz(1+z^2)\right],$$

$$\sigma_1(x,y,z) = x(y^3z - 2y^5z) + x^2(y^2 - y^2z^2 + 2y^4z^2) - x^4y^2,$$

$$\sigma_2(x,y,z) = xy\left[2x^2z + z(2y^2 - 1) - x(y + 2yz^2)\right],$$

$$\tau_1(x,y,z) = x^2(y^2 + y^2z^2 - y^4) + x^3yz + 2x^4y^2z^2,$$

$$\tau_2(x,y,z) = xy\left[2x^2z + z(2y^2 - 1) - x(y + 2yz^2)\right]$$

B. Expression for $T(k, p, \theta_1, \theta_2, \phi_1, \phi_2)$

The expression given by Eq. (7.72) can be expressed using spherical polar coordinate as

$$T(k,p,\theta_1,\theta_2,\phi_1,\phi_2) = 2kp^5\rho_3(x,y,z) + 2k^2p^4\sigma_3(x,y,z) + 2k^3p^3\tau_3(x,y,z)$$

$$-4k^2p^4\frac{(px+ky)^2}{k^2+p^2+2kpz}\xi(x,y,z), \tag{7.110}$$

where

$$\rho_3(x,y,z) = (x^2y^2z - x^3y - x^4y^2z + x^5y),$$

$$\sigma_3(x,y,z) = (xy^3z + x^2y^4 - 2x^2y^2 + x^3yz - x^3y^3z + x^4y^2),$$

$$\tau_3(x,y,z) = (x^2y^2z - x^2y^4z - xy^3 + xy^5),$$

$$\xi(x,y,z) = xy\left[x^2z + y^2z - xy(1+z^2)\right]$$

Chapter 8

Summary and Conclusions

The main focus of the thesis has been theoretical studies of statistical properties of a few non-equilibrium stochastic processes, such as surface growth and fluid turbulence. We study the surface growth processes via the most paradigmatic equations, namely, KPZ and VLDS equations. Further, it is well known that turbulent fluid flow is governed by the Navier-Stokes equation. In this Chapter, a general conclusion and scope of the thesis is presented.

The universality class of a dynamical stochastic system is an important statistical property. In the earlier studies on surface growth, the universality class was usually determined via the scaling exponents. In the last two decades, it has been realized that despite the same scaling exponents, the distribution functions can be entirely different due to different initial conditions corresponding to different sub-universality classes. Thus, the distribution function contains more statistical information about the system than the scaling exponents. Because of these facts, the full information about the PDF enables one to classify many similar problems into varying universality classes. However, an analytical calculation of the full PDF is an extremely difficult task, whereas the calculation of higher order moments such as the skewness, kurtosis, and hyper-skewness are a more viable approach to economize on the amount of calculation.

This thesis work develops a perturbative renormalization scheme to study the higher-order cumulants of PDF and to validate the scheme by comparing the outcome with the existing numerical, experimental and other theoretical estimations. In the literature, so far, we have not seen any consistent method which finds the higher order cumulants of PDF for various non-linear systems. This motivated us to carry out this thesis work.

In Chapter-2, 3, and 4, we followed Yakhot-Orszag's renormalization approach

and obtained the renormalized surface tension and noise amplitude for one-dimensional KPZ equation. This scheme is slightly different from the usual perturbative renormalization group analysis. Similar to the other calculations, the renormalized surface tension and the strength of the noise correlation are found to be renormalized in the same way so that $D(r)/\nu(r)$ is r-independent, a consequence of fluctuation- dissipation theorem for the case of $(1+1)$ dimensional KPZ equation. At the asymptotic limit of scale parameter r, we obtained $\nu(k)$ and $D(k)$ by identifying $\Lambda_0 e^{-r} = k$ and thereby from the expressions for $\nu(r)$ and $D(r)$, scaling exponents are obtained. Our obtained scaling exponents for one dimensional KPZ system agree with the one-loop RG results. Moreover, we have developed a perturbative renormalization scheme in order to obtain numerical values of normalized third order cumulant (in Chapter-2), normalized fourth order cumulant (in Chapter-3) and normalized fifth order cumulant (in Chapter-4) where the calculation for second cumulant is common to all.

We obtain a value of skewness $S = 0.3237$ for the flat geometry in the stationary state in $(1+1)$ dimensions. In the recent seminal paper on PNG model of Prähofer and Spohn, the estimated skewness value is $S = 0.35941$ [153]. The experiment of slow combustion fronts of a paper sheet yielded the skewness value $S = 0.32$ for flat initial conditions in the saturation regime [129]. The investigation [108] of the stationary state skewness for the SSM model with random uncorrelated spins led to estimate $|S| \approx 0.33$.

Our obtained kurtosis value is $Q = 0.1523$ at one loop renormalization scheme in one dimension. The recent studies [153] of PNG model yields different kurtosis values for different initial conditions, namely, $Q = 0.0934$ for curved, $Q = 0.1652$ for flat, and $Q = 0.289$ for stationary initial conditions. In the subsequent studies, the DPRM with different configurations such as point-to-point, point-to-line, and stationary cases, by Halpin-Healy and Lin [61], leading to GUE-TW, GOE-TW and Baik-Rains F_0 distributions, respectively. They have estimated the stationary state kurtosis value to be $Q = 0.278$. They have also studied the distributions of deposition models (BD, SSM, and RSOS) that strongly agree with DPRM/SHE results and they turn out to be the Baik-Rains distribution.

Although there have been many studies on the lower order normalised moments such as skewness and kurtosis for one-dimensional KPZ equation in the steady state, the study of hyperskewness remains a rarity. However, there have been studies based on numerical models that focus on the probability distribution function belonging to the KPZ universality class and the distributions have been shown to be identical

with the Baik-Rains distribution with zero mean in the steady state. From Fredholm determinant representation as well as from the numerical data via the solution of the Painlevé-II, the value for hyperskewness is 0.3092. This value which come from Baik-Rains distribution, is distinctly higher than our calculated value $\tilde{S} = 0.0835$. There are a few reasons due to which our approach underestimate the result. First, the perturbative RG calculation is carried out only at one-loop order. The dynamics is governed by a white noise following a Gaussian distribution and it appears that the Gaussian white noise plays a more dominant role in the perturbative calculations for the higher order moments, namely, kurtosis and hyperskewness. In this regard, calculations which incorporate higher order contributions in the perturbative expansions are expected to yield better estimates for these higher order moments.

In practice, the growth of a surface in Nature occurs on a two-dimensional surface. The motivation of calculating skewness and kurtosis values of PDF for $(2+1)$-dimensional KPZ equation comes from the unavailable analytical methodology directly from the dynamical equation in the existing literature. To do the calculations, we use the value of roughness exponent $\chi \approx 0.39$ as an input from the various extensive numerical simulations. We employed perturbation theory directly on the KPZ equation and obtain skewness $S = 0.2879$ and the kurtosis value $Q = 0.1995$ in the stationary state. The skewness and kurtosis values yield the Derrida-Appert ratio $R_{DA} = 0.41547$. Our obtained values are comparable to other numerical estimations. The values are compared with those estimations in a table in Chapter-5 to validate the proposed theory.

We find that the cumulants depend on the infrared cutoff μ in both ($(1+1)$ and $(2+1)$) the dimensions. This is expected because the cumulants obey the semi-extensive property $W_n \sim L^{n\chi}$ in the stationary state, so that we identify $\mu \sim L^{-1}$ where $(L \times L)$ is the substrate size. It is very important to note that the obtained values for the skewness, kurtosis, in one and two dimensions and hyperskewness in one dimension are found to be independent of the model parameters (λ_0, D_0, and ν_0) of the KPZ equation and the UV and IR cutoffs (Λ_0, μ), suggesting its universality.

It is very important to emphasize that the method can also be generalized for $(d+1)$-dimensional systems, such as, KPZ-type surface growth. We can express the renormalized quantities as $\nu(k) \sim k^{-\chi}$ and $D(k) \sim k^{-3\chi+2-d}$ in d dimensions where k is the wavenumber. Similarly, the renormalized amputated part of the diagrams (excluding external legs) can also be expressed in a general $(d+1)$ dimensions. For example, the scalings for the loop functions are $L_2(k) = C_2\, k^{-3\chi-d+2}$, $L_3(k) = C_3\, k^{-4\chi-2d+2}$, $L_4(k) = C_4\, k^{-5\chi-3d+2}$, and $L_5(k) = C_5 k^{-6\chi-4d+2}$ in d dimensions where

the constants C_2, C_3, C_4 and C_5 are obtained directly from the KPZ equation by using the perturbative approach. Subsequently, we substitute the expressions for the loop functions in the diagrams and carry out the frequency and momentum integrations to calculate the value of skewness, kurtosis and hyperskewness.

In Chapter-6, we study the statistical properties of a one-dimensional, nonlinear, conserved growth equation (VLDS equation) driven by a stochastic Gaussian white noise. The studied properties are the scaling exponents and the skewness of the PDF of surface height fluctuations. Employing our approach, we obtain the renormalized diffusivity in the large-scale long-time limit and thereby the value of roughness exponent $\chi = 1$ is obtained, which is consistent with the previous RG results obtained by Lai and Das Sarma. Our obtained skewness value, $S = -0.0441$, is negative. The value is consistent with the numerical prediction of Das Sarma *et al.* ($S = -0.1 \pm 0.15$) in the steady state. According to their suggestions, the skewness value is likely to be negative, although a zero or slightly positive value is not excluded. It is to be mentioned that a large error bar to the result has been estimated due to a dominant role of fluctuations in their numerical model. However, our calculated value asserts that the probability distribution function is negatively skewed. We also note that, similar to the previous calculations, the VLDS skewness is also independent of the model parameters (λ_0, D_0, and ν_0) of VLDS equation and the UV and IR cutoffs (Λ_0, μ).

In Chapter-7, we study the velocity derivative skewness of incompressible isotropic turbulent velocity field governed by Navier-Stokes equation. We implement a renormalized perturbative scheme to calculate the second and third-order cumulants of the velocity derivative. The perturbative renormalization scheme is directly applied on Navier-Stokes equation and subsequently, we obtain various loop diagrams for the third and second order moments of the velocity derivative. We calculate the skewness by excluding and including the dissipation range. This leads to the velocity derivative skewness value $S = -0.647$ when only the innertial range is included and the dissipation range is excluded. When we include the dissipation range by considering Pao's model for the energy spectrum, the skewness value turns out to be $\mathcal{S} = -0.682$. This is quite surprising because the skewness value does not differ drastically from the previous value when the dissipation range is included.

In summary, we have developed a perturbative renormalization scheme to calculate the normalised cumulants for nonlinear stochastic dynamical systems. To validate the theory, we apply the scheme on different systems in different dimensions such as surface growth equations KPZ, VLDS, and the Navier-Stokes equation.

We find that the our theoretically predicted values agree better with experimental and numerical estimations when the dimensionality of the system increases. This is of course expected because the role of Gaussian fluctuations coming from the stochastic noise term diminishes when the system dimension increases.

Bibliography

[1] S. Ayyalasomayajula, A. Gylfason, and Z. Warhaft. *J. Fluid Mech.* **501**, 213 (2004).

[2] F. D. A. Aarão Reis. *Phys. Rev. E* **70**, 031607 (2004).

[3] F. D. A. Aarão Reis. *Phys. Rev. E* **69**, 021610 (2004).

[4] R. A. L. Almeida, S. O. Ferreira, T. J. Oliveira, and F. D. A. Aarão Reis. *Phys. Rev. B* **89**, 045309 (2014).

[5] S. G. Alves, T. J. Oliveira, and S. C. Ferreira. *Phys. Rev. E* **90** 020103 (2014).

[6] J. G. Amar and F. Family. *Phys. Rev. A* **41** 3399 (1990).

[7] J. G. Amar and F. Family. *Phys. Rev. A* **45** 5378 (1992).

[8] J. C. André and M. Lesieur. *J. Fluid Mech.* **81**, 187 (1977).

[9] J. Baik and E. M. Rains. *J. Stat. Phys.* **100** 523 (2000).

[10] R. Baiod, D. Kessler, P. Ramanlal, L. Sander, and R. Savit. *Phys. Rev. A* **38** 3672 (1988).

[11] A.-L. Barabási and H. E. Stanley. *Fractal Concepts in Surface Growth.* (Cambridge University Press, Cambridge, England, 1995).

[12] D. P. Barkey, R. H. Muller and C. W. Tobias. *J. Electrochem. Soc.* **136**, 2199 (1989).

[13] M. C. Bartelt and J. W. Evans. *J. Phys. A: Math. Gen.* **26**, 2743 (1993).

[14] G. K. Batchelor. *The Theory of Homogeneous Turbulence.* Cambridge University Press, (1953).

[15] F. Belin, J. Maurer, P. Tabeling, and H. Willaime. *Phys. Fluids* **9**, 3843 (1997).

[16] A. Berera and L.-Z. Fang. *Phys. Rev. Lett.* **72**, 458 (1994).

[17] F. Bornemann. *A Markov Processes Relat. Fields*, **16** 803 (2010).

[18] J. P. Bouchaud and M. E. Cates. *Phys. Rev. E* **47** R1455 (1993).

[19] P. Burattini, P. Lavoie, and R. A. Antonia. *Exp. Fluids* **45**, 523 (2008).

[20] P. Calabrese, P. Le Doussal, and A. Rosso. *Europhys. Lett.* **90**, 20002 (2010).

[21] P. Calabrese, P. Le Doussal *Phys. Rev. Lett.* **106** 250603 (2011).

[22] L. Canet, H. Chaté, B. Delamotte, and N. Wschebor. *Phys. Rev. Lett.* **104** 150601 (2010).

[23] A. C. K. Chan, H. Wang, and M. J. Chan. *IEEE Electron Device Letters*, **22**,

384 (2001).
[24] L. Chevillard, B. Castaing, E. Lévéque, and A. Arneodo. *Physica D* **218**, 77 (2006).
[25] N. Chia and R. Bundschuh. *Phys. Rev. E* **72** 051102 (2005).
[26] C. -S. Chin and M. den Nijs. *Phys. Rev. E* **59** 2633 (1999).
[27] J.-P. Chollet and M. Lesieur. *J. Atmos. Sci.* **38**, 2747 (1981).
[28] F. Colaiori and M. A. Moore. *Phys. Rev. Lett.* **86**, 3946 (2001).
[29] W. E. H. Culling. *J. Geol.* **71**, 127 (1963).
[30] S. Das Sarma. *arxiv.org/abs/cond-mat/9705118v2*, 1997.
[31] S. Das Sarma and R. Kotlyar. *Phys. Rev. E* **50** R4275 (1994).
[32] S. Das Sarma, C. J. Lanczycki, R. Kotlyar, and S. V. Ghaisas. *Phys. Rev. E* **53**, 359 (1996).
[33] S. Das Sarma and P. Tamborenea. *Phys. Rev. Lett.* **66**, 325 (1991).
[34] C. DeDominicis and P. C. Martin. *Phys. Rev. A* **19**, 419 (1979).
[35] U. Deker and F. Haake. *Phys. Rev. A* **11**, 2043 (1975).
[36] B. Derrida and C. Appert. *J. Stat. Phys.* **94**, 1 (1999).
[37] J. P. Doherty, M. A. Moore, J. M. Kim, and A. J. Bray. *Phys. Rev. Lett.* **72**, 2041 (1994).
[38] P. Le Doussal and P. Calabrese. *J. Stat. Mech.* **P06001** (2012).
[39] M. Eden.
Proceedings of the Fourth Berkeley Symposium on Mathematical Statistics and Probability, Volume 4: Contributions to Biology and Problems of Medicine edited by J. Neyman (University of California Press, Berkeley, 1961), pp.223-239
[40] D. Ertaş and M. Kardar. *Phys. Rev. Lett.* **69**, 929 (1992).
[41] D. Ertaş and M. Kardar. *Phys. Rev. Lett.* **73**, 1703 (1994).
[42] F. Family and T. Vicsek (eds.). *Dynamics of Fractal Surfaces*. (World Scientific, Singapore, New Jersey) 1991.
[43] F. Family and T. Vicsek. *J. Phys. A: Math. Gen.* **18**, L75 (1985).
[44] F. Family. *Physica A: Statistical Mechanics and its Applications* **168**, 561, 1990.
[45] D. S. Fisher and D. A. Huse. *Phys. Rev. B* **43**, 10728 (1991).
[46] B. M. Forrest and L.-H. Tang. *Phys. Rev. Lett.* **64**, 1405 (1990).
[47] D. Forster, D. R. Nelson, and M. J. Stephen. *Phys. Rev. A* **16**, 732 (1977).
[48] E. Frey and U. Claus Täuber. *Phys. Rev. E* **50**, 1024 (1994).
[49] E. Frey, U. Claus Täuber, and T. Hwa. *Phys. Rev. E* **53**, 4424 (1996).
[50] U. Frisch. *Turbulence: A Legacy of A. N. Kolmogorov*. Cambridge University Press, Cambridge (1999).
[51] S. V. Ghaisas. *Phys. Rev. E* **73**, 022601 (2006).

[52] M. J. Giles. *Phys. Fluids* **7**, 2785 (1995).
[53] F. Ginelli and H. Hinrichsen. *J. Phys. A: Math. Gen.* **37**, 11085 (2004).
[54] N. Goldenfeld. *Lectures on Phase Transitions and the Renormalization Group.* Addison-Wesley, Reading (1976).
[55] T. Gotoh, D. Fukayama, and T. Nakano. *Phys. Fluids* **14**, 1065 (2002).
[56] T. Halpin-Healy and K. A. Takeuchi. *J. Stat. Phys.* **160**, *794* (2015).
[57] T. Halpin-Healy and Y. C. Zhang. *Phys. Rep.* **254**, 215 (1995).
[58] T. Halpin-Healy. *Phys. Rev. A* **44**, R3415 (1991).
[59] T. Halpin-Healy. *Phys. Rev. Lett.* **109**, 170602 (2012).
[60] T. Halpin-Healy. *Phys. Rev. E* **88**, 042118 (2013).
[61] T. Halpin-Healy and Y. Lin. *Phys. Rev. E* **89**, 010103 (2014).
[62] T. Halpin-Healy and G. Palasantzas. *Europhys. Lett.* **105**, 50001 (2014).
[63] T. Halpin-Healy and Y.-C. Zhang. *Phys. Rep.* **254**, 215, (1995).
[64] S. Havlin, S. V. Buldyrev, H. E. Stanley, and G. H. Weiss. *J. Phys. A: Math. Gen.* **24**, L925 (1991).
[65] S. P. Hastings and J. B. McLeod. *Archive for Rational Mechanics and Analysis*, **73**, 31, (1980).
[66] P. C. Hohenberg and B. I. Halperin. *Rev. Mod. Phys.* **49**, 435 (1977).
[67] E. Holland-Moritz, J. Gordon, K. Kanazawa, and R. Sonnenfeld. *Langmuir* **7**, 1981 (1991).
[68] R. E. Horton. *Bulletin Geological Soc. America* **56**, 275 (1945).
[69] Z.-F. Huang and B.-L. Gu. *Phys. Rev. E* **54**, 5935 (1996).
[70] Z.-F. Huang and B.-L. Gu. *Phys. Rev. E* **57**, 4480 (1998).
[71] M. A. C. Huergo, M. A. Pasquale, A. E. Bolzán, A. J. Arvia, and P. H. González. *Phys. Rev. E* **82**, 031903 (2010).
[72] M. A. C. Huergo, M. A. Pasquale, P. H. González, A. E. Bolzán, and A. J. Arvia. *Phys. Rev. E* **84**, 021917 (2011).
[73] D. A. Huse and C. L. Henley. *Phys. Rev. Lett.* **54**, 2708 (1985).
[74] D. A. Huse and C. L. Henley, and D. S. Fisher. *Phys. Rev. Lett.* **55**, 2924 (1985).
[75] T. Hwa. *Nature (London)* 399, 1999.
[76] T. Hwa and E. Frey. *Phys. Rev. A*, **44**, R7873 (1991).
[77] T. Hwa and M. Lässig. *Phys. Rev. Lett.* **76**, 2591 (1996).
[78] T. Imamura and T. Sasamoto. *Phys. Rev. Lett.* **108**, 190603 (2012).
[79] T. Imamura and T. Sasamoto. *J. Stat. Phys.* **150**, 908 (2013).
[80] T. Ishihara, Y. Kaneda, M. Yokokawa, K. Itakura, and A. Uno, *J. Fluid Mech.* **592**, 335 (2007).
[81] E. Jackson, Z. S. She and S. A. Orszag. *J. Sci. Comput.* **3**, 407 (1988).
[82] H. K. Janssen. *Phys. Rev. Lett.* **78**, 1082 (1997).

[83] K. Johansson. *Communications in Mathematical Physics*, **209**, 437 (2000).
[84] R. Jullien and R. Botet. *Phys. Rev. Lett.* **54**, 2055 (1985).
[85] Y. Kaneda. *Phys. Fluids A* **5**, 2835 (1993).
[86] M. Kardar, G. Parisi, and Y.-C. Zhang. *Phys. Rev. Lett.* **56**, 889 (1986).
[87] M. Kardar and Y.-C. Zhang. *Phys. Rev. Lett.* **58**, 2087 (1987).
[88] E. Katzav. *Phys. Rev. E* **65**, 032103 (2002).
[89] J. Kelling and G. Ódor. *Phys. Rev. E* **84**, 061150 (2011).
[90] R. M. Kerr. *J. Fluid Mech.* **153**, 31 (1985).
[91] A. R. Kerstein and W. T. Ashurst. *Phys. Rev. Lett.* **68**, 934 (1992).
[92] S. Kida and S. Goto. *J. Fluid Mech.* **345**, 307 (1997).
[93] Y. Kim and J M. Kim *Phys. Rev. E* **55**, 3977 (1997).
[94] J. M. Kim, M. A. Moore, and A. J. Bray. *Phys. Rev. A* **44**, 2345 (1991).
[95] J. M. Kim and S. Das Sarma. *Phys. Rev. Lett.* **72**, 2903 (1994).
[96] J. M. Kim and S. Das Sarma. *Phys. Rev. E* **51**, 1889 (1995).
[97] J. M. Kim and J. M. Kosterlitz. *Phys. Rev. Lett.* **62**, 2289 (1989).
[98] Y. Kim, D. K. Park, and J. M. Kim *J. Phys. A: Math. Gen.* **27**, L553 (1994).
[99] T. Kloss, L. Canet, B. Delamotte, and N. Wschebor. *Phys. Rev. E* **89**, 022108 (2014).
[100] T. Kloss, L. Canet, B. Delamotte, and N. Wschebor. *Phys. Rev. E* **86**, 051124 (2012).
[101] A. N. Kolmogorov. *C. R. (Dokl.) Acad. Sci. SSSR* **30**, 299 (1941).
[102] J. Kondev, C. L. Henley, and D. G. Salinas. *Phys. Rev. E* **61**, 104 (2000).
[103] R. H. Kraichnan. *Phys. Rev. Lett.* **65**, 575 (1990).
[104] T. Kriecherbauer and J. Krug. *J. Phys. A: Math. Gen.* **43**, 403001 (2010).
[105] J. Krug. *Adv. Phys.*, **46**, 139 (1997).
[106] J. Krug and H. Spohn. *Phys. Rev. A* **38**, 4271 (1988).
[107] J. Krug *Phys. Rev. A* **36**, 5465 (1987).
[108] J. Krug, P. Meakin, and T. Halpin-Healy. *Phys. Rev. A* **45**, 638 (1992).
[109] A. Kuo and S. Corrsin. *J. Fluid Mech.* **50**, 285 (1971).
[110] Y. Kuramoto. *Chemical Oscillations, Waves, and Turbulence.* Dover Books on Chemistry Series. Dover Publications, 2003.
[111] Z.-W. Lai and S. Das Sarma. *Phys. Rev. Lett.* **66**, 2348 (1991).
[112] L. D. Landau and E. M. Lifshitz. *Fluid Mechanics.* Pergamon Press, Oxford, London (1987).
[113] M. Lässig. *Phys. Rev. Lett.* **80**, 2366 (1998).
[114] M. Lesieur. *Turbulence in Fluids.* Springer, 4th edition, The Netherlands (2008).
[115] M. Lesieur and S. Ossia. *J. Turbulence* **1**, 7 (2000).
[116] D. C. Leslie. *Developments in the Theory of Turbulence.* Clarendon Press, Oxford (1973).

[117] Y. Li and C. Meneveau. *Phys. Rev. Lett.* **95**, 164502 (2005).
[118] S. K. Ma and G. Mazenko. *Phys. Rev. B* **11**, 4077 (1975).
[119] F. Mallamace and H. E. Stanley. *The Physics of Complex Systems*. IOS Press, Amsterdam, Oxford, Tokyo, Washington DC (1996).
[120] B. B Mandelbrot, E. Dann Passoja, and Alvin J. Paullay. *Nature* **308**, 721 (1984).
[121] E. Marinari, A. Pagnani, and G. Parisi. *J. Phys. A: Math. Gen.* **33**, 8181 (2000).
[122] M. Marsili, A. Maritan, F. Toigo, and J. R. Banavar. *Rev. Mod. Phys.* **68**, 963 (1996).
[123] P. C. Martin, E. D. Siggia, and H. A. Rose. *Phys. Rev. A* **8**, 423 (1973).
[124] J. Maunuksela, M. Myllys, O.-P. Kähkönen, J. Timonen, N. Provatas, M. J. Alava, and T. Ala-Nissila. *Phys. Rev. Lett.* **79**, 1515 (1997).
[125] W. D. McComb. *The Physics of Fluid Turbulence*. Oxford University Press, New York (1990).
[126] P. Meakin. *Phys. Rep.* **235**, 189 (1993).
[127] P. Meakin, P. Ramanlal, L. M. Sander, and R. C. Ball. *Phys. Rev. A* **34**, 5091 (1986).
[128] E. Medina, T. Hwa, M. Kardar, and Y.-C. Zhang. *Phys. Rev. A* **39**, 3053 (1989).
[129] L. Miettinen, M. Myllys, J. Merikoski, and J. Timonen. *Eur. Phys. J. B* **46**, 55 (2005).
[130] V. G. Miranda and F. D. A. A. Reis. *Phys. Rev. E* **77**, 031134 (2008).
[131] A. S. Monin and A. M. Yaglom. *Statistical Fluid Mechanics*, volume 2. MIT Press, Cambridge, MA (1975).
[132] M. Moskovits. *Rev. Mod. Phys.* **57**, 783 (1985).
[133] W. W. Mullins. *J. of Appl. Phy.* **30**, 77 (1959).
[134] M. Myllys, J. Maunuksela, M. Alava, T. Ala-Nissila, J. Merikoski, and J. Timonen. *Phys. Rev. E* **64**, 036101 (2001).
[135] O. Narayan and D. S. Fisher. *Phys. Rev. Lett.* **68**, 3615 (1992).
[136] T. Nattermann and W. Renz. *Phys. Rev. B* **38**, 5184 (1988).
[137] T. Nattermann and L.-H Tang. *Phys. Rev. A* **45**, 7156 (1992).
[138] M. Nelkin. *Phys. Rev. A* **42**, 7226 (1990).
[139] V. Ng, J. F. Hu, A. O. Adeyeye, J. P. Wang, and T. C. Chong. *J. Appl. Phys.* **91**, 7206 (2002).
[140] G. Ódor, B. Liedke, and K.-H. Heinig. *Phys. Rev. E* **81**, 031112 (2010).
[141] I. C. Oppenheim, D. J. Trevor, C. E. D. Chidsey, P. L. Trevor, and K. Sieradzki. *Science* **254**, 687 (1991).
[142] S. A. Orszag and G. S. Patterson. *Phys. Rev. Lett.* **28**, 76 (1972).

[143] A. Pagnani and G. Parisi. *Phys. Rev. E* **92**, 010101 (2015).
[144] T. Paiva and F. D. A. A. Reis. *Surf. Sci.* **601**, 419 (2007).
[145] G. Palasantzas, D. Tsamouras, and J. Th. M. De Hosson. *Surf. Sci.* **507**, 357 (2002).
[146] Y.-H. Pao. *Phys. Fluids* **8**, 1063 (1965).
[147] G. Parisi. *J. Phys. France* **51**, 1595 (1990).
[148] P. Pfeifer, D. Avnir, and D. Farin. *Surf. Sci.* **126**, 569 (1983).
[149] M. Předota and M. Kotrla. *Phys. Rev. E* **54**, 3933 (1996).
[150] M. Plischke, Z. Rácz, and D. Liu. *Phys. Rev. B* **35**, 3485 (1987).
[151] M. Plischke and Z. Rácz. *Phys. Rev. Lett.* **53**, 415 (1984).
[152] M. Plischke and Z. Rácz. *Phys. Rev. A* **32**, 3825 (1985).
[153] M. Prähofer and H. Spohn. *Phys. Rev. Lett.* **84**, 4882 (2000).
[154] M. Prähofer and H. Spohn. *J. Stat. Phys.* **115**, 255 (2004).
[155] J. Qian. *Acta Mechanica Sinica* **10**, 12 (1994).
[156] J. Qian. *Phys. Rev. E* **58**, 7325 (1998).
[157] J. Qian. *Phys. Rev. Lett.* **84**, 646 (2000).
[158] R. Rabady and I. Avrutsky. *J. Opt. Soc. Am. B* **20**, 2174 (2003).
[159] S. M. Rossnagel and T. S. Kuan. *J. Vac. Sci. Technol. B*, **22**, 240, (2004).
[160] M. A. Rubio, C. A. Edwards, A. Dougherty, and J.P. Gollub. *Phys. Rev. Lett.* **63**, 1685 (1989).
[161] T. Sasamoto and H. Spohn. *J. Stat. Mech.* **P11013** 2010.
[162] T. Sasamoto and H. Spohn. *Phys. Rev. Lett.* **104**, 230602 (2010).
[163] M. Schwartz and S. F. Edwards. *Europhys. Lett.* **20**, 301 (1992).
[164] Z. S. She and S. A. Orszag. *Phys. Rev. Lett.* **66**, 1701 (1991).
[165] Y. Shim and D. P. Landau. *Phys. Rev. E* **64**, 036110 (2001).
[166] M. Siegert and M. Plischke. *Phys. Rev. Lett.* **68**, 2035 (1992).
[167] G. I. Sivashinsky. *Acta. Astron.* **4**, 1177 (1977).
[168] T. Singha and M. K. Nandy. *J. Stat. Mech.* **023205** (2016).
[169] T. Singha and M. K. Nandy. *Phys. Rev. E* **90**, 062402 (2014).
[170] T. Singha and M. K. Nandy. *J. Stat. Mech.* **P05020** (2015).
[171] L. M. Smith and W. C. Reynolds. *Phys. Fluids A* **4**, 364 (1992).
[172] T. R. Smith and F. P. Bretherton. *Water Resources Research* **8**, 1506 (1972).
[173] K. R. Sreenivasan and R. A. Antonia. *Annu. Rev. Fluid Mech.* **29**, 435 (1997).
[174] K. R. Sreenivasan, P. Kailasnath and G. Stolovitzky. *Phys. Rev. Lett.* **68**, 2766 (1992).
[175] T. Sun, H. Guo, and M. Grant. *Phys. Rev. A* **40**, 6763 (1989).
[176] K. A. Takeuchi. *preprint*, 2012.
[177] K. A. Takeuchi. *Phys. Rev. Lett.* **110**, 210604 (2013).
[178] K. A. Takeuchi and M. Sano. *Phys. Rev. Lett.* **104**, 230601 (2010).
[179] K. A. Takeuchi and M. Sano, T. Sasamoto, and H. Spohn. *Sci. Rep.* **1**, 34

(2011).
[180] K. A. Takeuchi and M. Sano. *J. Stat. Phys.* **147**, 853 (2012).
[181] L. H. Tang. *J. Stat. Phys.* **67**, 819, (1992).
[182] L. H. Tang, B. M. Forrest, and D. E. Wolf. *Phys. Rev. A* **45**, 7162 (1992).
[183] L. H. Tang and T. Nattermann. *Phys. Rev. Lett.* **66**, 2899 (1991).
[184] T. Tatsumi, S. Kida, and J. Mizushima *J. Fluid Mech.* **85**, 97 (1978).
[185] C. A. Tracy and H. Widom. *Comm. Math. Phys.* **159**, 151 (1994).
[186] D. Tsamouras, G. Palasantzas, and J. Th. M. De Hosson. *Appl. Phy. Lett.* **79**, 1801 (2001).
[187] Y. Tu. *Phys. Rev. Lett.* **73**, 3109 (1994).
[188] Y. Tu. *Phys. Rev. A* **46**, R729 (1992).
[189] H. van Beijeren, R. Kutner, and H. Spohn. *Phys. Rev. Lett.* **54**, 2026 (1985).
[190] W. van Saarloos and G. H. Gilmer. *Phys. Rev. B* **33**, 4927 (1986).
[191] T. Vicsek, M. Cserz, and V. K. Horvth. *Physica A* **167**, 315 (1990).
[192] J. Villain. *J. Phys. I* **1** , 19 (1991).
[193] A. Vincent and M. Meneguzzi. *J. Fluid Mech.* **225**, 1 (1991).
[194] M. J. Vold. *J. Colloid Science* **14**, 168 (1959).
[195] M. J. Vold. *J. Phys. Chem* **63**, 1608 (1959).
[196] D. D. Vvedensky, A. Zangwill, C. N. Luse, and M. R. Wilby. *Phys. Rev. E* **48**, 852 (1993).
[197] D. D. Vvedensky, M. R. Wilby and A. Zangwill. *Phys. Rev. B* **46**, *12896* (1992).
[198] L. P. Wang, S. Chen, J. G. Brasseur, and J. C. Wyngaard *J. Fluid Mech.* **309**, 113 (1996).
[199] D. R. Wilkinson and S. F. Edwards. *Proc. Roy. Soc. London Ser. A* **381**, 17 (1982).
[200] K. G. Wilson and J. Kogut *Phys. Rep.* **12**, 75 (1974).
[201] K. G. Wilson. *Rev. Mod. Phys.* **55**, 583 (1983).
[202] D. Wolf and J. Villain. *Europhys. Lett.* **13**, 389 1990.
[203] D. E. Wolf and J. Kertsz. *Europhys. Lett.* **4**, 651 (1987).
[204] D. E. Wolf and J. Villain. *Europhys. Lett.* **13**, 389 (1990).
[205] H. W. Wyld. *Ann. Phys. (N.Y.)* **14**, 143 (1961).
[206] V. Yakhot. *Phys. Rev. E* **49**, 2887 (1994).
[207] V. Yakhot and S. A. Orszag. *Phys. Rev. Lett.* **57**, 1722 (1986).
[208] V. Yakhot and S. A. Orszag. *J. Sci. Comput.* **1**, 3 (1986).
[209] H. Yan. *Phys. Rev. Lett.* **68**, 3048 (1992).
[210] S. H. Yook, J. M. Kim, and Y. Kim. *Phys. Rev. E* **56**, 4085 (1997).
[211] S. H. Yook, C. K. Lee, and Y. Kim. *Phys. Rev. E* **58**, 5150 (1998).

Vita

Tapas Singha was born on 20th March 1989 in West Bengal, India. He did his B.Sc. with Physics Honours in 2009 from Ramakrishna Mission Residential College Narendrapur, under University of Calcutta, Kolkata and M.Sc. in Physics from Indian Institute of Technology Guwahati, Guwahati in 2011. He enrolled into the Ph.D programme at Indian Institute of Technology Guwahati in 2011. He qualified both Graduate Aptitude Test in Engineering (GATE) and CSIR-UGC NET in 2011. He earned the Senior Research Fellowship in 2013 by Indian Institute of Technology Guwahati, Guwahati.